



ARISTOTLE UNIVERSITY OF THESSALONIKH

SCHOOL OF GEOLOGY

MSc Hydrocarbon Exploration and Exploitation



VOUTA STYLIANI

Graduate Geologist

**TURBIDITES AND MASS MOVEMENTS IN DEEP WATER CONTINENTAL
SLOPES. CURRENT ISSUES AND LABORATORY EXPERIMENTS
APPROACH.**

MASTER THESSIS



Thessaloniki 2024



VOUTA STYLIANI

Graduate Geologist

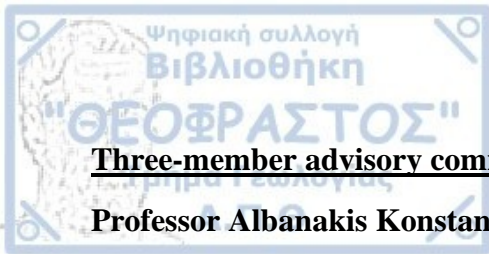
Turbidites and mass movements in deep water continental slopes.

Current issues and laboratory experimental approach.

Submitted to the Department of Geology as part of the Master's Program of Study

Hydrocarbon exploration and exploitation

Date of oral examination:



Three-member advisory committee:

Professor Albanakis Konstantinos, supervisor professor

Associate Professor Pechlivanidou Sofia member of the advisory committee

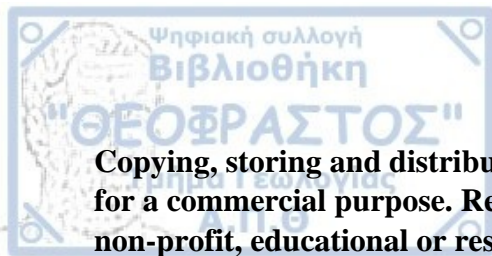
Associate Professor Maravelis Angelos member of the advisory committee

Department of Geology Scientific Yearbook Supplement Number No

© Styliani, I. Vouta, 2024

All right reserved

Turbidites and mass movements in deep water continental slopes. Current issues and laboratory experimental approach.



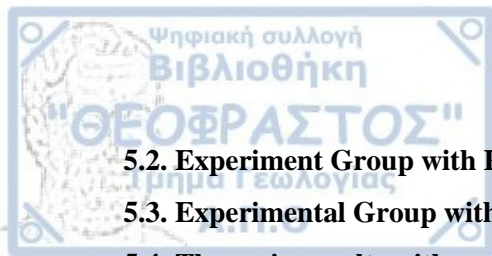
Copying, storing and distribution of this work is prohibited, ex in whole or in part, for a commercial purpose. Reprinting is permitted, storage and distribution for non-profit, educational or research purposes nature, provided that the source of origin is mentioned and the present message. Questions regarding the use of the work for profit should be addressed to the author.

The opinions and conclusions contained in this document express the author and should not be interpreted as expressing the official positions of AUTH.



CONTENTS

Acknowledgments.....	VI
1. Introduction	1
2. Deep water processes that effect the sedimentation in deep water continental slopes.	2
2.1. Turbidites	2
2.1.1. <i>Rheology of Newtonian fluids.....</i>	<i>2</i>
2.1.2 <i>Characteristics of turbulent flows</i>	<i>3</i>
2.1.3. <i>The turbidity's architectural elements.....</i>	<i>5</i>
2.1.4. <i>The turbidites sequence stratigraphy and controlling factors.....</i>	<i>20</i>
2.2. Mass flows	24
2.2.1. <i>Rheology of Bingham plastic flows</i>	<i>24</i>
2.2.2. <i>Categories of mass flows processes.....</i>	<i>24</i>
2.3. Hyperpycnal flows	30
2.3.1. <i>The formation of hyperpycnal flows</i>	<i>30</i>
2.3.2. <i>High density turbidity currents.....</i>	<i>34</i>
2.4. Initiation of gravity flows.....	35
2.4.1. <i>Oceanic processes</i>	<i>35</i>
2.4.2. <i>Failure gravity flows</i>	<i>36</i>
2.4.3. <i>Submarine flows as a continuum of a river flow</i>	<i>37</i>
2.5 Flow transformation in sediment- gravity flows.....	39
3. Currents that affect the sedimentation in deep water continental slopes.....	42
3.2. Geostrophic thermohaline circulation.....	43
3.3. Contour currents- Contourites.....	45
3.3.1. <i>Processes of transport and deposition.....</i>	<i>46</i>
4.2. Preparation of Hyper-Saline Solution	49
4.3. Sample Collection	50
4.4. Sample Processing	52
4.6. Video Recording of Experiments	53
4.7. Processing and Analysis of Experiment Videos.....	53
4.8. Boundary conditions	54
5. Discussion and Results	55
5.1. Group of experiments with a particle size range of 1-1.5 ϕ (mean 1.25ϕ).....	57



5.2. Experiment Group with Particle Size Range of 2-2.5 ϕ (Mean 2.25 ϕ)	62
5.3. Experimental Group with Sediment Material Grain Size Range -1.5 to >4	68
5.4. The main results with graphical approaches.	73
6. For further research.....	83
7. Bibliography.....	84
APPENTIX I	100
APPENTIX II	155



This Thesis was conducted as part of the Postgraduate Program in Hydrocarbons Exploitation and Exploitation at the Department of Geology of Aristotle University of Thessaloniki.

At this point, I would like to thank my supervisor, the professor at the Department of Geology of Aristotle University of Thessaloniki Dr. Konstantinos Albanakis, for selecting the topic of my thesis and for his valuable guidance, as well as for the scientific discussions and observations he provided regarding my thesis. I would also like to express my gratitude to the other two members of the advisory committee, the associate professor Dr. Sofia Pechlivanidou and the associate professor Dr. Maravelis Angelos, for their advice and support. Finally, I would like to thank the doctor Dr. Kalliopi Koliadimou, who is part of the laboratory teaching staff at the Department of Geology of Aristotle University of Thessaloniki, for her assistance with various laboratory aspects of my thesis.

Above all, however, I would like to thank my family, for their patience and support throughout all these years of my hard work...

Vouta Styliani



1. Introduction

The purpose of this specialized thesis is the detailed study of turbiditic gravity flow processes in marine environments. For this reason, an extensive literature review is initially presented, followed by the results of a total of 48 laboratory experiments were conducted at the laboratory of sedimentology Department of Geology, Aristotle University of Thessaloniki.

Turbidites are the result of turbidity currents [2], which are sediments gravity flows [3] with Newtonian rheology [4] and turbulent state [2]. Turbidity currents are usually characterized by a low sediment concentration, commonly below 9% by volume [5]

Mass flows is a general term that is used to describe flows under gravity. They are separated into debris flows and turbidity currents. Cable failures, are an impact of their action on human in fractures and their classification is based on their sedimentary deposits.

The purpose of this specialization thesis is to study the movement of sand in the ripples of the deep sea. The choice of sand as the main material for the experimental study was not random. Sands, and by extension, the sandstone rocks, are what provide the best petroleum reservoirs, with the easiest and less costly extraction of oil.

Specifically, an attempt will be made to simulate the sand movements of through turbidity currents and debris flows in closed and open sea environments. This will be achieved through the study of the movements of different grain sizes of sand in an experimental tube and in a setting of freshwater and super-saline water solution.

A total of 48 experiments were conducted in order to understand the movement of sands grains and, consequently, the granulometry of the deep-sea sandstone reservoir.

2. Deep water processes that effect the sedimentation in deep water continental slopes.

A coarse-grained sediment can be transferred hundreds of kilometres away from the continental slopes. It's very important to understand the mechanism of transfer and deposition in deep sea. Turbidites, slides, slumps and debris flows (mass flows) are the major sediment gravity processes, which play an important role for the sedimentation of the continental slopes [1].

2.1. Turbidites

Turbidites are the result of turbidity currents [2], which are sediments gravity flows [3] with Newtonian rheology [4] and turbulent state [2]. Turbidity currents are usually characterized by a low sediment concentration, commonly below 9% by volume [5]. Sedimentation occurs by the sediment suspension, which result in normal grading [4, 2, 3, 6, 7].

2.1.1. Rheology of Newtonian fluids

Rheology of Newtonian fluids is called the relationship between the applied shear stress and the rate of shear strain (Fig. 1). Newtonian fluids are the fluids without inherent strength such as water. Their deformation is linear and begins when a shear stress is applied. The turbulence in Newtonian fluids begins when the Reynolds number is greater than the value of 2000 (Fig.1). The Reynolds number is the ration between inertia and viscous forces.

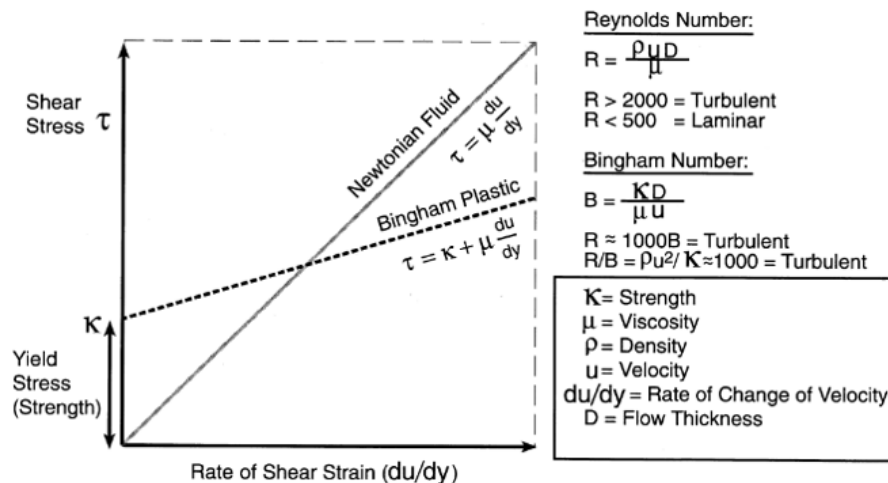


Figure 1. Rheology (stress-strain relationships) of Newtonian fluids (e. g., turbidity currents) and Bingham plastics (e.g., debris flows), compiled from several [4, 8, 9, 10, 11]. This graph shows that a fundamental rheological difference between debris flows (Bingham plastics) and turbidity currents (Newtonian fluids) is that debris flows exhibit strength, whereas turbidity current do not. In general, turbidity currents are turbulent and debris flows are laminar in state [7].

Many scientists, say that in the deep-water environments, the turbidity currents are represented by the Newtonian rheology [4, 8, 9, 10, 11]. There is an option that turbidity currents are sediment-gravity flows and fluidal flows too [12, 13]. According to Oakeshott 1989 [14], turbidity currents cannot be the both flows at the same time, because in sediment-gravity flows the sediments are moved by gravity, whereas in fluidal flows the fluids are moved by gravity [3]. According to Middleton (1993) [15], a turbidity current is a sediment gravity flow with Newtonian rheology in which the sediments are held in suspension by fluid turbulence.

2.1.2 Characteristics of turbulent flows

2.1.2.a. Morphology of turbulent flows

The turbulent flows consisting parts are the head, the neck (which is not always observed), the body and the tail (Fig. 2A). The head has usually a bulge shape because of the flow dynamic of the turbulent flow. Is observed, that the fluid which is inside the head, has a circular motion from the front to the top of the head. In this part of the turbidity current, are concentrated the coarser grains (Fig. 2B). For these reasons, the head is the most erosional part of the turbidity current. Neck is a transitional part between the head and the body of the turbidity. The body is located behind the neck and it is mainly the depositional part of the turbulent flow. The tail is the last part of the turbulent flow which is very diluted [16].

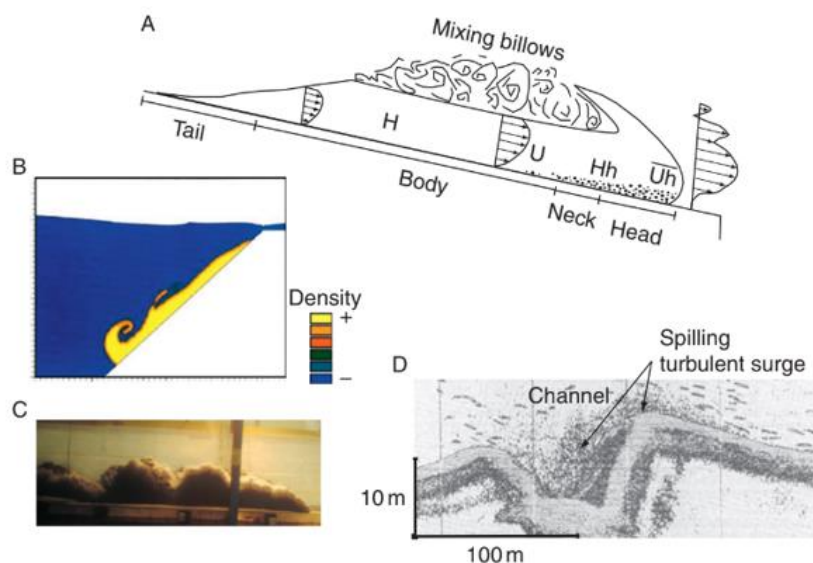


Figure 2. Examples of turbulent-flow morphology. (A) Morphology of a turbulent surge [16]. (B) Numerical simulation of a turbulent surge [17]. (C) Basin experiment of a turbidite surge. Flow is 10 to 20 cm thick. (D) Very high-resolution seismic profile showing a turbidity current spilling over a channel wall [18]. Copyright 1987 American Geophysical Union. Reproduced with permission from American Geophysical Union.

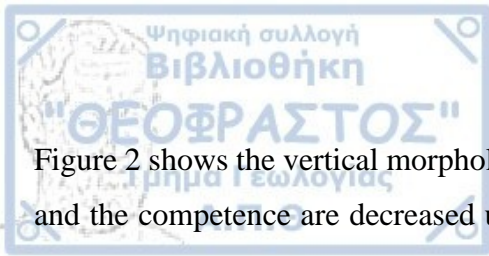


Figure 2 shows the vertical morphology of the turbulent flow, which is stratified. The flow density and the competence are decreased upward (Fig.2B) [17]. There is a vertical decrease of the flow velocity, with the maximum value in the flow's lower part. The phenomenon of the flow splitting and stripping is explained with the upward velocity behaviour (Fig. 2C&D) [18].

2.1.2.b. Velocity of turbulent flows

The numerical modelling of the velocity of a turbulent flow can be assessed by the using of a simple 1D approach. The Chezy's equation is the first equation which usually used for the velocity calculation of a turbulent flow and a fluvial current [19].

$$U^2 = cg'Hs \sin s / (1 + \alpha) C_f$$

s = the slope of the seafloor

c = the volume concentration of sediment

C_f = the friction coefficient along the bed (value = 0.035-0.005)

[20, 19]

α = the friction coefficient that is related to both Reynolds and Froude numbers

[21]

The Chezy's equation is simple but applied only to uniform and stationary 1D flows with the value of seafloor slope different than zero. As it's known, the natural phenomenon of the turbulent flow is highly non-uniform and non-stationary. In addition, this equation can be used only as a first estimate of the turbulent flow's velocity, because the most of the parameters in this equation are very difficult to measure or quantify such as density and flow thickness.

This equation is the first which try to calculate the flow velocity of a turbulent phenomenon. The recent equations include non-stationary models [22], stationary non-uniform models based on the theory of boundary layers and interaction methods [23, 24], mixing models based on Navier-Stokes equation [17, 25] and cellular automata models [26].

2.1.2.c. Erosion by turbulent flows

The erosional ability of the turbulent flows is very important. Giant scours and erosional surfaces occur at the base of the turbidity beds. The erosion effect can be happened by the turbulent flow or due to the concentrated flow forming the base of turbidity flows. Historical events show that the volume of a turbidity deposit by one event can be larger than the volume in the initial failure. Some paradigms, in the Nice event the initial slide was 0.08 km^3 and the turbidity was 2 km^3 [27]. In the Grand Banks event, the initial failure was 20 km^3 and the turbidity was 200 km^3 in the Sohm abyssal plain [28, 29]. The seafloor erosion could be increased by the conduit flushing [30].

2.1.3. The turbidity's architectural elements

The main architectural elements of deep sea as a result of turbidity systems are a) Canyons, b) Gullies, c) Shelf- break deltas, d) Channels and levees, e) Terraces in submarine f) Canyons and channels, g) Lobes. All the descriptions of the upward elements are provided by the study of recent systems such as the Amazon [31, 32], the Capbreton Canyon [33, 34, 35], the La Jolla fan valley and others [36].

2.1.3.a. Canyons

The main way for the sediment transfer from the continent to oceans are the canyons (Fig. 3). The canyons are usually hundreds of metres and frequently more than a kilometre deep and narrow a few kilometres. Their walls are steep and formed by erosion of the continental slope and outer shelf [37]. According to Gaudin (2006) [38] and Gaudin et al. (2006b) [34], except the erosion, the canyons shape is a result of alternating stages of filling and incision. There are sinuous or meandering and straight canyons. In the meandering canyons, there is one sheer erosive and another smoother depositional flank, where terraces are formed. For this reason, the canyon is asymmetrical. The straight canyons have a symmetric V or U shape [35, 27]. The start of the canyons is usually the mouth of the rivers such as Zair, Amazon and Onirico in the Atlantic Ocean, Indus in the Indian Ocean, Ebro in Mediterranean. But there are canyons which aren't connected with any river mouth such as Dume and La Jolla canyons off southern California.

The determination of the canyon formation is a very difficult process. So, there are four possible processes a) after a subaerial phase of erosion by a river system, b) backward

(retrogressive) submarine erosion, c) forward erosion by continuous steady flows (hyperpycnal flows) d) by passing on rapidly progradating margins.

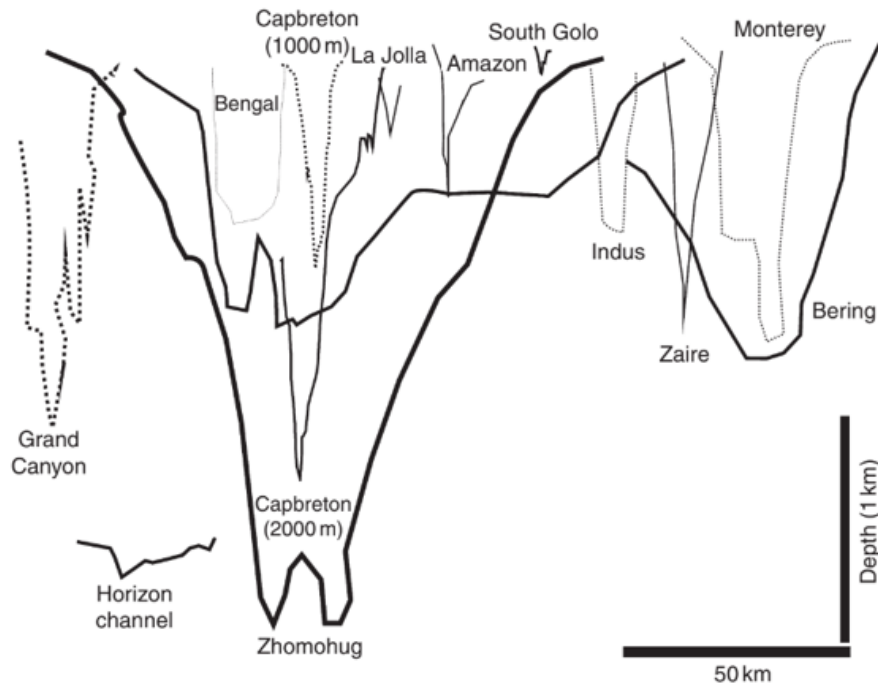


Figure 3. Canyon morphology and detailed morphology of meandering channels and terraces. Am: abandoned meander. Compared cross section of submarine canyons with one continental canyon the Grand Canyon. Vertical exaggeration =48.5 [39].

- A characteristic paradigm is the canyons which created in the Mediterranean Sea during the Messinian period. There are canyons which are created when the sea level fall extremely by river erosions [40].
- At the canyon head, so the supply as the accumulation of the sediments is huge. This suggest that retrograde processes can be form and maintain canyons. The simplest explanation for canyon formation is the submarine retrogressive erosion. Thus, the canyon head moves progressively towards the land, so numerous slumps are observed at some of them (Fig.4) [41].

- c) Hyperpycnal flows [42], are erosive sediment gravity flows which take part to the canyon erosion [43]. The discovery of hyperpycnites in the Var Canyon [44] is the proof of this assumption. In addition, this assumption is supported by the insitu measurements of the laden flows in submarine canyons [45, 46, 35, 47, 48].
- d) The canyon structures are narrow areas with a low rate of sedimentation. Their margins do not prograde so quickly as the rest of the margins [49]. This hypothesis has effect only for margins with a high progradation

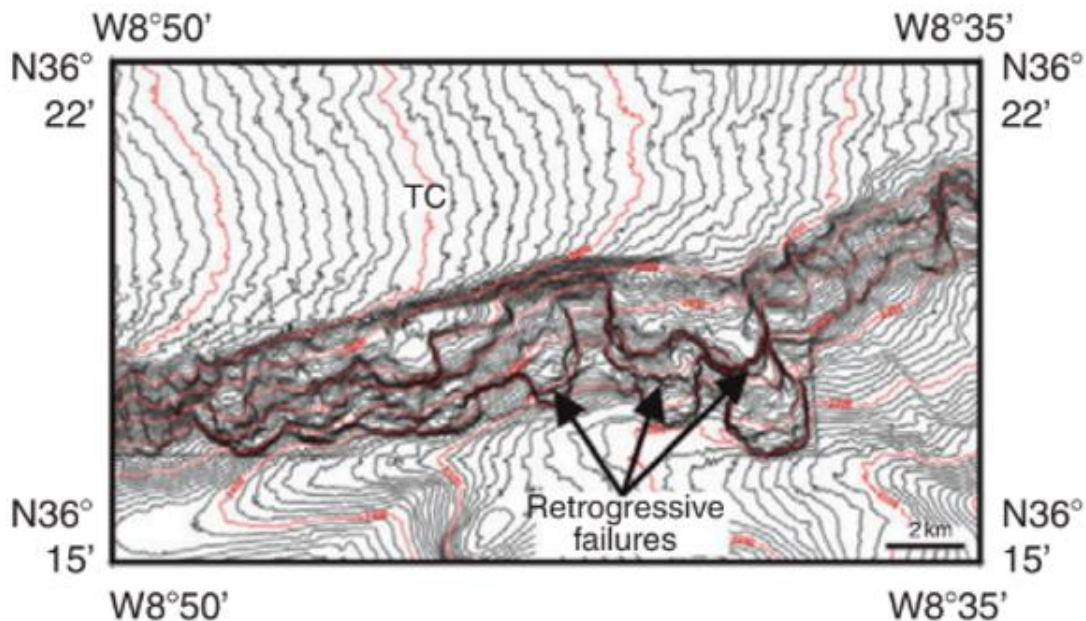


Figure 4. Retrogressive slumps on the wall of a channel at the Gulf of Cadiz.

2.1.3.b. Gullies

Gullies, are usually small and straight submarine valleys with 100-250m width and 5-50 m depth. Their flanks are steep with failure scars. Their morphology is similar to subaerial badlands. Continental slope and self are incised by gullies, which usually form a connected

network. Gullies origin is from retrogressive erosion or from density cascading like Eel River [50].

2.1.3.c. Shelf-break deltas

The shelf-break deltas can be found from the continental shelf to the slope. They usually formed when the rate of relative sea level fall rise is not able to exceed sedimentation rate (lowstand), particularly during the regression processes [51, 52]. But, they continue to formed during the high stand like the Mississippi and Nile river deltas [53]. Their deposits thickness can be 140m. A typical prograding order of a self- break begins with the turbidites and debris flows, the mouth bar, the delta front deposits and at the end of the sequence are the river deposits [54]. As the result of gravity processes (turbidites and gravity flows) which include various types of slump and mudflow, is the rapid progradation of the delta front and the river mouth bar [55]. The deep mass flow deposits are influenced by the storm waves and swell. In the swallower sea parts these deposits are influenced by the tidal. These upward processes can change completely the continental slope.

2.1.3.d. Channels and levees

The processes of erosion and deposition control the deep-sea channel morphology (Fig. 5). The channel's erosion is reduced from upstream to downstream, while the deposition is increased. There are two kind of channels. The first kind is the incising channels which are deep, with small or none lateral levees because the sediment flow doesn't fall out of them, like Zaire river [56]. The second kind of channels are the aggrading channels in which the sediments are concentrated vertically and 'quickly' like the Amazon river (Fig. 6) [32].

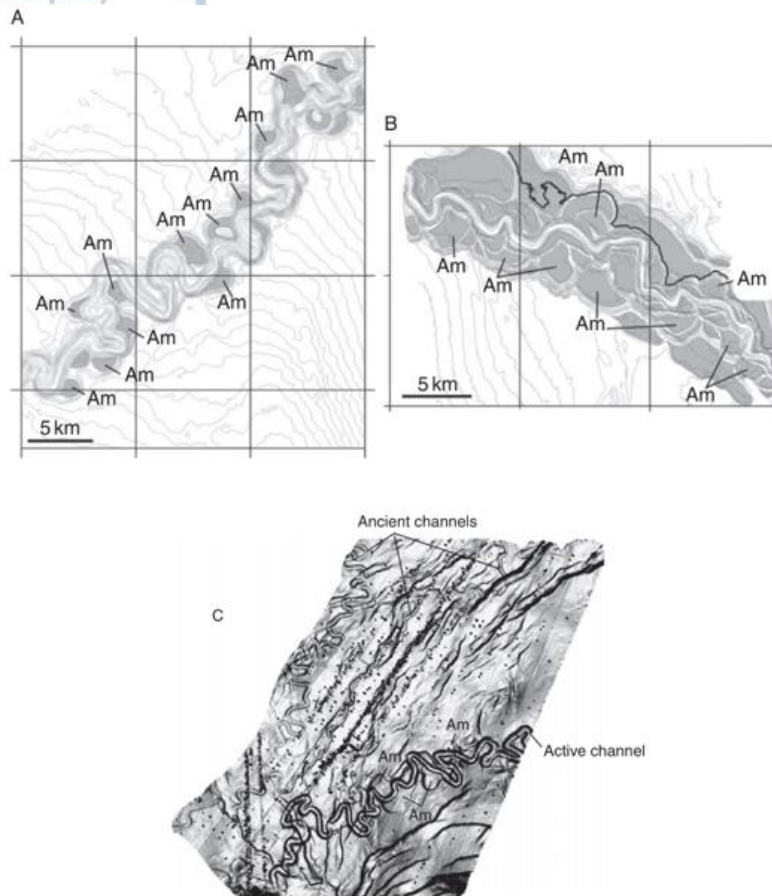


Figure 5. Deep sea fans, A and B is the Zaire deep sea fan (A) EM12 bathymetric map and (B) EM 300 bathymetric map [56, 57]. Terraces are in grey. Most of them are abandoned meanders acting as nested levees. (C) Indus deep sea fan [58].

The morphology of the channels depends on the characteristics of the transferred sediment. For example, channels with coarse-grain sediments are wide, straight and shallow. Channels with fine grained sediments are narrow, deep and create meanders with levees.

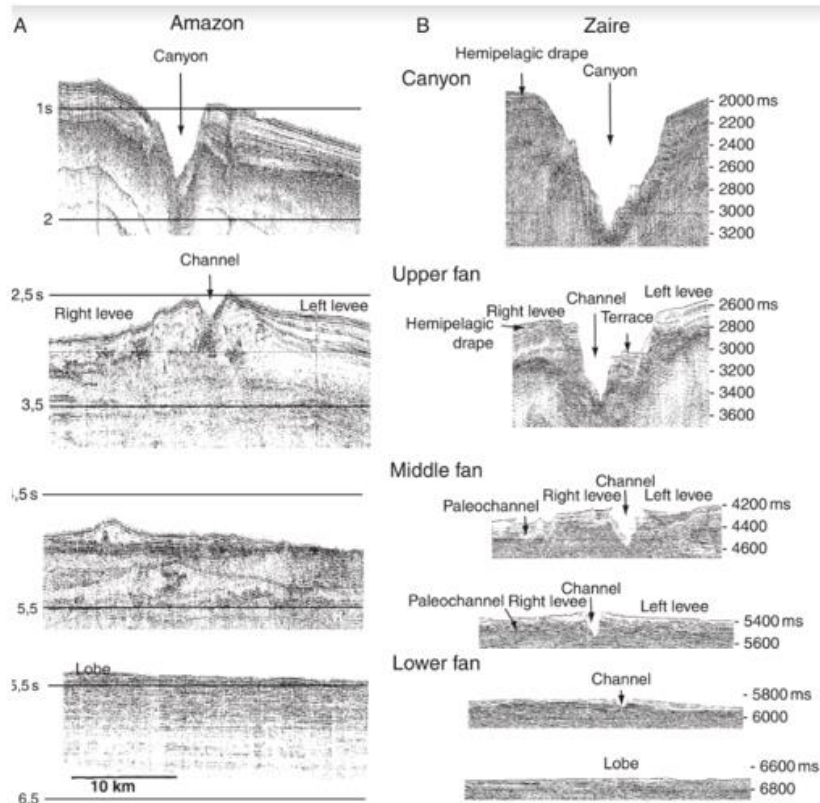


Figure 6. Longitudinal evolution of the seismic structure of modern deep-sea fans. (A) Amazon [32] (B) Zaire [56, 57]. Reproduced with permission from Geological Society, London.

The channels aren't permanent structures. 'Avulsion' is a phenomenon which happens because of a fault action (Fig.7) [59] in areas with steep slope, such as the Amazon fan [60, 61, 62]. When the 'avulsion' is occurred, the next turbidity flow, follows the new path and gradually a new levee is created. The geological formation 'avulsion lobes' [32] are the structures which are formed at the base of the new levee.

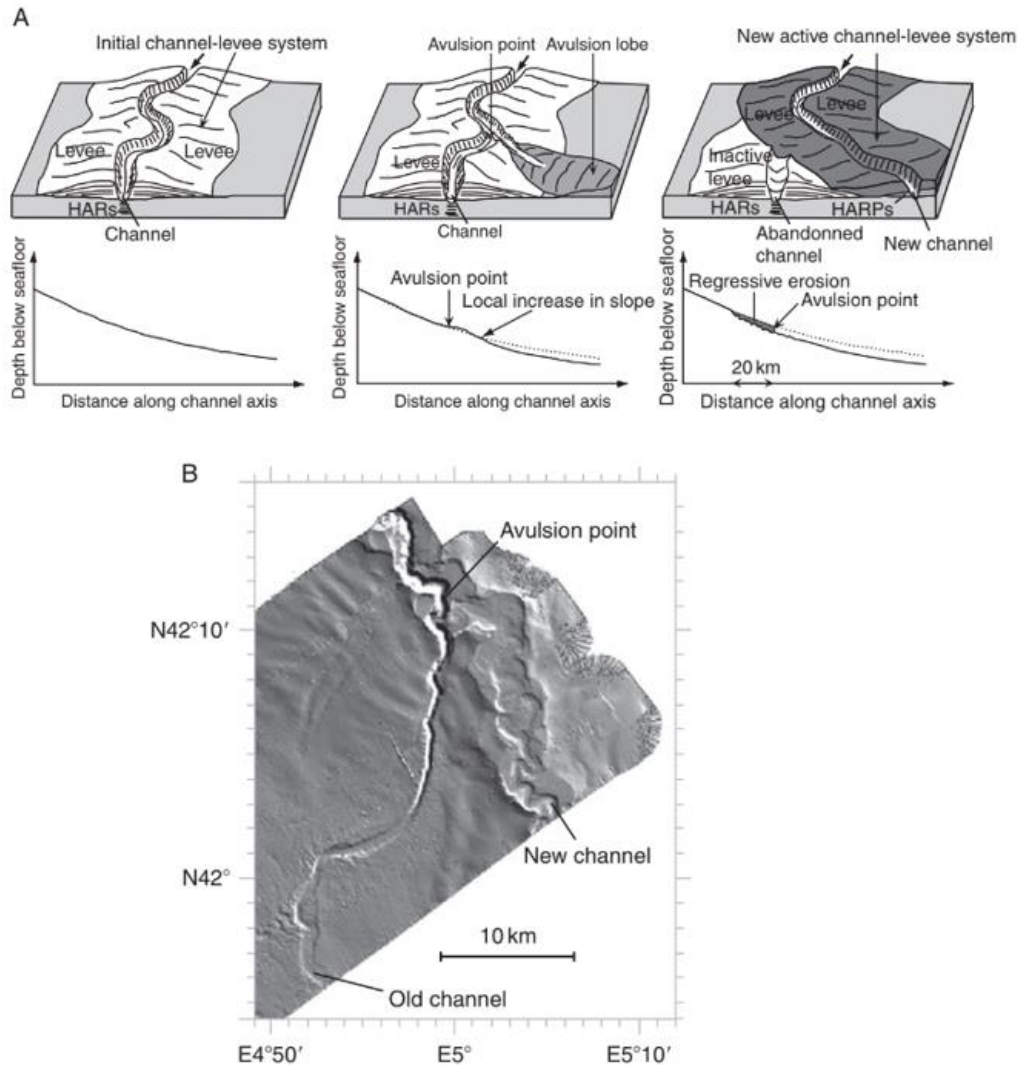


Figure 7. Channel ‘avulsion’ Channel avulsion. (A) Channel avulsion and evolution of the downslope morphology of a channel during and after avulsion [56]. Bold arrow indicates direction of the channelized flow. (B) Last avulsion point of the Rho'ne deep-sea fan (that led to the formation of the Rhone neofan) [63].

The ‘alvusion’ doesn’t happen in canyons. Rarely happens at the upper channel- levee complex. More frequently happens downward the channel- levee complex. The ‘alvusion’ becomes very frequent in lobe channels.

Levees are topographic highs which begin from the canyon’s mouth and neighbouring with the channel side. The levee’s height from the channel to the top of it can reach from e few

hundred to several tens of metres (upstream to downstream). So, the total sediment thickness of a channel- levee complex can be reaching the 1000-1500 metres [64]. The final levees extend can be reach at the 50 km on each side of a channel.

Levees at the mid-latitude, are usually asymmetrical. On the right side is more developed than the left one. This happens because of the Coriolis force [65, 66, 67, 68, 69]. The opposite happens in the south hemisphere [70].

Levees can be easily recognized on the seismic profiles by their special topography and characteristic shape of the bird-wing or moustache shape. Levees created by the process of spillover of the upper part of turbidity currents. This happen because of the flow thickness is greater than the levee height (Fig. 8 A) [71].

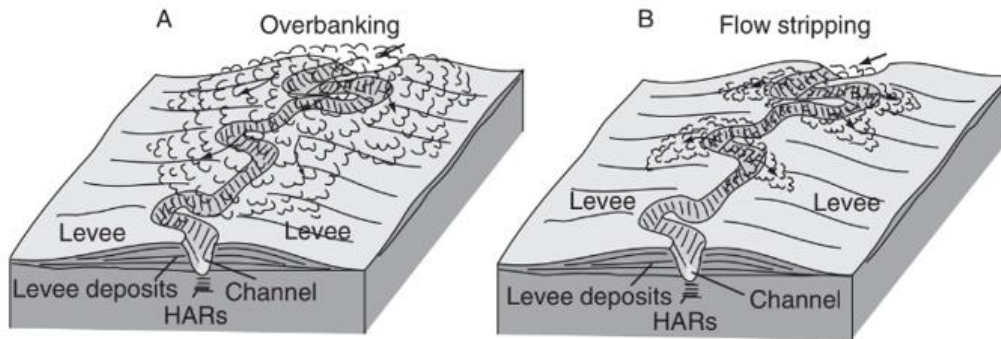


Figure 8. (A) Overbanking or overspilling [71]. (B) Flow stripping [72]. Bold arrow indicates direction of the channelized flow [56].

Flow stripping is the process in which, the flow separated due to the centrifugal force and the abrupt change of the channel direction (in a bend or a meander), into bipartite flow [72] (Fig. 8B). The denser part of the flow, concentrated on the bottom as a channelized flow. The upper, the diluted turbulent flow, spills (falls out) and spreads over the levees. Secondary channels can be formed, in areas in which the fall out (spillover process) is intensive [73]. In areas, where the levees are low (meanders), 'crevasse splay deposits' (channelized deposits) can be developed by the outer erosion during the spillover [73].

Levee grow up vertical and depends on the type (volume, intensity, sediments grain size) and the frequency of turbidity currents. If for some reasons the type, the frequency or the

characteristics of the turbidity currents change, the levee decryption, is a difficult procedure such as the levees of Amazon river [71, 74].

At the outer side of the levee also seems slumps which are covered with sediment waves [75, 76, 77]. A particular characteristic of the sediment waves is their progradation upstream and upslope. They are created by the turbidity currents and have a crest direction vertical to the flow. Their morphology is asymmetrical, with an upstream (progradational) side, which is steeper and shorter than the downstream side [78, 79, 80]. Their sediment deposition happens on the upstream side. On the other hand, erosion and less deposition processes happen on the downstream side [75, 76] due to the flow velocity change (Fig. 9).

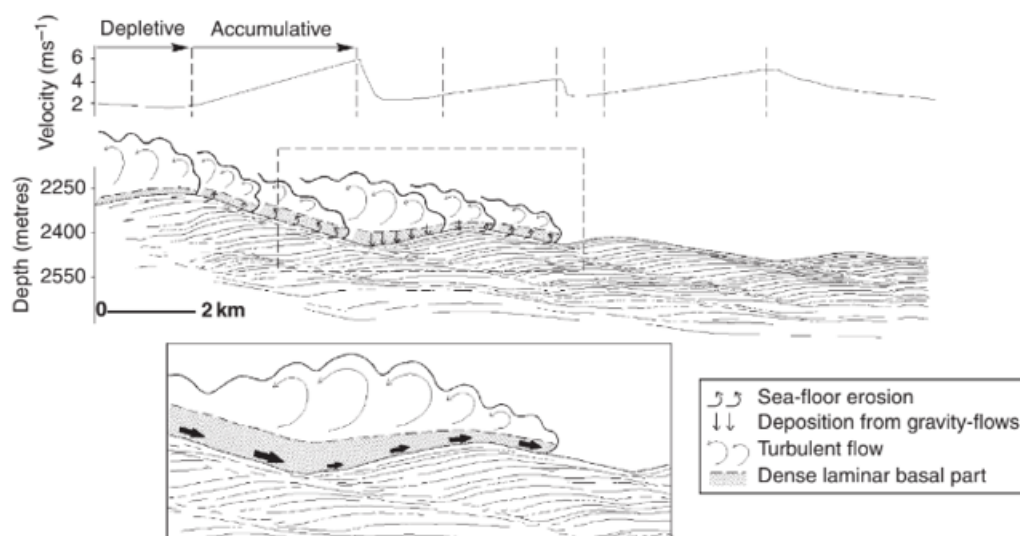


Figure 9. Longitudinal changes in a turbulent flow spilling over the sedimentary levee in the Var deep-sea fan [75, 76]. The location of dominant erosion or deposition explains the formation of sediment waves on the distal (outer) side of the levee. Reproduced with permission from S. Migeon and from Elsevier.

The seafloor and the flow velocity, play an important role for the processes of erosion and deposition. The flow moves along the abrupt upstream wave side until the lowest point of the channel. After that, an important sediment deposition happens because of the rapidly flow deceleration. Behind the wave crest, the flow accelerates again along the downstream flank.

2.1.3.e. Terraces in submarine canyons and channels

Terraces are flat structures of several metres to several tens of metres above the talweg. The development of submarine channels by 'plug and cut migrations' [81] means, alternative of channel fill and incision phases. Downward are the submarines terrace formation processes.

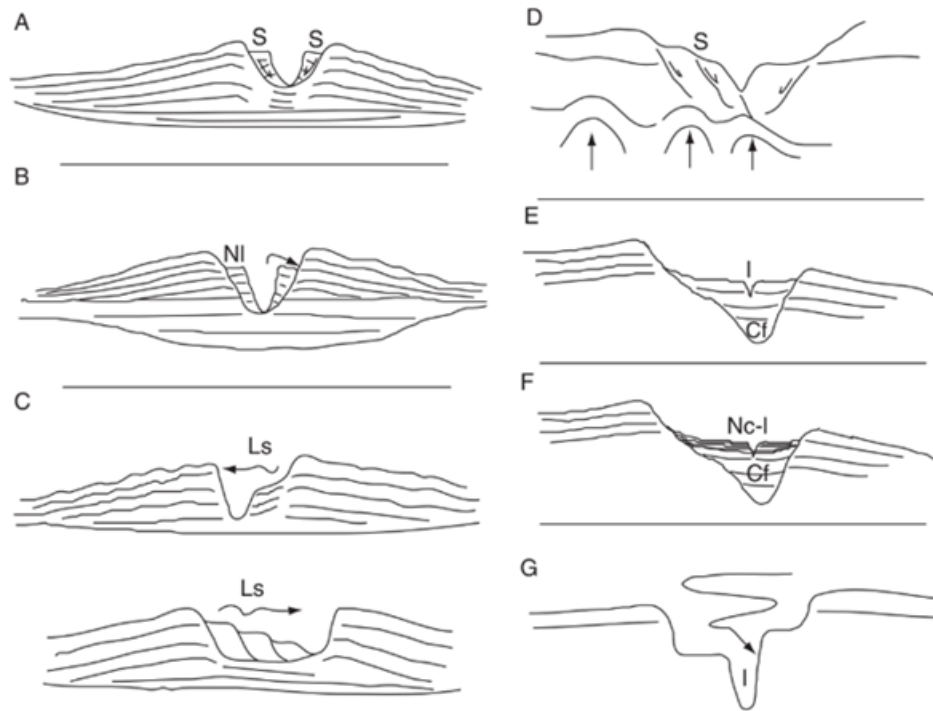


Figure 10. Models for terrace interpretation in deep-sea turbidite channels. **(A)** Slumps (S) on canyon/channel flanks (e.g. Indus Channel: [83]. **(B)** Formation of nested levees (NI) during sea-level rise (e.g. Bengal Channel: [86]; Hueneme Channel: [69]. **(C)** Filling of the canyon/channel because of lateral shifting (Ls) of the canyon/channel or of decrease in the volume of the channelized flows (e.g. Amazon Channel: [87]; Toyama Channel: [88]; Indus Channel: [89]. **(D)** Deformation and slumping (S) due to gravitational tectonics (e.g. Kaoping Canyon: [90]; Zaire Canyon: [91]. **(E)** Incision (I) of a talweg in the canyon/channel fill (Cf) because of an avulsion that occurred downstream (e.g. Rhoˆne Canyon: [92]. **(F)** Formation of a nested channel-levee (Nc-l) system in the canyon/channel fill (Cf) (e.g. Rhoˆne Canyon: [93]. **(G)** Meander abandonment and talweg incision I (e.g. Basin Arequipa Canyon: [94]; Indus Canyon: [95]. From Babonneau et al. (2004) [57]. Reproduced with permission from Geological Society, London.

1. Failure of the canyon side walls (Fig. 10 A & D) [82]. There are slumps (S) on canyon – channel flanks like in Indus channel [83].
2. Flat terraces with or without topographic height are created due to lateral shift of the channel in confined levees (Fig. 10 B- D and F) [57, 84]. The origin of the terraces is the slump, the meander cut or the channel shift.
3. Incision due to avulsion upstream or meander abandonment (Fig. 10 E-G)
4. Horse terraces are formed because of the meander cut off and abandonment. The abandoned part of the meander, is filled by sediments [85] (Fig. 11). Before the total abandonment, the lower part of the flow still moves in the first, ancient meander, while the upper part moves eroding to a new path [56, 57].

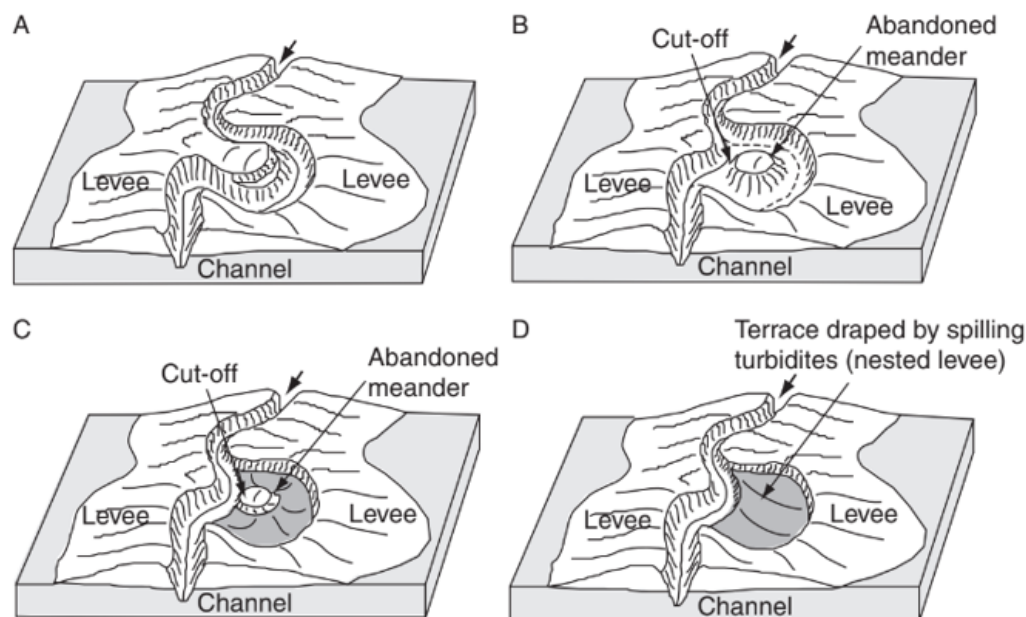


Figure 11. Scenario for meander abandonment [56, 57]. (A) Lateral shift of a talweg. A meander forms. (B) Meander cut-off. (C) Beginning of the filling by spilling of turbidity current in the abandoned meander. (D) Formation of a terrace that acts as a nested levee. Bold arrow indicates direction of the channelized flow. Reproduced with permission from Geological Society, London.

Zaire system is an example of cut off abandoned meanders, with migration and flat terraces with hemipelagic sediments [56, 57] (Fig. 12).

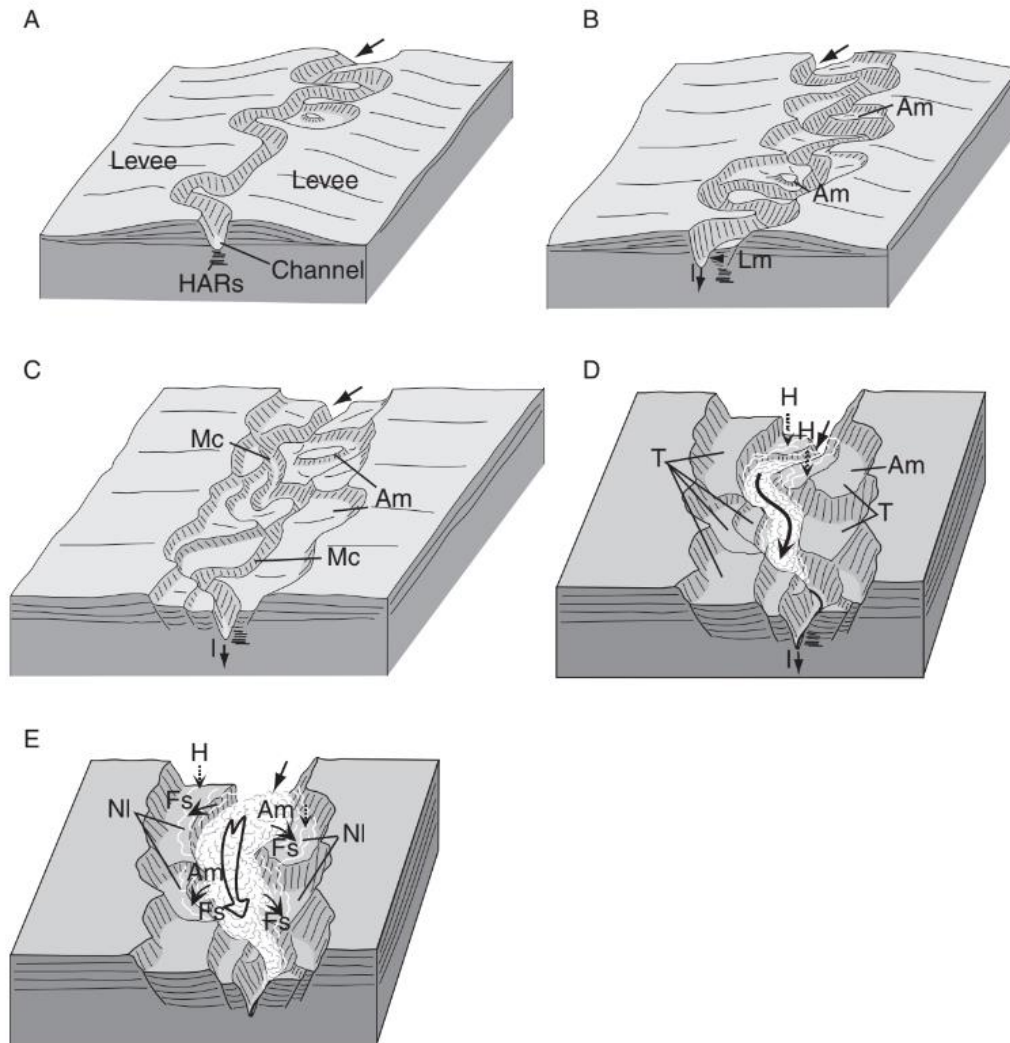


Figure 12. Recent evolution of the Zaire Valley [56, 57]. Reproduced with permission from Geological Society, London. (A) Sinuous channel/levee system with few meander cut-offs (Mc). (B) Simultaneous channel-floor incision (I) and lateral migration (Lm) of meanders. Meander cut-off generates abandoned meanders (Am) and terraces (T). (C) Continuation of both incision and lateral migration of the channel. (D, E) Present time: entrenchment of the talweg inside the deep valley. (D) Low-volume channelized flows. (E) Large-volume, spilling flows (Fs and arrows) forming a nested levee (NI). Bold arrow indicates direction of the channelized flow. Dashed vertical arrow indicates hemipelagic (H) sedimentation.

There is a sinuous channel-levee, which meander is locally abandoned by the existence of interruption (Fig.12 A). The talweg, incises and migrates the channel. So, the meander turned into an abandoned meander. Then it is filled with sediments and finally flat terraces are generated (Fig. 12 B). The incision and the migration of the talweg create a meander belt, in which the fine grades turbidites reduce the flat terraces so, hemipelagic sediments are settled (Fig. 12 C). The present situation of the Zaire system is, that flows with low volume are channelized and cannot spill over the terraces, which are covered with hemipelagites. But, large volume flows (turbidites), can fall out the terraces and fine grained of sedimentation can happen. Finally, nested levees are aggraded (Fig. 12 D).

2.1.3.f. Lobes

Lobes represent the furthest part of a channel- levee system. They are corresponded the initial suprafan lobe and lower fan definition [96, 97]. A lobe is formed, when a levee is failed. Then the flow path is deviated from the existing channel. The flow which is generated, forms a high amplitude packets of reflection (HARPs) on the acoustic reflectivity maps (Fig.13)

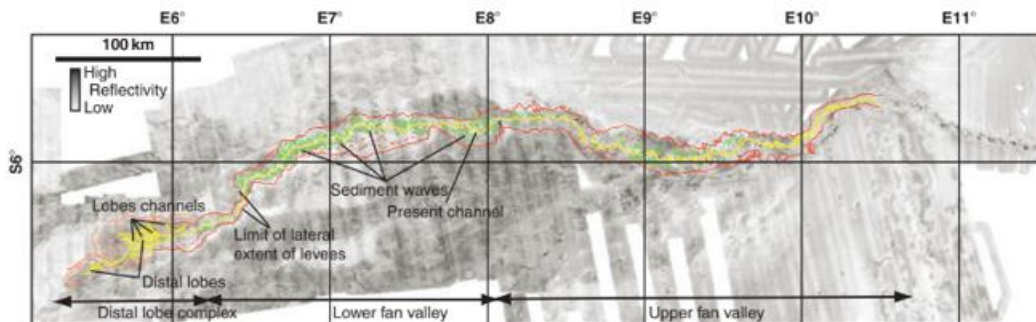


Figure 13. Acoustic imagery (EM12) of the present Zaire deep-sea fan, including the mapping and imagery of main sedimentary bodies [56, 57]. Reproduced with permission from Geological Society, London.

The lobes have the following features:

- 1) They are formed at the submarine channel or valley mouth, when erosional processes happen. Chaotic high amplitude seismic facies are generated [98, 99]. This zone called 'channel lobe transition zone' (CLTZ) (Fig. 14) [100, 101, 102]. This zone has a high

sand/clay ratio and exists only in turbidity systems like Navy and Agadir Channel, Laurentian and Valentia Fan [103, 104, 105, 102]. In mud dominated turbidity systems like Zaire [106] or Mississippi [107] the channel lobe transition zone can be missing.

- 2) Their shape is ovoid with an extent from a few tens of metres to a few tens of kilometres.
- 3) Lobes have a convex –up (positive) topography and a difference in elevation (relief) that is 25 m above of the surrounding sea floor. The lobe's slopes are smooth in small turbidity systems, such as Navy and San Lucas [96]. Lobes have different thicknesses. Mississippi's lobe thickness is 10-40m, Amazon's 10-25m [101], Zaire's 5-10m, Rhone's 12m, South Golo's 60m and Var's 20-30m.
- 4) Their depositional areas, have a lateral large extent [108].

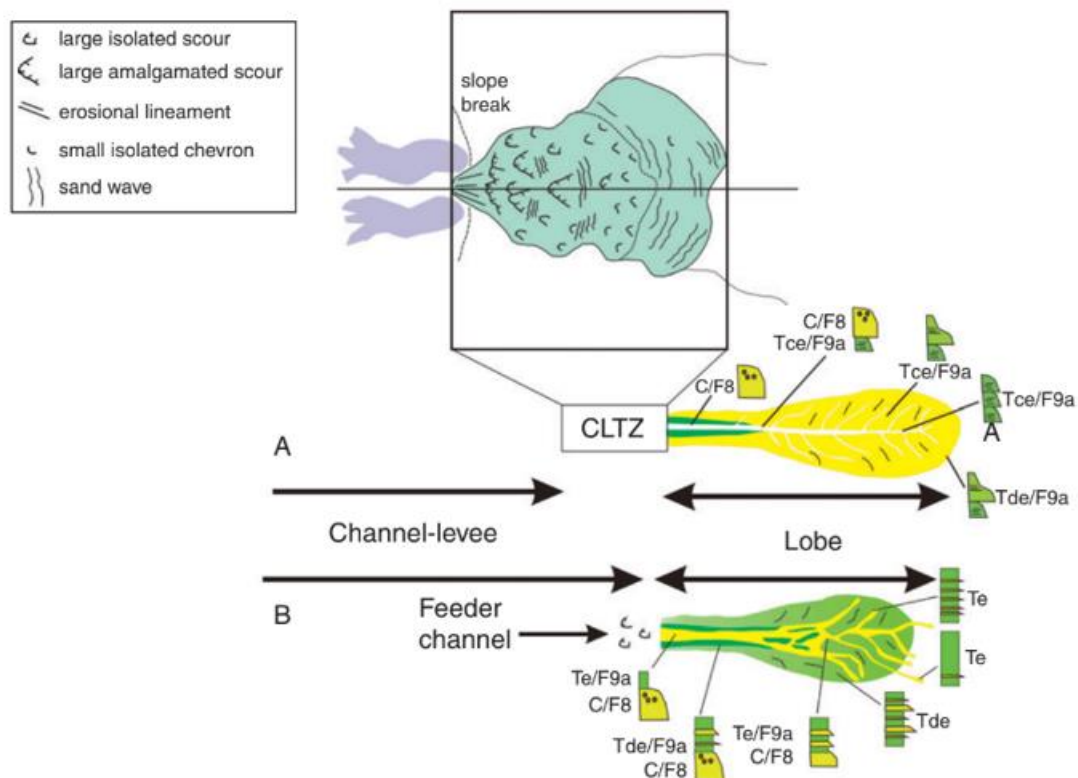


Figure 14. Subdivisions used to describe lobe and channel-lobe transition zone morphology and depositional faces in lobes. (A) sandy lobe; (B): muddy lobe. CLTZ: channel-lobe transition zone. (C) concentrated flow deposits [102, 63]. Reproduced with permission from AAPG and C. Bonnel.

- 5) The lobes are subdivided and are the levee channel continuation (Fig.15 A). In figure 15 B seems a fringe lobe deposit. This deposit is a non-channelized lobe (without channels) with a non-rough surface (Fig. 15 B). For example, in the Monterey System the channel depth doesn't exceed the 10m and decreases progressively downstream [109]. The main channel of the Var Zaire fans, can be reach at the 20m deep [63]. The non-channelized lobe has a small surface and is created from the rapid deposition of sandy flows like Zaire System [101]. Hemipelagites and other fine-grained sediments can be cover the lobe fringe.
- 6) The lobes are mainly composed of sand. For example, the Amazon lobe contains 50-80% massive fine to very fine sand. This happens due to the increasing clay fraction flow over the levees. If the channel is deep and incise, then the rate of clay can be important, such as Zaire lobes [56, 63].
- 7) The lobe shape is influenced by its confinement. So, if the spatial confinement is low, the lobe shape is rounded to ovoid like Zaire lobes with 20-40km length and 10-40 km width [110]. If the confinement is high, the lobes are elongated, like Amazon lobes with 6.5-25 km width and 21-83 km length. The Monterey's lobe length is 130 km and width is 45 km. The lengths of channel levee complexes of Rhone Neofan are 25-125 km and the widths are 5-35 km [101].
- 8) Sometimes the lobes are separated from the channel mouth. This happens by the existence of a scoured area like the Zaire lobe and Rhone Neofan lobes [63]. This happens when retrogressive erosion take place in this scouring zone. Then any interaction between the lobe channel and feeder channel is lost.

Figurer 15 shows a complex of nested lobes of the eastern Corsica [98, 99, 111]. The lobes are usually organized in groups on the erosion zone over the channel-lobe transition zone due to progradation processes.

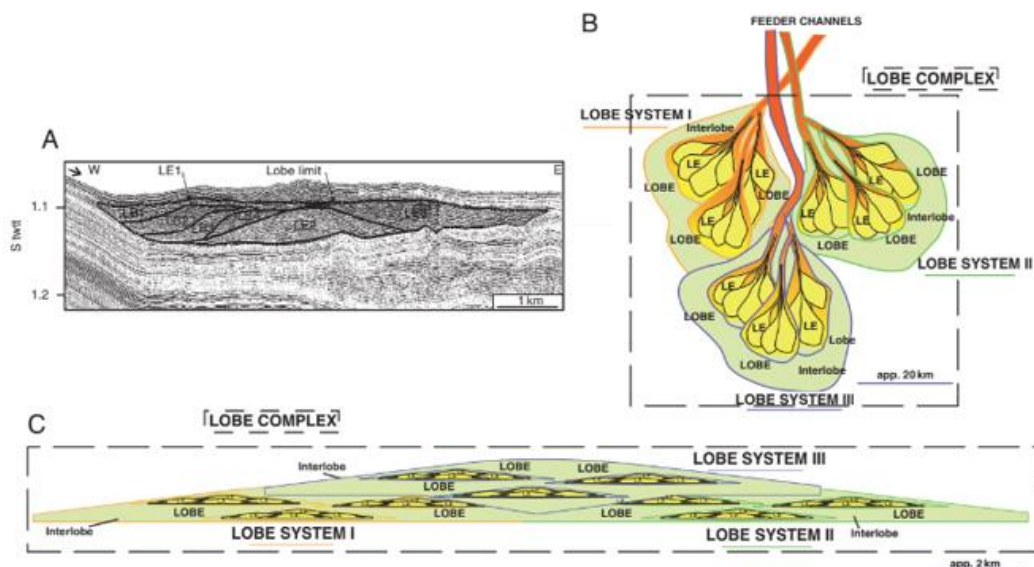


Figure 15. Terminology used for lobe geometry. Lobes correspond to nested depositional bodies from lobe complex (basin scale) to lobe bed (depositional process). Modified from Prelat et al. (2009) [112], and Mulder and Etienne (2010) [113]. (A) Structure of the South Golo lobe, E. Corsica [98, 114]. The lobe is composed of three elements (LE1, LE2 and LE3). LE1 is composed of four lobe beds (LB1, LB2, LB3 and LB4). (B) Plane view of lobe hierarchy in a lobe complex. LE: lobe elements. (C) Transverse view of a lobe complex.

With the term ‘lobe’, is an architectural element which is connected with the mother channel. Its length and width are several of kilometres and its thickness is several of metres [112]. A lobe consists of lobe units and sub-units [98, 114]. The lobe’s elements shift rapidly by the process of avulsion (which is very frequent) and fill nearby topographic lows by the action of turbidity flows [101].

2.1.4. The turbidites sequence stratigraphy and controlling factors.

The sequence stratigraphy in deep sea turbidity systems, depends on the accommodation space which is a result of the sea level changes, the sediment supply and the basin physiography. The total accommodation space, is measured from a reference point which is located on the base layer before the sedimentation starting [115].

The upward parameters, depend on the tectonic movements, the activity of oceanic currents, the river load, the climate's changes (rainfall, temperature), the morphology of the drainage basin (size, maximum elevation), the nature of the bedrock in the drainage basin and the extent of the vegetation cover [116, 117]. The balance between the sedimentation rate (S) and the total accommodation (A) determine the stratigraphic architecture and the spatial distribution of the deposits [118, 119]. According to Homewood et al. (2000) [120],

- if $A/S > 1$, the architecture is retrograding;
- if $A/S = 1$, the architecture is only aggrading
- if $1 > A/S > 0$, there is creation of available space, and the architecture is prograding and aggrading
- if $A/S = 0$, the available space is constant and the architecture is only prograding
- if $A/S < 0$, there is a rapid downward shift as a response to available space destruction.

All these hypotheses are possible for low deep-water environments, in which the small variations in the sea level, are recorded in sedimentary facies. While, in deep sea the small changes of the sea level (a few hundreds of metres maximally), have a small impact in sedimentary facies [59, 121]. In the Figure 16 seems the comparison of sequence stratigraphy models.

In Figure 16A, a maximum fall of sea level happen and a deep-sea turbidity system is generated in the basin, with a siliclastic supply. Erosion increases because of the river tends to reach it's equilibrium profile. According to Schumm, 1993 [123] the incision happens when the level of the sea falls below of the continental edge. The new deposits of this new system, are created above of this erosion surface.

In Figure 16B, the sea level is stabilized, and a mud structured turbidity system is growing with well-constructed channels and levees.

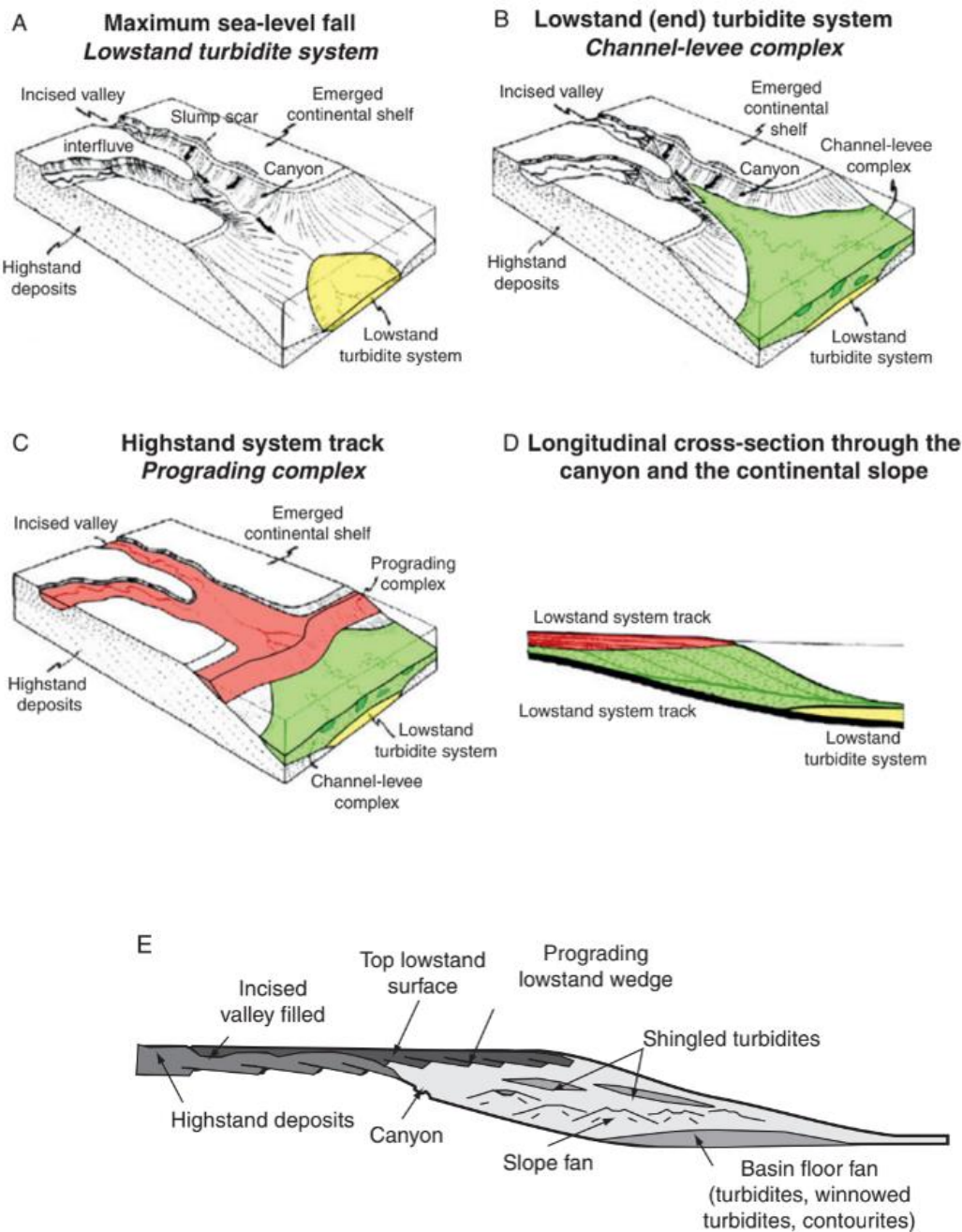


Figure 16. Comparison of sequence stratigraphy models. (A-D) Posamentier and Vail (1988) [115] model for sequence stratigraphy. (A) Fall of sea level: maximum turbidite-system development. (B) Sea-level lowstand: muddy channel-levee complex development. (C) Sea-level rise: formation of prograding complexes. (D) Cross-section to compare with E. (E) Mutti model for sequence stratigraphy [122].

In Figure 16C, the sea level is risen and progradation happens. The sea fills the incised valleys and canyons and shingled turbidites take place. When the sea level is stabilized, hemipelagites are accumulated. Finally, the sea level defines the canyon's activity and its sedimentary supply [124].

In Figure 16 D-E, sedimentary supply controls the stratigraphic evolution of the deep sea. There are three types of turbidity systems according to the sea level fluctuation [122].

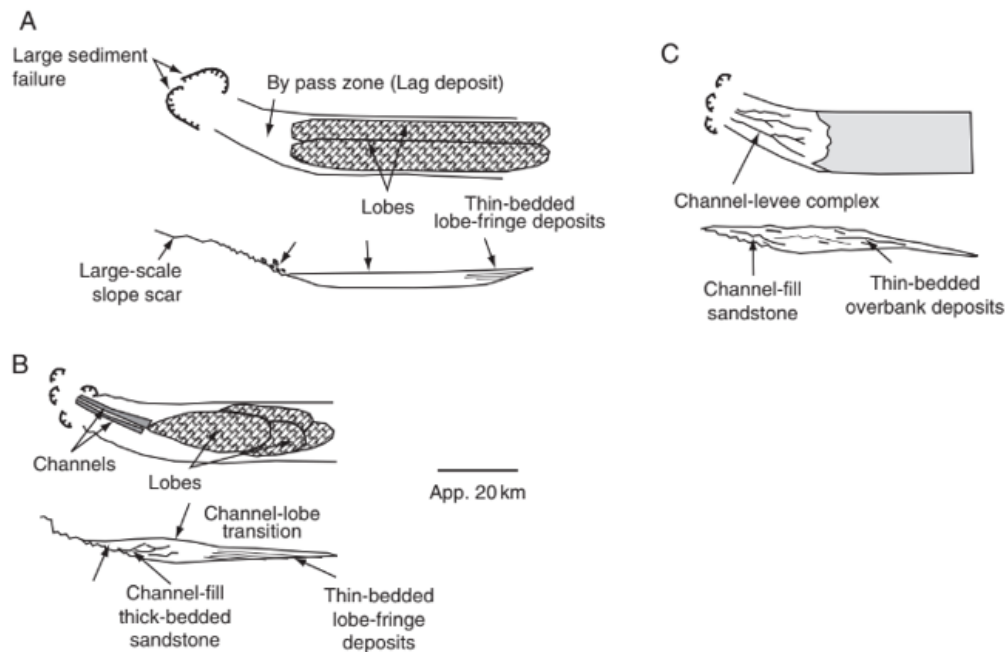


Figure 17. Model of gravity-flow system evolution [122]. (A) Type 1 systems with high transport capacity. (B) Type 2 systems with low transport capacity. (C) Type 3 systems corresponding to large modern mud-rich fans.

For more details, in Figure 17 A, is a system with high transport capacity. Many failures happen on the shelf and channelized flows supply thick sand rich sediments. Lobes are generated, which are separated from the source by a bypass or erosion zone. In Figure 17B, there is a system with low transport capacity, amalgamated channels and sandy lobes [122, 97]. In Figure 17C, there are large modern mud structured fans, with well-constructed channel and levees. Lobes are missing and sand is gathered in the proximal part of the channels.

2.2. Mass flows

The mass flows are the result of gravity processes in deep sea environments. Cable failures, are an impact of their action on human in fractures. The Bingham's model is the most appropriate to estimate the flow's rheology behaviour. Their classification is based on their sedimentary deposits. So the main types of the mass flows are the rock avalanches, the creeping failures, the slides and slumps, the cohesive flows, the non- cohesive flows and the water dominated flows.

2.2.1. Rheology of Bingham plastic flows

The mass flows rheology is based on Bingham's model. This means that, the mass flows are natural material which are not deformed until the yield stress will be exceeded. After this point, their deformation is linear (Fig. 1). These flows which have fluids 'with strength' (with a plastic rheology) are called plastic debris flows. Some of these, can develop a turbulence behaviour [8, 13]. The limit-border between the Newtonian and plastic flows is the 20-25% of the sediment concentration by volume (Fig. 18). There is an exception, the high turbidity current in which coexist the Newtonian and the plastic flow.

The rheology of a flow, depends on the sediment concentration, the grain size and the physical – chemical properties of the transported grains [9]. Generally, rheology is a parameter with many complexities [10] and it is very difficult to measured it accurately.

2.2.2. Categories of mass flows processes

The categorization of the mass flows processes, based on the deposits of ancient environments. Sedimentary facies and their evolution along the pathway of the flows are studied.

2.2.2.a. Rock avalanches

The size of the rock avalanching blocks is usually some of metres to hundreds of metres. Avalanches with the upward blocks are happen when steep slopes and undersea cliffs are formed by consolidated sediments or rock outcrops. Volcaniclastics, are the most frequent environments in which processes of rock avalanching are happen [133].

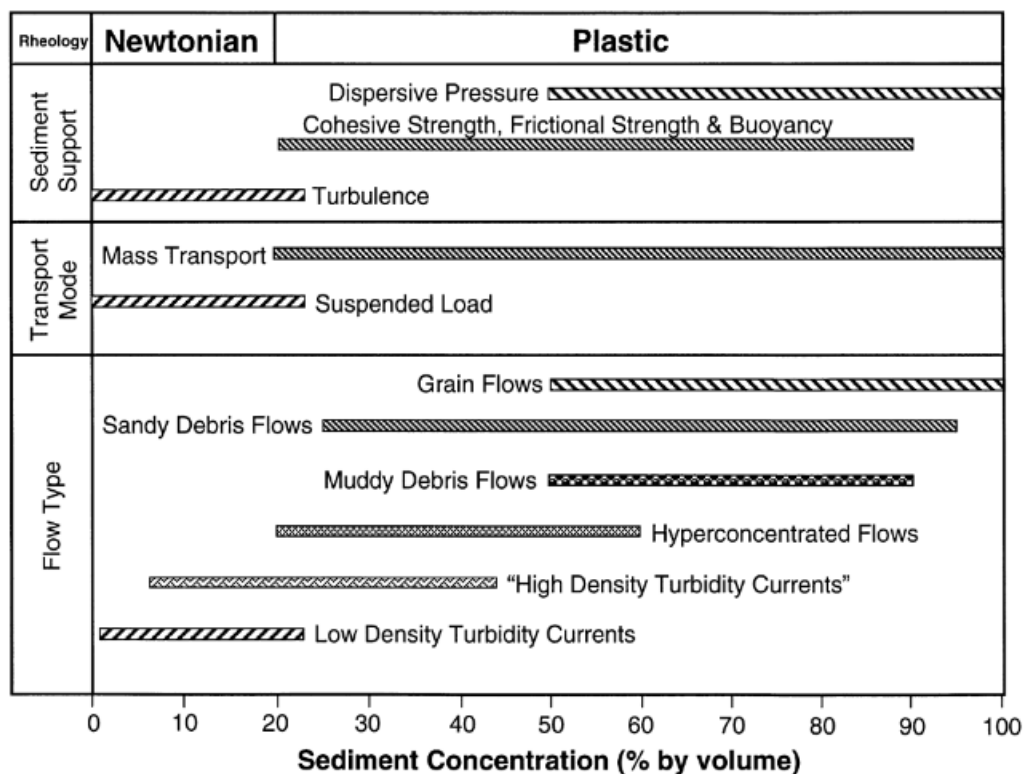
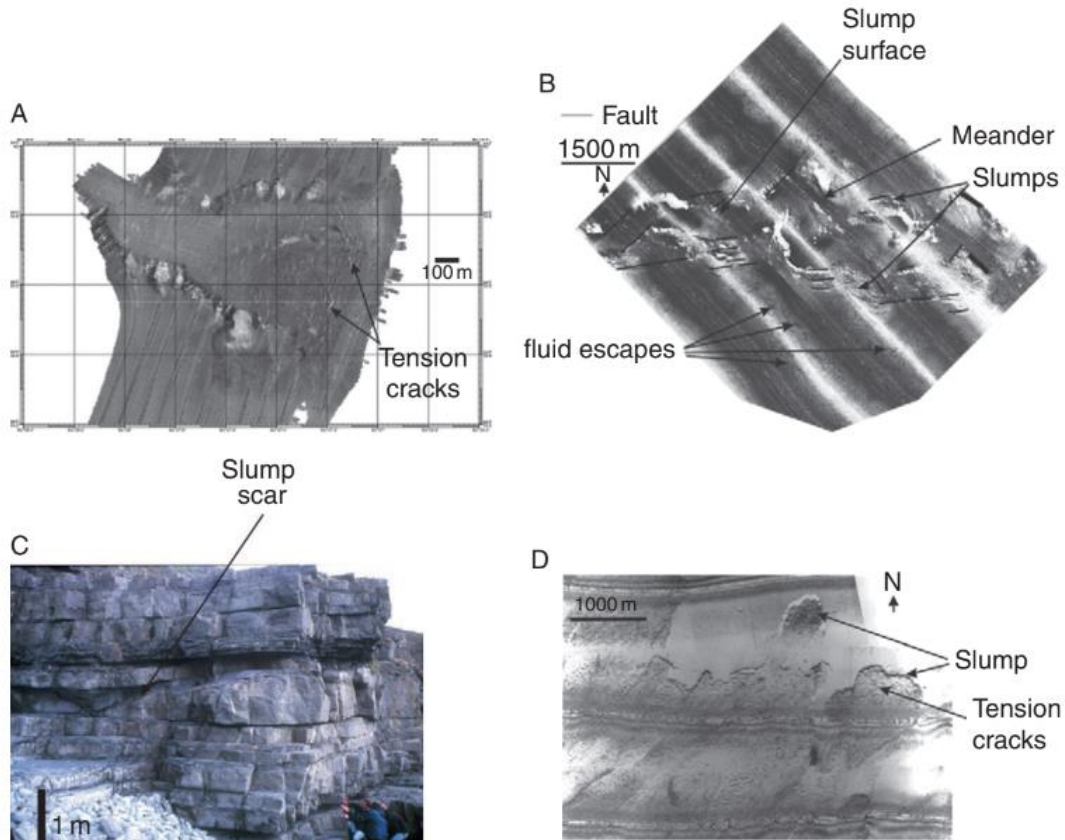


Figure 18. A classification of subaqueous gravity flows, based on fluid rheology, showing two general types, Newtonian and Plastic [4]. Turbidity currents are Newtonian flows whereas all mass flows (muddy debris flows, sandy debris flows and grain flows) are Plastic flows. Turbidity currents occur only as subaqueous flows, whereas debris flows and grain flows can occur both as subaerial and as subaqueous flows. For purposes of comparison, subaerial flows (river currents and hyperconcentrated flows) are included. Sediment concentration is the most important property in controlling fluid rheology. Published values of sediment concentration by volume % are: (1) river currents (1-5%) [125], (2) low- density turbidity currents (1-23%) [126, 15], (3) high-density turbidity currents (6-44%) [126], (4) hyper concentrated flows (20-60%) [9], (5) cohesive- muddy debris flows (50-90%) [128], (6) sandy debris flows (25-95%) [7, 127, 126, 129, 130, 131], (7) cohesion less-grain debris flows (50-100%) [132, 131, 9].

2.2.2.b. Creeping and failures

Creeping is the process of progressive sediment deformations which lead to failure surfaces [13]. The velocity of these deformations is very low [134]. These sediment failures can be divided into slides and slumps, in which large volumes of sediments or rocks can be moved along the failure surfaces. The size of the failure surfaces can be reach hundreds or thousands of square metres (Stow et al., 1996. In Figure 19 are presented the typical morphological characteristics of the sediment failures. Extensions structures such as tensions cracks and normal

faults, existing at the head of the failure (Fig. 19 A and D). Instead of the head, compressive structures such as folds, inverse folds and over thrusts existing at the toe of the failure.



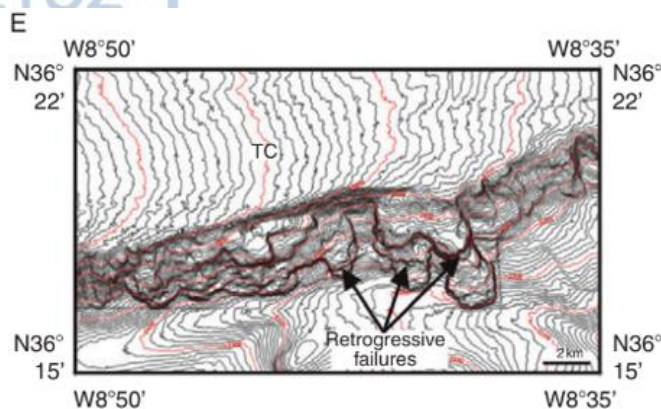


Figure 19. Examples of deep-sea sediment failures. (A) Retrogressive (backward) slumps at the head of the Capbreton Canyon [136, 34]. (B) Slumps on the wall of the deep channel of the Orinoco [137]. (C) Slump in Silurian deposits (Aberystwyth Grits Formation at New Quay/Aberarth, West Wales). (D) Slumps in the source area of the Grand Banks turbidity current (photograph courtesy P. Cochonat). (E) Retrogressive slumps on the wall of a channel (Gulf of Cadiz).

2.2.2.c. Slides and slumps

Slides and slumps, are structures which happen when sediment deformations lead to failure surfaces by the process of the creeping. When the slides are rotational, they called slumps (Fig. 19 A, B, C) and their failure surface is upward concave. The ratio D/L (D is the maximum depth of the slide surface, L is the total length of the slump) can determine the structures of slides and slumps. So, when the ratio D/L is between 0.15 and 0.33 the geological structures are slumps [138]. When the ratio D/L is < 0.15 the structures are slides. Usually, the slide spreading, can generate internal vertical tension faults to the failure surfaces which cut the original slide into several slabs or blocks. According to the Figure 19, slides and slumps can form complex of structures with upslope propagation of the failure (retrogressive failures) (Fig. 19 E). Steep escarpment can be formed at the failure head by tensional faults. A failure downslope propagation creates successive slumps or slides (domino slumps or slides) [134] which overload the located sediments at the failure toe, so a new failure is generated.

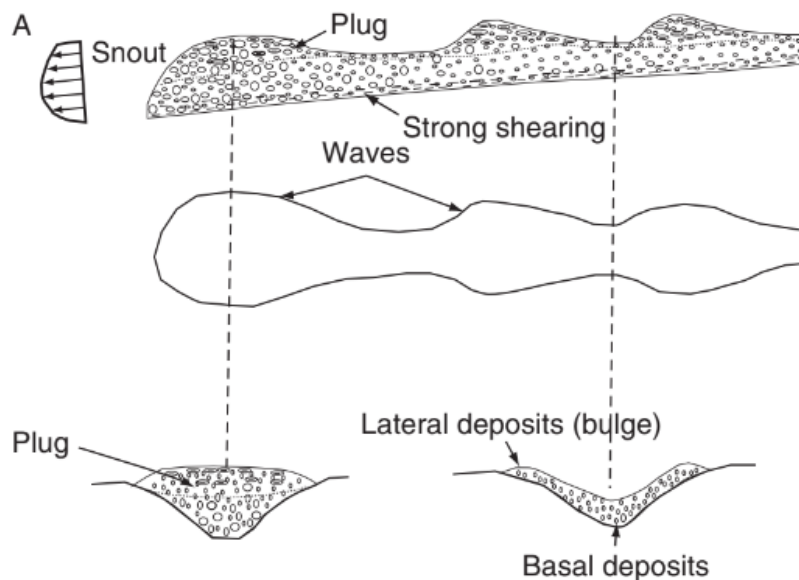
2.2.2.d. Cohesive flows (muddy debris flows)

Cohesive flows have a matrix strength because of the cohesion between their fine particles such as clays and fine silts. According to their percentage participation, cohesive flows can be subdivided to clay and silt mudflows. So, flows with clay percentage participation less than

25%, are called silt mudflows, while flows with clay percentage participation over than 40% are classified as clay mudflows.

As regard the morphology of the cohesive flows, their head is thick (Fig.20 A). Their motion depends on the permeability of the matrix. When the matrix is very fine, the rate of the flow diluted water is small so, the flow resistance is big [135]. The phenomenon of ‘hydroplaning’ according to Mohrig [139] happens when a layer of water is trapped under the body of the flow. This process reduces the flow resistance (friction power) and the flow erosional power (Fig. 20 C).

When the cohesive debris flow has large matrix strength (large density) then, boulder size clasts, very large rafts or olistoliths can be transport many kilometres away from their initial place (Fig.20 B) [140, 141, 142, 143, 144].



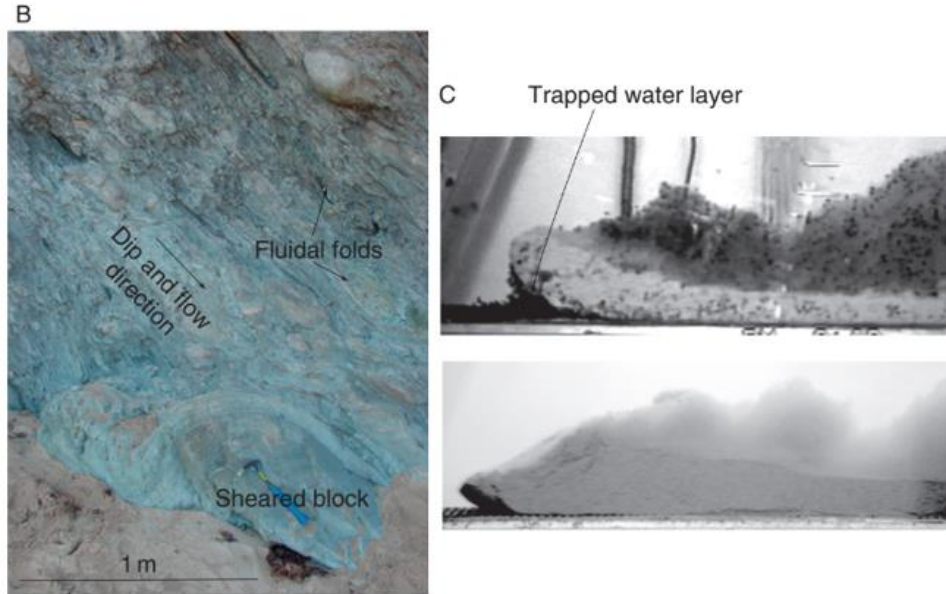


Figure 20. Characteristics of cohesive flows. (A) Morphology of a partially channelized debris flow (Johnson, 1984). Longitudinal structure mimics sediment waves. Flow head (snout) mimics a depositional lobe. Lateral deposits (bulge) mimic sedimentary levee; decametre to hectometre scale. (B) Sedimentary deformation in a cohesive debris flow due to laminar flow regime: sheared (sigmoid) deformation and fluidal (sheath) folds (Cretaceous flysch of the Basque Country, Baiede Loya, France). (C) Hydroplaning forming at the base of a flow during a laboratory experiment [139].

2.2.2.e. Non- cohesive flows (grain- cohesion less flows)

In non- cohesive (granular) flows, dispersive pressures exist because of the interactions between the grains of the flows [3]. These interactions usually become bigger because of the seafloor erosion which cause an increasing grains concentration. These processes are happened in steep slopes ($>18^\circ$) with sand or coarse slit grains. Frictional strengths are developed at the base of the flows.

2.2.2.f. Sandy debris flows

The term “sandy debris flow” represents an intermediate process between the muddy debris flows (cohesive flows) with cohesive strengths and the grain flows (cohesion less flows) with frictional strengths [7]. Sandy debris flows can be developed in slurries of any grain size (very fine sand to gravel), sorting (poor to well) and clay content (low to high) [6, 7].

2.2.2.g. Water- dominated flows

Water dominated flows are generated when a forcing event like earthquake, surge wave or sudden upward motion, happens. In water dominated flows, the flow pore pressure increasing by the destruction of the fabric of the sediment flows [145, 3]. Then, high porosity sediments are created like quick sands. The water transport capacity dominates flows which depends on the permeability of the sediments. This capacity is larger than the hydrostatic pressure.

2.3. Hyperpycnal flows

2.3.1. *The formation of hyperpycnal flows*

Hyperpycnal flows are generated by the erosion of the geological formations due to particular geological conditions and climate with intense and sustained rainfalls.

Hyperpycnal flows can occur in different river locations, due to the different types of external catastrophic events. These events can be floods under hot arid climates, rapid ice melting in periglacial streams or sudden dam break.

1. Hot arid climates

The streams which are in hot- arid climates, have an intermittent flow. The streams bed usually stays dry during the year. Sporadic and intense rainfalls (cyclones and hurricanes) can create hyperpycnal flows in the streams such as Wadis stream in North Africa and streams in west Mexico [146].

2. Cold climates

Hyperpycnal flows under cold climates, can be generated by two ways. In first way, the flows are generated by the ice melting from the volcano action (catastrophic ice melting). So, when a glacier covers an active volcano, a large volume of ice melting. Then a subglacial lake can be formed. If the ice wall of the subglacial lake will be breaking, millions of cubic metres of water will be released and mixed with volcanic and glacial deposits. Hyperpycnal flows are generated which are flowed to the oceans. This geological phenomenon can be last a few hours to a few days and it's very frequent in Iceland and Alaska.

In second way, the hyperpycnal flows are generated by the ice melting from the season alteration (winter/summer variations). Every spring, the ice melts and large floods are generated, which erosion the natural domes [147]. Then hyperpycnal flows are formed which flowed to the oceans. In these high latitudes, usually appear laminated geological beds [148, 149], landslides and submarine slides in fine- grained formations which show long periods of severe floods [150].

3. Particular geological conditions

Loess is a geological formation which consist of 20% clays and equal part of sand and silt. All the components are soldered by calcium carbonate. Generally, is a homogeneous, high porous, soft and easily erodible sediment rock. Some areas of the world (China and others) are covered by loess. So, during the monsoon rains loess is eroded and concentrated at the river mouths (the Daling, Haile and Huanghe rivers) and hyperpycnal flows are generated [151, 152, 153].

Easily erodible black sales there are in Alps which participate on hyperpycnal flows at the Var river mouth. Lahars are flows which are rich of water and volcanic ashes. They follow the continent hydrographic network and when they arrive at the sea, they are transformed into hyperpycnal flows. These geological phenomena are frequent in Indonesia.

4. Climate, precipitations and floods of the rivers

Floods are the main reason of the hyperpycnal flows creation at the river's mouth. They depend on every region climate. By the using of the 147 rivers global database, 55% of the world rivers can create hyperpycnal flows with frequency less than every 100 years. While, 77% can form with a frequency less than every 1000 years [154]. In Table 1, seems some of the largest rivers which cannot create hyperpycnal flows. The producing ability of hyperpycnal flows is larger in small and medium rivers than the bigger. This happen because of particle of the sediment load is diluted by the volume of the river water so their concentration is reduced. Another reason is that the big rivers trap much of their sediment loads in their flood plains, subaerial deltas or in both of them, so only a small amount of the sediment load can be reach in the deep sea.

River	Q_{av} ($m^3 s^{-1}$)	Cs_{av} ($kg m^{-3}$)	Cc ($kg m^{-3}$)	Cs_{flood} ($kg m^{-3}$)
Orinoco (Venezuela)	34,500	0.14	36.2	< 1
Mississippi (USA)	15,500	0.8	42.7	11
Amazon (Brazil)	17,500	2.0	36.2	14
Paraná (Argentina)	13,600	0.18	38.9	3
Columbia (USA)	7960	0.06	42.7	2
Mekong (Vietnam)	14,800	0.3	38.9	4
Danube (Romania)	6420	0.3	42.7	25
Yukon (USA)	6120	0.3	42.7	26
Zambezi (Mozambique)	17,600	0.09	38.9	< 1
MacKenzie (Canada)	9750	0.14	43.6	4
Amur (Russia)	10,600	0.16	42.7	4
Zaire (= Congo) (Zaire)	41,200	0.03	36.2	< 1
Pechora (Russia)	3370	0.06	43.6	13
Niger (Nigeria)	6140	0.21	36.2	17
Volga (Russia)	17,200	0.03	42.7	0.4
Ob (Russia)	10,300	0.05	43.6	1
Lena (Russia)	16,200	0.02	43.6	0.3
Yenisey (Russia)	18,000	0.02	43.6	0.2
S. Dvina (Russia)	3660	0.04	43.6	8
Kolyma (Russia)	2840	0.07	43.6	25
Sao Francisco (Brazil)	3040	0.06	36.2	21
St. Lawrence (Canada)	14,900	0.01	42.7	0.1

Table 1. Examples of large rivers that cannot produce hyperpycnal flows. Cs_{av} , average annual suspended-particle concentration values; Q_{av} , average annual discharge values; Cc , concentration threshold to generate hyperpycnal flows [154]; Cs_{flood} , maximum flood concentration in suspended particle. Rivers that easily form hyperpycnal flows by re-concentration of a hyperpycnal plume are underlined.

5. Sediment re- concentration

Sediment re-concentration is a very important process which influence the hyperpycnal flows suspended load. Mass flows can be generated by dynamic processes how take place on the continental shelves. Intensive storms can be affect the deposition of the hyperpycnal flows like the Pennsylvanian's deposits in Colorado [155, 156].

The re-concentration importance was proved by two laboratory simulation experiments. In the first one was proved by the process of double diffusion sedimentation and in the second was proved by the process of convective sedimentation (Fig. 21). In both of them is simulated the replacement of fresh water by cooler and denser brine. In Figure 21 A and B, double diffusion

(salt fingering) is occurred when a warm brine is situated above a colder so a denser water mass [157]. Then millimetre large fingers are appeared because of the different diffusivity and warmth between the brine and the rest water mass. Figure 21 C and D preserve the process of settling convection [158, 159]. Hyperpycnal flows are created by the discharge of the fresh water above a cooler and denser brine. Then small sediment fingers are appeared between the two flows because of the gravity instability [157]. These two laboratory simulations differing in the size of the convective figures and the space between them.

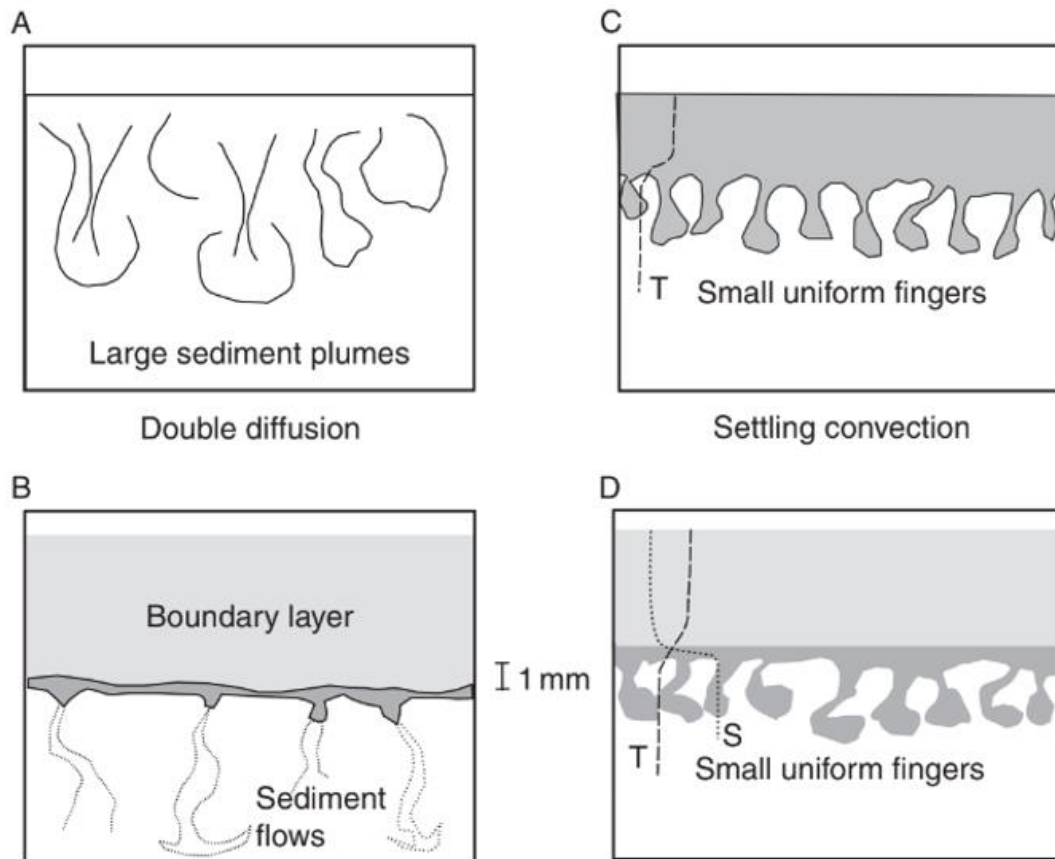


Figure 21. Comparison of reconcentration processes observed during laboratory experiments [159]. Darker grey tone indicates increasing density. (A, B) Double diffusion. (C, D) Settling convection. T: temperature; S: salinity.

2.3.2. High density turbidity currents

A high-density turbidity current, is an intermediate current with an intermediate flow, both turbulent and laminar flows [160, 6]. This flow composed of two different layers. The first layer, which is lower, denser (with high sediment concentration such as mudstone clasts and quartz granules) with laminar flow and plastic rheology. The second layer is an upper layer with low sediment concentration, turbulent flow and Newtonian rheology (Fig. 22). In addition, a high-density turbidity current is defined based on the driving force (Fig 23). The basal traction carpet which is known as inertia- flow layer is driven by the overriding turbidity current [160]. Also, these currents are defined based on grain size [161], rapid deposition and flow density [162].

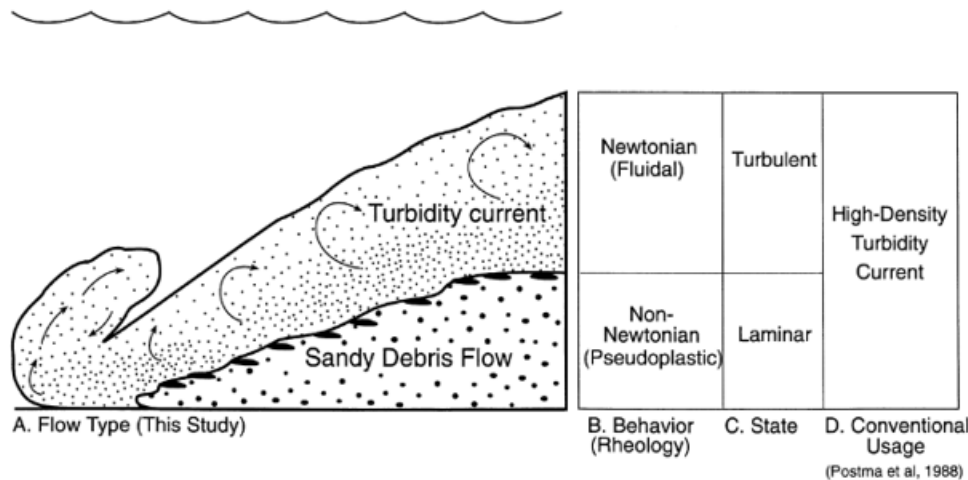


Figure 22. (A) An experimental view of high density turbidity currents [160] who suggested that the basal high concentration layer labeled as sandy debris flow was driven by the upper low-concentration layer labeled as turbidity current. Both upper and lower layers comprise the high-density turbidity currents [160]. The upper and lower layers as rheologically different entities and therefore separate flow processes [6]. (B) Lower and upper layers represent non-Newtonian and Newtonian rheology respectively [160]. (C) Lower and upper layers represent laminar and turbulent states [160]. The basal laminar layer (sandy debris flow) is variously termed as inertia- flow layer, traction carpet, flowing- grain layer etc. By various authors [6], the basal layer with high sediment concentration promotes hindered settling and allows development of floating mudstone clasts and quartz granules. (D) Because sediment-gravity flows are classified on the basis of rheology and sediment- support mechanism [160, 161], a single flow (i.e., high-density turbidity current) cannot be both Newtonian and non-Newtonian in rheology and laminar and turbulent in state at the same time. This type represents gravity flow transformation of Fisher (1983). From Shanmugam (1997a).

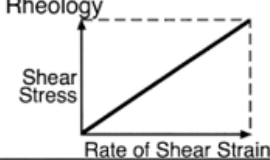
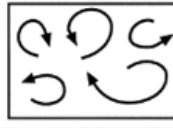
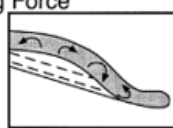
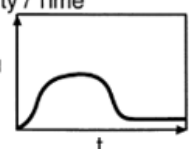
Criteria	Type	Deposit
Rheology 	Newtonian (Dott, 1963)	Evidence Preserved
Support 	Turbulent (Middleton & Hampton, 1973)	
Driving Force 	High Density (Postma et al., 1988)	Evidence Not Preserved
Velocity / Time 	Waxing / Waning (Kneller, 1995)	

Figure 23. Four different definitions of turbidity currents based on (1) rheology of fluids (2) sediment-support mechanism (3) driving force and (4) velocity/time factors. Of these four types, only the Newtonian and turbulent types are useful in interpreting the behaviour of flow because evidence for fluid rheology and sediment- support mechanism is preserved in the deposit. However, evidence for driving force and waxing velocity is not always preserved [164].

2.4. Initiation of gravity flows

Gravity is the main reason for the flows start. Gravity flows are usually happened in oceanic environments. For example, when a canyon slope collapses, a submarine slide is happened or when a direct flow incurs from rivers to submarine environment [165, 124]. In the second case, the volume of the sediments which come of the rock erosion is huge and accumulate to sedimentation areas such as submarine sedimentary basins.

2.4.1. Oceanic processes

The oceanic processes are related with the gravity flows creation. According to Bjerrum (1971) [166] it is usual in Norwegian fjords to happen subaqueous slope failures. These failures are created during low or extreme low tides. It isn't clear the reasons how acted in this overloading which leded to these slope failures. The first reason seems to be the big pressure which happen

due to the sediment emergence. The second reason is the reduction of hydrostatic pressure which act cumulatively to overloading.

Storm waves can affect the ancient slide deposits such as Huanghe Delta. By the using of accelerometer and pore –water pressure sensor is observed that this reactivation of the storm waves can cause gentle and gradual motion as kind of liquefaction process or as thixotropic behaviour [167]. Another example is the Capbreton Canyon, when a strong storm hit the north Atlantic coast. Then because of the wave stress or other oceanic processes, slump in the canyon head is happened (Fig. 19A) due to the exceptional pore pressure [168]. There are many other examples in the geological bibliography which are observed the relationship between the mass-turbidity flows and oceanic processes [169, 109, 30, 170, 171, 172].

2.4.2. *Failure gravity flows*

The failure in gravity flows is a phenomenon which is correlated with the sedimentary cycles and with the presence of earthquakes or volcanos. With the geological term sedimentary cycles means the continental denudation and sediment accumulation along the continental margins and mainly depends on climate changes.

According to sediment accumulation, the overloading and oversteepening are the usual processes in which the failure in gravity flows is happened such as the British Columbia fjords [173].

The earthquake shake is a possible reason for the gravity flows, and is suggested when there isn't another reason to explain this phenomenon. There are many examples such as the submarine cable failures which are occurred a few hours later the earthquake action like the Marmara Sea [174], Algeria [175], Sumatra [176]. It seems that the alteration of silt and clay beds is favoured the sediment liquefaction. In addition, when an earthquake happens, the pore water- gas pressure is increased. So sediment collapse is occurred by the gas and water upward moving. This circular depression called 'pockmarks' and are related to fluid escape [177].

Pockmarks are geological structures which their shape and size depend on the characteristics of the bottom sediments. Their granulometry size is usually from clay to sand [178]. Pockmarks have an elongated, elliptic shape and their diameter is from few to several hundreds of metres, rarely reach to 1000 metres such as Skagerrak, North Sea [179] and north Gabon [180]. Their

depth is usually less than 10 metres and depends on the thickness and the sediment texture of the sedimentary cover [181]. They are almost associated with tectonic structures like faults, diapirs, syncline and anticlines. On seismic lines they suggest gas presence [182].

In volcanic arcs, are usually generated low magnitude earthquakes by the upward moving of magma in magmatic chambers. Then giant tsunamigenic landslides on the volcano's steep slopes (such as in Hawaii) can occurred by the reduce of the sediment shear resistance.

Mud flows are occurred when the mud volcanos are erupted due to the methane presence and escape. The mud volcanos have a positive topography with an elongated, elliptical or conical shape. Their size is from several tens of metres to several hundreds of kilometres. Their escaping material is fluid mud which is mixed with water, gas or oil (mud breccia) [183].

2.4.3. Submarine flows as a continuum of a river flow

Rivers are the most common way to transport the continental sediments to the oceans (89% of the global sediment transport). Glaciers are the second larger sediment supplier with the proportion of the 7% of the global sediment transport. Winds support the 2.5% of the global sediment transport and the 1.5% is responsible for the coastal erosion [184].

The density difference between the flow (p_f) and the surrounding water (p_w) plays an important role for the flow evolution (Fig. 24). For this reason, there are three categories of flows [185]:

- a) The overflow-hypopycnal flow, if $p_f < p_w$
- b) The homopycnal flow, if $p_f = p_w$
- c) The underflow-hyperpycnal flow, if $p_f > p_w$
- d) The intraflow-mesopycnal flow, if p_f is between the density of two layers p_{w1} and p_{w2} [186]. This flow usually appears in areas with hypersaline like Mediterranean Sea [187] or in areas with well stratified water masses.

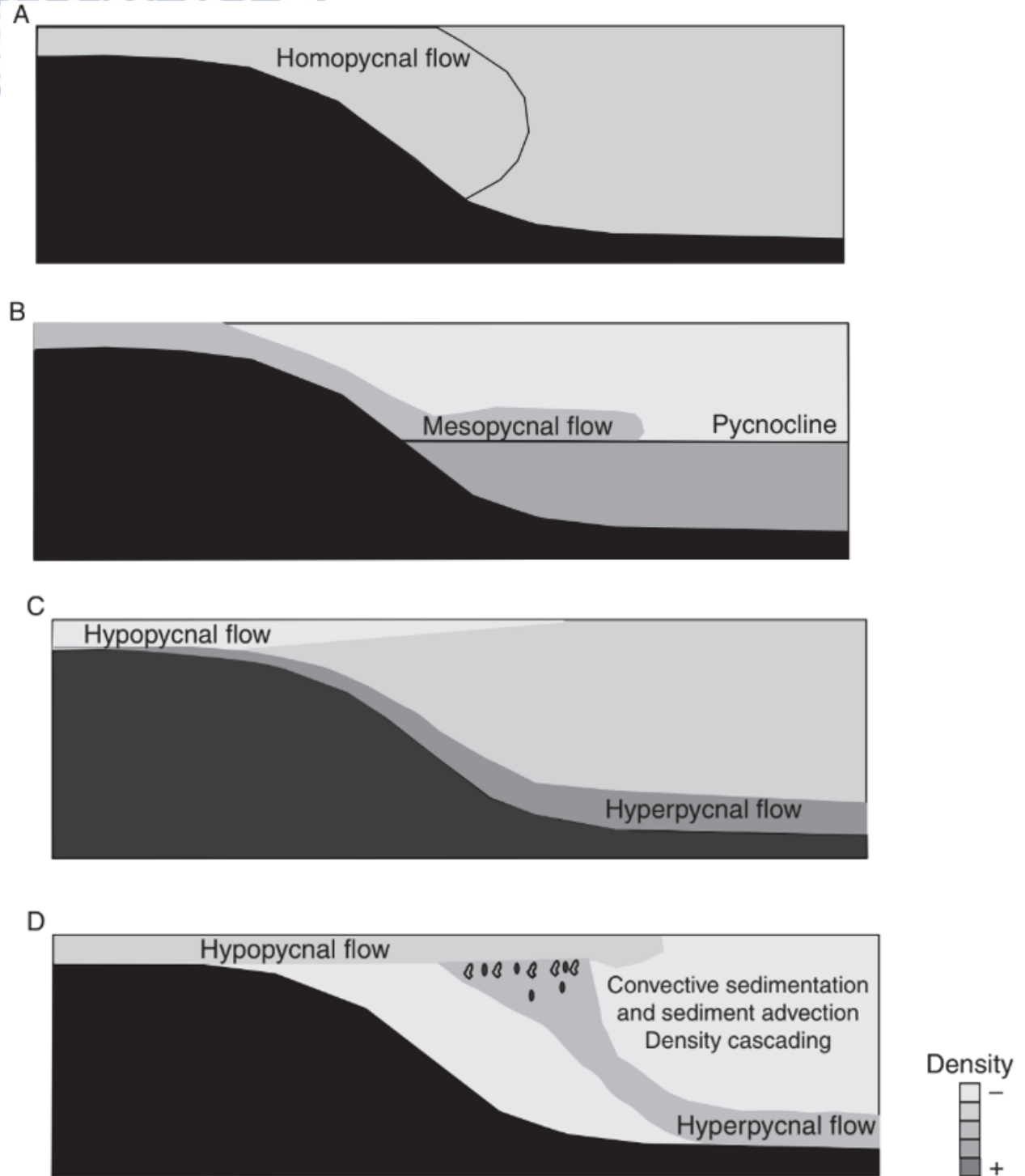


Figure 24. Types of density flows [188, 186]. ρ_f =density of flow; ρ_w = density of ambient fluid (ρ_{w1} , ρ_{w2} : densities of water in stratified body). (A) Homopycnal flow: $\rho_f = \rho_w$. (B) Mesopycnal flow: $\rho_{w1} < \rho_f < \rho_{w2}$. (C) Hypopycnal flow: $\rho_f < \rho_w$ and hyperpycnal flow $\rho_f > \rho_w$, formed by direct plunging. (D) Hyperpycnal flow formed by density cascading generated by both double diffusion and settling convection. Reproduced with permission from John Wiley and Sons.

There are two definitions of the hyperpycnal flows. The first one, hyperpycnal flow is the flow which moving on the basin floor. The second one, is the flow which is the direct continuation of a river flow. According to the second definition, there are two kinds of hyperpycnal flows:

- a. Hyperpycnal flows *sensu stricto*, which are turbidity flows with suspension
- b. Bedload dominated hyperpycnal flows, which are formed at stream mouths [189, 190]. These flows are usually in active tectonic basins with abrupt slopes. These flows can be transformed into turbidity flows.

2.5 Flow transformation in sediment- gravity flows

There are transformations of one type of flow to another such as slumping to mud flow [162] or laminal debris flow to turbidity current [4, 144]. The flows constitute is the base of the deposits classification [191]. According to Fisher (1983) there are five types of flows transformation (Fig. 25):

- A. There is a transformation from a laminar to turbulent flow without volume change. There isn't any fluid loss or surrounding fluid entrainment [192, 19].
- B. There is a transformation from a laminar to turbulent flow with volume change. There is a volume increase after the hydraulic jump [193] and erosion with quick deposition close to the slope break.
- C. There is a gravitational transformation of the initial turbulent to a basal laminar flow, because of the increase in flow concentration. The upper flow part remains turbulent [161, 160].
- D. There is a flow transformation due to the entrainment of the surrounding fluids. According to the laboratory experiments, initially there is a fluid progressive mixing. Latterly, flow dilution and concentration decrease happens so the turbulent phenomenon can occur [194].
- E. There is a flow transformation due to the combination of the elutriation and the progressive fluidization. The fine particles are progressively removed upwards and a turbulent cloud is formed above the denser basal part of the flow [195].

With the term 'high density turbidity current' means, that in turbidity currents can developed basal debris (laminar) flow by the gravity flow transformation (Fig. 22 & 26) [160]. With the term 'low density debris flow' means, that in laminar debris flows can created an upper diluted turbulent cloud by the flow transformation phenomenon (Fig. 26) [144, 196].

According to Parker (1982) [197], the dense of laminar flow is affected from the water entrainment and is transformed to a diluted turbulent flow. So, the flow fine particles are moved upward (suspension) and the coarser are left behind.

A decrease in slope can generate a hydraulic jump (slope break) and an increase in the flow thickness with simultaneous water entrainment. The flow velocity is decreased and the coarse grains are sat down. These deposits are called 'slope break deposits' [198, 199, 195, 194, 200, 201].

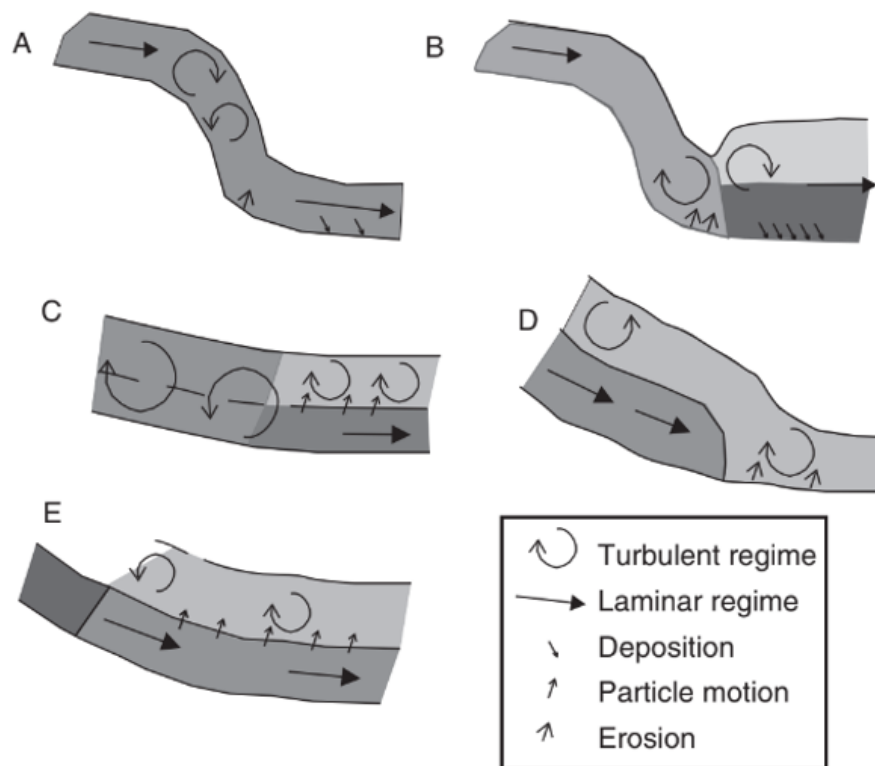


Figure 25. Hydrodynamic transformation of a flow (modified from Fisher, 1983 [163] with the authorization of the Geological Society of America). (A) Transition laminar/turbulent without change in volume of interstitial flow (body transformation). (B) Transition laminar/turbulent with increase in volume of interstitial flow (hydraulic jump). (C) Gravitational transformation: formation of a high-concentration (hyperconcentrated or concentrated) laminar basal flow and a top concentrated flow by grain-size segregation under the action of gravity. (D) Surface transformation: progressive formation of a turbulent upper part in a flow by dilution and flow entrainment. (E) Elutriation: formation of a turbulent, low-concentration upper part in a flow by upward motion of fine particles and interstitial fluid.

All the flows are progressively changed along their transport path because of the decrease in sediment concentration and the rate of the entrainment fluid. The rate of the entrainment fluid depends on the velocity and on the flow thickness. In addition, different hydrodynamic changes such as sedimentary levees or diapirs have an impact in sedimentary depositions. So, there is a better sedimentation by the increasing of the topographic high erosion. Then a better grain size sorting happened [202, 80, 199].

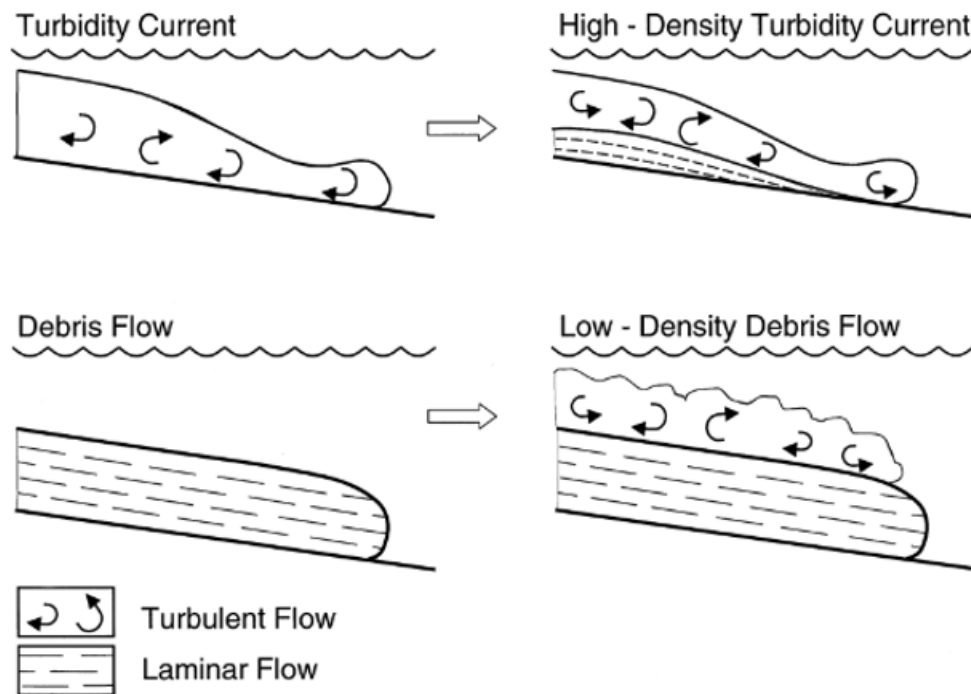


Figure 26. Problems in classifying sediment-gravity flows based on driving forces. Top: If a turbidity current generates a basal high-concentration laminar layer due to gravity flow transformation [160] would call it a 'high-density turbidity current'. This is because the basal high concentration layer is derived from and driven by over-riding turbidity currents. Open arrow shows direction of transport. Bottom: If a laminar debris flow generates an upper turbulent cloud (i.e., turbidity current) due to surface flow transformation through dilution [144], we should call it a 'low-density debris flow' if we follow the reasoning of Postma et al., 1988 for high-density turbidity current. These weak turbidity currents are not capable of transporting sand and gravel in suspension. Open arrow shows direction of transport.

3. Currents that affect the sedimentation in deep water continental slopes

There are surface and deep oceanic currents that affect the deep-sea erosion, sediments transport, distribution and deposition. The wind derived circulation process (geostrophic circulation), controls the surface currents such as the pelagic and semi-pelagic sediment depositions. The thermohaline circulation process, controls the bottom depositions by the currents of contourites.

3.1. Surface geostrophic circulation

Coriolis is a force which is created by the Earth's spin and the ocean morphology. Due to the Coriolis force, large wind currents exist at the ocean surface which transport the water molecules to the right of the wind direction on the northern and to the left on the southern hemisphere. The transport velocity is decreased with the water depth by the increasing friction. The Ekman's spiral is the spiral water morphology which can reach down to thousands of metres. These currents follow cyclonic and anticyclonic gyres (Fig. 27).

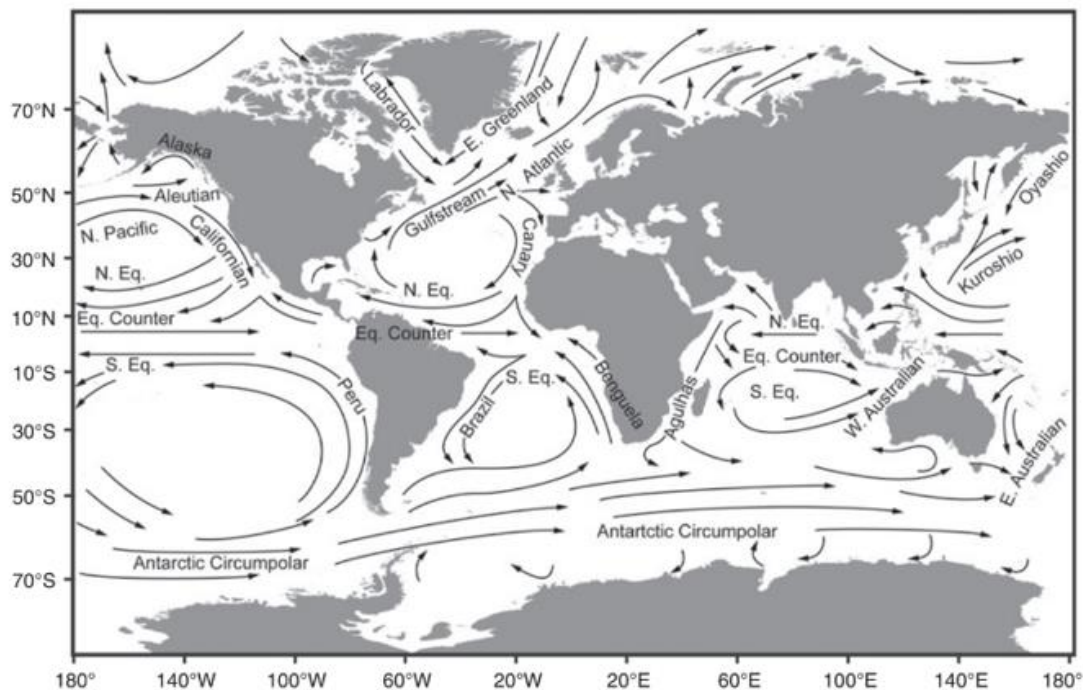


Figure. 27 Major surface currents of the oceans.

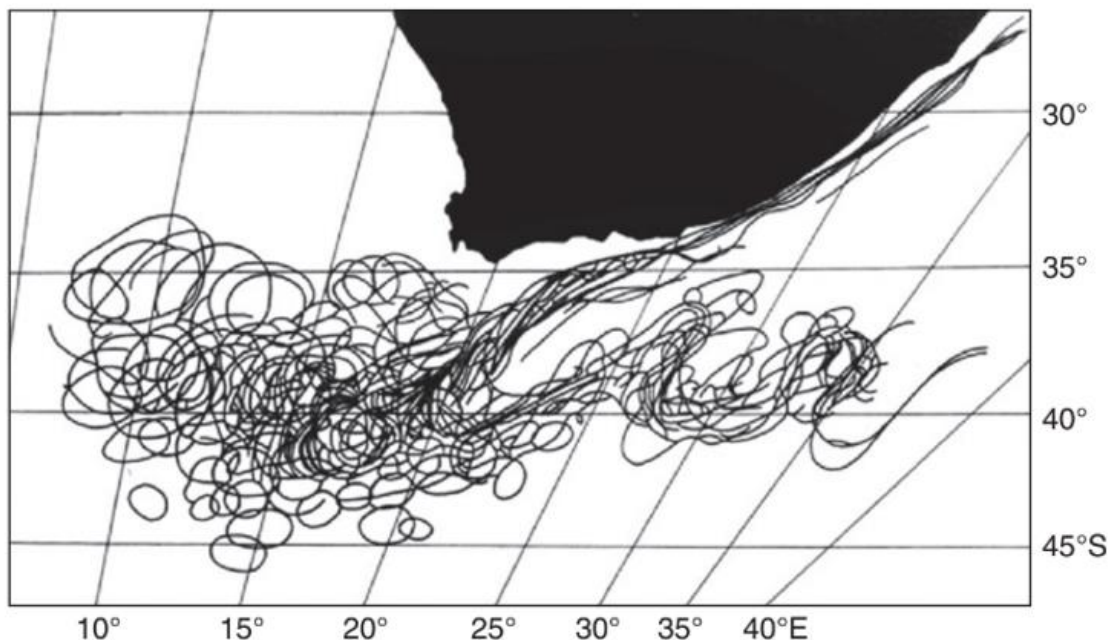


Figure 28. The Agulhas Current the period from December 1984 to December 1985. Modified from Lutjeharms, 1996 [203].

The Gulf stream and the Agulhas current (North Africa) have a ‘‘spaghetti’’ water transport shape (Fig. 28). Brazil Current, Kuroshio Current (Japan) and the Antarctic Circumpolar Current are driven by the western wind. These currents cross all the oceanic system from the continental slope to the deep sea. Firstly, the currents deepest parts erode the deep-sea bottoms along the continental slopes. Then, they transport and finally they deposit the sediments to the deep sea.

3.2. Geostrophic thermohaline circulation

The geostrophic thermohaline circulation phenomenon, exists because of the temperature and salinity difference of the oceanic water (Fig.29). The polar regions are the two sources of the dense surface water. This water is very dense due to its low temperature and its increased salinity. For these reasons, the dense water is sunk and stratified accordingly to its temperature and salinity value (density equilibrium). The denser water is formed around the Antarctica polar ocean particularly, in the Weddell and the Ross Sea. These sea areas feed firstly the Atlantic and secondly the India and the South Pacific Ocean. The

Arctic Ocean feed with dense water the North Atlantic Ocean. The North Atlantic Deep Water (NADW) flows southern and above the Northward Antarctic Bottom Water (AABW). The NADW participates on the deep-water circulation phenomenon (Fig 30).

The Mediterranean Sea is a close sea and is another source of dense water, because of the appearance of evaporates. The ambient water getting richer and warmer so, it participates to the global thermohaline circulation by the Gibraltar Strait and forms the Mediterranean Outflow Water (MOW). A second similar source of warm and dense water is the Caribbean Sea, which is injected to the Northwest Atlantic Ocean across the Florida Strait (Fig. 29).

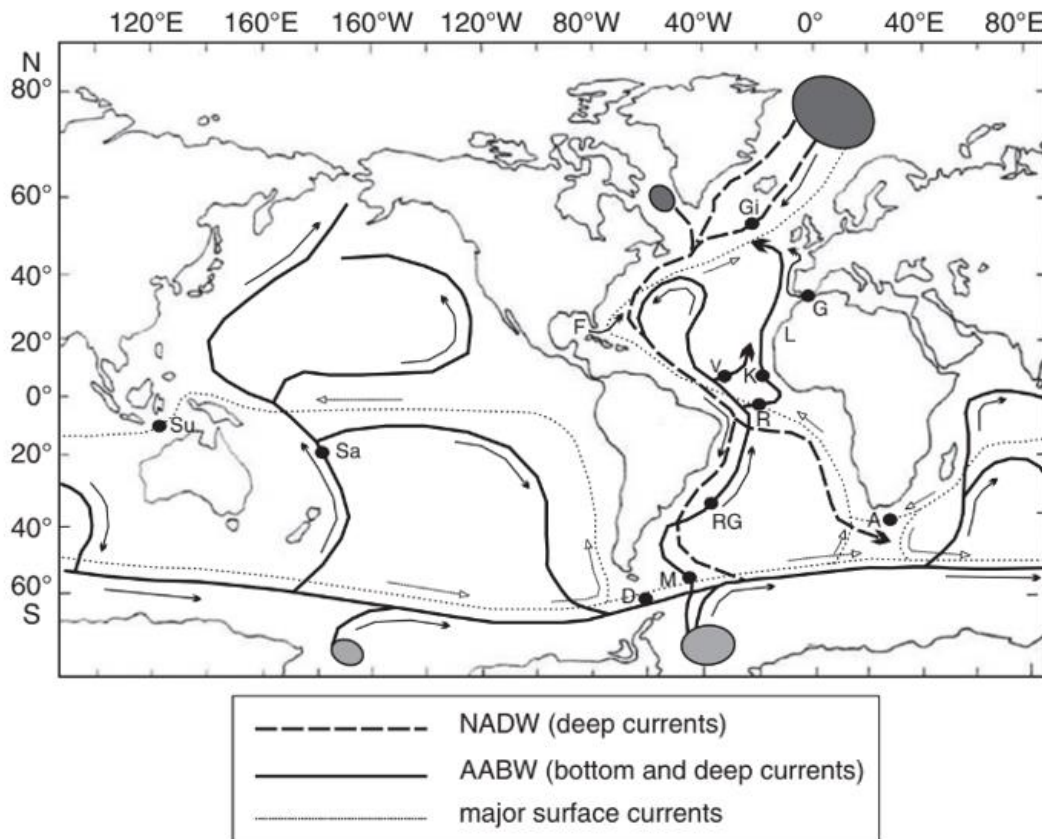


Figure 29. The Global thermohaline circulation. currents. A, Agulhas Gateway; D, Drake Passage; F, Florida Strait; G, Gibraltar Strait; Gi, Gibbs fracture zone; K, Kane Gap; M, Falklands Channel; RG, Rio Grande Rise and Vema deep channel; R, Romanche Gap; S, Samoan Gateway; Su, Sumba Strait; V, Vema Fracture Zone.

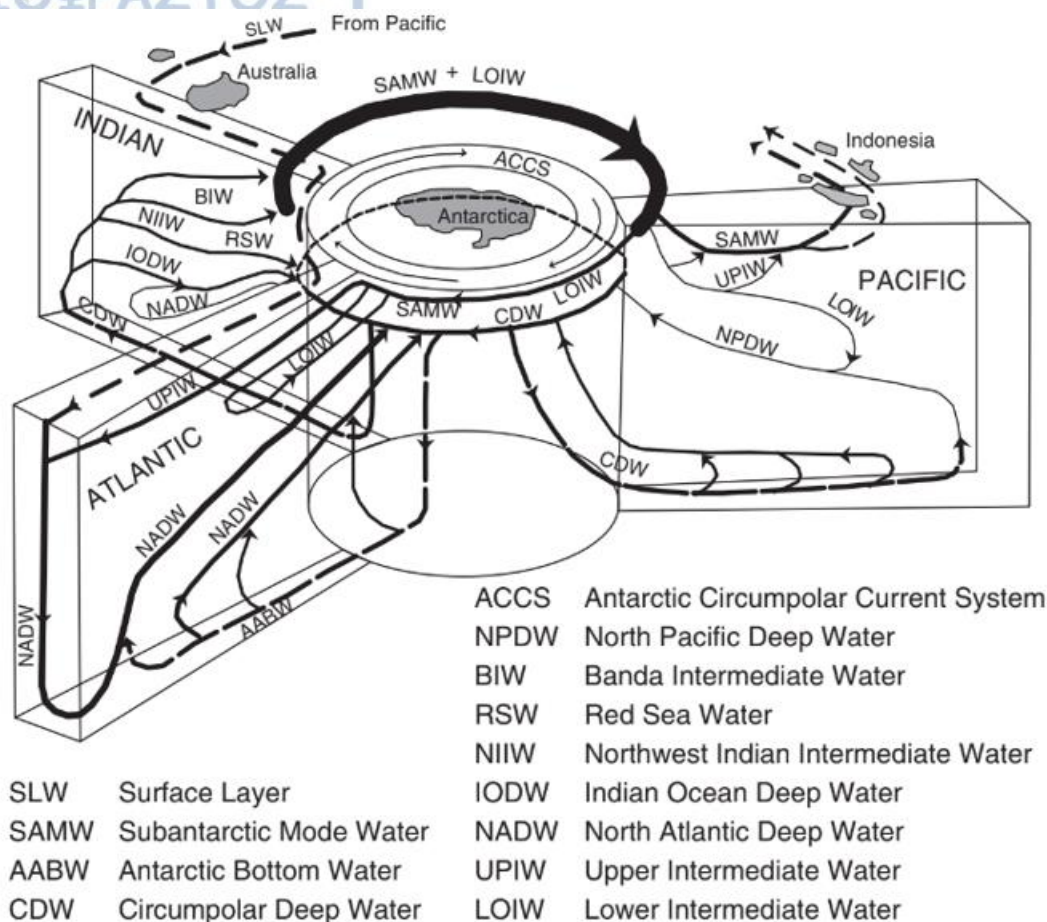


Figure 30. The thermohaline circulation. The Atlantic, Pacific and Indian Oceans are shown essentially as continent enclosed arms radiating from the central Southern Ocean [204].

3.3. Contour currents- Contourites

The Contour Currents- Contourites are oceanographic phenomena which called and 'along slope process' (Fig. 31). They play an important role in the deep-sea bottom shape because they are efficient agents of sediment transport and depositions. The sedimentation processes are depending on the volume and the kind of the sediments. The main forces which are response for contourites are the thermohaline force, Coriolis force and the wind force which transfers the surface energy downwards to the water column during strong storms. In addition, there are chemical forces which are due for dissolution and cementation processes.

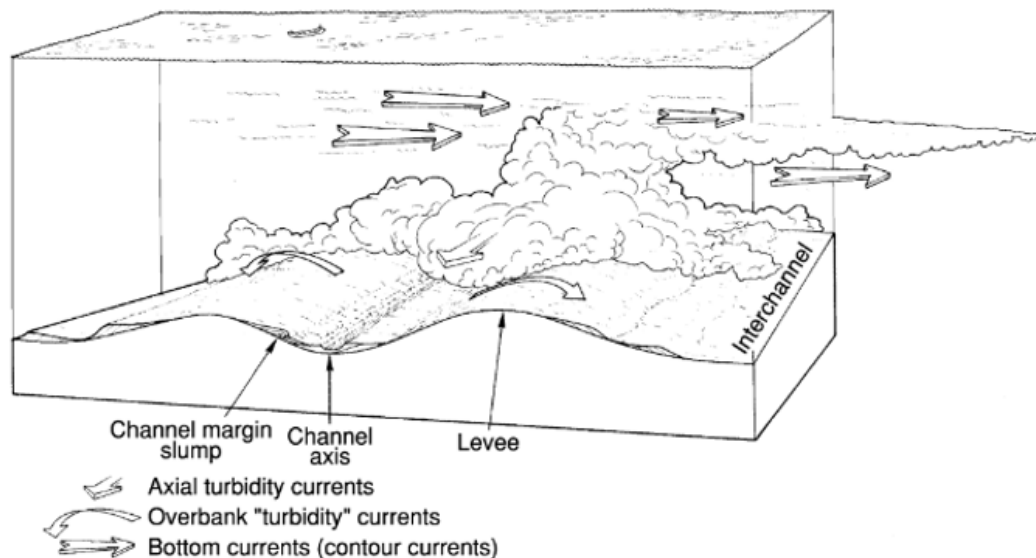


Figure 31. Conceptual model which shows the relationship between gravity flows (turbidity currents-turbidites) and along slope processes (contourites) [164].

3.3.1. Processes of transport and deposition

The contourites sediments are mainly consist of clays, fine silts and biogenic origin materials like mollusc shells, foraminifers, coccoliths, diatoms and radiolarians. These sediments are transformed by a nepheloid layer over thousands of kilometres. For example, sediments from the Norwegian sea can transported to the Blake Bahamas drift after 15 years and 6500km distance [205]. In addition, chlorite and diatom rich sediments from the south Atlantic Ocean, are transported for 3000 km to the Argentine and Brazilian margins [206]. A nepheloid layer can be shaped by high velocity contourites like the Western Boundary Undercurrents (WBUCs). This current is developed along the western Atlantic margins Scotia and Argentine margins (Fig. 31) [207, 208, 209]. Generally, the nepheloid layers seems to appear superimposed layers with a gentle upward density decrease with intermediate discontinuities (isopycnal surfaces) at certain depths (Fig. 32) [205].

The sedimentation of the nepheloid layer suspended particles, is a complicated process and is depended on their size. The largest silt particles (10-20 μ m) appear a faster settling-sedimentation than the largest clay particles (2-4 μ m). So, the smaller particles have the smaller velocity and finally they traverse the longer distance until their deposition.

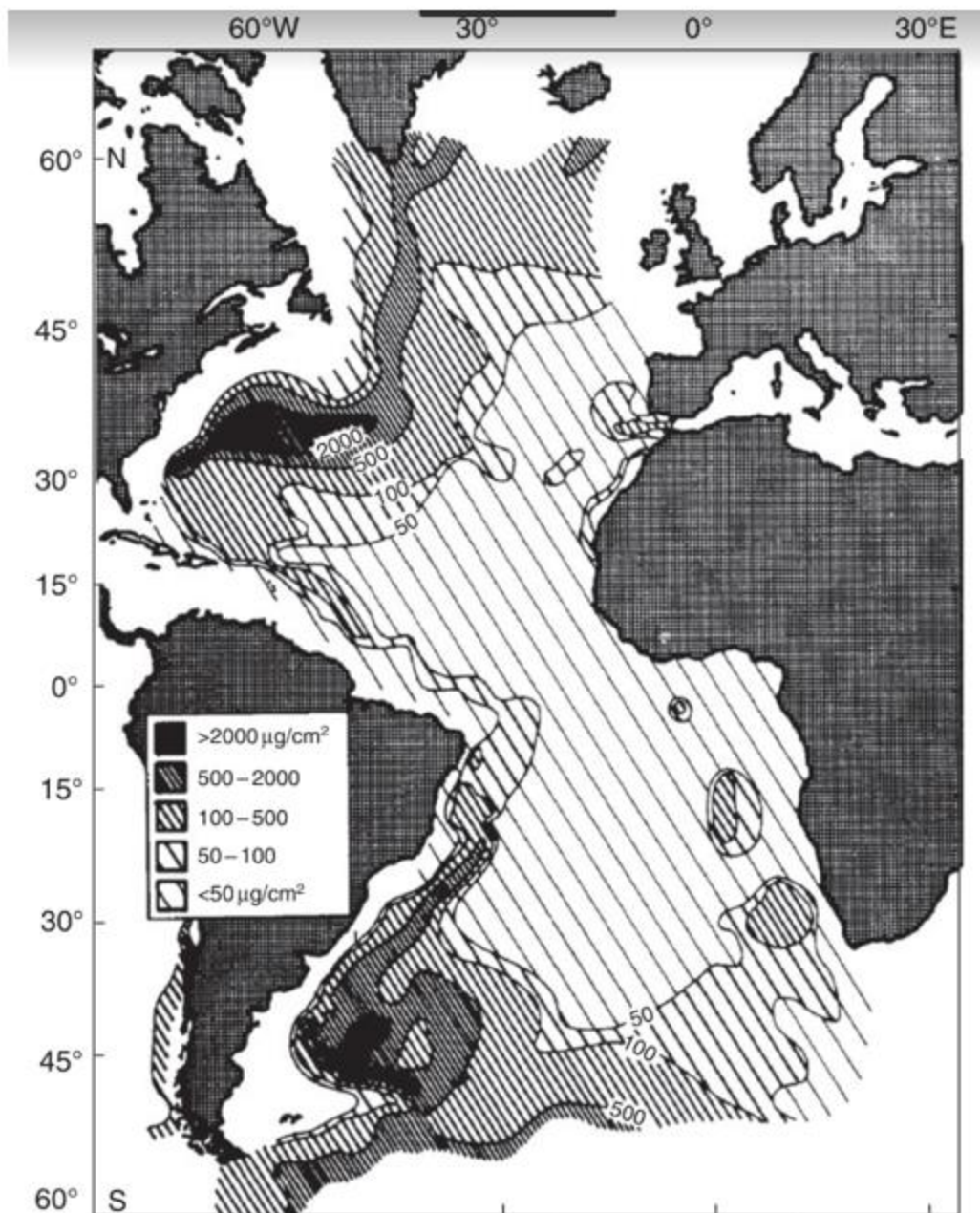


Figure 32. The nepheloid layer from WBUC contour current [207].

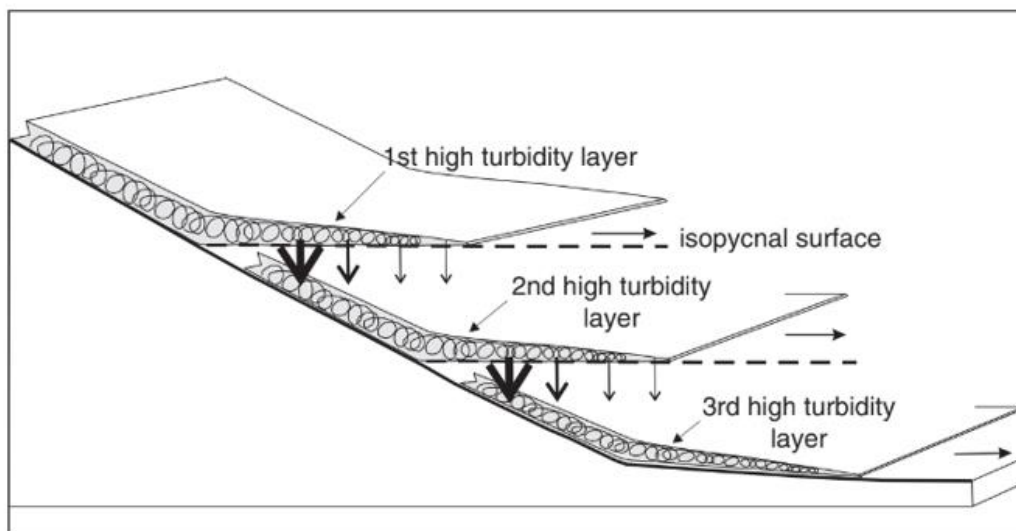


Figure 33. The superimposed layers of a nepheloid layer, 900m thick with isopycnal surfaces [205, 210]



4. Material and methods

In the present Thesis an experimental transparent tube was used, with a diameter of 6 cm and a length of 1.5m, full of liquid (fresh water and hyper-saline solution) to form a slope where turbidites and sediment mass flows were simulated. The whole experiment was recorded by a high-definition camera, to observe and calculate the sediment movement by video-frame analysis.

The stages followed in detail were as follows:

4.1. Preparation of the experimental pipe

An experimental transparent pipe was used, made in the Department's workshop, by Professor Konstantinos Albanakis. Its length is 1.5 m (the transparent part). The inner and outer diameter are 5 and 6 cm respectively. The material of the tube is plexiglass with a PVC non-transparent curved pipe on the upper part to help the introduction of the sample and a 2-inch ball-valve, at the lower end, to empty the experimental materials (hypersaline waters, tap water and solid materials).

4.2. Preparation of Hyper-Saline Solution

To prepare the hyper-saline solution, deionized water, salt, a 20-liter capacity pot, and an electric stove were used. The salt intentionally used was not pure but had various impurities. This was done to simulate as closely as possible both turbiditic and gravity flow processes that occur in nature, specifically in conditions of a closed hyper-saline sea. The preparation of the solution was carried out under normal conditions, namely at a temperature of 20°C and a pressure of 1 atm. It is noted that for the easier and quicker dissolution of salt in deionized water, it was previously ground into a powder form. The average amount of salt that managed to dissolve in one litre of deionized water is 400 to 450 gr per litre. It is calculated that the specific gravity of the resulting hyper-saline solution is 1160.45.

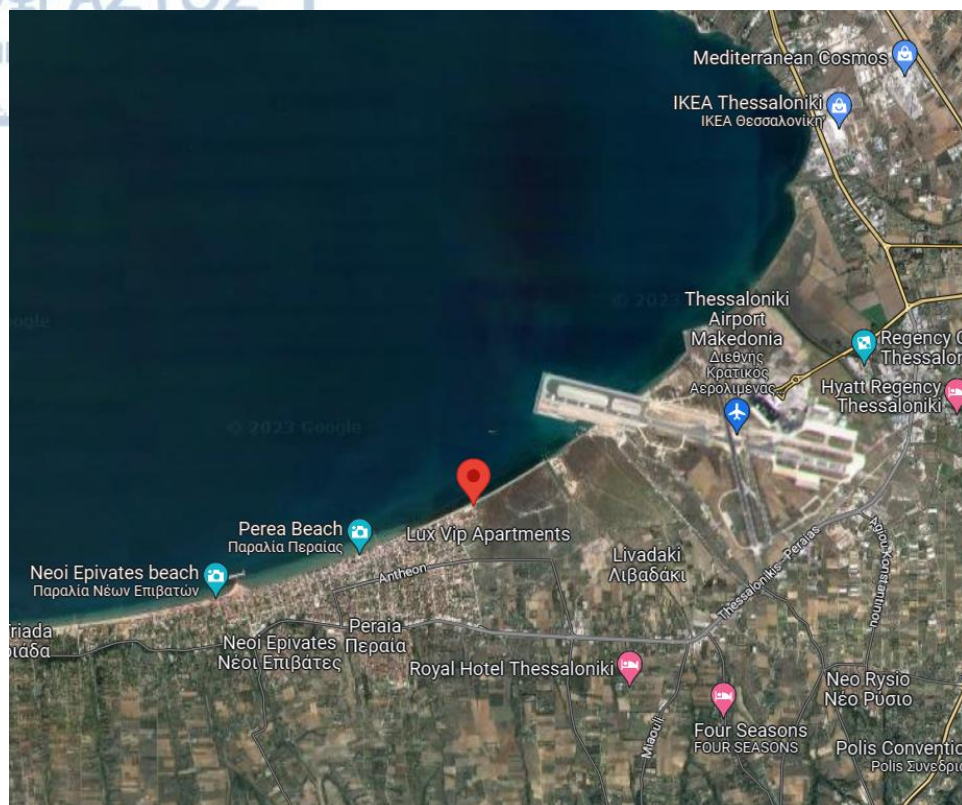
4.3. Sample Collection

As previously mentioned, a total of three samples were collected from the broader marine area of Perea in the Thessaloniki region. The first sample was collected from the upper beach area, specifically from the seagrass zone, with coordinates $40^{\circ}30'49.214''\text{N}$ and $22^{\circ}56'14.905''\text{E}$. This sample consists of uniform and fine-grained sediment.

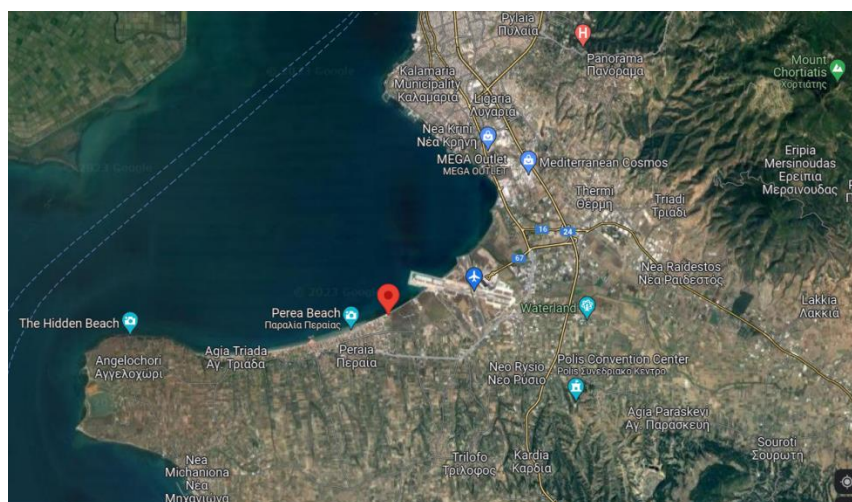


Satellite Image 1. Coordinates of sand samples from the marine area of Perea, Thessaloniki region.

The second sample was collected from the upper beach zone and has coordinates $40^{\circ}30'49.377''\text{N}$ and $22^{\circ}56'14.865''\text{E}$, and it is of medium grain size. The third and final sample was taken from the sea backwash zone and has coordinates $40^{\circ}30'49.537''\text{N}$ and $22^{\circ}56'14.795''\text{E}$, and it is of coarse grain size (Satellite Images 1, 2, 3).



Satellite Image 2. Collection point (in red) of the samples from the broader area of Perea, Thessaloniki region.



Satellite Image 3. Similarly.

4.4. Sample Processing

Subsequently, the samples were processed in the sedimentology laboratory of the Department of Geology at Aristotle University of Thessaloniki. The processing of the samples began with their drying in the department's dryer (Image 1a). Next, a random and independent quantity of the collected samples (fine-grained, medium-grained, coarse-grained) was selected and sieved through sieves with the following size ranges: 0.0-0.5φ, 0.5-1.0φ, 1.0-1.5φ, 1.5-2.0φ, 2.0-2.5φ, 2.5-3.0φ, 3.0-3.5φ, 3.5-4.0φ, and 4.0- <4.0φ (Image 1b). The quantities of sand falling within the same grain size range were then combined. Through this process, all sand grains within the same grain size range were derived from the three collection points. Finally, after the combination of the grains, they were divided into eight equal parts using the rotary sample divider type PT 100 in the laboratory (Image 1c).



(a)



(b)



Image 1a. Dryer where the samples were dried.

Image 1b. Sieves for separating the samples into individual portions of specific grain size ranges (ϕ).

Image 1c. Separation of the samples using the rotary sample divider type PT 100.

(c)

4.5. Granulometry of the sand samples

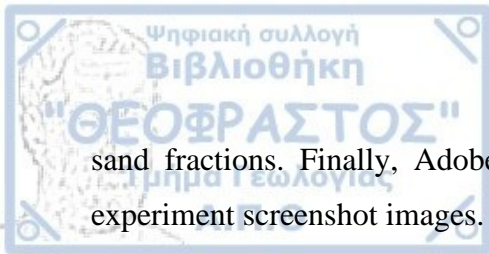
The range of the samples granulometry is 1-1.5 ϕ and 2-2.5 ϕ with average 1.25 and 2.25 ϕ respectively. Also as mentioned above, experiments were done with a part of the amount of the fine-grained material taken from the upper part of the beach (Dunes).

4.6. Video Recording of Experiments

The video recording of the experiments was carried out using a high-resolution camera from a Xiaomi Redmi 9T mobile phone, at 1080P-30FPS. To make the turbiditic and mass flows of the samples within the tube more distinguishable, a blue-coloured background cloth was used. This helped in achieving more detailed and clearer recording of the flows.

4.7. Processing and Analysis of Experiment Videos

The processing and analysis of the experiment videos were performed using Wondershare Filmora 12 software. Specifically, video montage, zooming, and capturing screenshots of the experiments were done to study the turbiditic and mass flow movements of various



sand fractions. Finally, Adobe Photoshop CS6 software was used for processing the experiment screenshot images.

4.8. Boundary conditions

The boundary conditions under which the following experiments were conducted are as follows and pertain to:

1. The quantity of material.

The quantity of material used in the experiments ranged from 12.8 to 13.4gr. This range was sufficient to form a turbidite of satisfactory length in the specific experimental tube.

2. The angle of inclination of the experimental tube.

The rolling initiation angle of the material is the angle of inclination of the experimental tube at which the internal friction angle of the material, specific to its granulometry, is overcome, causing it to start rolling. This angle ranges from 22 to 24 degrees. The angle of inclination of the experimental tube at which a turbidite of sufficient length, capable of being observed, is formed is 35 degrees. The range of inclination angles for the experimental tube during the experiments was between 22-35 degrees.

3. Experimental tube.

The tube's length is 1.5m, and its internal diameter is 5cm. In these dimensions of the tube, combined with the amount of material used and its angle of inclination, turbiditic events are created and evolve. This indicates that the tube, and consequently its length and diameter, are adequate for the experiments.

5. Discussion and Results

In this thesis specialization, a total of 48 experiments were conducted. As previously mentioned, the solutions used were fresh water and a hyper-saline solution (brine) with a specific gravity of $S.G = 1160.45$. The grain size range of the sand fractions used was 1-1.5 ϕ and 2-2.5 ϕ with corresponding average grain sizes of 1.25 ϕ and 2.25 ϕ , respectively. Additionally, a portion of the material from the upper beach area (dunes), specifically from the seagrass zone, was used. Prior to this, grain size analysis was conducted (Table 1), and a grain size distribution curve was generated using the Gradistat version 6.0 program (Blott, 2008) (Figure 1).

The total experiments were divided into three groups based on the average grain size of the sand used in each. Thus, the first group of experiments with an average grain size of 1.25 ϕ included a total of sixteen (16) experiments. The second group with an average grain size of 2.25 ϕ included a total of fourteen (14) experiments. Finally, the third group, which used material from the seagrass zone, comprised a total of eighteen (18) experiments.

Single Sample Data Input Screen

Sample Identity: **DUNE**
Analyst: **1**
Date: **13/06/2023**
Initial Sample Weight: **140,14**

Aperture (microns)	Class Weight Retained (g or %)
90000	
63000	
45000	
31500	
22400	
16000	
11200	
8000	
5600	
4000	
2800	0,016
2000	0,072
1400	0,382
1000	1,467
710	8,676
500	25,828
355	20,092
250	17,914
180	17,049
125	6,428
90	1,229
63	0,218

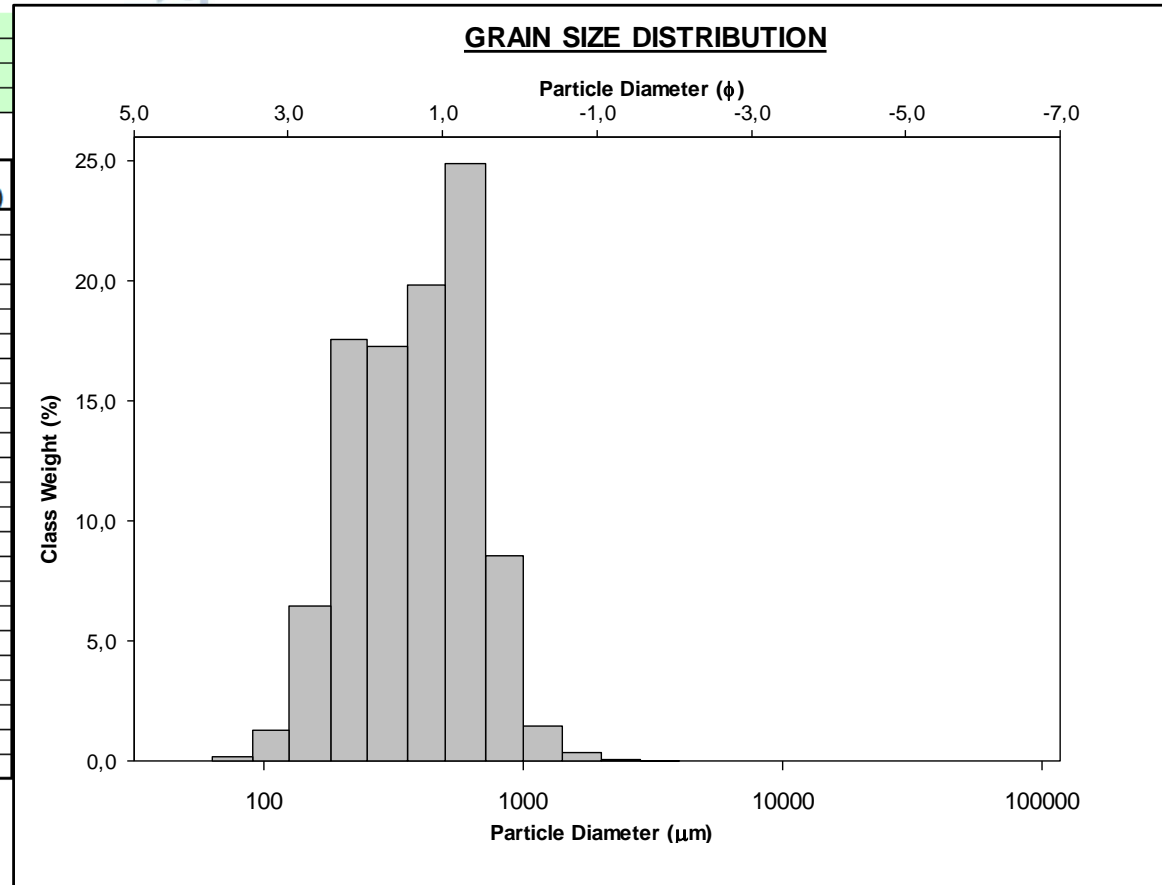


Table 1. Grain Size Analysis of the dunes sample.

Figure 1. Grain Size Distribution Frequency Curve in the Gradistat 6 Program (Blott, 2008)

5.1. Group of experiments with a particle size range of 1-1.5 ϕ (mean 1.25 ϕ).

In this group, a total of sixteen (16) experiments were conducted. The initial quantity of solid material used was 13.4gr. Out of these experiments, five (5) were conducted in fresh water, seven (7) in hypersaline water, and four (4) with nearly double the quantity of solid material, 28.1gr in hypersaline and fresh water (Table 5.1).

From these experiments, it was observed that the slope angle of the experimental tube, where the particles begin to roll as a mass (laminal sheet flow), is 24 degrees for fresh water and 25 degrees for the supersaturated hypersaline water (brine). The corresponding velocities of the particles are 0.5 and 0.3cm/sec, respectively. It can be seen from the above results that both the initiation angle of rolling and the velocity of sedimentation are affected by the surrounding solution's viscosity. Specifically, the greater the viscosity of the solution, the larger the initiation angle of the tube where the solid material begins to roll, and the slower the velocity.

Turbulence of the solid material is observed only in the hypersaline water, which is maintained in the first 0.18cm of the tube at a frontal velocity of 16cm/sec. Additionally, in fresh water and at an angle of 35 degrees in the experimental tube, turbulence is observed, which is maintained in the first 0.4 to 0.42m of the tube with a frontal velocity ranging from 20 to 23cm/sec. In the hypersaline water and at an angle of 27 degrees in the experimental tube, turbulence is observed, which is maintained in the first 0.2m of the tube with a frontal velocity of 17cm/sec. In the same environment and at an angle of 35 degrees in the tube, the turbulence formed is maintained in the first 0.29 to 0.45m of the tube, with frontal velocities ranging from 18 to 22cm/sec. From the above, it can be concluded that the duration of turbulence and the velocity of the material depend on the tube's initiation angle. The larger the angle, the longer the turbulence duration and its velocity. It also depends on the viscosity of the respective water; the higher the viscosity, the slower the frontal velocity.

Furthermore, the formation of particle groups is observed (clusters). Thus, at a 35-degree angle in fresh water, 5 to 6 groups of clusters are formed every 10sec. The velocity of these particle groups ranges from 8 to 10cm/sec, compared to the velocity of the rest of the material, which ranges from 4 to 7cm/sec. In a 35-degree angle in the hypersaline water, 6

to 8 groups are formed every 30sec, with velocities ranging from 5 to 7cm/sec, while the velocity of the rest of the material ranges from 3 to 4cm/sec. It should be noted that at the initiation angles of solid material rolling, the organization of particles into groups is not observed. From the above, it can be concluded that the solution's viscosity affects the wave length of the clusters, their velocity, and the velocity of the hole material.

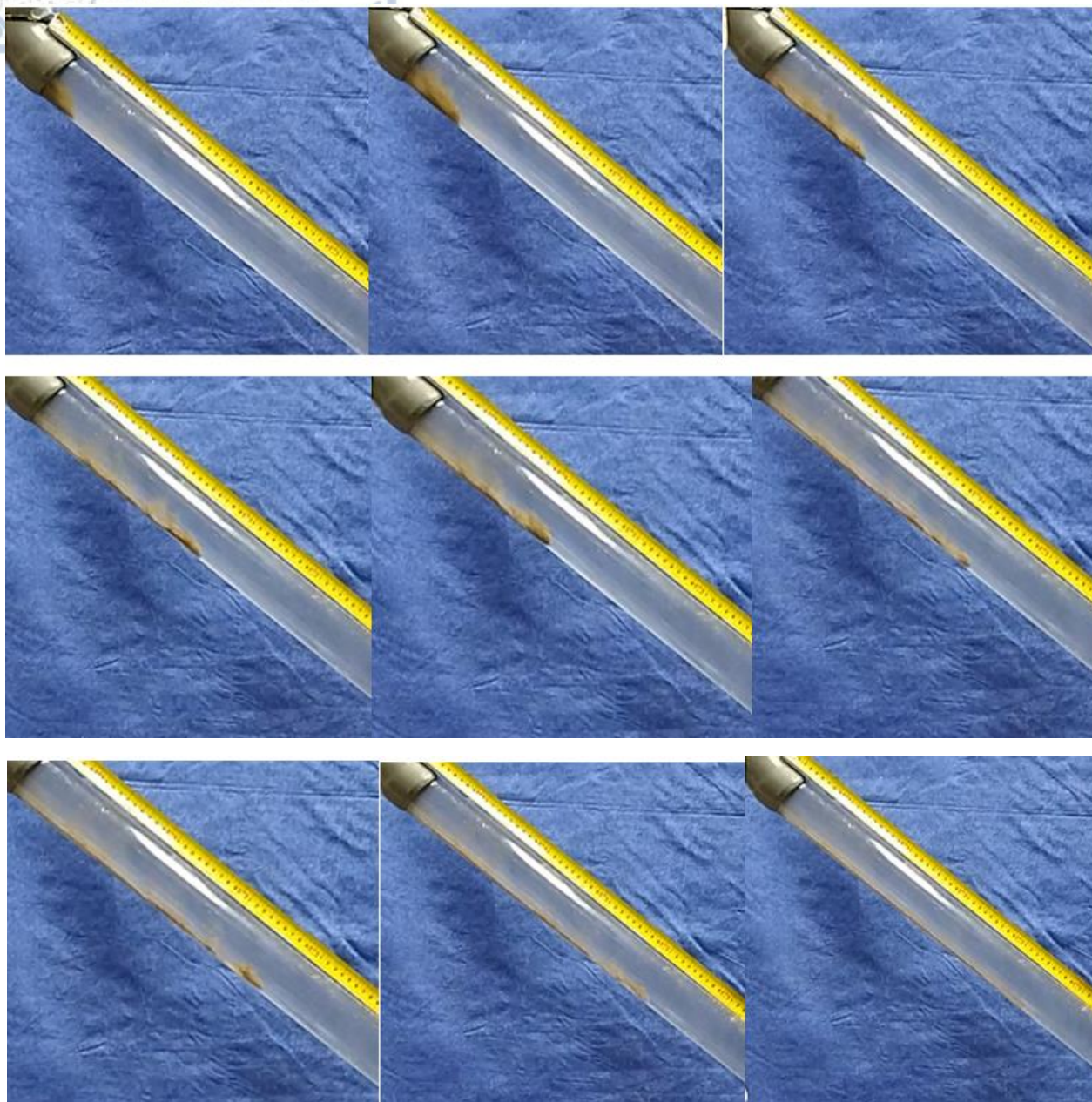
Next, four (4) experiments were conducted in the two aforementioned solutions, using a quantity of solid material of 28.1gr. This was done to determine whether the quantity of material affects the initiation angle of its rolling and its velocity in the experimental tube. From the above experimental results, it can be observed that in fresh water, the initiation angle of rolling decreases from 24 to 22 degrees, while the rolling velocity of the particles remains the same at 0.5cm/sec. At a 24-degree angle of the double quantity of solid material, the rolling velocity increases to 0.8cm/sec. Similar results are observed in hypersaline water (brine), with a reduction in the initiation angle of particle rolling from 25 to 23 degrees, accompanied by an increase in velocity from 0.3 to 0.6cm/sec. From the above, it can be concluded that as the quantity of solid material increases, the initiation angle of rolling in the experimental tube decreases, and its velocity increases at the same angle. Additionally, the velocity of the material is influenced by the viscosity of the respective solution. The higher the viscosity, the lower the material's velocity.

Finally, the remaining material at the beginning of the tube appears to be higher in the hypersaline water with the nearly double quantity of the solid material compared to fresh water. This happens and with the single quantity of the solid material. This quantity primarily concerns from sheet materials that, due to their large surface area, remain immobilized at the beginning of the experimental tube. Therefore, the viscosity of the solution affects the movement of the material. The higher the viscosity, the higher the concentration of solid material at the beginning of the tube. Representative images in the experiment with 13.4gr of material in hypersaline water (Image Groups 5.1.a.-5.1. b.).

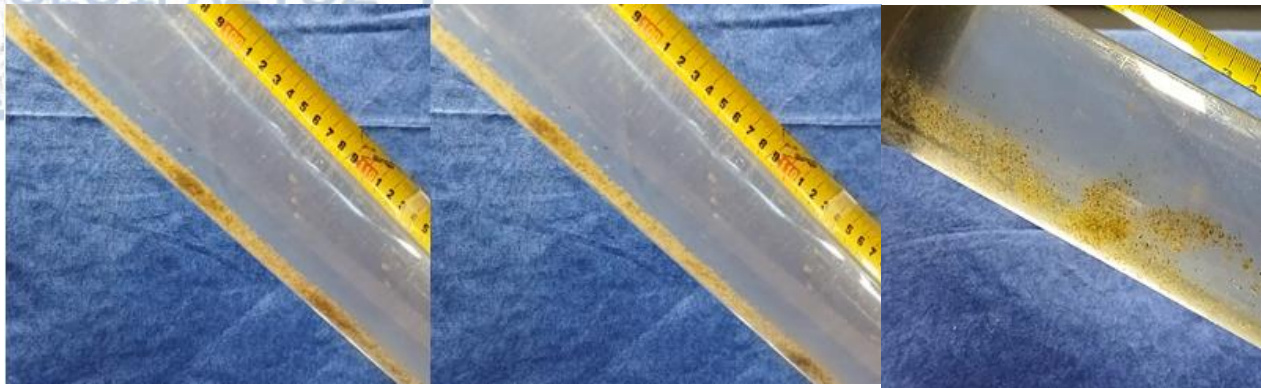
GRAIN SIZE RANGE 1-1.5 ϕ (average 1.25 ϕ)

	FRESH WATER								
	MATERIAL 13.4 gr					MATERIAL 28.1 gr			
EXPERIMENTS (7)	1	2	3	4	5	1	2		
PIPE INCLINATION (ankles)	22	24	35	35	35	24	22		
GRAIN ROLL	NO	YES	YES	YES	YES	YES	YES		
TURBIDITE	NO	NO	YES	YES (0.4 m)	YES (0.42m)	YES (0.16 m)	YES (0.1 m)		
GRAVITY FLOW	NO	YES	YES	YES	YES	YES	YES		
GRAIN GROUPS / 10 sec	NO	NO	5	5	6	NO	NO		
GRAIN GROUPS SPEED (cm/sec)	NO	NO	10	9	8	NO	NO		
SPEED MATERIAL (cm/sec)	NO	0.5	7	4	5	0.8	0.5		
REMAINIG MATERIAL	YES	YES	YES	YES	YES	YES	YES		
TURBIDITE FRONT SPEED (cm/sec)	NO	NO	-	23	20	19	11		
	HYPERSALINE WATER (SG=1160.45)								
	MATERIAL 13.4 gr						MATERIAL 28.1 gr		
EXPERIMENTS (9)	1	2	3	4	5	6	7 (+2% clay)	1	2
PIPE INCLINATION (ankles)	22	25	27	35	35	35	35	23	23
GRAIN ROLL	NO	YES	YES	YES	YES	YES	YES	YES	YES
TURBIDITE	YES (0.16 m)	YES (0.18 m)	YES (0.2m)	YES (0.45 m)	YES (0.44 m)	YES (0.29 m)	YES (0.32 m)	-	-
GRAVITY FLOW	NO	YES	YES	YES	YES	YES	YES	YES	YES
GRAIN GROUPS / 30 sec	NO	NO	NO	7	6	7	8	NO	NO
GRAIN GROUPS SPEED (cm/sec)	NO	NO	NO	5	7	5	6	NO	NO
SPEED MATERIAL (cm/sec)	NO	0.3	1	-	4	3	3	0.6	0.4
REMAINIG MATERIAL	YES	YES	YES	YES	YES	YES	YES	YES	YES
TURBIDITE FRONT SPEED (cm/sec)	14	16	17	19	22	18	18	-	-

Table 5.1. Presentation of experimental results with a material grain size range of 1-1.5 ϕ (Average 1.25 ϕ).



a)



b)

Image Group 5.1.a. Presentation of turbidity development with a range of particles 1-1.5 ϕ in a hypersaline solution and a 35-degree inclination angle of the experimental tube.

Image Group 5.1.b. Distinguishing sediment groups-clusters (on the left) and the remaining material at the beginning of the tube (on the right).

5.2. Experiment Group with Particle Size Range of 2-2.5 ϕ (Mean 2.25 ϕ)

In this group, a total of fourteen (14) experiments were conducted. The initial quantity of solid material used was 12.8gr. Out of these experiments, six (6) were carried out in fresh water, four (4) in a hypersaline water, and four (4) with nearly double the amount of solid material, which was 28.7gr in the hypersaline water and fresh water (Table 5.2).

From these fourteen (14) experiments, it was observed that the angle of inclination of the experimental tube, where particle rolling begins in mass form (laminal sheet flow), was 25 degrees in both types of solutions. However, the particle rolling velocities were 0.5 cm/sec in fresh water and ranged from 0.2 to 0.3cm/sec in the hypersaline water. It can be concluded that the velocity of sediments is affected by the properties of the surrounding solution, specifically, the higher the viscosity of the solution, the lower the sediment rolling velocity.

Additionally, the formation of turbidity was observed within the first 0.22cm in fresh water with a front velocity of 18cm/sec and within the first 0.24cm of the experimental tube in the hyper saline environment (brine) with a corresponding front velocity of 11cm/sec. Turbidity of the material was also observed at a 35-degree inclination angle of the tube in fresh water, lasting from the first 0.3 to 0.55m of the experimental tube, with front velocities ranging from 17 to 23cm/sec. Turbidity was also observed at 27 degrees, lasting up to the first 0.2m of the tube with a front velocity of 19cm/sec. In the hyper saline environment and at a 35-degree tube inclination angle, turbidity was formed, lasting up to the first 0.3m of the tube with a front velocity of 13cm/sec. From the above results, it can be inferred that the viscosity of the respective solution affects the duration and the velocity of turbidity. The higher the viscosity of the solution, the shorter the duration and the lower the velocity of the turbidity.

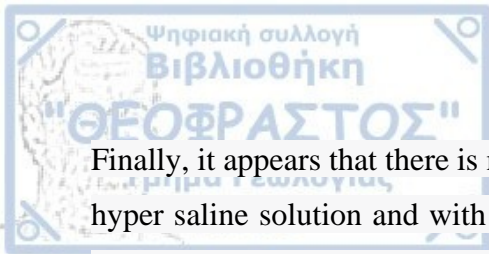
Furthermore, the tube's inclination angle also affected the formation of turbidity. The greater the angle, the longer the duration and the higher the velocity of turbidity.

It is also worth noting the creation of particle groups (clusters) apart from the starting angles of solid material rolling (laminal sheet sand). In this regard, at a 35-degree tube

inclination angle in fresh water, from 8 to 11 groups formed every 30sec. The velocity of these particle groups (clusters) ranged from 5 to 7cm/sec, compared to the velocity of the remaining mass of material, which ranged from 5 to 6cm/sec. In a hyper saline environment at a 35-degree tube inclination angle, from 4 to 7 clusters formed every 30sec, with velocities ranging from 2 to 2.5cm/sec, while the velocity of the laminal sheet sand was 3cm/sec. It is worth noting that there was a delay in the of these groups due to the smaller particle size of the material and the short length of the experimental tube, which acted as a constraining factor (if it were larger, they would have appeared sooner). From the above, it can be concluded that the solution environment and its viscosity affect the rate of particle organization into clusters. The higher the viscosity, the lower the rate of their organization into groups. Viscosity also inversely affects the velocity of both groups with the same particle size and the remaining mass of material.

Subsequently, four (4) experiments were conducted in both of the aforementioned solutions with a solid material quantity of 28.7gr. This was done, as mentioned earlier, to determine how the quantity of material affects the angle at which it begins to roll and its velocity in the experimental tube. From the experimental results, it was observed that in fresh water, the angle of initiation of rolling decreased from 25 to 22 degrees, while the rolling velocity of the particles increased from 0.5cm/sec to 0.6 to 0.7cm/sec. Similar results were observed in the hyper saline solution (brine), with the angle of initiation decreasing from 25 to 23 degrees, and a slight increase in velocity from 0.2 to 0.3cm/sec to 0.3 to 0.4cm/sec. It is therefore concluded that as the quantity of solid material increases, the angle at which it begins to roll in the experimental tube decreases, while its rolling velocity increases.

Turbidity of the material was also observed in both solution environments. In fresh water, turbidity was maintained up to the first 0.38cm of the experimental tube, with turbidity front velocities ranging from 22 to 23cm/sec, while in the hypertonic solution, it was maintained up to 0.3cm with a corresponding front velocity of 19cm/sec. As the viscosity increases, the front velocity of the turbidity and its maintenance in the experimental tube decrease. In the experiments with a material quantity of 28.7gr, the formation of particle groups was not observed.

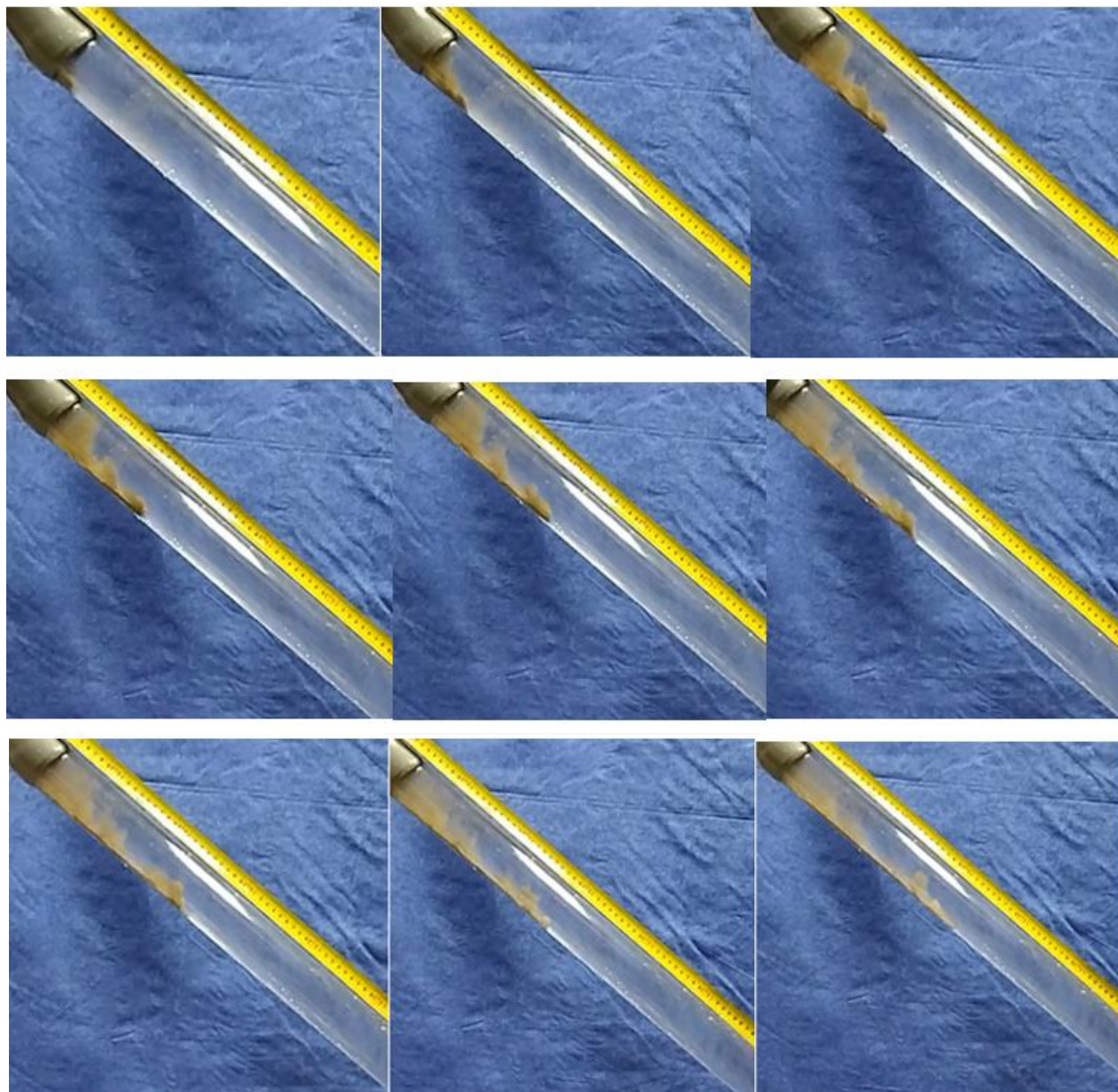


Finally, it appears that there is more remaining material at the beginning of the tube in the hyper saline solution and with the nearly double quantity of solid material, compared to fresh water and the single quantity of material. This quantity seems to mainly consist of phylloid minerals which, due to their large surface area, become immobilized at the beginning of the experimental tube such as the biotite and muscovite. Representative images of the turbidity created in the experiment with 12.8gr of material in fresh water are presented below (Image Groups 5.2.a. - 5.2.b.).

GRAIN SIZE RANGE 2-2.5 ϕ (average 2.25 ϕ)								
	TAP WATER							
	MATERIAL 12.8 gr						MATERIAL 28.7 gr	
EXPERIMENTS (8)	1	2	3	4	5	6	1	2
PIPE INCLINATION (ankles)	22	25	27	35	35	35	22	22
GRAIN ROLL	NO	YES	YES	YES	YES	YES	YES	YES
TURBIDITE	YES (0.2 m)	YES (0.22 m)	YES (0.29 m)	YES (0.3 m)	YES (0.52m)	YES (0.45 m)	YES (0.38 m)	YES (0.26 m)
GRAVITY FLOW	NO	YES	YES	YES	YES	YES	YES	YES
GRAIN GROUPS / 30 sec	NO	NO	NO	8	10	11	NO	NO
GRAIN GROUPS SPEED (cm/sec)	NO	NO	NO	5	7	6	NO	NO
SPEED MATERIAL (cm/sec)	NO	0.5	1.5	5	6	6	0.6	0.7
REMAINIG MATERIAL	YES	YES	YES	YES	YES	YES	YES	YES
TURBIDITE FRONT SPEED (cm/sec)	17	18	20	17	22	23	23	22
	HYPERHALINE WATER (SG=1160.45)							
	MATERIAL 12.8 gr				MATERIAL 28.7 gr			
EXPERIMENTS (6)	1	2	3	4	1	2		
PIPE INCLINATION (ankles)	25	25	35	35	23	23		
GRAIN ROLL	YES	YES	YES	YES	YES	YES		
TURBIDITE	YES (0.1 m)	YES (0.24 m)	YES (0.3 m)	-	YES (0.3 m)	-		
GRAVITY FLOW	YES	YES	YES	YES	YES	YES		
GRAIN GROUPS / 30 sec	NO	NO	7	4	NO	NO		
GRAIN GROUPS SPEED (cm/sec)	NO	NO	2.5	2	NO	NO		
SPEED MATERIAL (cm/sec)	0.3	0.2	3	3	0.3	0.4		
REMAINIG MATERIAL	YES	YES	YES	YES	YES	YES		
TURBIDITE FRONT SPEED (cm/sec)	-	11	13	-	19	-		

Table 5.2. Presentation of Experimental Results with Material Particle Size Range of 2-2.5 ϕ (Mean 2.25 ϕ)

a)





b)

Image Group 5.2.a: Presentation of turbidity development with particle size range of 2-2.5 ϕ in fresh water and an experimental tube slope angle of 35 degrees.

Image Group 5.2.b: Distinguishing sediment groups-clusters.

5.3. Experimental Group with Sediment Material Grain Size Range -1.5 to >4

In this group, a total of eighteen (18) experiments were conducted. The initial quantity of solid material used was 13.2gr. Out of these experiments, five (5) were conducted in fresh water solution, and seven (7) were conducted in a hyper-saline solution. Additionally, six (6) experiments were carried out with nearly double the amount, 30gr, of material in the hypersaline water and fresh water (Table 5.3).

From these experiments, it was observed that the angle of inclination of the experimental tube, where the particles begin to roll as a mass, was 22 degrees for fresh water and 23 degrees for the hyper-saline solution. The corresponding velocities of the particles were 0.4cm/sec and 0.2cm/sec. It can be concluded that both the angle of inclination and the velocity of sediments are influenced by the solution's viscosity. Specifically, a higher viscosity in the solution leads to a larger angle of tube inclination where the rolling of solid material begins and a slower velocity.

At 20 degrees of tube inclination in both solutions, although the material remains stationary and doesn't roll, turbidites form in the first 0.2m of the tube with a velocity front of 19cm/sec in fresh water and 15cm/sec in the hyper-saline environment. At 35 degrees of tube inclination, turbidization of the material occurs and is sustained from the first 1.23 to 1.34m of the total length in fresh water and from 0.64 to 0.7m in the hyper-saline solution. The velocity of the turbidity front in the respective solutions ranges from 26 to 28cm/sec and from 18 to 22cm/sec. Turbidites are also observed in the hyper-saline solution at a 25-degree tube inclination in the first 0.2m of the length with a velocity front of 20cm/sec and a material velocity of 1.5m/sec. From the above, it is inferred that the viscosity of the solution affects the duration and velocity of turbidites. The higher the viscosity of the solution, the shorter the duration and velocity of the front.

Furthermore, it is concluded that the velocity of the turbidity front depends on the tube's angle of inclination; the larger the angle, the longer the duration and the higher the velocity of the turbidity.

At the starting angles of sediment rolling, no organization of particles into groups is observed due to their similar sizes and velocities. At a 35-degree tube inclination, approximately 11

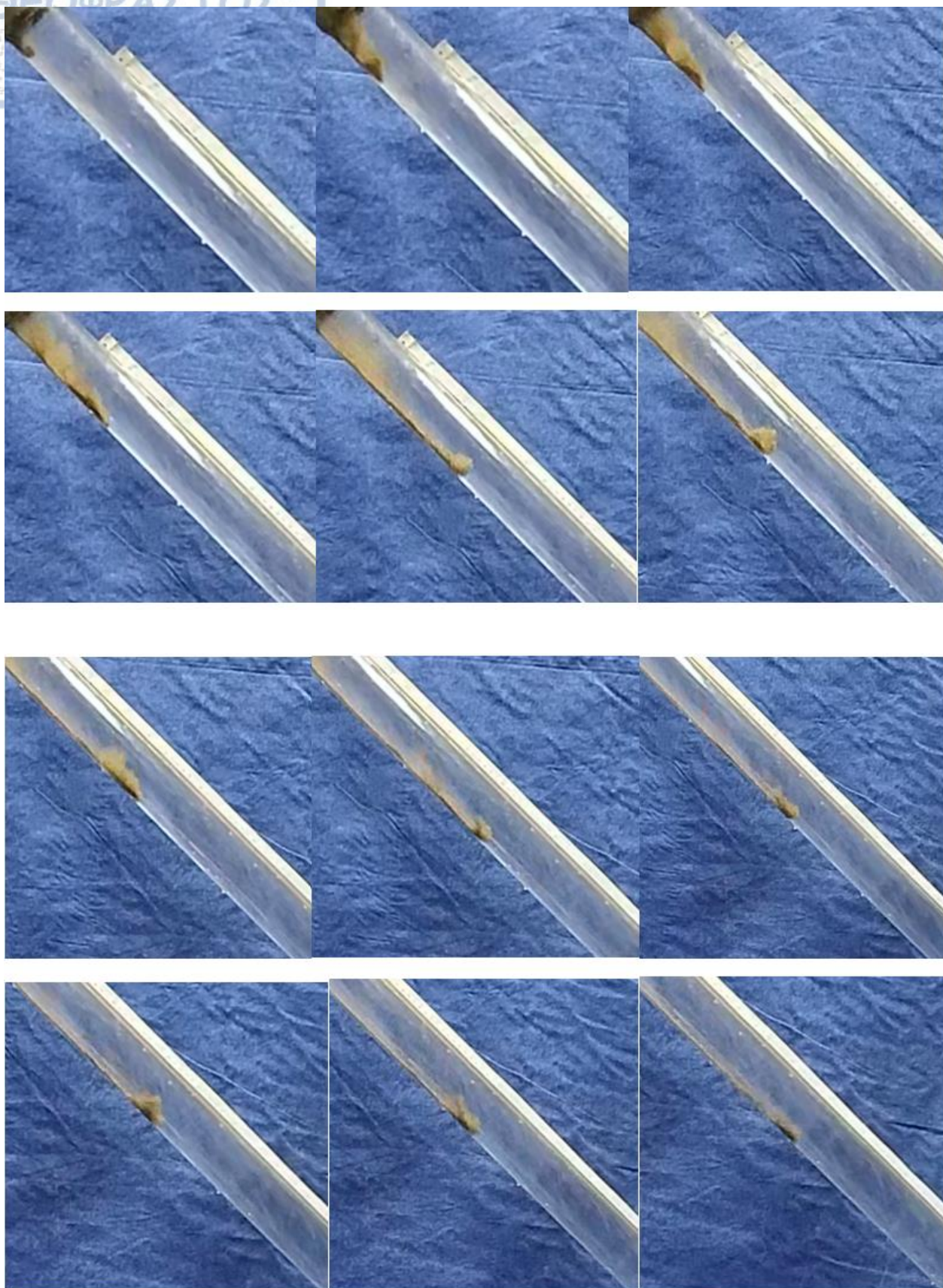
to 13 groups are formed per 10sec in fresh water and 4 to 9 groups per 30sec in the hyper-saline solution, with corresponding velocities ranging from 16 to 18cm/sec and from 6.5 to 12cm/sec. The velocity of the material mass in fresh water ranges from 20 to 21cm/sec and in the hyper-saline solution is 9cm/sec. It is noted that the velocity of the material mass in fresh water is higher than the velocity of the sediment groups. This occurs because the measurements were taken at the end of turbidity action (material mass) and at the beginning of group formation. The length of the experimental tube played a significant role in the experiment's development and, consequently, in the measurements of the above velocities. From the above, it is inferred that the solution's viscosity affects the rate of organizing sediment particles into groups. The higher the viscosity of the solution, the slower the rate of organization into groups, and the lower the velocity of solid material.

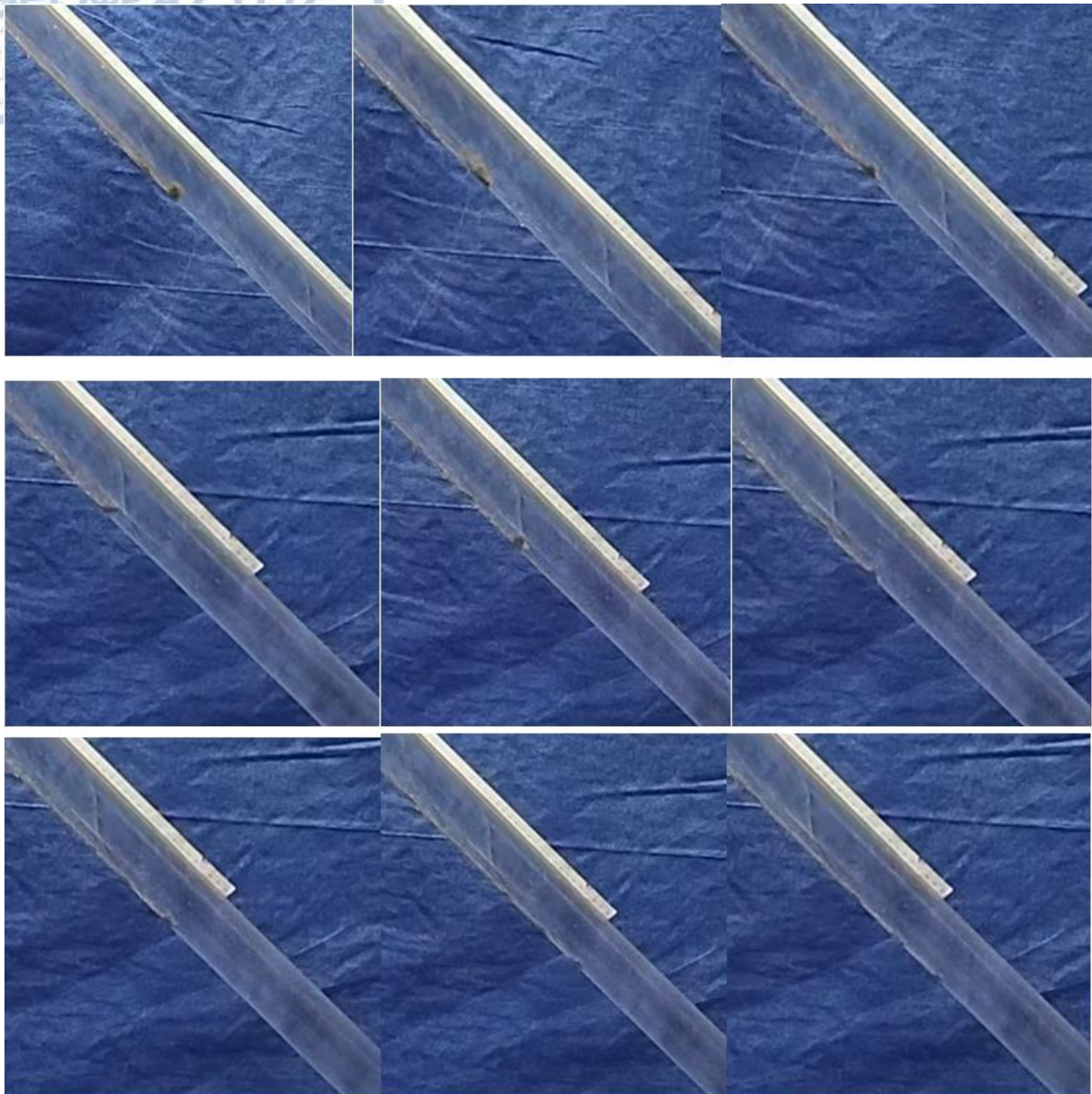
Subsequently, a total of six (6) experiments were conducted in the same solutions with a quantity of solid material of 30gr. This was done to determine whether the material quantity affects the angle of the beginning of its rolling and its velocity in the experimental tube. Turbidization of the material is observed in both solutions at a 22-degree tube inclination. In fresh water, it is sustained up to the first 0.35 meters with a velocity front ranging from 18 to 23cm/sec, and in the hyper-saline solution, it is sustained up to 0.24m with a corresponding velocity front of 15cm/sec. Additionally, the velocity of the solid material increased from 0.4 to 0.6-1cm/sec in fresh water and from 0.2 to 0.8-0.9cm/sec in the hyper-saline solution. Groups of sediment particles with a large wave length are also formed at the 22-degree tube inclination in fresh water.

Finally, concerning the remaining material at the beginning of the tube, the results are similar to the previous experiments. More material appears to remain in the hyper-saline solution and with nearly double the quantity of solid material compared to fresh water and the single quantity of material. This quantity seems to mainly consist of flake-like materials that, due to their large surface areas, become immobilized at the beginning of the experimental tube. Below are representative images of the turbidity created in the experiment with 13.2gr of material in a fresh water environment and a 35-degree tube inclination (Image Groups 5.3.a. - 5.3.b.).

	DUNE MATERIAL (-1.5- >4 φ)									
	TAP WATER									
	MATERIAL 13.2 gr					MATERIAL 30 gr				
EXPERIMENTS (9)	1	2	3	4	5	1	2	3	4	
PIPE INCLINATION (ankles)	20	22	35	35	35	22	22	22	22	
GRAIN ROLL	NO	YES	YES	YES	YES	YES	YES	YES	YES	
TURBIDITE	YES (0.2 m)	-	YES (1.34m)	YES (1.23m)	YES (1.25m)	YES (0.2 m)	YES (0.24 m)	YES (0.35 m)	-	
GRAVITY FLOW	NO	YES	YES	YES	YES	YES	YES	YES	YES	
GRAIN GROUPS / 10 sec	NO	NO	12	13	11	YES (bigger)	NO	NO	YES (bigger)	
GRAIN GROUPS SPEED (cm/sec)	NO	NO	16	16	18	-	-	-	-	
SPEED MATERIAL (cm/sec)	NO	0.4	20	20	21	1	0.6	0.8	0.6	
REMAINIG MATERIAL	YES	YES	YES	YES	YES	YES	YES	YES	YES	
TURBIDITE FRONT SPEED (cm/sec)	19	-	27	26	28	18	18	23	-	
	HYPERSALINE WATER (SG=1160,45)									
	MATERIAL 13.2 gr					MATERIAL 30 gr				
EXPERIMENTS (9)	1	2	3	4	5	6	7	1	2	
PIPE INCLINATION (ankles)	20	23	25	35	35	35	35	22	23	
GRAIN ROLL	NO	YES	YES	YES	YES	YES	YES	YES	YES	
TURBIDITE	YES (0.13m)	-	YES (0,2m)	YES (0,69 m)	YES (-)	YES (0,64m)	YES (0,7m)	YES (0.24 m)	-	
GRAVITY FLOW	NO	YES	YES	YES	YES	YES	YES	YES	YES	
GRAIN GROUPS / 30 sec	NO	NO	NO	-	-	9	4	NO	NO	
GRAIN GROUPS SPEED (cm/sec)	NO	NO	NO	-	-	6.5	12	NO	NO	
SPEED MATERIAL (cm/sec)	NO	0.2	1.5	-	-	-	9	0.9	0.8	
REMAINIG MATERIAL	YES	YES	YES	YES	YES	YES	YES	YES	YES	
TURBIDITE FRONT SPEED (cm/sec)	15	-	20	18	22	20	21	15	-	

Table 5.3. Presentation of Experimental Results with Sediment Material of Grain Size Range -1.5 to >4φ.





a)



b)

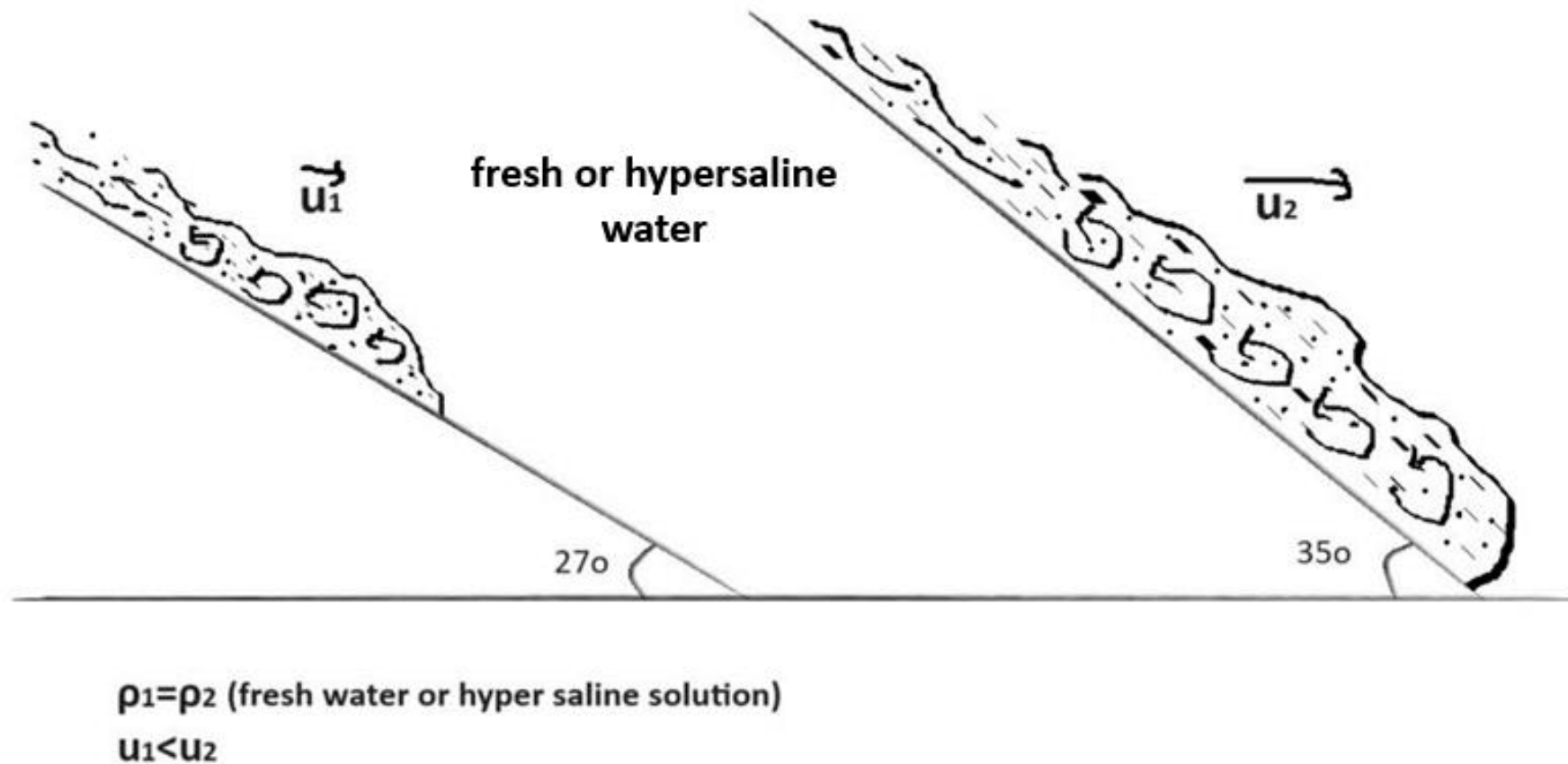
Image group 5.3.a. Presentation of the development of turbidity with sediment material of grain size range -1.5 to $>4\phi$ in fresh water and a 35-degree angle of inclination of the experimental tube.

Image group 5.3.b. Distinguishing sediment groups-clusters (on the left) and the remaining material at the beginning of the tube (on the right).

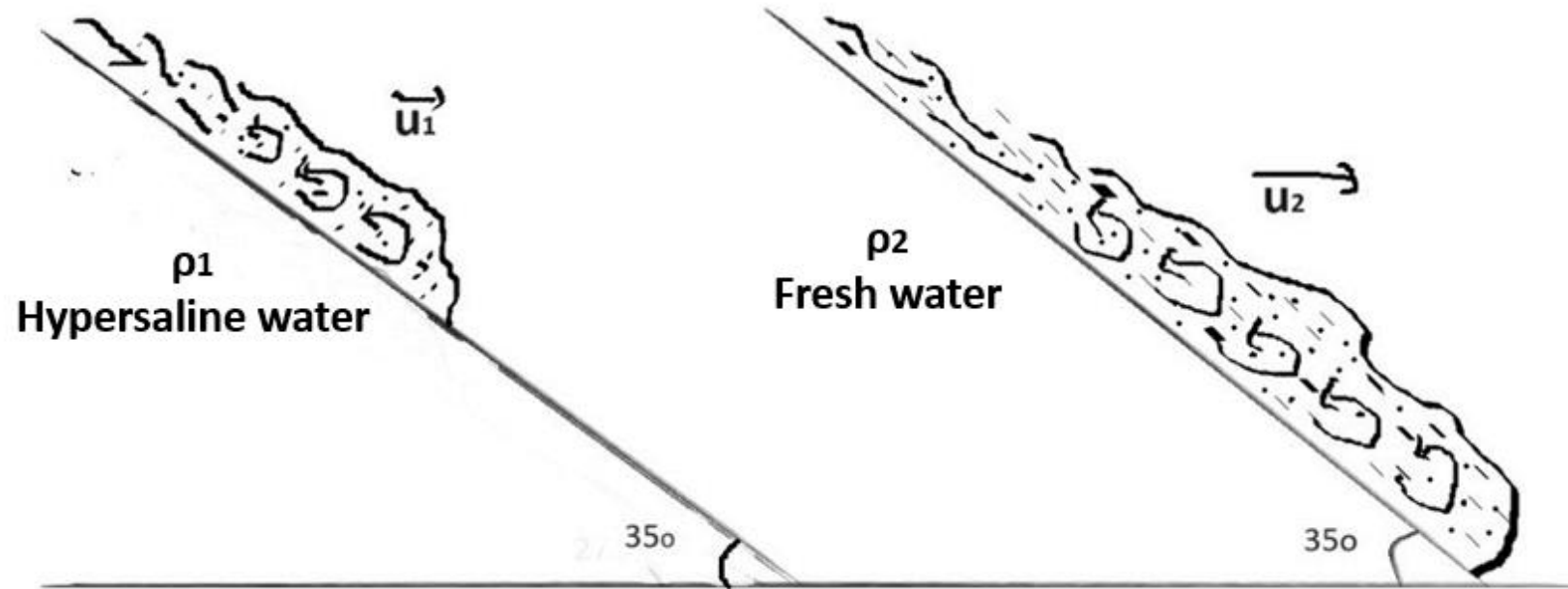
5.4. The main results with graphical approaches.

The overall results of the 48 experiments are summarized as follows, involving average grain size samples of 1.25φ, 2.25φ, and dune's material with grain size ranging from -1.5 to >4.

- The duration of turbidity and the velocity of the forming turbidity-front depend on the slope angle of the tube, the larger the slope angle, the longer the turbidity duration and the higher the velocity of the turbid front (Graphic 1).
- The duration of turbidity and the velocity of the turbidity-front are also influenced by the viscosity of the solution; the higher the viscosity, the shorter the duration and the velocity of the turbidity current (Graphic 2).
- A sheet of sand grains at the bottom of the flow was observed moving with laminar flow. The velocity of the laminal sheet of sand is influenced by the viscosity of the solution, the higher the viscosity, the lower the velocity (Graphic 3).
- The coarser grains of dunes roll at higher velocity than the finer grains, independent of the type of water and the tube angle. (Graphic 4).
- A critical factor in the movement of material within the tube is the amount used. When nearly double the amount of material was used, a higher movement speed of the material was observed at the same inclination angle of the experimental tube compared to the speed with a single quantity of material. Additionally, smaller inclination angles of the experimental tube were noted, where the material started rolling. (Graphic 5).
- It has been observed that after the turbidism of the material, laminal sheet flow of the grains happens as it flows downhill and is organized into clusters forming, something like embryonic sand waves. These clusters are moving with almost double speed than the speed of the initial sheet flow (Graphic 6).
- The wavelength of the forming cluster depends on the viscosity of the solution. The higher the viscosity, the bigger the wavelength of the forming clusters. (Graphic 7).
- The inclination angle of the experimental tube affects the wavelength of the clusters. The greater the inclination angle of the experimental tube, the smaller the wavelength of the clusters. Conversely, the smaller the inclination angle of the tube, the larger the wavelength of the clusters. (Graphic 8).
- The wavelength of the forming clusters depends on the sediment granulometry. The coarser the material, the smaller the wavelength of the clusters. (Graphic 9).



Graphic 1. The duration of turbidity and the velocity of the forming turbidity front depend on the slope angle of the tube, the larger the slope angle, the longer the turbidity duration and the higher the velocity of the turbidity front.

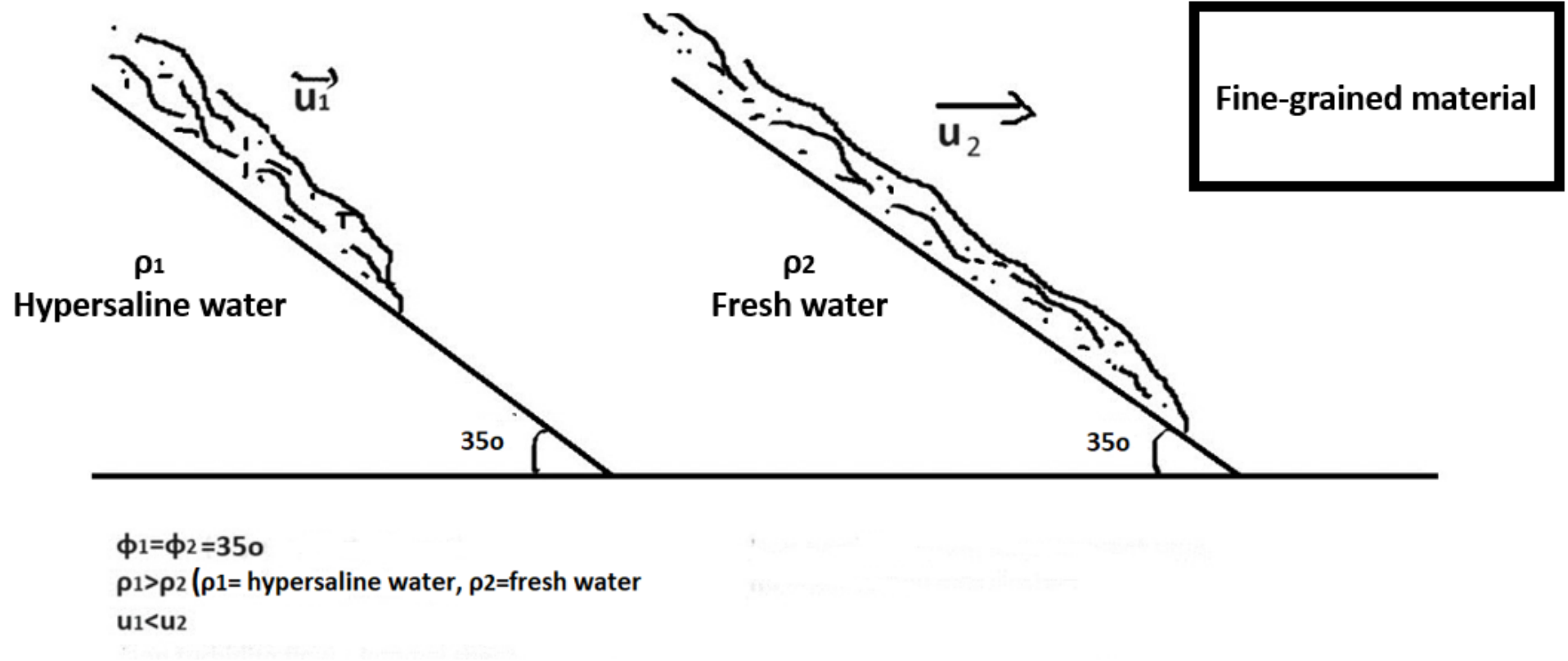


$\rho_1 > \rho_2$ (ρ_1 = hypersaline water, ρ_2 = fresh water)

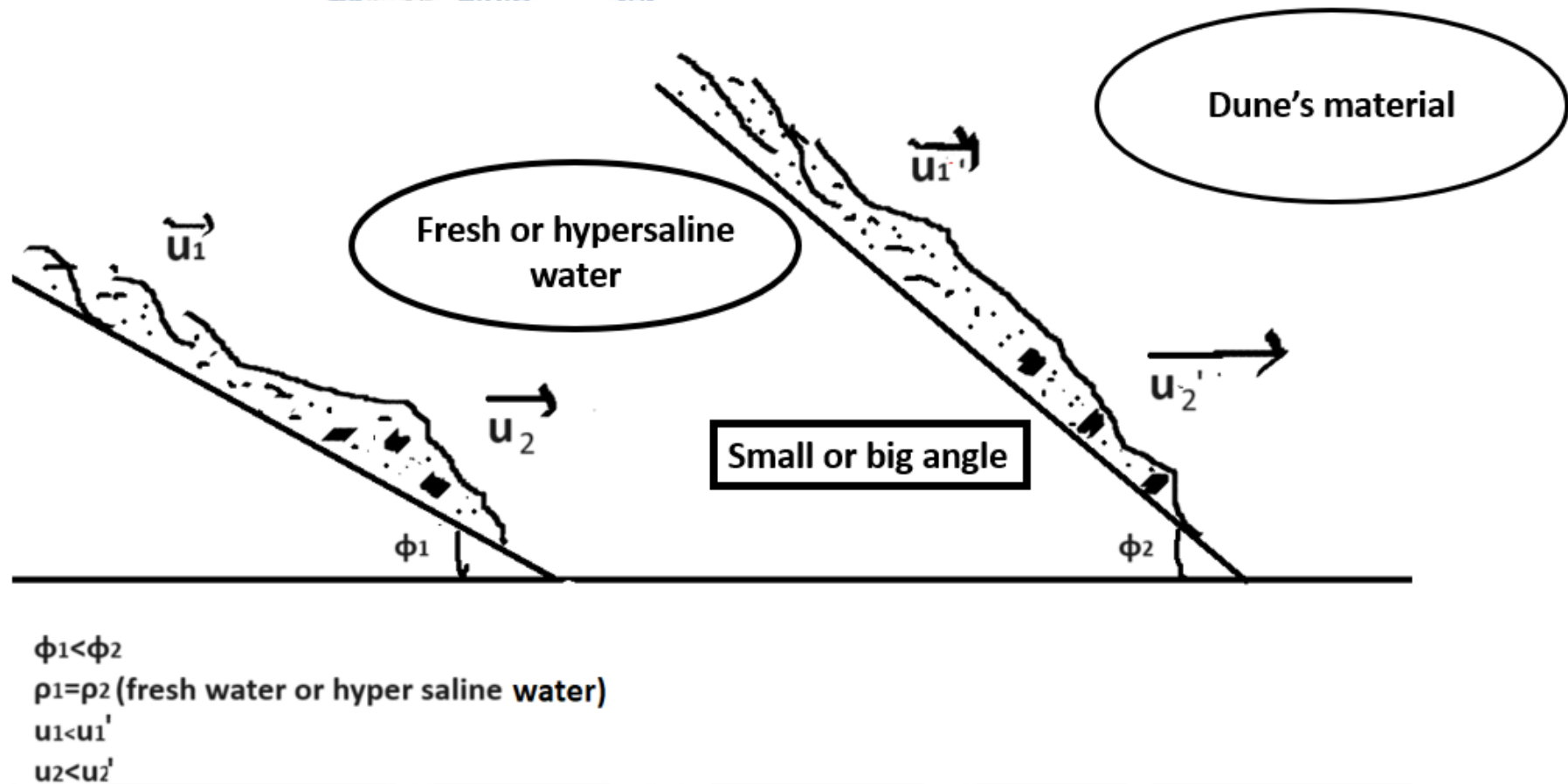
$\phi_1 = \phi_2 = 35^\circ$

$u_1 < u_2$

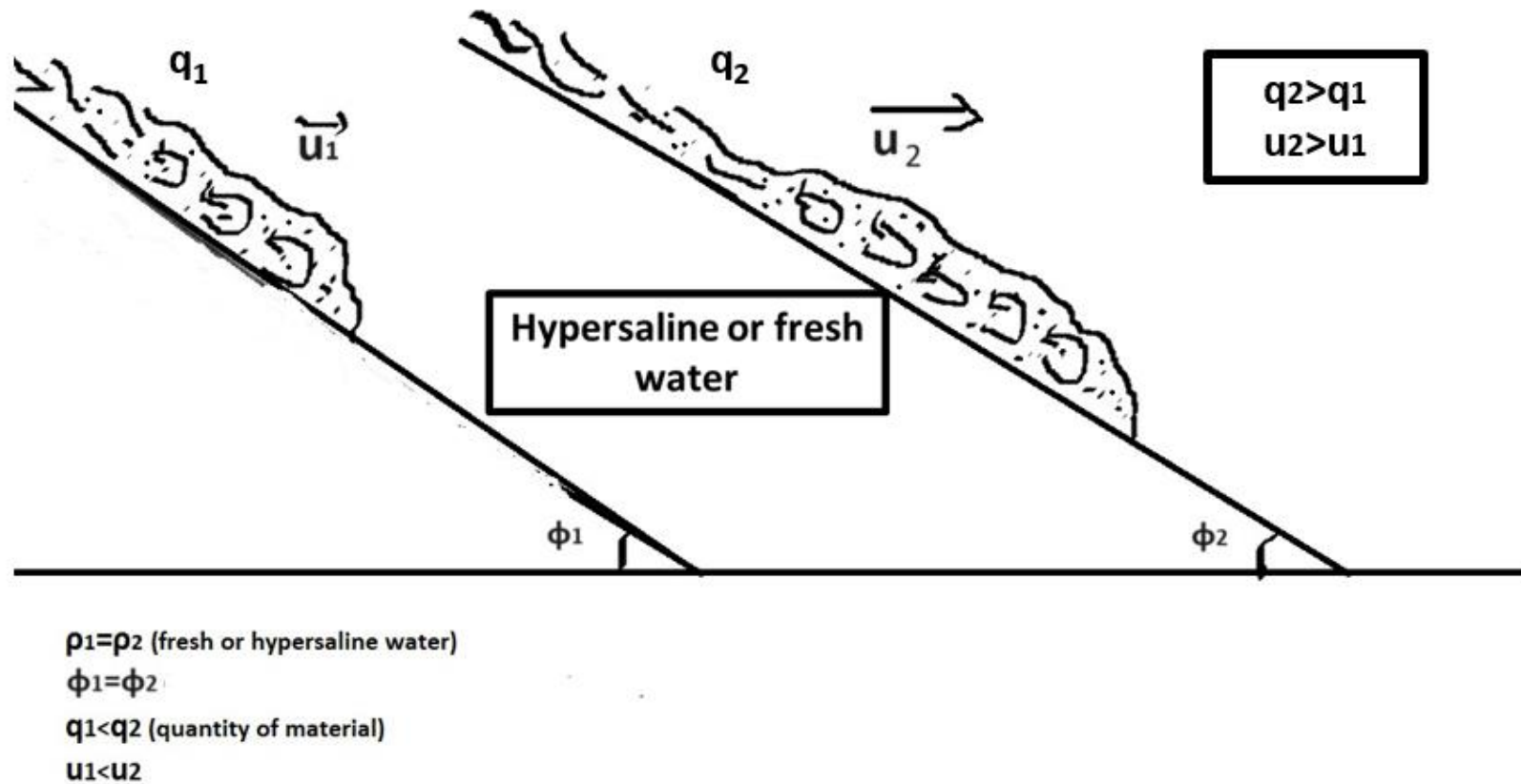
Graphic 2. The duration of the turbidity and the velocity of the forming turbidity-front are also influenced by the viscosity of the respective solution, the higher the viscosity, the shorter the duration and the velocity of the turbidity current.



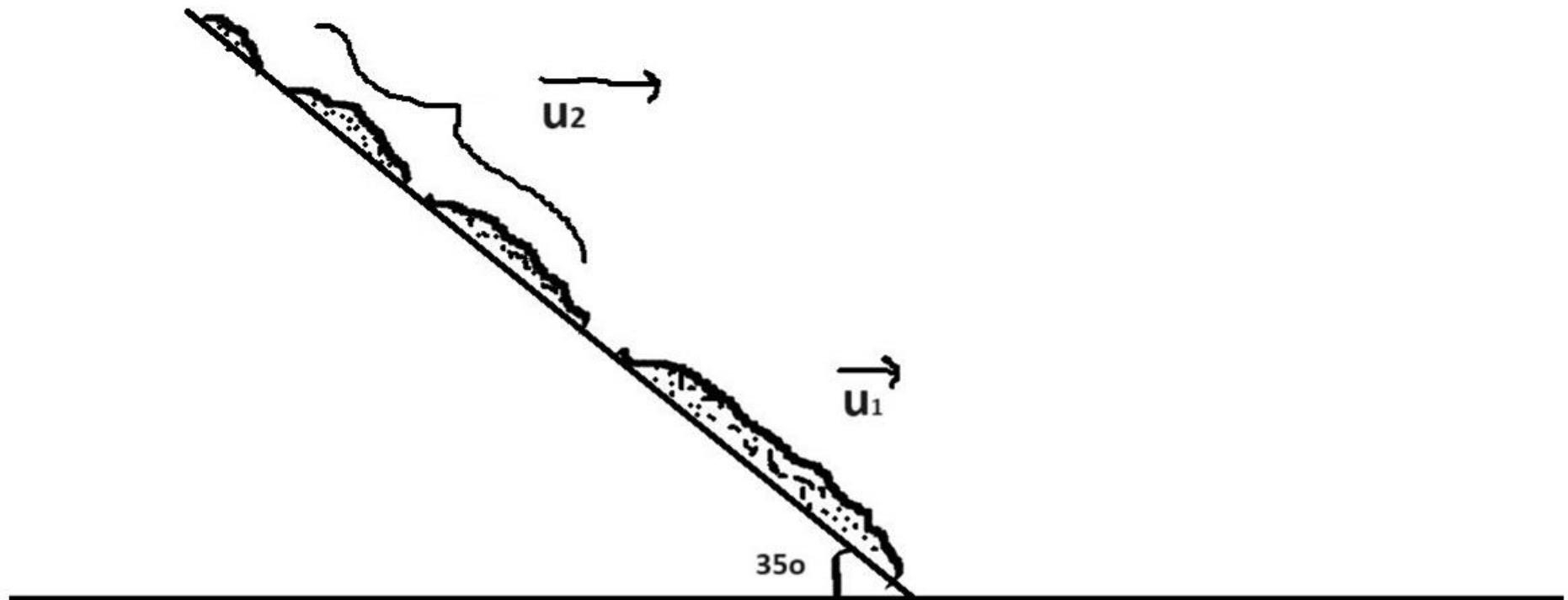
Graphic 3. The fine-grained sand material, moving with laminar flow at the bottom of the pipe. The velocity of the laminar sheet of sand is influenced by the viscosity of the solution, the higher the viscosity, the lower the velocity.



Graphic 4. The coarser grains of the dunes roll at higher velocity independent of the type of water and the tube angle.



Graphic 5. Double the amount of material was used, a higher movement speed of the material was observed at the same inclination angle of the experimental tube compared to the speed with a single quantity of material. Additionally, smaller inclination angles of the experimental tube were noted, where the material started rolling.

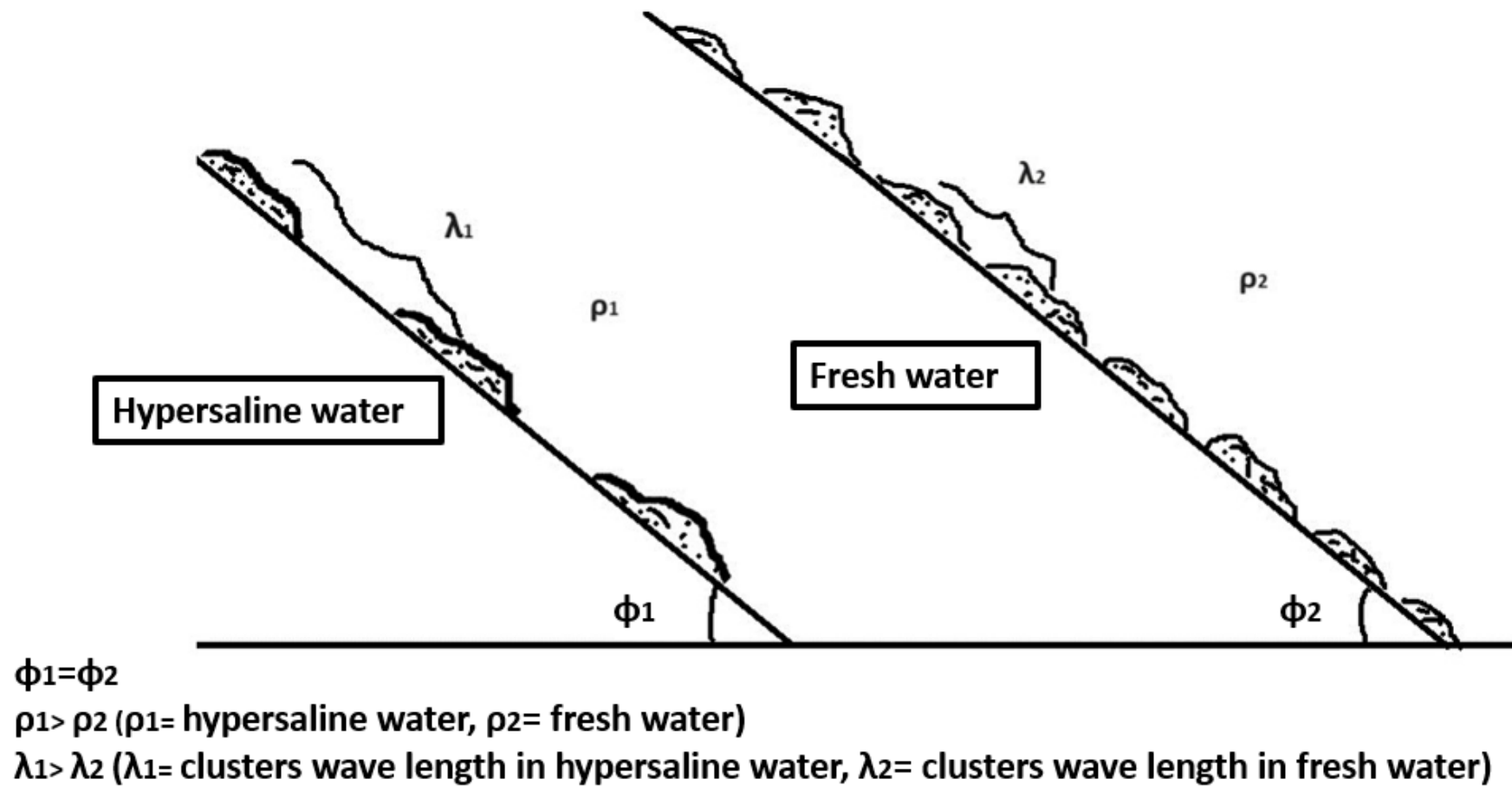


$$|u_2| > |u_1|$$

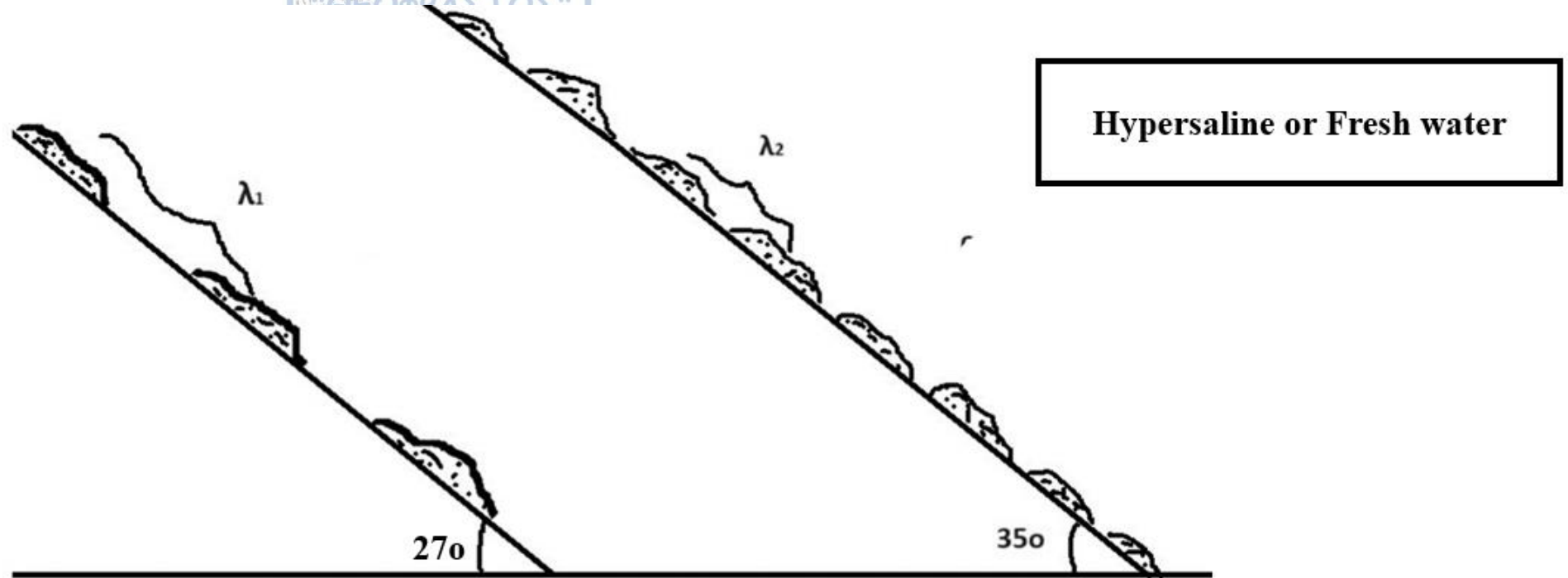
$$|u_2| \approx 2|u_1|$$

u_2 = The velocity of the clusters
 u_1 = The velocity of the unified
sheet

Graphic 6. The laminal sheet flow organized into clusters with almost double speed than the initial sheet flow.

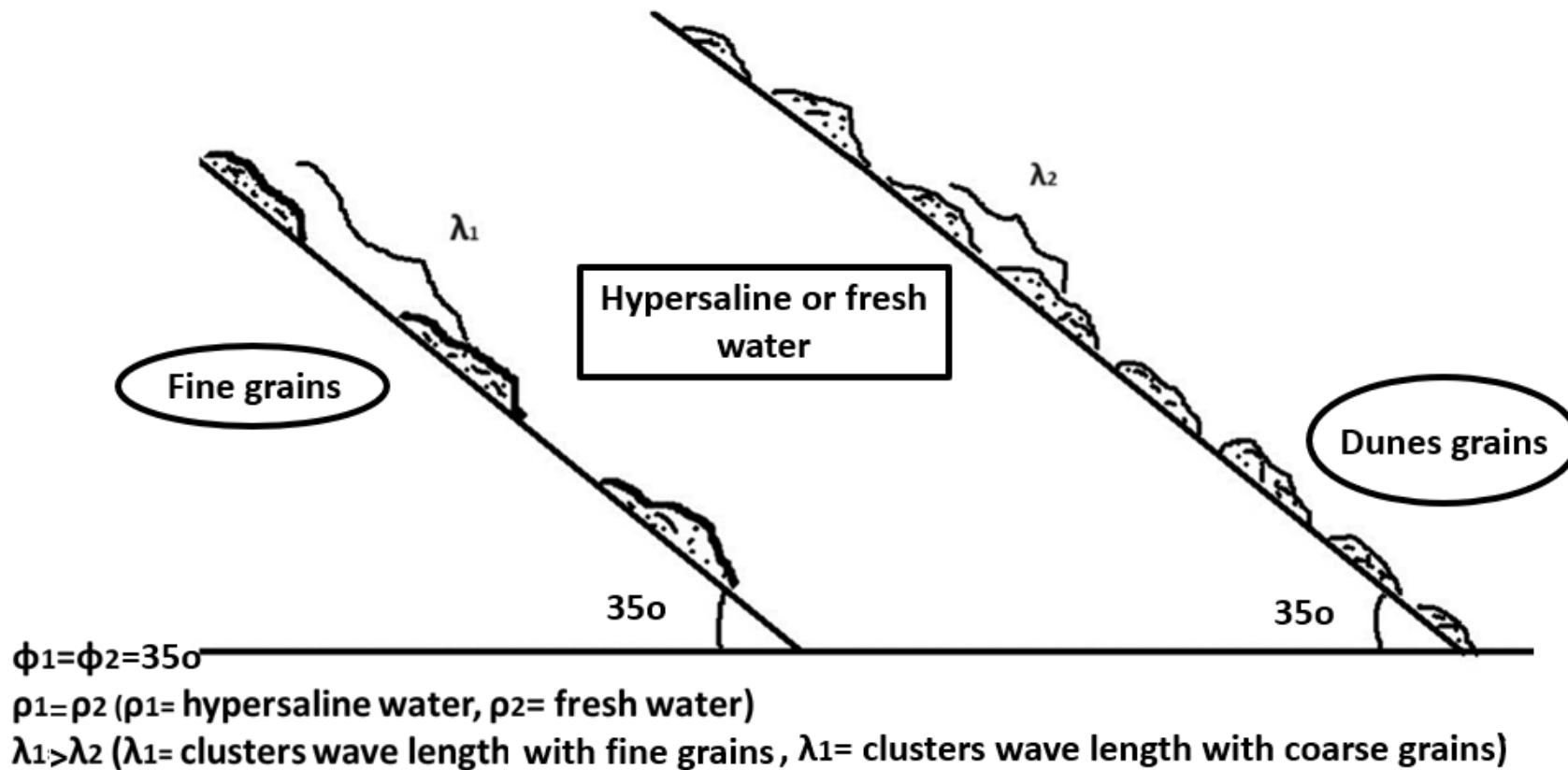


Graphic 7. The wavelength of the forming cluster depends on the viscosity of the solution. The higher the viscosity, the bigger the wavelength of the forming clusters.



$\lambda_1 > \lambda_2$ (λ_1 = clusters wave length with fine grains, λ_2 = clusters wave length with coarse grains)

Graphic 8. The inclination angle of the experimental tube affects the wavelength of the clusters. The greater the inclination angle of the experimental tube, the smaller the wavelength of the clusters. Conversely, the smaller the inclination angle of the tube, the larger the wavelength of the clusters.



Graphic 9. The wavelength of the forming clusters depends on the sediment granulometry. The coarser the material, the smaller the wavelength of the clusters.



6. For further research...

- The turbidity current flows with its coarse-grained material at the front and fine-grained material at the tail. Therefore, at the bottom of the marine basin, the coarse grains are deposited first, followed by the fine grains. The same occurs after the turbidity event has passed, when the material follows a laminar flow. Coarse-grained materials flow at a higher speed than fine-grained ones. As a result, a graded layer of grains/materials forms in the deposition basin, with the coarsest at the base of the basin and the finest toward the top. This means that oil reservoirs have better permeability and porosity, and therefore better recoverability, at the deeper parts of the subsea basin, properties that diminish with decreasing depth due to the smaller size of the grains deposited there. Experiments were conducted not only with tap water but also with hypersaline water. This was done in order to better simulate the conditions that prevailed in the enclosed hypersaline sea of the Mediterranean at the beginning of the Messinian Salinity Crisis.
- From the above experiments, it is concluded that after the end of the turbidity event, the material follows a laminar flow. At that point, it begins to organize into clusters due to the similar grain size and speed of the particles. It is estimated that if the length of the experimental tube were longer, these clusters would form ripples. According to Bouma, ripples are formed due to the flow of water over fine-grained sediment. From the above experiments, it is inferred that ripples can also be created by the consolidation of the forming clusters, that is, by the sediment mass itself flowing toward the base of the basin.

7. Bibliography

- [1] Shanmugam, G. (2000). 50 years of the turbidity paradigm (1950s-1990s): deep- water processes and facies models- a critical perspective (pp. 285-342). Marine and petroleum geology.
- [2] Sanders, J. E. (1965). Primary sedimentary structures formed by turbidity currents and related resedimentation mechanisms. In G. V. Middleton, Primary sedimentary structures and their hydrodynamic interpretation (pp. 192-219), Society of Economic Paleontologists and Mineralogists Special Publication, Vol. 12.
- [3] Middleton. G. V., & Hampton, M. A. (1973). Sediment gravity flows: mechanics of flow and deposition. Proceedings of Pacific Section Society of Economic Paleontologists and Mineralogists, Los Angeles G. V. Middleton, & A. H. Bouma, Turbidites and deep- water sedimentation, 1-38.
- [4] Dott Jr, R. H. (1963). Dynamics of subaqueous gravity depositional processes. American Association of Petroleum Geologists Bulletin, 47, 104-128.
- [5] Bagnold, R. A. (1962). Auto-suspension of transported sediment; turbidity currents. Royal Society of London Proceedings, Series A, 265, 315-319.
- [6] Shanmugam, G. (1996a). High-density turbidity currents: Are they sandy debris flows? Journal of Sedimentary Research, 66, 2-10.
- Shanmugam, G.(1996b). Perception vs reality in deep-water exploration. World Oil, 217, 37-41.
- [7] Shanmugam, G. (1997a). The Bouma Sequence and the turbidity mind set. Earth-Science Reviews, 42, 201-229.
- Shanmugam, G. (1997b). Slope turbidity packets in a fore-arc basin fill sequence of the Plio-Pleistocene Kakegawa Group: Their formation and sea-level changes_ Discussion. Sedimentary Geology, 112, 297-300.
- Shanmugam, G. (1997c). Deep-water exploration: Conceptual models and their uncertainties. NAPE (Nigerian Association of Petroleum Explorationists) Bulletin, 12/01, 11-28.
- [8] Enos, P. (1977). Flow regimes in debris flow. Sedimentology, 24, 133-142.
- [9] Pierson, T. C., & Costa, J. E. (1987). A rheologic classification of subaerial sediment-water flows. In J. E. Costa, & G. F. Wieczorek, Debris flows/ avalanches: process, recognition and mitigation, vol. VII (pp. 1-12)., Geological Society of America Reviews in Engineering Geology.
- [10] Philips, C. J., & Davies, T. R. H. (1991). Determining rheological parameters of debris flow material. *Geomorphology*, 4, 101-110.
- [11] Middleton, G. V. & Wilcock, P. R. (1994). In Mechanics in the earth and environmental sciences (pp.459). Cambridge, UK: Cambridge University Press.

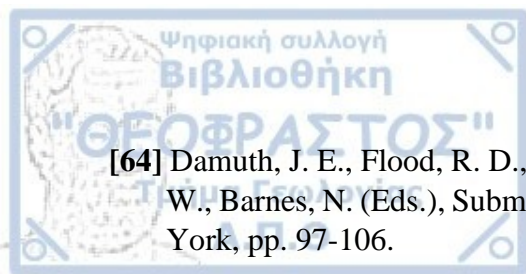
- [12] Lowe, D. R. (1979). Sediment gravity flows: their classification and some problems of application to natural flows and deposits. In L. J. Doyle, & O. H. Pilkey, *Geology of Continental Slopes* (pp. 75-82), Society of Economic Paleontologists and Mineralogists Special Publication, Vol 27.
- [13] Nardin, T. R., Hein, F. J., Gorsline, D. S. & Edwards, B. D. (1979). A review of mass movement processes, sediment and acoustic characteristics and contrasts in slope and base of slope systems versus canyon fan basin floor systems. In L. J. Doyle, & Pilkey, *Geology of continental slopes* (pp. 61-73), Economic Paleontologists and Mineralogists Special Publication, Vol. 27.
- [14] Oakeshott, J. M. (1989). Aspects of depositional mechanisms of high concentration sediment gravity flows. Unpublished Ph. D. thesis, Keele, University of Keele, 502 pp.
- [15] Middleton, G. V. (1993). Sediment deposition from turbidity currents. *Annual Review Earth Planetary Sciences*, 21, 89-114.
- [16] Pickering, K. T., Hiscott, R. N. & Hein, F. J. (1989). In *Deep-marine environments* (pp. 416). London: Unwin Hyman.
- [17] Assier-Rzadkiewicz, S., 1997. Etude numérique et expérimentale d'un glissement de sédiments le long d'une pente sous-marine et des vagues générées. Thèse de doctorat, Univ. Montpellier II.
- [18] Hay, A.E., 1987. Turbidity currents and submarine channel formation in Rupert Inlet, British Columbia 2. The roles of continuous and surge-type flow. *J. Geophys. Res.* 92, 2883–2900.
- [19] Komar, P.D., 1977. Computer simulation of turbidity current flow and the study of deep-sea channels and fan sedimentation. In: Goldberg, E.D., McCave, I.N., O'Brien, J.J., Steele, J.H. (Eds.), *The Sea*, v.6, Marine Modelling. John Wiley, New York, pp. 603–621.
- [20] Bowen, A.J., Normark, W.R., Piper, D.J.W., 1984. Modelling of turbidity currents on Navy Submarine Fan, California Continental Borderland. *Sedimentology* 31, 169-185.
- [21] Middleton, G.V., 1966b. Experiments on density and turbidity currents: II. Uniform flow of density currents. *Can. J. Earth Sci.* 3, 627–637.
- [22] Beghin, P., 1979. Etude des bouffées bidimensionnelles de densité en écoulement sur pente avec application aux avalanches de neige poudreuse. Thèse de doctorat, Université Scientifique et Médicale de Grenoble et Institut National Polytechnique de Grenoble, 120pp.
- [23] Hinze, J. O., 1960. On the hydrodynamics of turbidity currents. *Geol. Mijnbouw* 39, 18-25.
- [24] Plapp, J. R., Mitchell, J. P., 1960. A hydrodynamic theory of turbidity currents. *J. Geophys. Res. B.* 65 (3), 983-992.
- [25] Naaïm, M., 1995. Modelisation numerique des avalanches aerosols. *Houille Blanche* 6 (5), 56-62.

- [26] D' Ambrosio, D., Di Georgio, S., Iovine, G., 2003. Simulating debris flows through a hexagonal Cellular Automata model: Sciddica S3-hex. *Nat. Hazards Earth Syst. Sci.* 3, 545-559.
- [27] Piper, D. J. W., Savoye, B., 1993. Process of late Quaternary turbidity current flow and deposition on the Var deep-sea fan, north-west Mediterranean Sea. *Sedimentology* 40, 557-583.
- [28] Nisbet, E. G., Piper, D. J. W., 1998. Giant submarine landslides: Slumps, megaturbidites and their impact. *Nature* 392, 329-330.
- [29] Piper, D. J. W., Asku, A. E., 1987. The source and origin of the 1929 Grand Banks turbidity current inferred from sediment burgets. *Geo-Mar. Lett.* 7, 177-182.
- [30] Piper, D. J. W., Normark, W. R., 2009. Process that initiates turbidity currents and their influence on turbidites: A marine geology perspective. *J. Sediment. Res.* 79 (5), 347-362.
- [31] Flood, R. D., Damuth, J. E., 1987. Quantitative characteristics of sinuous distributary channels on the Amazon deep-sea fan. *Geol. Soc. Am. Bull.* 98, 728-738.
- [32] Flood, R. D., Manley, P. L., Kowsmann, R. O., Appi, C. J., Pirmez, C., 1991. Seismic facies and late Quaternary growth of Amazon submarine fan. In: Weimer, P., Link, M. H. (Eds.), *Seismic Facies and Sedimentary Process of Modern and Ancient Submarine Fans and turbidity systems*. *Frontiers in sedimentary geology*. Springer-Verlag, New York Inc., 415-433.
- [33] Cirac, P., Bourillet, J.-F., Griboulard, R., Normand, A., Mulder, T., The ITSAS Shipboard Scientific Party, 2001. Le canyon de Capbreton: Nouvelles approches morphostructurales et morphosedimentaires Premiers resultants de la campagne Itsas. *C. R. Acad. Sci. Paris* 332, 447-455.
- [34] Gaudin, M., Mulder, T., Cirac, P., Berne, S., Imbert, P., 2006b. Past and present sedimentary activity in the Capbreton Canyon, southern Bay of Biscay. In: Mulder, T. (Ed.), *Geo-Marine Letters*, vol. 26 (6), 331-345 *Secial Issue on 'Deep-Sea Turbidity Systems on French Margins'*.
- [35] Shepard, F. P., Dill, R. F., 1966. *Submarine Canyons and other Sea-Valleys*. Rand McNally, Chicago, IL381pp.
- [36] Rigaut, F., 1997. Analyse et evolution recente d'un systeme turbiditique meandriforme: l'eventail profond du Zaire. Unpubl. Ph. D. thesis, Univ. Bretagne Occidentale., 209pp.
- [37] Shepard, F. P., 1981. Submarine canyons: multiple causes and long-time persistence. *Am. Assoc. Pet. Geol. Bull.* 65, 1062-1077.
- [38] Gaudin, M., 2006. Processus et enregistrements sedimentaires dans les canyons sour-marins Bourcart et de Capbreton Durant le dernier cycle clymatique. Unpubl. Ph. D. thesis, Univ. Bordeaux 1, no. 3122, 296pp.
- [39] Normark, W. R., Carlson, P. R., 2003. Giant submarine canyons: Is size any clue to their importance in the rock record. In: Chan, M. A., Archer, A. W. (Eds.), *Extreme Depositional*

Environments: Mega end members in Geologic time, Geological Society of America, Special Paper, 1-15.

- [40] Clauzon, G., 1978. The Messinian Var Canyon (Provence, southern France). Paleogeographic implications. *Mar. Geol.* 27 (3/4), 231-246.
- [41] Guillocheau, F., Pautot, G., Auzende, J.-M., 1983. Les canyons du Var et du Paillon (marge des Alpes meridionales-Mediterranee occidentale): une origine quaternaire par glissement. *C. R. Acad. Sci. Paris* 296, 91-96.
- [42] Mulder, T., Cirac, P., Gaudin, M., Bourillet, J.-F., Tranier, J., Normand, A., et al., 2004. Understanding continent-ocean sediment transfer. *EOS American Geophysical Union Transaction* 257, 261-262.
- [43] Pratson, L. F., & Haxby, W. F. (1996). What is the slope of the US continental slope, *Geology*, 24, 3-6.
- [44] Mulder, T., Zaragosi, S., Razin, P., Grelaud, K., Lanfumey, V., Bavoil, F., 2009b. A new conceptual model for the deposition process of homogenite: Application to a Cretaceous megaturbidity of the western Pyrenees (Basque region, SW France). *Sediment. Geol.* 222, 263-273.
- [45] Genesseeux, M., Guibout, M., Lancombe, H., 1971. Enregistrement de courants de turbidity dans la vallee sous-marine du Var (Alpes-Maritimes). *C. R. Acad. Sci. Paris D* 273, 2456-2459.
- [46] Inman, D. L., 1970. Strong currents in submarine canyons. *Abstr. Trans. Am. Geophys. Union* 51, 319.
- [47] Shepard, F. P., McLoughlin, P. A., Marshall, N. F., Sullivan, G. G., 1977. Current-meter recordings of low-speed turbidity currents. *Geology* 5, 297-301.
- [48] Shepard, F. P., Marshall, N. F., McLoughlin, P. A., Sullivan, G. G., 1979. Currents in submarine canyons and other sea valleys. *American Association of Petroleum Geologists, Studies in Geology*, No. 8, 173pp.
- [49] Pratson, L. F., Ryan, W. B. F., Mountain, G. S., Twichell, D. C., 1994. Submarine canyon initiation by downslope-eroding sediment flows: evidence in late Cenozoic strata on the New Jersey continental slope. *Geol. Soc. Am. Bull.* 106, 395-412.
- [50] Palanques, A., Guillen, J., Puig, P., Durrieu de Madron, X., 2008. Storm-driven shelf-to-canyon suspended sediment transport at the southwestern Gulf of Lions. *Cont. Shelf Res.* 28 (15), 1947-1956.
- [51] Porebski, S. J., Steel, R. J., 2003. Self-margin deltas: their stratigraphic significance and relation to deep water sands. *Earth Sci. Rev.* 62 (3-4), 283-326.
- [52] Posamentier, H., Allen, G. P., James, D. P., Tesson, M., 1992. Forced regression in a sequence stratigraphic framework: Concepts, examples and exploration significance. *Am. Assoc. Pet. Geol. Bull.* 76, 1687-1709.

- [53] Rouillard, P., 2010. Modele architectural et lithologique du systeme de Rosetta (Delta du Nil, Mediterranee Orientale): Implications pour un analogue actuel de reservoir petrolier. Unpubl. Ph. D. thesis, Universite de Nice Sophia-Antipolis, 375pp.
- [54] Sydow, J., Roberts, H. H., 1994. Stratigraphic framework of Late Pleistocene shelf-edge delta, northeast Gulf of Mexico. Am. Assoc. Pet. Geol. Bull. 78, 1276-1312.
- [55] Coleman, J. M., Prior, D. B., Lindsay, J. F., 1983. Deltaic influences on shelf edge instability process. In: Stanley, D. J., Moore, G. T. (Eds.), The Shelf break, Critical Interface on Continental Margins, 121-137.
- [56] Babonneau, N., 2002. Mode de fonctionnement d'un chenal turbiditique meandriforme: cas du systeme turbiditique actuel du Zaire. Unpubl. Ph. D., Univ. Bordeaux 1, 308pp.
- [57] Babonneau, N., Savoye, B., Cremer, M., Bez, M., 2004. Multiple terraces within the deep incised Zaire Valley (ZaiAngo Project): Are they confined levees. In: Lomas, S., Joseph, P., (Eds.), Confined Turbidity Systems, Geological Society, London, Special Publication, 222, 91-114.
- [58] Garlan, T., 2004. Apports de la modelisation dans l' etude de la sedimentation marine recente. Memoire d' Habilitation a Diriger les Recherches, Universite des Sciences et Techniques de Lille 158pp.
- [59] Ferry, J.-N., 2004. Developpement et geometrie des corps sableux de pente, de glaciais et du bassin profond, sur le prisme sedimentaire progradant (Oligocene Pliocene) de la marge ouest africaine entre le Sud-Gabon et l' Angola. Unpubl. Ph. D. thesis, Univ. Bordeaux 1, 482pp.
- [60] Beaubouef, R. T., Friedmann, S. J., 2000. High resolution seismic/sequence stratigraphic framework for the evolution of Pleistocene intra slope basins, Western Gulf of Mexico: Depositional models and reservoir analogs. In: Weimer, P., Slatt, R. M., Coleman, J., Rosen, N. C., Nelson, H., Bouma, A. H., Styzen, M. J., Lawrence, D. T. (Eds.), Deep-water reservoirs of the world. GCSSEPM Foundation 20th Annual research conference, Dec. 3-6, Houston, Gulf Coast Section-SEPM Special Publication, pp, 40-60.
- [61] Pirmez, C., Flood, R. D., 1995. Morphology and structure of Amazon Channel. Proceedings of the Ocean Drilling Program, Initial Reports 155, 23-45
- [62] Pirmez, C., Beaubouef, R. T., Friedmann, S. J., Mohrig, D. C., 2000. Equilibrium profile and baselevel in submarine channels: Examples from Late Pleistocene systems and implications for the architecture of deep-water reservoir. In: Weimer, P., Slatt, R. M., Coleman, J., Rosen, N. C., Nelson, H., Bouma, A. H., Styzen, M. J., Lawrence, D. T. (Eds.), Deep-water reservoirs of the world, GCSSEPM, Foundation 20th Annual research conference, Dec. 3-6, Houston, Gulf Coast Section-SEPM Special Publication, pp, 782-805.
- [63] Bonnel, C., 2005. Mise en place des lobes distaux dans les systemes turbiditiques actuels: Analyse compare des systemes du Zaire, Van et Rhone. Unpubl. Ph. D. thesis, Univ. Bordeaux 1, 293pp.

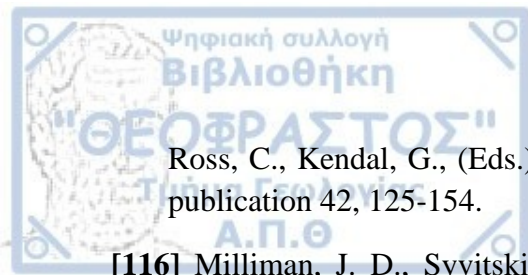


- [64] Damuth, J. E., Flood, R. D., 1985. Amazon fan, Atlantic Ocean. In: Bouma, A., Normark, W., Barnes, N. (Eds.), Submarine fans and related turbidity systems. Springer-Verlag, New York, pp. 97-106.
- [65] Cremer, M., 1983. Approches sedimentologiques et geophysiques des accumulations turbiditiques. L'eventail profond du Cap-Ferret (Golfe de Gascogne), La serie des gres d' Annot (Alpes de Hautes Provence). Unpubl. Thesis, Univ. Bordeaux 1, 334pp.
- [66] Piper, D. J. W., Stow, D. A. V., Normark, W. R., 1984. Laurentian Fan: Sohm abyssal plain. *Geo-Mar. Lett.* 3, 141-146.
- [67] Savoye, B., Piper, D. J. W., Droz, L., 1993. Plio-pleistocene evolution of the Var deep-sea fan on the French Riviera. *Mar. Pet. Geol.* 10, 550-571.
- [68] Klaucke, I., Hesse, R., Ryan, W. B. F., 1998. Seismic stratigraphy of the Northwest Atlantic Mid-Ocean channel: growth pattern of a mid-ocean channel-levee complex. *Mar. Pet. Geol.* 15, 575-585.
- [69] Piper, D. J. W., Hiscott, R. N., Normark, W. R., 199b. Outcrop scale acoustic facies analysis and latest Quaternary development of Hueneme and Dune submarine fans, offshore California. *Sedimentology* 46, 47-78.
- [70] Komar, P. D., 1969. The channelized flow of turbidity currents with application to Monterey deep sea Fan channel. *J. Geophys. Res. B* 74, 4544-4558.
- [71] Hiscott, R. N., Hall, F. R., Pirmez, C., 1997. Turbidity current overspill from the Amazon channel: texture of the silt/sand load, paleo flow from anisotropy of the magnetic susceptibility, and implications for flow processes. In: Flood, R. D., Piper, D. J. W., Klaus, A., Peterson, L. C. (Eds.), *Proc. ODP, Sci. Results*, 155, 53-78, College Station, TX.
- [72] Piper, D. J. W., Normark, W. R., 1983. Turbidity depositional patterns and flow characteristics. Navy Submarine fan, California Borderland, *sedimentology* 30, 681-694.
- [73] Masson, D. G., Kenyon, N. H., Gardner, J. V., Field, M. E., 1995. Monterey fan: Channel and overbank morphology. In: Pickering, K. T., Hiscott, R. N., Kenyon, N. H., Ricci, Luchi, Smith, R. D. A. (Eds.), *Atlas of deep-water environments: Architectural style in turbidity systems*. Chapman et Hall, London, pp. 74-79.
- [74] Piper, D. J. W., Deptuck, M., 1997. Fine-grained turbidites of the Amazon Fan: Facies characterization and interpretation. In: Flood, R. D., Piper, D. J. W., Klaus, A., Peterson, L. C. (Eds.), *Proc. ODP, Sci. Results*, 155, 79-108 College Station, TX.
- [75] Migeon, S., 2000. Dunes Geantes et levees Sedimentaires en domaine marin profond: approches morphologique, sismique et sedimentologique. These, Universite Bordeaux I, 288pp.
- [76] Migeon, S., Savoye, B., Zanella, E., Mulder, T., Faugeres, J-C., Weber, O., 2001. Detailed seismic-reflection and sedimentary study of turbidity sediment waves on the Var sedimentary Ridge (SE France): significance for sediment transport and deposition and for the mechanisms of sediment-waves construction. *Mar. Pet. Geol.* 18, 179-208.

- [77] Skene, K. I., 1998. Architecture of submarine channel levees. Unpubl. Ph. D. thesis, Dalhousie University, Halifax, 413pp.
- [78] Allen, J. R. L., 1982. Sedimentary structures: their characters and physical basis, in Developments in Sedimentology, v I and II. Elsevier, Amsterdam.
- [79] Flood, R. D., 1988. A lee wave model for deep-sea mud wave activity. Deep-Sea Res. 35, 973-983.
- [80] Kneller, B. C., Buckee, C., 2000. The structure and fluid mechanics of turbidity currents: a review of some recent studies and their geological implications. Sedimentology 57 (Suppl. 1), 62-94.
- [81] Deptuck, M. E., Sylvester, Z., Pirmez, C., O'Byrne, C., 2007. Migration-aggradation history and 3D seismic geomorphology of submarine channels in the Pleistocene Benin-major Canyon, western Niger Delta slope. Mar. Pet. Geol., 24, 406-433.
- [82] Berne, S., Loubrieu, B., THE CALMAR Shipboard Party, 1999. Canyons et processus sedimentaires recents sur la marge occidentale du Golfe du Lion. Premiers resultats de la campagne Calmar. C. R. Acad. Sci. Paris 328, 471-477.
- [83] Kenyon, N. H., Amir, A., Cramp, A., 1995. Geometry of the younger sediment bodies of the Indus Fan. In: Pickering, K. T., Hiscott, R. N., Kenyon, N. H., Lucchi, Ricci, Smith, R. D. A. (Eds.), Atlas of Deep-Water Environments: Architectural style in turbidity systems. Chapman et Hall, London, pp. 89-93.
- [84] Pichevin, L., Mulder, T., Savoye, B., Cremer, M., Piper, D. J. W., Gervais, A., 2003. The Golo submarine system (east-Corsica margin): turbidity system morphology and processes of terrace formation from high resolution seismic Boomer profiles. Geo-Mar. Lett. 23 (2), 117-124.
- [85] Tranier, J., 2002. Etude des processus sedimentaires dans la parties superieure du canyon de Capbreton. Origine des terrasses. Unpubl. Master thesis, Univ. Bordeaux 1, 31pp.
- [86] Hubsher, C., Spiess, V., Breitzke, M., Weber, M. E., 1997. The youngest channel-levee system of the Bengal Fan: results from digital sediment echosounder data. Mar. Geol. 141, 125-145.
- [87] Damuth, J. E., Flood, R. D., Kowsmann, R. O., Belderson, R. H., Gorini, M. A., 1988. Anatomy and growth pattern of Amazon deep-sea fan as related by long-range side-scan sonar (GLORIA) and high resolution seismic studies. Am. Assoc. Pet. Geol. Bull. 72 (8), 885-911.
- [88] Nakajima, T., Satoh, M., Okamura, Y., 1998. Channel-levee complexes, terminal deep-sea fan and sediment wave fields, associated with the Toyama Deep-Sea Channel system in the Japan Sea. Mar. Geol. 149, 24-41.
- [89] Mc Hargue, T., Webb, J. E., 1986. Internal geometry, seismic facies and petroleum potential of canyons and inner fan channels of the Indus Submarine fan. Am. Assoc. Pet. Geol. Bull. 70, 161-180.

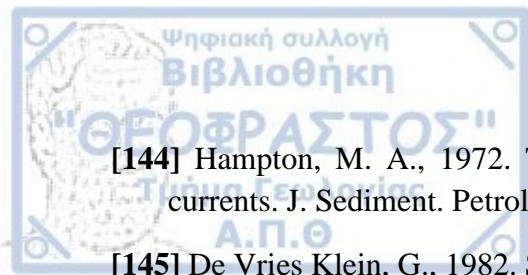
- [90] Liu, C. S., Lundberg, N., Reed, D. L., Lu, H. Y., 1993. Morphological and seismic characteristics of the Kaoping submarine canyon. *Mar. Geol.* 111, 93-108.
- [91] Cramez, C., Jackson, M. P. A., 2000. Superposed deformation straddling the continental oceanic transition in deep-water Angola. *Mar. Pet. Geol.* 17, 1095-1109.
- [92] O' Connel, S., McHugh, C., Ryan, W. B. F., 1995. Unique fan morphology in an entrenched Talweg channel on the Rhone fan. In: Pickering, K. T., Hiscott, R. N., Kenyon, N. H., Lucchi, Ricci, Smith, R. D. A. (Eds.), *Atlas of Deep-Water environments; Architectural style in turbidity systems*. Chapman et Hall, London, pp. 80-83.
- [93] Torres, J., Droz, L., Savoye, B., Terentieva, E., Cochonat, P., Kenyon, N. H., et al., 1997. Deep sea avulsion and morpho-sedimentary evolution of the Rhone Fan Valley and Neofan during the Late Quaternary (north-western Mediterranean Sea). *Sedimentology* 44, 457-477.
- [94] Hagen, R. A., Bergersen, D. D., Moberly, R., Coulbourn, W. T., 1994. Morphology of a large meandering submarine canyon system on the Peru- Chile forearc. *Mar. Geol.* 119, 7-38.
- [95] Von Rad, U., Tahir, M., 1997. Late Quaternary sedimentation on the outer Indus shelf and slope (Pakistan): evidence from high-resolution seismic data and coring. *Mar. Geol.* 138, 193-236.
- [96] Normark, W. R., 1970. Growth patterns of deep-sea fans. *Am. Assoc. Pet. Geol. Bull.* 54 (11), 2170-2195.
- [97] Normark, W. R., 1978. Fan valleys, channels and depositional lobes on modern submarine fans: characters for recognition of sandy turbidity environments. *Am. Assoc. Pet. Geol. Bull.* 62 (6), 912-931.
- [98] Gervais, A., 2002. Analyse multi-echelles de la morphologie, de la geometrie et de l'architecture d'un systeme turbiditique sableux profond (systeme du Golo, marge est-Corse, mer Mediterranee). Unpubl. Ph. D. thesis, Univ. Bordeaux 1, 288pp.
- [99] Gervais, A., Savoye, B., Mulder, T., Piper, D. J. W., Cremer, M., Pichevin, L., 2004. Present morphology and depositional architecture of a sandy submarine system: The Golo turbidity system (Eastern margin of Corsica). In: Lomas, S., Joseph, P. (Eds.), *Confined Turbidity Systems*, Geological Society, London, Special Publication, 222, 59-89.
- [100] Bouma, A., Normark, W., Barnes, N. (Eds.), 1985. *Submarine fans and related turbidity systems*. Springer-Verlag, New York 351pp.
- [101] Jerou, I., 2008. Etude de la transition chenel/levee/lobe dans les systemes turbiditiques recents. Application a l'eventail turbiditique de l'Amazone et au neofan du Petit-Rhone. Unpubl. Ph. D. thesis, Univ. Bretagne Occidentale 1, 351pp.
- [102] Wynn, R. B., Kenyon, N. H., Masson, D. G., Stow, D. A. V., Weaver, P. P. E., 2002. Characterization and recognition of deep water channel-lobe transition zones. *Am. Assoc. Pet. Geol. Bull.* 86 (8), 1441-1446.

- [103] Normark, W. R., Piper, D. J. W., Hess, G. R., 1979. Distributary channels, sand lobes and mesotopography of navy submarine fan, California Borderland with application to ancient fan sediments. *Sedimentology* 26, 749-774.
- [104] Normark, W. R., Piper, D. J. W., Stow, D. A. V., 1983. Quaternary development of channels, levees and lobes on middle Laurentian Fan. *Am. Assoc. Pet. Geol. Bull.* 67 (9), 1400-1409.
- [105] Morris, W. R., Kenyon, N. H., Limonov, A., Alexander, J., 1998. Downstream changes of large scale bedforms in turbidites around the Valencia channel mouth, north west Mediterranean: implications for paleo flow reconstruction. *Sedimentology* 45 (2), 365-377.
- [106] Savoye, B., Cochonat, P., Apprioual, R., Bain, O., Baltzer, A., Bellec, V., et al., 2000. Structure and recent evolution of the Zaire deep sea fan: preliminary results of the Zaiango 1&2 cruises (Angola- Congo margin). *C. R. Acad. Sci. IIA* 331 (3), 211-220.
- [107] Twitchell, D. C., Kenyon, N. H., Parsons, L. M., Mc Gregor, B. A., 1991. Depositional patterns of the Mississippi fan surface: Evidence from GLORIA II and high-resolution seismic profiles. In: Link, M. L. (Ed.), *Seismic facies and sedimentary process of submarine fans and turbidity systems*. Springer-Verlag New York, pp. 349-363.
- [108] Mutti, E., Ricci Lucchi, F., 1972. Le torbiditi dell' Appennino settentrionale: introduction all' analisi de facies. *Mem. Soc. Geol. It.* 11, 161-199.
- [109] Gardner, J. V., Bohannon, R. G., Field, M. E., Masson, D. G., 1996. The morphology, process and evolution of Monterey Fan: a revisit. In: Gardner, J. V., Field, M. E., Twitchell, D. G., (Eds.), *Geology of United States seafloor. The view from GLORIA*. Cambridge University Press, Cambridge, UK, pp. 193-220.
- [110] Jerou, I., Savoy, B., Primez, C., Droz, L., 2008. Channel mouth lobe complex of the recent Amazon fan: the missing piece. *Mar. Geol.* 252, 62-77.
- [111] Deptuck, M. E., Piper, D. J. W., Savoye, B., Gervais, A., 2008. Dimensions and architecture of late Pleistocene submarine lobes off the northern margin of East Corsica. *Sedimentology* 926, 1-32.
- [112] Prelat, A., Hodgson, D. M., Flint, S. S., 2009. Evolution, architecture and hierarchy of distributary deep water deposits: a high-resolution outcrop investigation from the Permian Karoo Basin, South Africa, *Sedimentology* 56, 2132-2154.
- [113] Mulder, T., Etienne, S., 2010. Lobes in deep sea turbidity systems State of the art. In: Mulder, T. (Ed.), *Sedimentary Geology* 211, 75-80 Special Issue on Lobes in Deep Sea Turbidity Systems.
- [114] Gervais, A., Mulder, T., Savoye, B., 2006. Sandy modern turbidity lobes: a new insight from high resolution seismic data. *Mar. Pet. Geol.* 23, 485-502.
- [115] Posamentier, H. W., Vail, P. R., 1988. Eustatic controls on classic deposition II sequence and systems tract models. In: Wilgus, C., Hastings, B., Posamentier, H., Van Wagoner, J.,



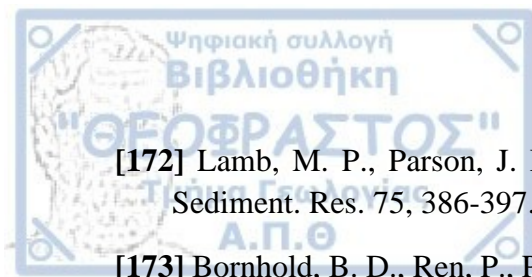
- Ross, C., Kendal, G., (Eds.), Sea level changes: An integrated approach, SEPM, special publication 42, 125-154.
- [116] Milliman, J. D., Syvitski, J. P. M., 1992. Geomorphic tectonic control of sediment discharge to the ocean: the importance of small mountainous rivers. *J. Geol.* 100, 525-544.
- [117] Schumm, S. A., 1963. Disparity between modern rates of denudation and orogeny, USGS Prof. Paper 454-H 13pp.
- [118] Jervey, M. T., 1988. Quantitative geological modelling of siliciclastic rock sequence and their seismic expression. In: Wilgus, C., Hastings, B., Posamentier, H., Van Wagoner, J., Ross, C., Kendall, G., (Eds.), Sea level changes: An intergraded approach, EEPM Spec. Publ., 42, 48-69.
- [119] Posamentier, H. W., Allen, G. P., 1999. Siliciclastic sequence stratigraphy concepts and applications, SEPM concepts in sedimentology and Palaeontology no. 7 210pp.
- [120] Homewood, P., Mauriaud, P., Lafont, F., 2000. Vade-Mecum de straitigraphie sequentielle, Elf EP editions Memoire, 25 81pp.
- [121] Ferry, J. N., Mulder, T., Parize, O., Raillard, S., 2005. Equilibrium profile in deep water turbidity systems: effects of local physiographic changes on deposits geometries and nature of sedimentary process. In: Hodgson, D. M., Flint, S. S., (Eds.), Submarine slope systems. Processes and products, *Geol. Soc., London, Special Publication*, 244, 181-193.
- [122] Mutti, E., 1985. Turbidity systems and their relations to depositional sequences. In: Zuffa, G. (Ed.), Provenance of ankerites, D. Reidel Publishing Co, Dordrecht, Holland, 65-93.
- [123] Schumm, S. A., 1993. River response to base level change: implication for sequence stratigraphy. *J. Geol.* 101, 279-294.
- [124] Normark, W. R., Piper, D. J. W., Romans, B. W., Covault, J. A., Dartnell, P., Sliter, R. W., 2009. Submarine canyons and fan systems of the California Borderland. *The Geol. Soc. America, Spec. Paper* 454, pp.141-168.
- [125] Galay, V., 1987. In erosion and sedimentation in the Nepal Himalaya (pp. 10.11). Singapore: Kefford Press Pvt. Ltd.
- [126] Middleton, G. V. 1967. Experiments on density and turbidity currents III: deposition of sediment. *Canadian Journal of Earth Sciences*, 4, 475-505.
- [127] Middleton, G. V. 1966. Experiments on density and turbidity currents I: motion of the head. *Canadian Journal of Earth Sciences*, 3, 523-546.
- [128] Coussot, P., Meunier, M. 1996. Recognition, classification and mechanical description of debris flows. *Earth –science Reviews*, 40, 209-227.
- [129] Wallis, G. B. 1969. In one-dimensional two-phase flow (pp.408). New York: McGraw-Hill.

- [130] Lowe, D. R. 1982. Sediment gravity flows: II depositional models with special reference to the deposition of high-density turbidity currents. *Journal of sedimentary petrology*, 52, 279-297.
- [131] Shultz, A. W. 1984. Subaerial debris flow deposition in the upper Paleozoic Cutler formation, western Colorado. *Journal of sedimentary petrology*, 54, 759-772.
- [132] Rodine, J.D., Johnson, A. M. 1976. The ability of debris, heavily freighted with coarse clastic material to flow on gentle slopes. *Sedimentology*, 23, 213-234.
- [133] Carey, S. N., Schneider, J. L., 2011. Volcaniclastic processes and deposits in the deep sea. In: Huneke, H., Mulder, T. (Eds.), *Deep sea sediments. Developments in sedimentology*, Elsevier, Amsterdam, Vol. 63, pp. 457-515.
- [134] Mulder, T., Cochonat, P., 1996. Classification of offshore mass movements. *J. Sediment. Res.* 66, 46-57.
- [135] Stow, D. A. V., Reading, H. G., Collison, J D., 1996. Deep seas. In: Reading, H. G. (Ed), *Sedimentary environments processes, facies and stratigraphy*. Blackwell science, Oxford, pp. 395-453.
- [136] Gaudin, M., Berne, S., Jouanneau, J. M, Palanques, A., Puig, P., Mulder, T., et al., 2006a. massive sand beds attribute to deposition by dense water cascades in the Bourcart canyon head, Gulf of Lios (northwestern Mediterranean Sea). *Mar. Geol.* 234, 111-128.
- [137] Faugeres, J. C., Gonythier, E., Bodier, C., Griboulard, R. 1997. Tectonic control on sedimentary processes in the southern termination of the Barbados prism. *Mar. Geol.* 140, 117-140.
- [138] Skempton, A. W., Hutchinson, J. N., 1969. Stability of natural slopes and embankment foundations, State of the art report. In: *Proc. 7th Int. Conf. SMFE*, Mexico City, vol. 2291-335.
- [139] Mohrig, D., Whipple, K. X., Hondzo, M., Ellis, C., Parker, G., 1998. Hydroplaning of subaqueous debris flows. *Geol. Soc. Am. Bull.* 110 (3), 387-394.
- [140] Johnson, A. M., 1970. *Physical process in geology*, Cooper and Co., San Francisco, 577pp.
- [141] Johnson, A. M., 1984. Debris flow, In: Brunden, D., Prior, D. B. (Eds), *Slope instability*. Wiley, Toronto, pp.257-362.
- [142] Rodine, J. D., Johnson, A. M., 1976. The ability of debris, heavily freighted with coarse clastic materials, to flow on gentle slopes, *sedimentology* 23, 213-234.
- [143] Van Weerng, T. C. E., Nielsen, T., Kenyon, N. H., Akentieva, K., Kuijpers, A. H., 1998. Large submarine slides on the NE Faeroe continental margin. In: Stoker, M. S., Evans, D., Cramp, A. (Eds), *Geological processes on continental margins: sedimentation, Mass-wasting and stability*, *Geol. Soc. London, Spec. Publ.* 129, 5-17.



- [144] Hampton, M. A., 1972. The role of subaqueous debris flow in generating turbidity currents. *J. Sediment. Petrol.* 42, 775-793.
- [145] De Vries Klein, G., 1982. Sandstone depositional models for exploration for fossil fuels. Geological science series 209pp.
- [146] Warrick, J. A., Milliman, J. D. 2003. Hyperpycnal sediment discharge from semi-arid southern California rivers: implications for coastal sediments budgets. *Eology* 31 (9), 781-784.
- [147] Syvitski, J. P. M., Schafer, C. T., 1996. Evidence for an earthquake triggered basin collapse in
- [148] Hesse, R., Klauke, I., Ryan, W. B. F., Edwards, M. B., Piper, D. J. W., NAMOC study group, 1996. Imaging Laurentide ice sheet drainage into the deep sea: impact on sediments and bottom water. *Geol. Soc. Am. Today* 3-9.
- [149] Hesse, R., Khodabakhsh, S., 1998. Depositional facies of late Pleistocene Heinrich events in the Labrador Sea. *Geology* 26 (2), 103-106.
- [150] Schafer, C. T., Smith, J. N., 1987. Hypothesis for a submarine landslide and cohesionless sediment flows, resulting from a 17th century earthquake-triggered landslide in Quebec, Canada. *Geo-Mar. Lett.* 7, 31-37.
- [151] Wright, L. D., Yang, Z.-S., Bornhold, B. D., Keller, G. H., Prior, D. B., Wisenam Jr., W. J., 1986. Hyperpycnal flows and flow fronts over the Huanghe (Yellow River) delta front. *Geo-Mar. Lett.* 6, 97-105.
- [152] Wright, L. D., Wisenam Jr., W. J., Bornhold, B. D., Prior, D. B., Suhayda, J. N., Keller, G. H., et. al., 1988. Marine dispersal and deposition of Yellow River silts by gravity-driven underflows. *Nature* 332, 629-632.
- [153] Wright, L. D., Wisenam Jr., Yang, Z.-S., Bornhold, B. D., Keller, G. H., Prior, D. B., et. al., 1990. Processes of marine dispersal and deposition of suspended silts off the modern mouth of the Huanghe (Yellow River). *Cont. Shelf Res.* 10, 1-40.
- [154] Mulder, T., Syvitski, J. P. M., 1995. Turbidity currents generated at river mouths during exceptional discharges to the world oceans. *J. Geol.* 103, 285-299.
- [155] Myrow, P. M., Fisher, W., Goodge, J. W., 2002. Wave-modified turbidites: Combined-flow shoreline and shelf deposits, Cambrian, Antarctica. *J. Sediment. Res.* 72, 641-656.
- [156] Lamp, M. P., Myrow, P. M., Lukens, C., Houck, K., Strauss, J., 2008. Deposits from wave-influenced turbidity currents: Pennsylvanian Minturn Formation, Colorado, USA. *J. Sediment. Res.* 78, 480-498.
- [157] Hoyal, D. C., Bursik, M. I., Atkison, J. F., 1999. Settling driven convection: A mechanism of sedimentation from stratified fluids. *J. Geophys. Res.* 104, 7953-7966.

- [158] Chikita, K., 1991. Dynamic processes of sedimentation by river induced turbidity currents. II. Application of a two-dimensional, advective diffusion model. Jpn. Geomorphol. Union Trans 13-1, 1-18.
- [159] Parson, J. D., Bush, J., Syvitski, J. P. M., 2001. Hyperpycnal flow formation with small sediment concentrations. Sedimentology 48, 465-478.
- [160] Postma, G., Nemec, W., Zachariasse, W. J., 1988. Large floating clasts in turbidites: A mechanism for their emplacement. Sediment. Geol. 58, 47-61.
- [161] Lowe, D. R., 1982. Sediment gravity flows: II. Depositional models with special reference to the deposits of high-density turbidity currents. J. Sediment. Petrol. 52, 279-297.
- [162] Kuenen, P. H., 1950. Turbidity currents of high density. In: Geol. Congr., 18th, London, 1948, 44-52, rept. 8.
- [163] Fisher, R. V., 1983. Flow transformations in sediment gravity flows. Geology 11, 273-274.
- [164] Shanmugam 2000 Shanmugam (2000) 50 years of the turbidity paradigm (1950s–1990s): Deep-water processes and facies models—A critical perspective, Marine and Petroleum Geology 17: 285–342
- [165] Normark, W. R., Piper, D. J. W., 1991. Initiation processes and flow evolution of turbidity currents: Implications for the depositional record. SEPM Special Publication 46 pp. 207-229.
- [166] Bjerrum, L., 1971. Subaqueous slope failures in Norwegian fjords. Norge Geotech. Bull. No 88 pp. 1-8.
- [167] Prior, D. B., Suhayda, J. N., Lu, N.-Z., Bornhold, B. D., Keller, G. H., Wiseman, W. J., et. al., 1989. Storm wave reactivation of a submarine landslide. Nature 341, 47-50.
- [168] Mulder, T., Weber, O., Anschutz, P., Jorissen, F. J., Jouanneau, J.-M., 2001c. A few months-old storm-generated turbidity deposited in the Capbreton Canyon (Bay of Biscay, S-W France). Geo-Mar. Lett. 21 (3), 149-156.
- [169] Klaucke, I., Masson, D. G., Kenyon, N. H., Gardner, J. V., 2004. Sedimentary processes of the lower Monterey Fan channel and channel-mouth lobe. Mar. Geol. 206 (1-4), 181-198.
- [170] Mosher, D. C., Piper, D. J. W., Campbell, D. C., Jenner, K., 2004. Near surface geology and sediment-failure geohazards of the central Scotian Slope. Am. Assoc. Pet. Geol. Bull. 88, 703-723.
- [171] Puig, P., Ogston, A. S., Mullenbach, B. L., Nittrouer, C. A., Sternberg, R. W., 2003. Shelf to canyon sediment-transport processes on the Eel continental margin (northern California). Mar. Geol. 193, 129-149.



- [172] Lamb, M. P., Parson, J. D., 2005. High-density suspensions formed under waves. *J. Sediment. Res.* 75, 386-397.
- [173] Bornhold, B. D., Ren, P., Prior, D. B., 1994. High-frequency turbidity currents in British Columbia fjords. *Geo-Mar. Lett.* 14, 238-243.
- [174] Beck, C., Schneider, J.-L., Cremer, M., MercierdeLepinay, B., Cagatay, N., Labeyrie, L., et. al., 2003. Late Pleistocene major sedimentary reworking event (homogeneite) in Marmara Sea Central Basin: Preliminary results of giant piston-coring and high-resolution seismic reflection. In: EGS-AGU joint meeting 6-11 April, 2003, Nice, France.
- [175] Giresse, P., Pauc, H., Deverchere, J., Savoye, B., The MARADJA Scientific Party, 2004. Gravity induced transport on the Algerian margin. In: EGU 1st meeting Nice, France, 25-30 April, 2004.
- [176] Singh, S. C., 2005. Sumatra earthquake research indicates why rupture propagated northward. *EOS Trans. Am. Geophys. Union* 86 (48), 497-502.
- [177] King, L. H., Mac Lean, B., 1970. Pockmarks on the Scotian shelf. *Geol. Soc. Am. Bull.* 81, 3141-3148.
- [178] Hovland, M., Judd, A. G., 1988. Seabed pockmarks and seepages. Graham and Trotman, London, 293pp.
- [179] Boe, R., Rise, L., Ottesen, D., 1998. Elongated depressions on the southern slope of the Norwegian Trench (Skagerrak): morphology and evolution. *Mar. Geol.* 146 (1-4), 191-203.
- [180] Le Moigne, M., 1999. Compréhension des mécanismes de formation des pockmarks sur la pente du Golfe de Guinée. Unpubl. Master thesis, Univ. Sci. Tech Lille 1.
- [181] Josenhans, H. W., King, L. H., Fader, G. B., 1978. A side scan sonar mosaic of pockmarks on the Scotian Shelf. *Can. J. Earth Sci.* 15, 831-840.
- [182] Baraza, J., Ercilla, G., 1996. Gas-charged sediments and large pockmark like features on the Gulf of Cadiz slope (SW Spain). *Mar. Pet. Geol.* 13 (2), 253-261.
- [183] Dimitrov, L. I., 2002. Mud volcanoes the most important pathway for degassing deeply buried sediments. *Earth Sci. Rev.* 59 (1-4), 49-76.
- [184] Syvitski, J. P. M., 2003. Sediment fluxes and rates of sedimentation. In: Middleton, G. V. (Ed), *Encyclopedia of sediments and sedimentary rocks*. Kluwer Academic Publisher, Dordrecht, Netherlands, pp 600-606.
- [185] Bates, C. C., 1953. Rational theory of delta formation. *Bull. Am. Assoc. Pet. Geol.* 37 (9), 2119-2162.
- [186] Mulder, T., Alexander, J., 2001a. The physical character of sedimentary density currents and their deposits. *Sedimentology* 48, 269-299.

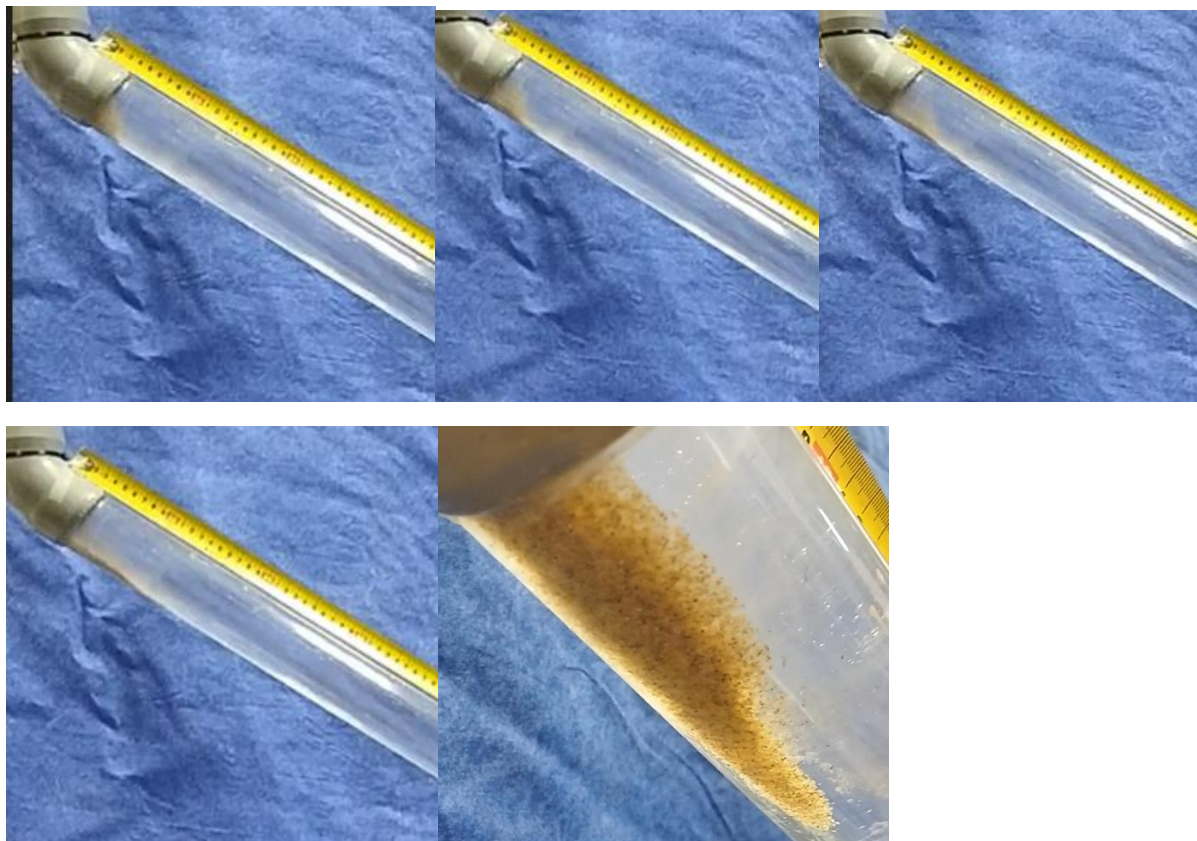
- [187] Rimoldi, B., Alexander, J., Morris, S. A., 1996. Experimental turbidity currents entering density stratified water: Analogues for turbidites in Mediterranean hypersaline basins. *Sedimentology* 43, 527-540.
- [188] Bates, C. C., 1953. Rational theory of delta formation. *Bull. Am. Assoc. Pet. Geol.* 37 (9), 2119-2162.
- [189] Mutti, E., Davoli, G., Tinterri, R., Zavala, C., 1996. The importance of ancient fluviodeltaic systems dominated by catastrophic flooding in tectonically active basins. *Sci. Geol. Mem.* 48, 233-291.
- [190] Mutti, E., Tinterri, R., di Biase, D., Fava, L., Mavilla, N., Angella, S., et. al., 2000. Delta front facies associations on ancient flood dominated fluvio deltaic systems. *Rev. Soc. Geol. Espana* 13 (2), 165-190.
- [191] Heezen, B. C., Ewing, M., 1952. Turbidity currents and submarine slumps and the 1929 Grand Banks earthquake. *Am. J. Sci.* 250, 849-873.
- [192] Komar, P. D., 1971. Hydraulic jumps in turbidity currents. *Geol. Soc. Am. Bull.* 82, 1477-1488.
- [193] Garcia, M. H., Parker, G., 1989. Experiments on hydraulic jumps in turbidity currents near a canyon- fan transition. *Science* 245, 393-396.
- [194] Mohrig, D., Elverhoi, A., Parker, G., 1999. Experiments on relative modify of muddy subaqueous and subaerial debris flows and their capacity to remobilize antecedent deposits. *Mar. Geol.* 154, 117-129.
- [195] Bates, R. L., Jckson, J. A., 1980. *Glossary of Geology*, second ed. American Geologicate institute, Falls Church, Virginia 751p.
- [196] Marr, J., Harff, P., Shanmugam, G., Parker, G. 1997. Experiments on subaqueous sandy debris flow. Supplement to EOS Transactions, AGU Fall Meeting, San Francisco, 78, Number 46, F 347.
- [197] Parker, G., 1982. Conditions for the ignition of catastrophically erosive turbidity currents. *Mar. Geol.* 46, 307-327.
- [198] Alexander, J., Morris, S., 1994. Observations on experimental, non-channelized, high concentration turbidity currents and variations in deposits around obstacles. *J. Sediment. Res. A* 64, 899-909.
- [199] Garcia, M. H., 1994. Depositional turbidity currents laden with poorly sorted sediment. *J. Hydraul. Eng.* 120, 1240-1263.
- [200] Mulder, T., Alexander, J., 2001b. Abrupt change in slope causes variation in the deposit thickness of concentrated particle driven density currents. *Mar. Geol.* 175, 221-235.
- [201] Ravenne, C., Beghin, P., 1983. Apport des experiences en canal a l'interpretation sedimentologyque des depots de cones detriques sous-marines. *Rev. Inst. Fr. Petrol.* 38, 279-297.

- [202] Pochat, S., 2003. Escarpement de faille syssedimentaire. Perturbation deseoulements gravitaires sous marins et determination de la cinetique des failles. Ph. D. Thesis, Univ. Rennes 1, Memoires Geosciences Rennes no. 105, 283 pp.
- [203] Lutjeharms, J. R. E., 1996. The exchange of water between the South Indian and South Atlantic oceans. In: Wefer, G., Berger, W. H., Siedler, G., Webb, D. J. (Eds). The south Atlantic: Presents and past circulation. Springer- Verlag, Berlin, Heidelberg, pp. 125-162.
- [204] Schmitz, W. J., 1996. On the world ocean circulation. The Pacific and Indian Oceans. A global Update. Technical report, WHOI-96-08, vol. II.
- [205] McCave, I. N., 1986. Local and global aspects of the bottom nepheloid layers in the world ocean. J. Sea Res. (Netherlands) 20 (2-3), 167-181.
- [206] Masse, L., Faugeres, J. C., Pujol, C., Pujos, A., Labeyrie, L. D., Bernat, M., 1996. Sediment flux distribution in the Southern Brazil Basin during the late Quaternary: The role of deep-sea currents. Sedimentology 43, 115-132.
- [207] Biscaye, P. E., Eitrem, S. L., 1977. Suspended particulate loads and transport in the nepheloid layer of the abyssal Atlantic Ocean. Mar. Geol. 23, 155-172.
- [208] Ewing, M., Thorndike, E. M., 1965. Suspended matter in deep ocean water. Science 147, 1291-1294.
- [209] Jerlov, N. G., 1953. Particle distribution in the ocean. Rep. Swed. Deep sea Expedition 3, 73-97.
- [210] McCave, I. N., 1984. Erosion, transport and deposition of fine-grained marine sediments. Geol. Soc. London, Sp. Pub. 15pp. 35-6

APPENTIX I

GRAIN SIZE RANGE 1-1.5 ϕ (average 1.25 ϕ)

Pipe inclination 22° degrees, tap water, material 13.4 gr



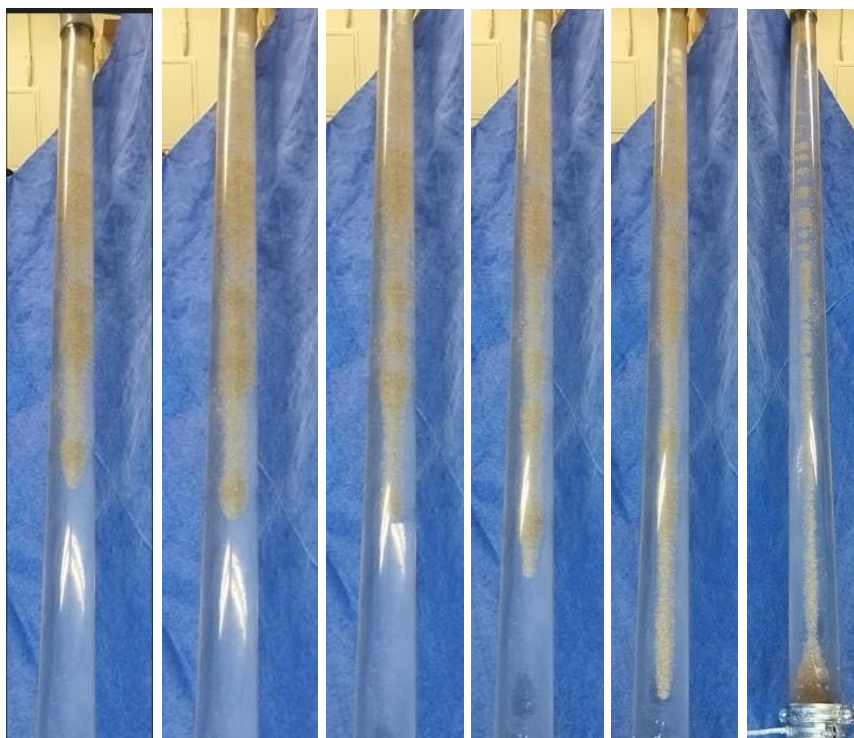
Pipe inclination 24° degrees, tap water, material 13.4 gr.



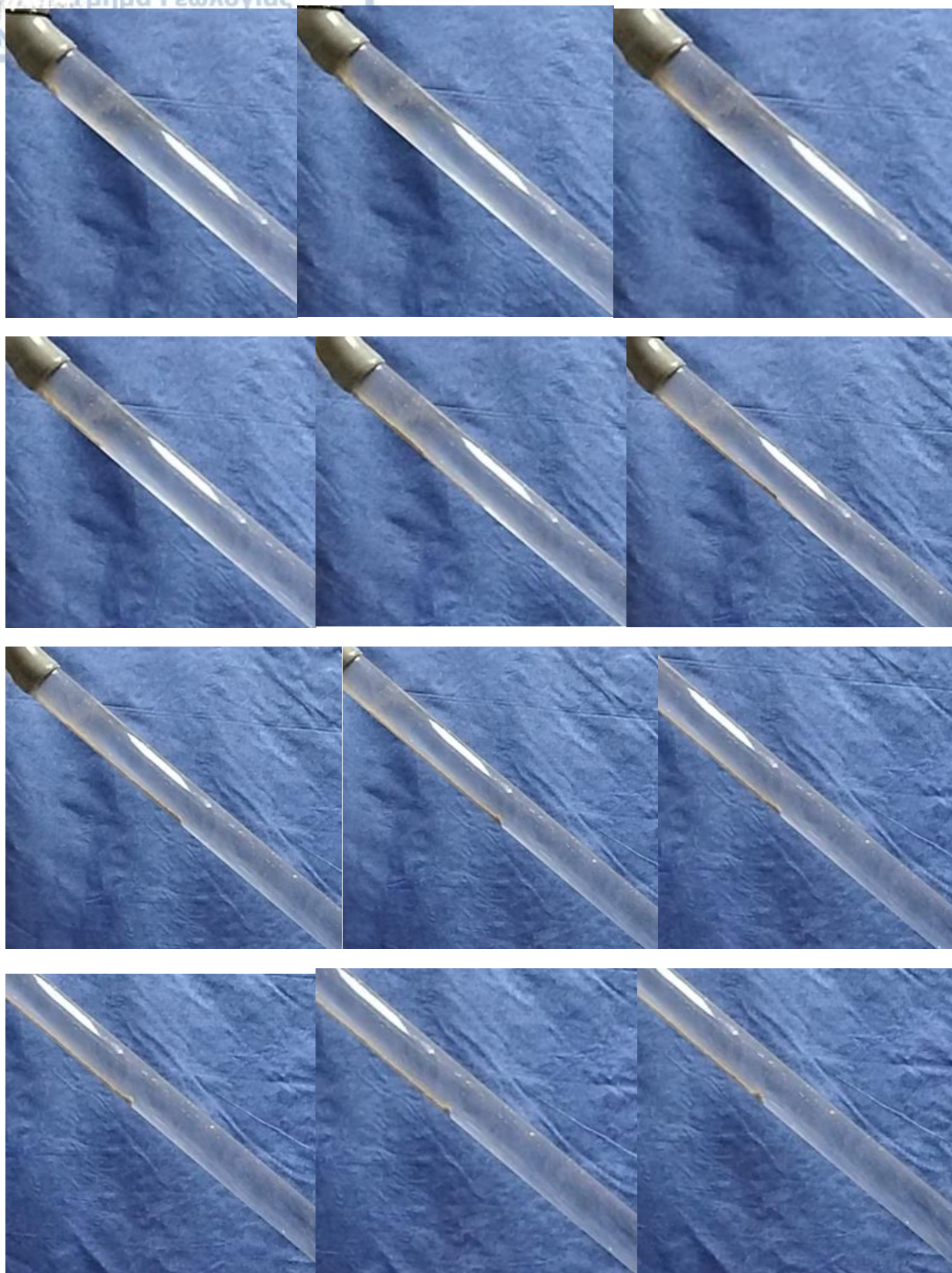


Pipe inclination 35°, tap water, material 13.4 gr.

a)

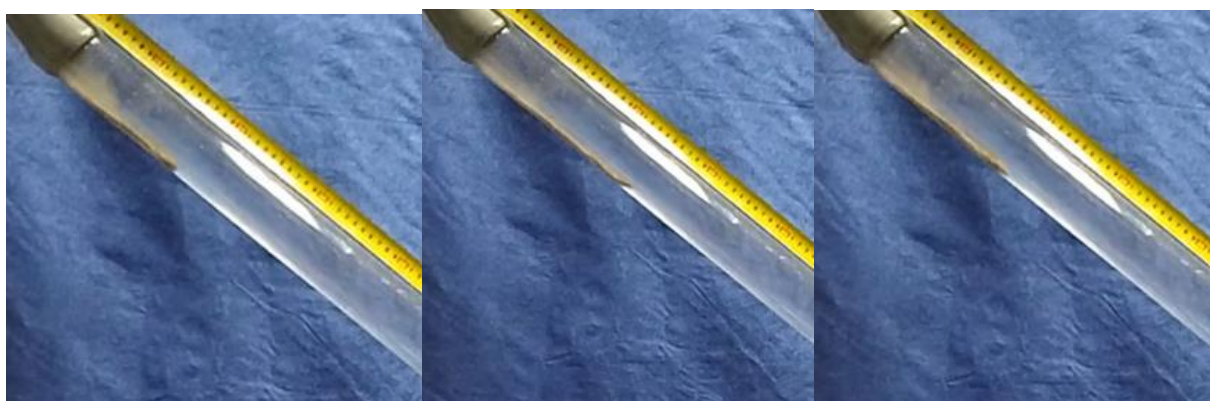


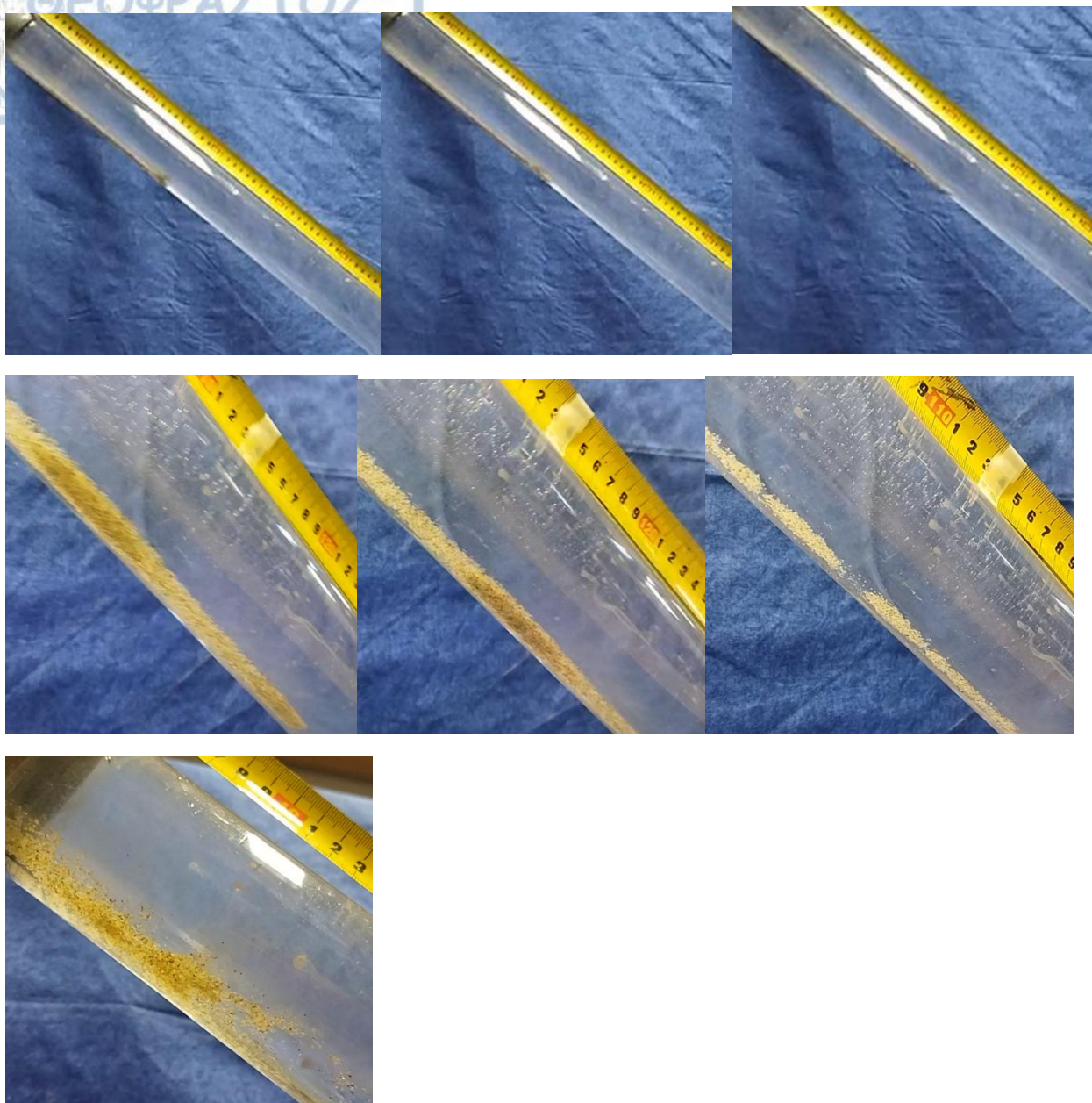
b)



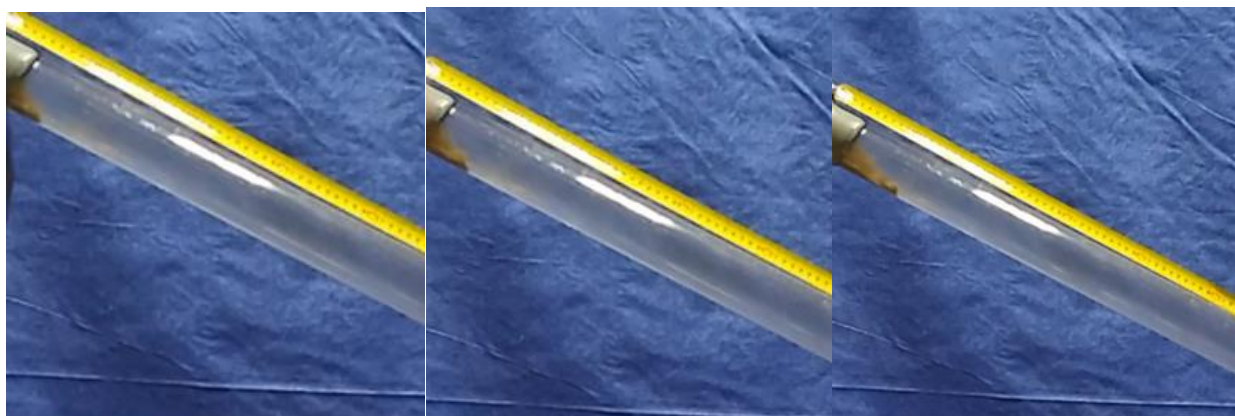


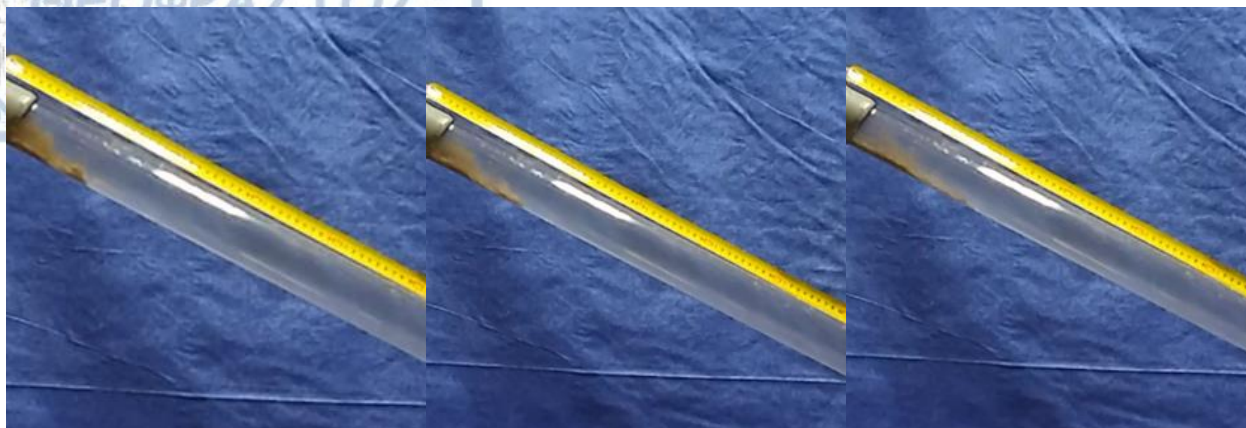
c)



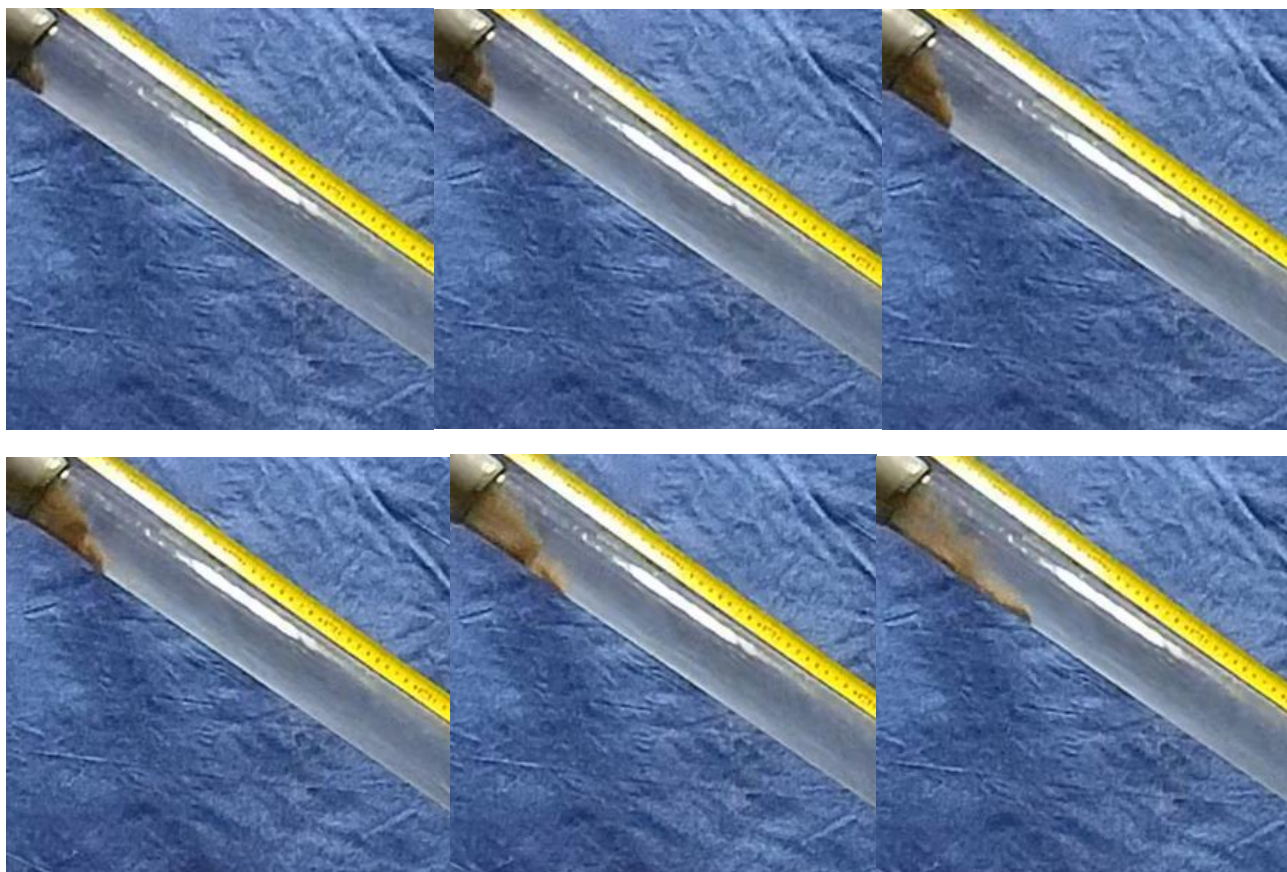


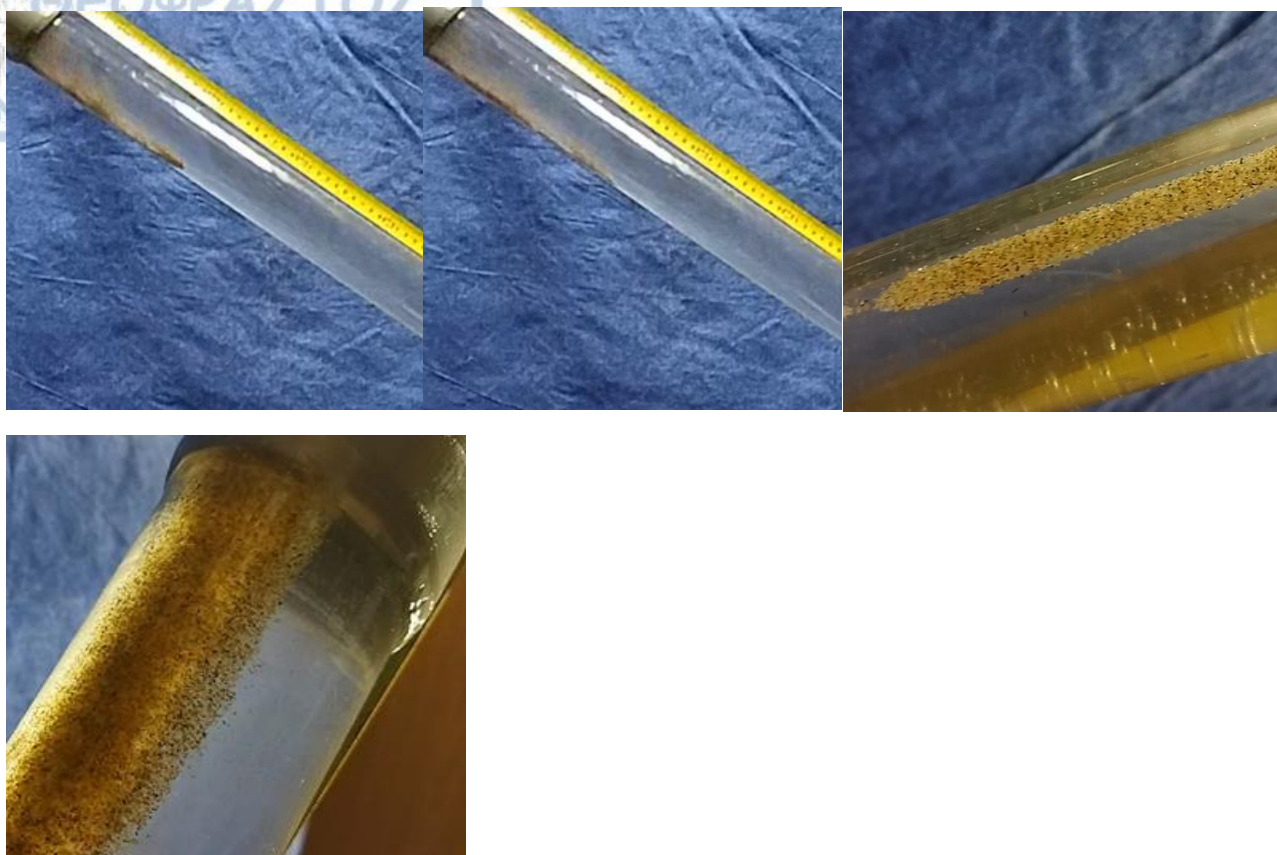
Pipe inclination 22° hypersaline water, material 13.4 gr.



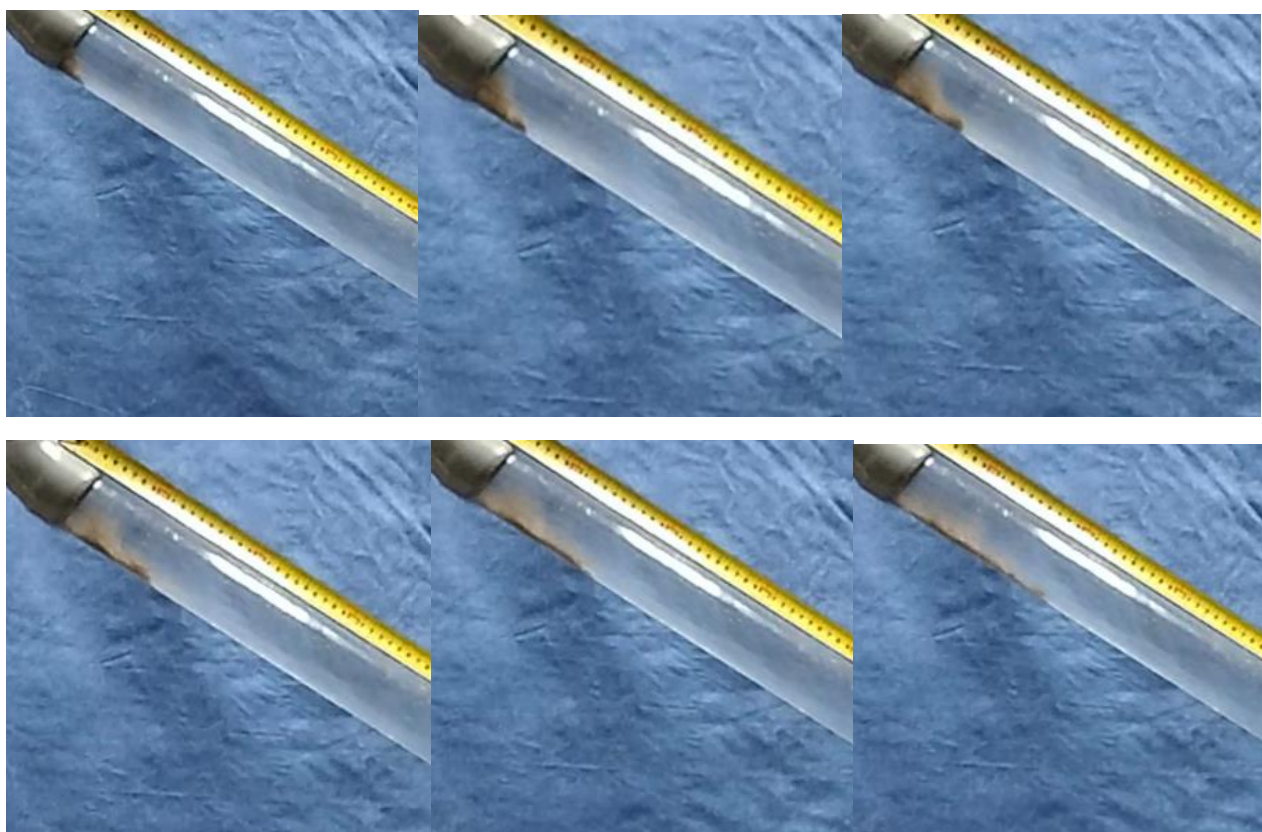


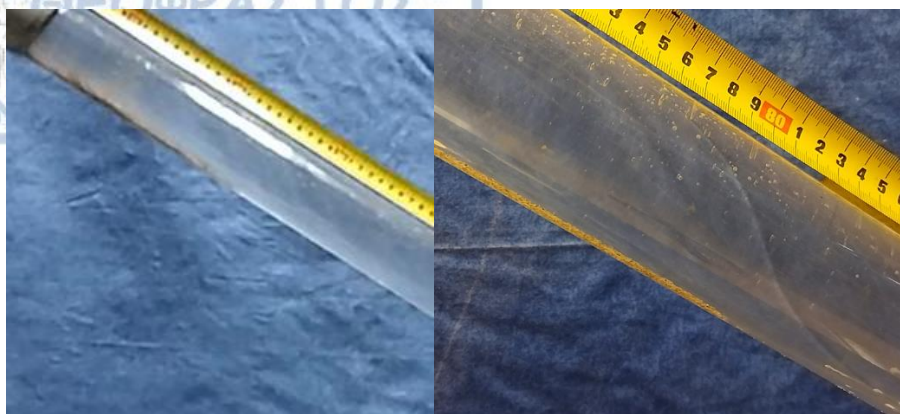
Pipe inclination 25°, hypersaline water, material 13.4 gr.





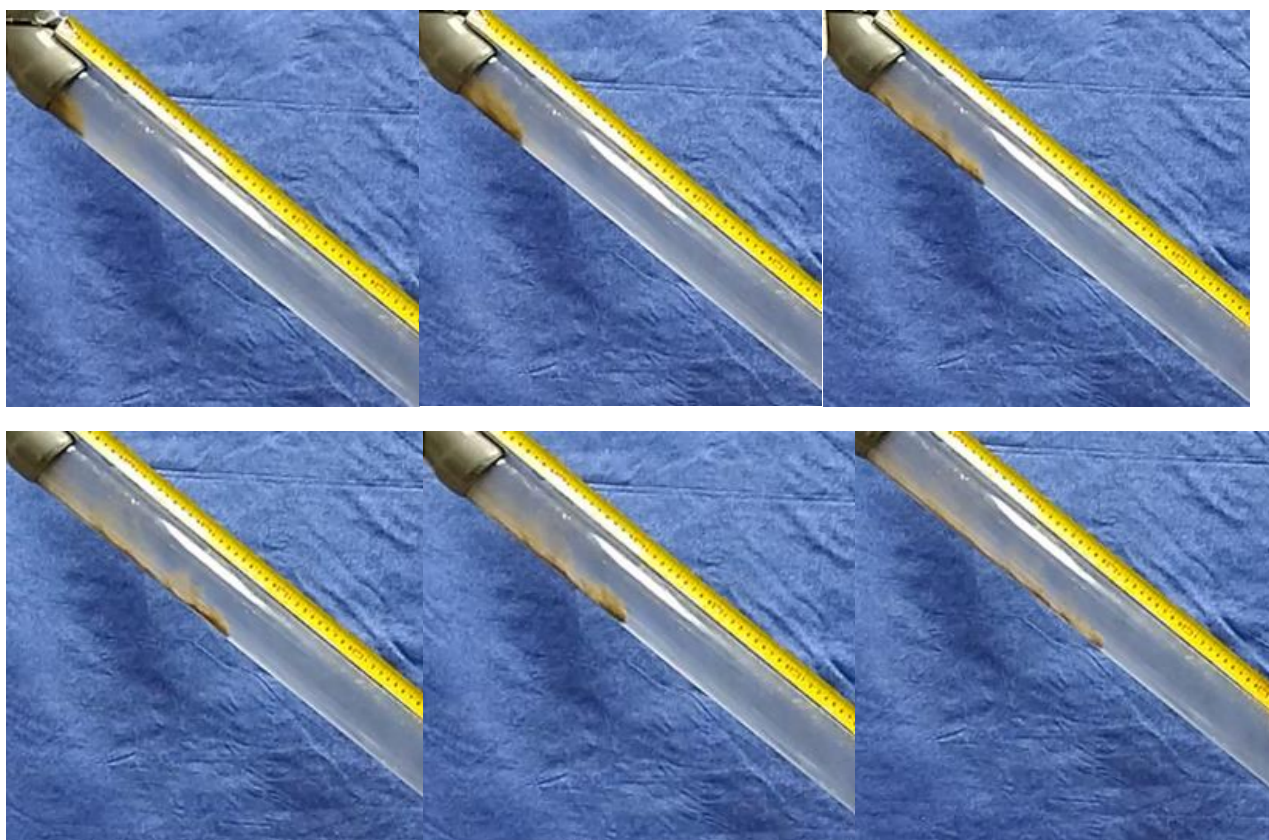
Pipe inclination 27°, hypersaline water, material 13.4 gr.

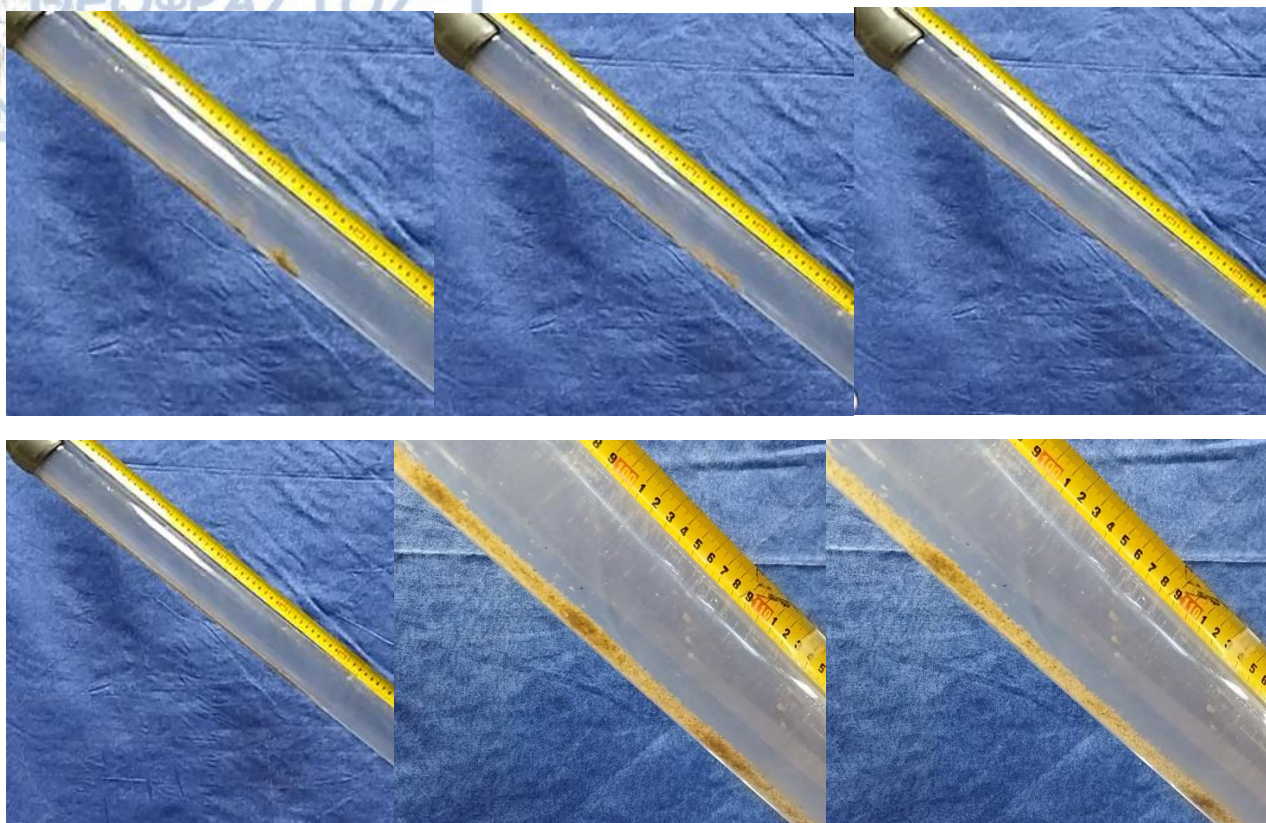




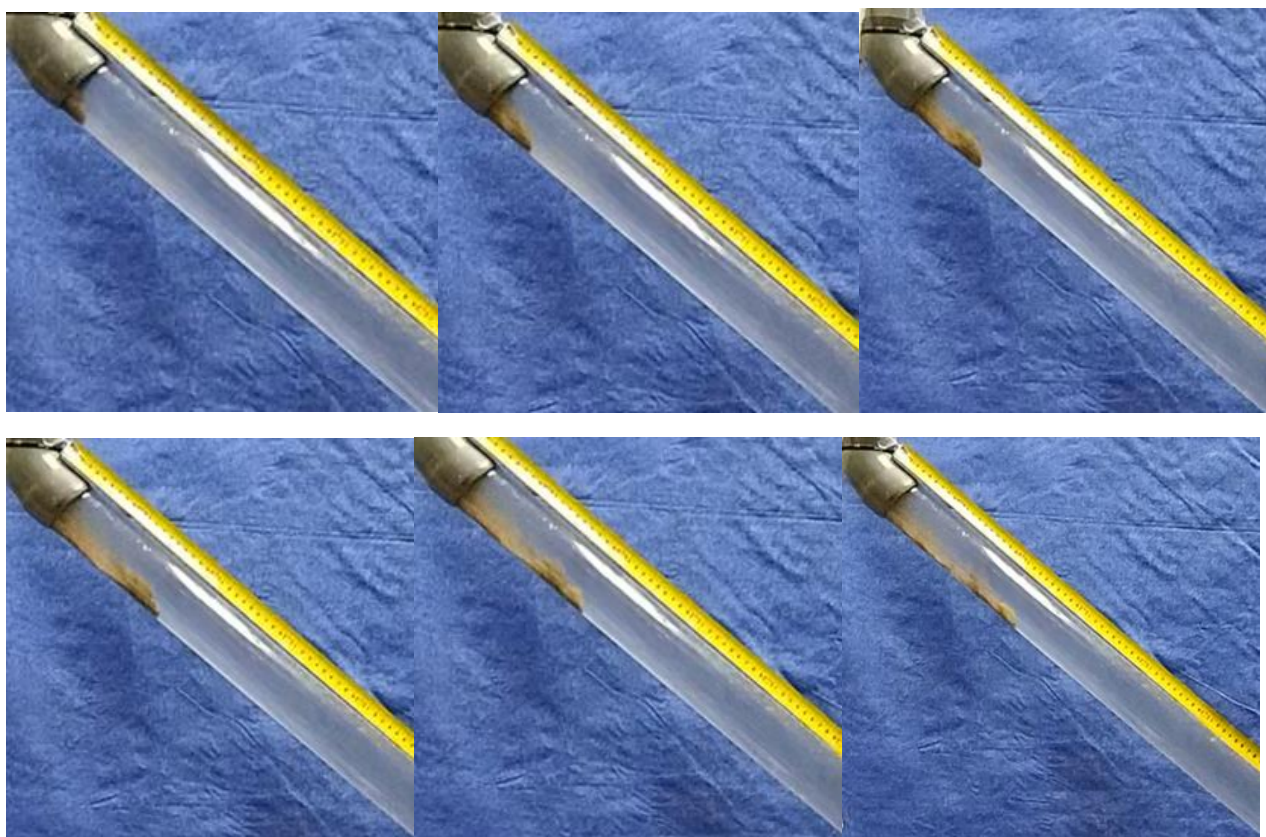
Pipe inclination 35°, hypersaline water, material 13.4gr.

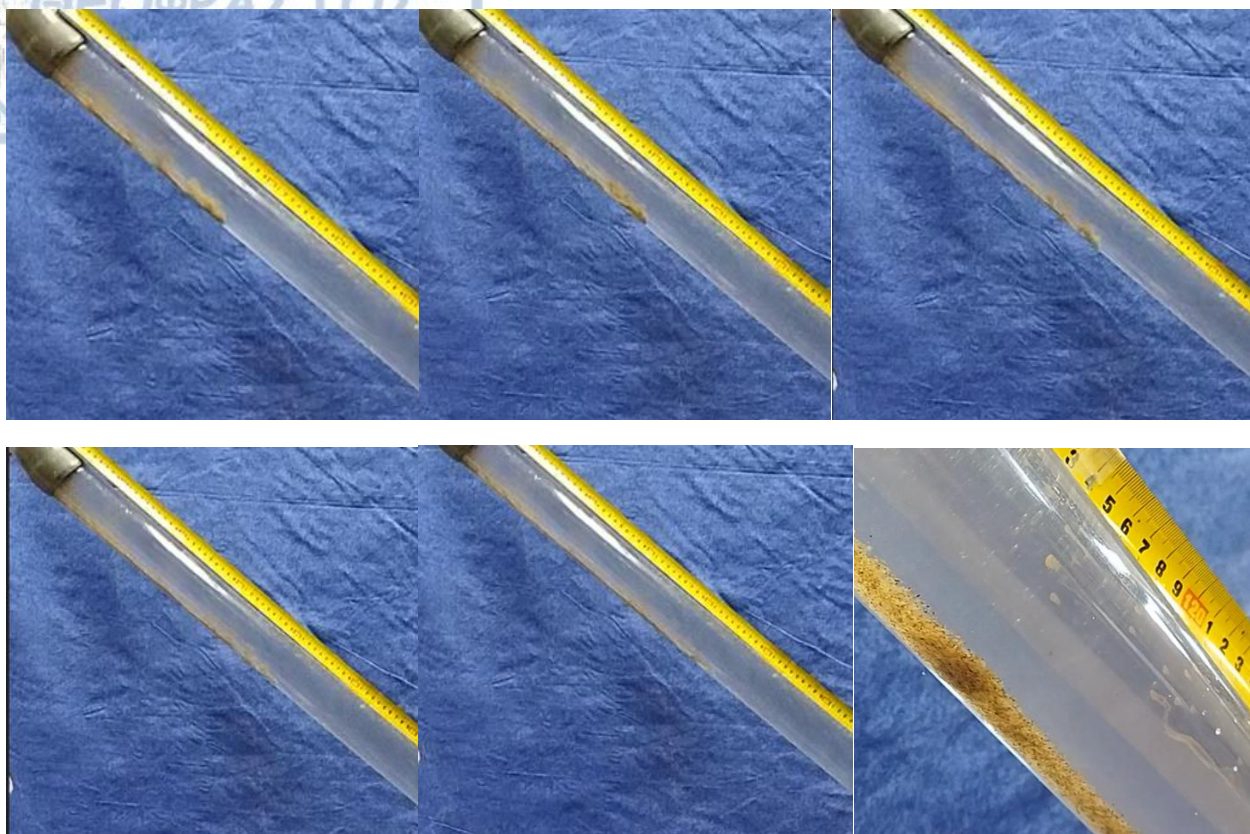
a)



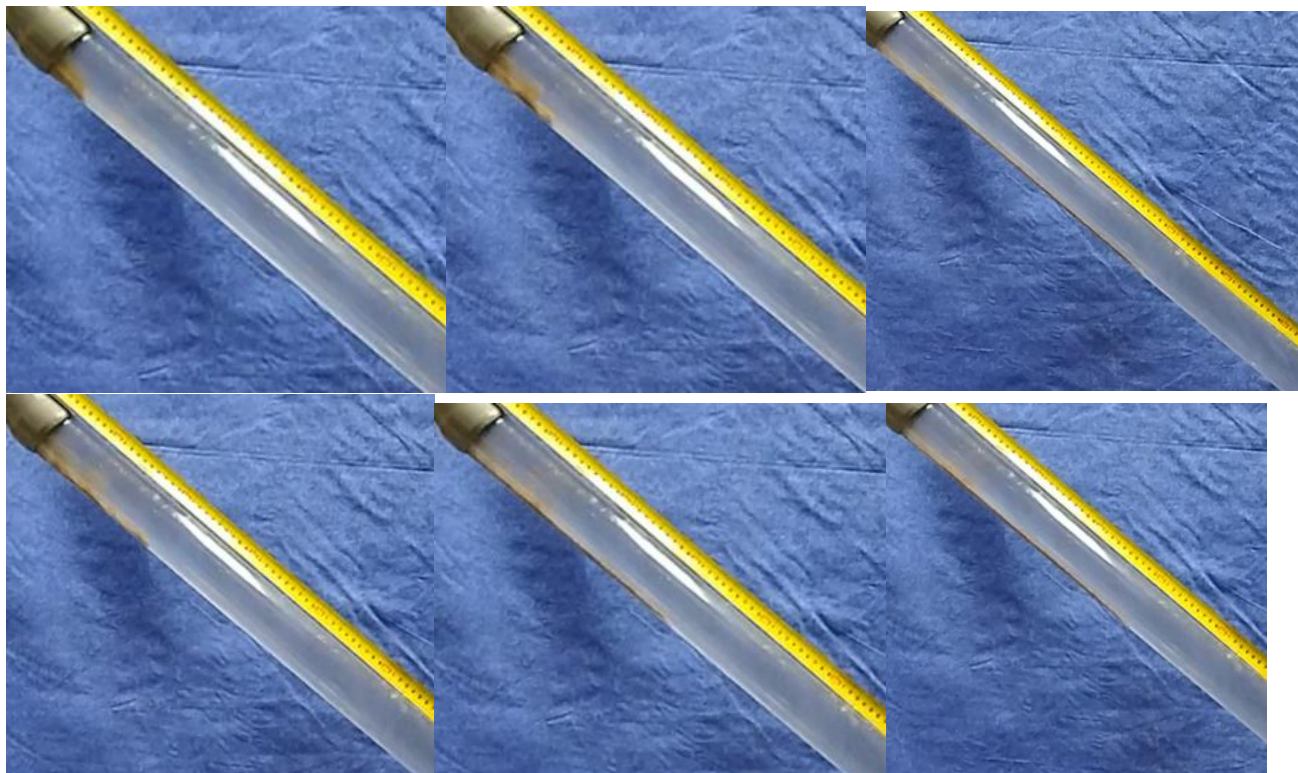


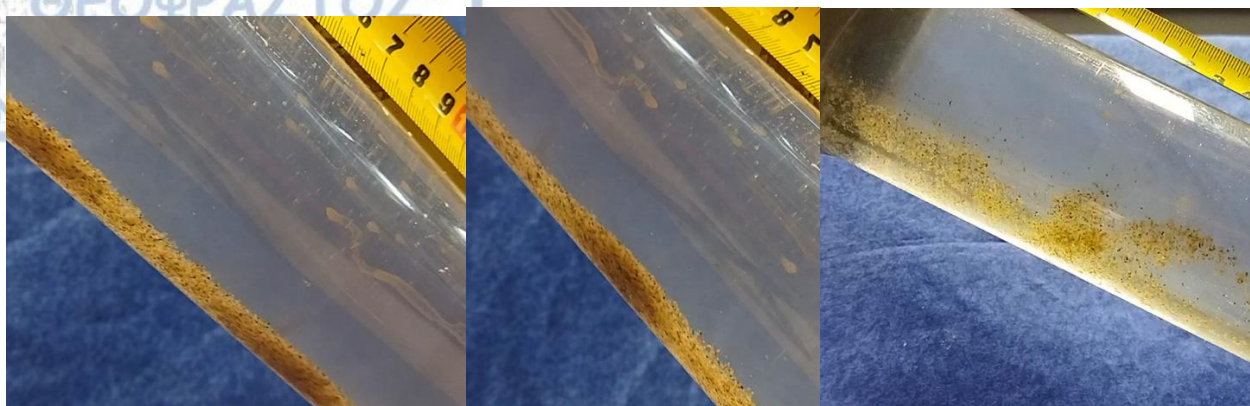
b)



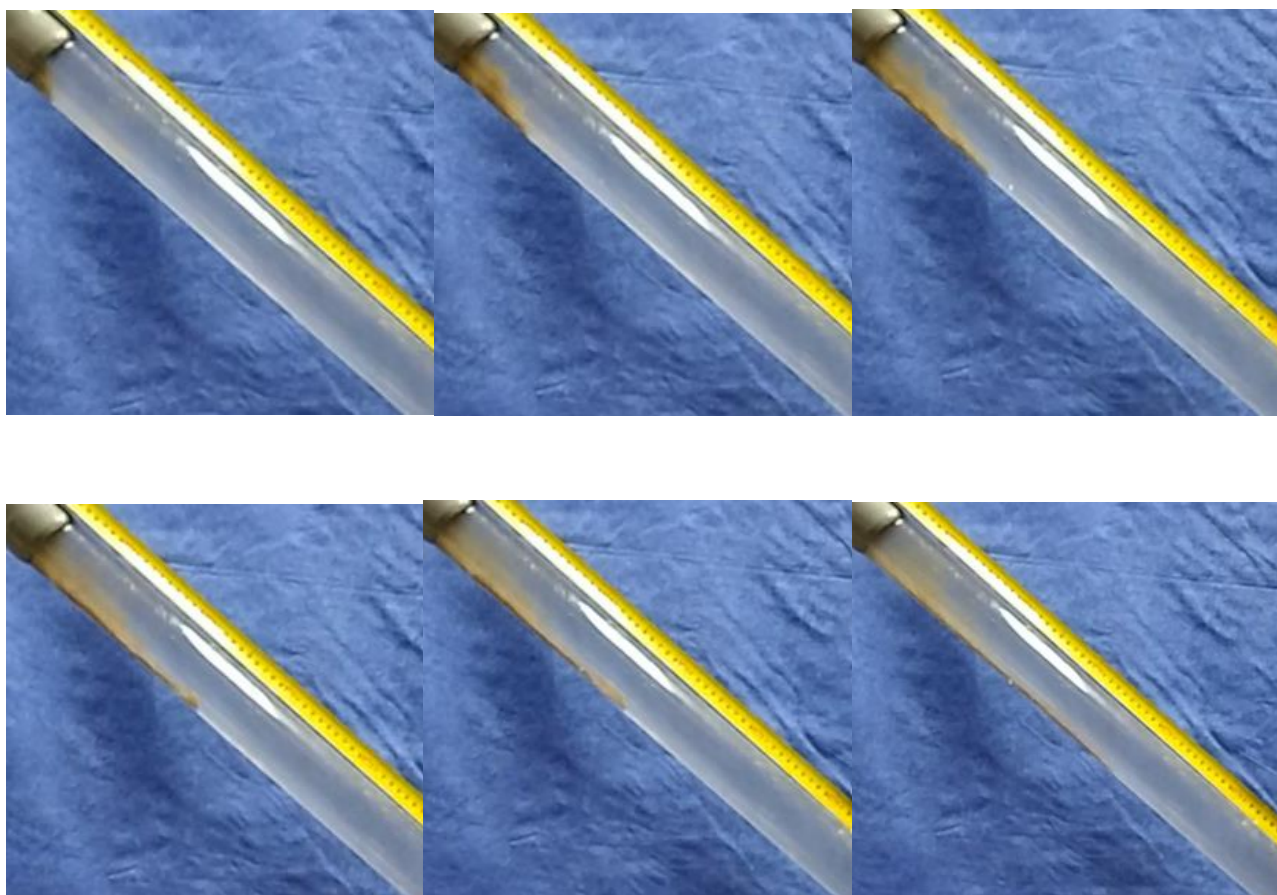


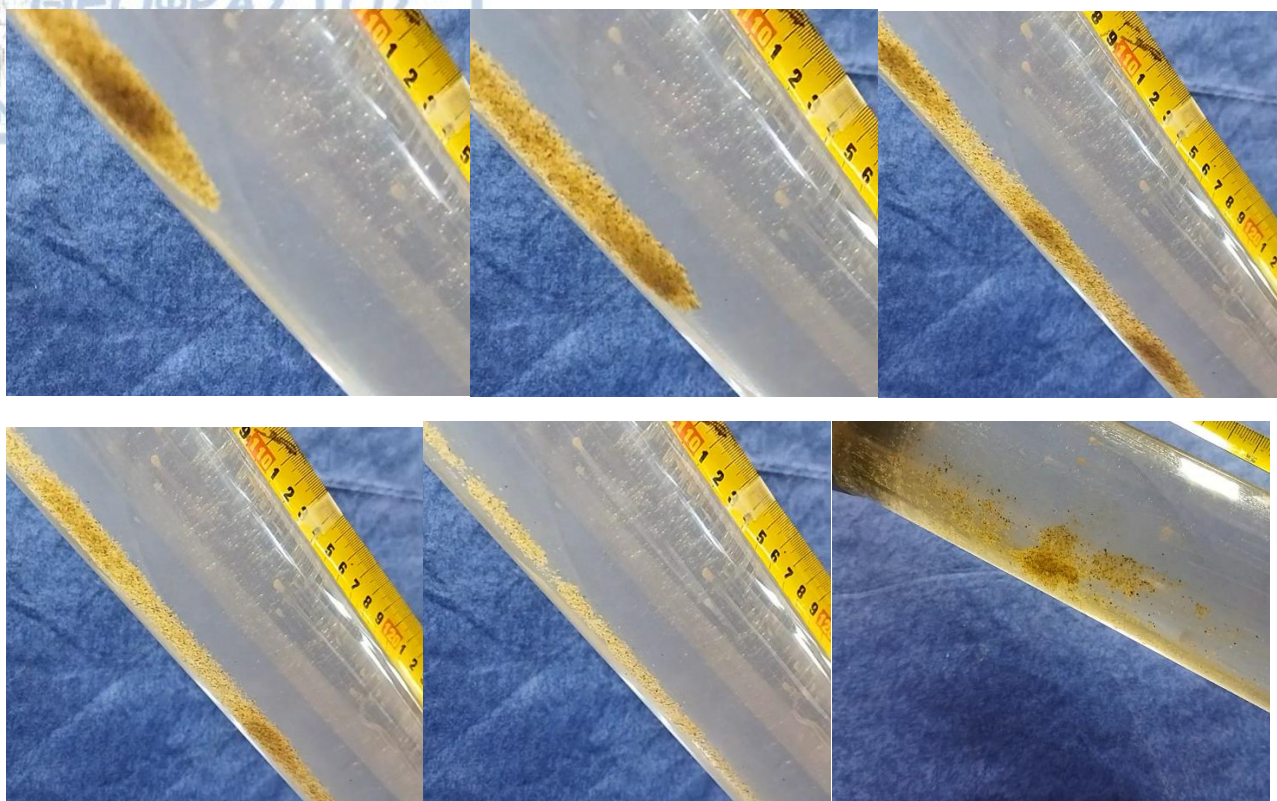
c)



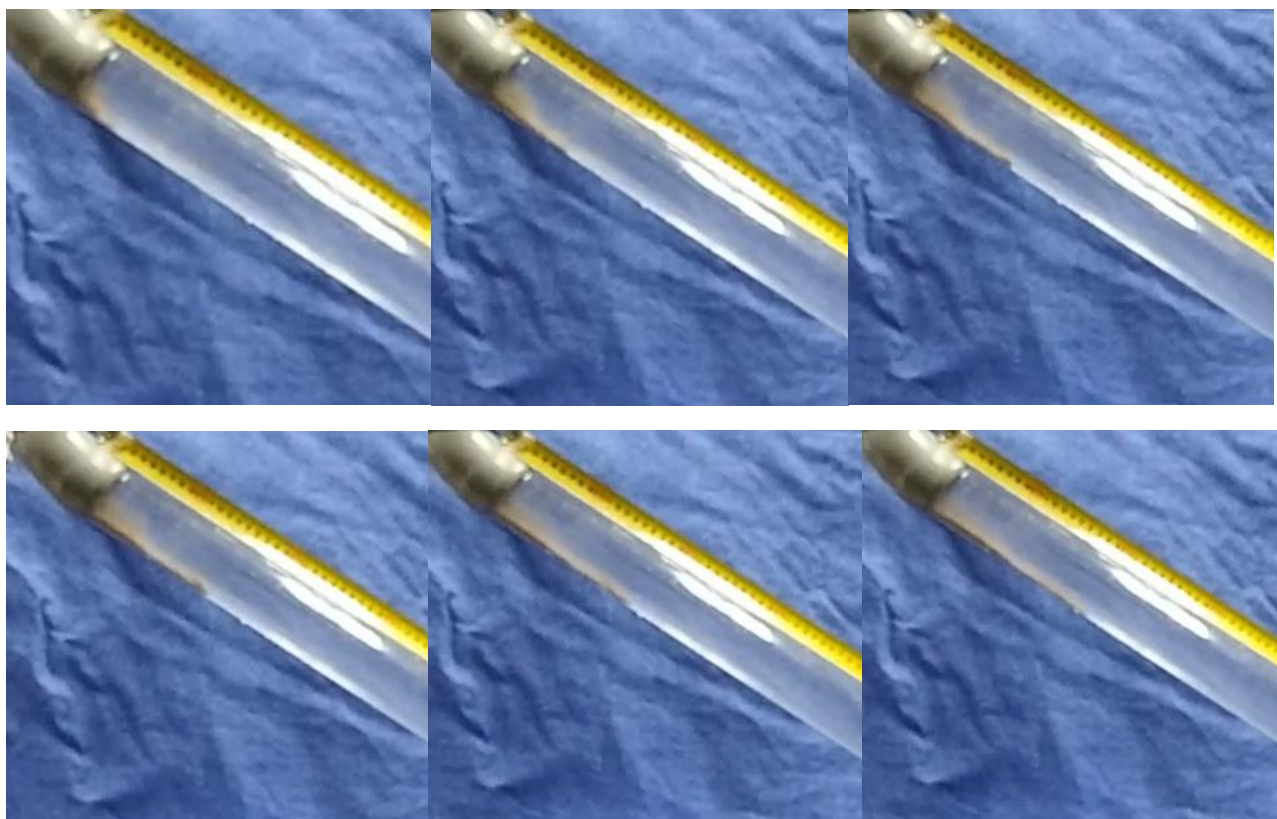


d) + 2% clays



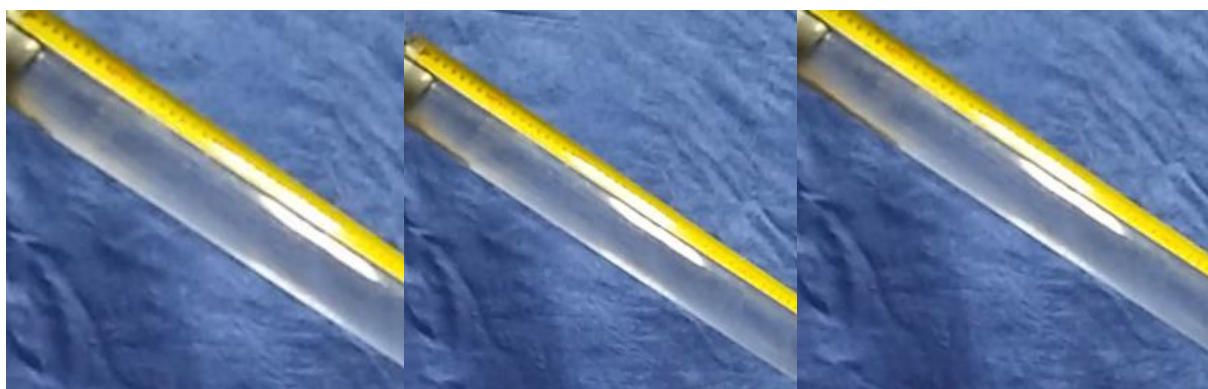


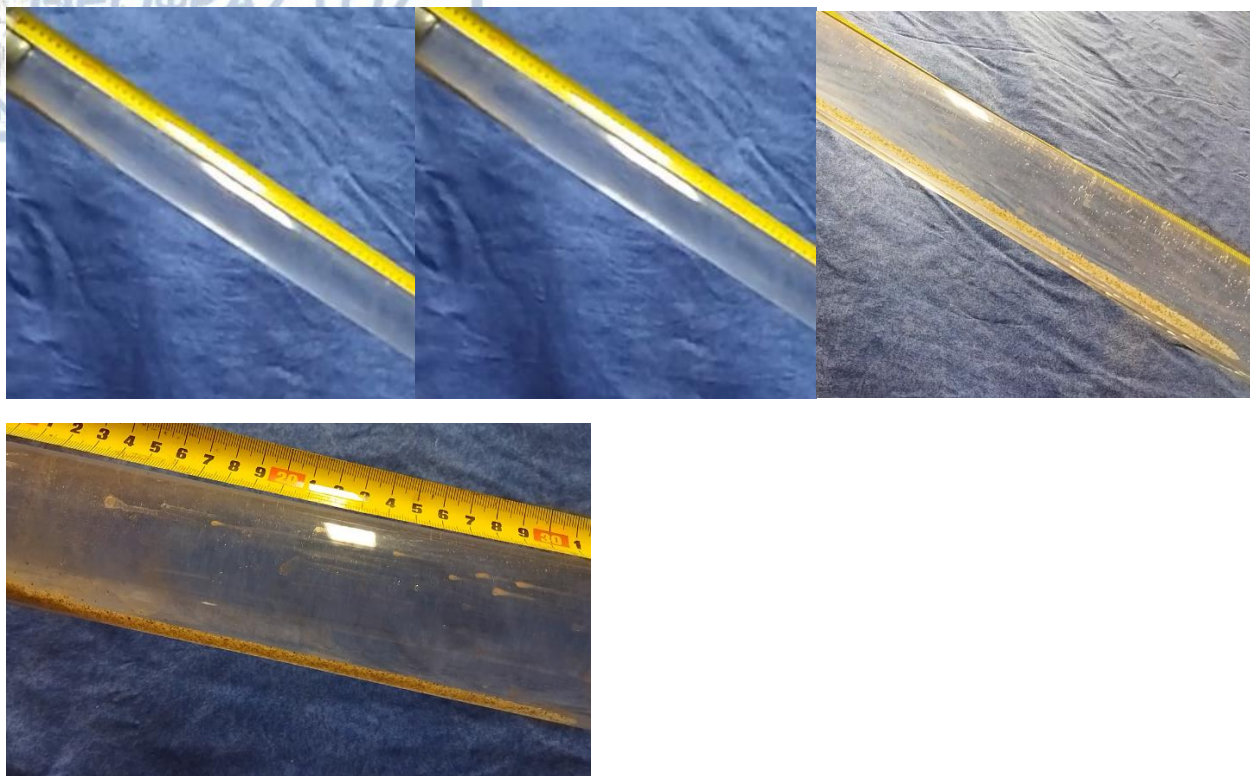
Pipe inclination 24°, tap water, material 28.13 gr.





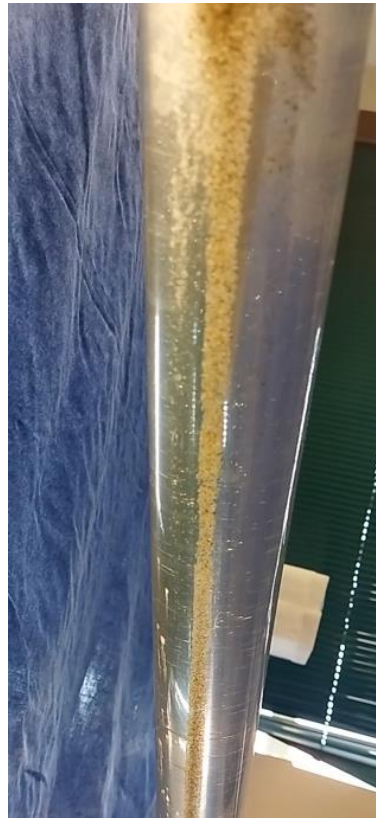
Pipe inclination 22°, tap water, material 28.13 gr.





Pipe inclination 23°, hypersaline water, material 28.13 gr.



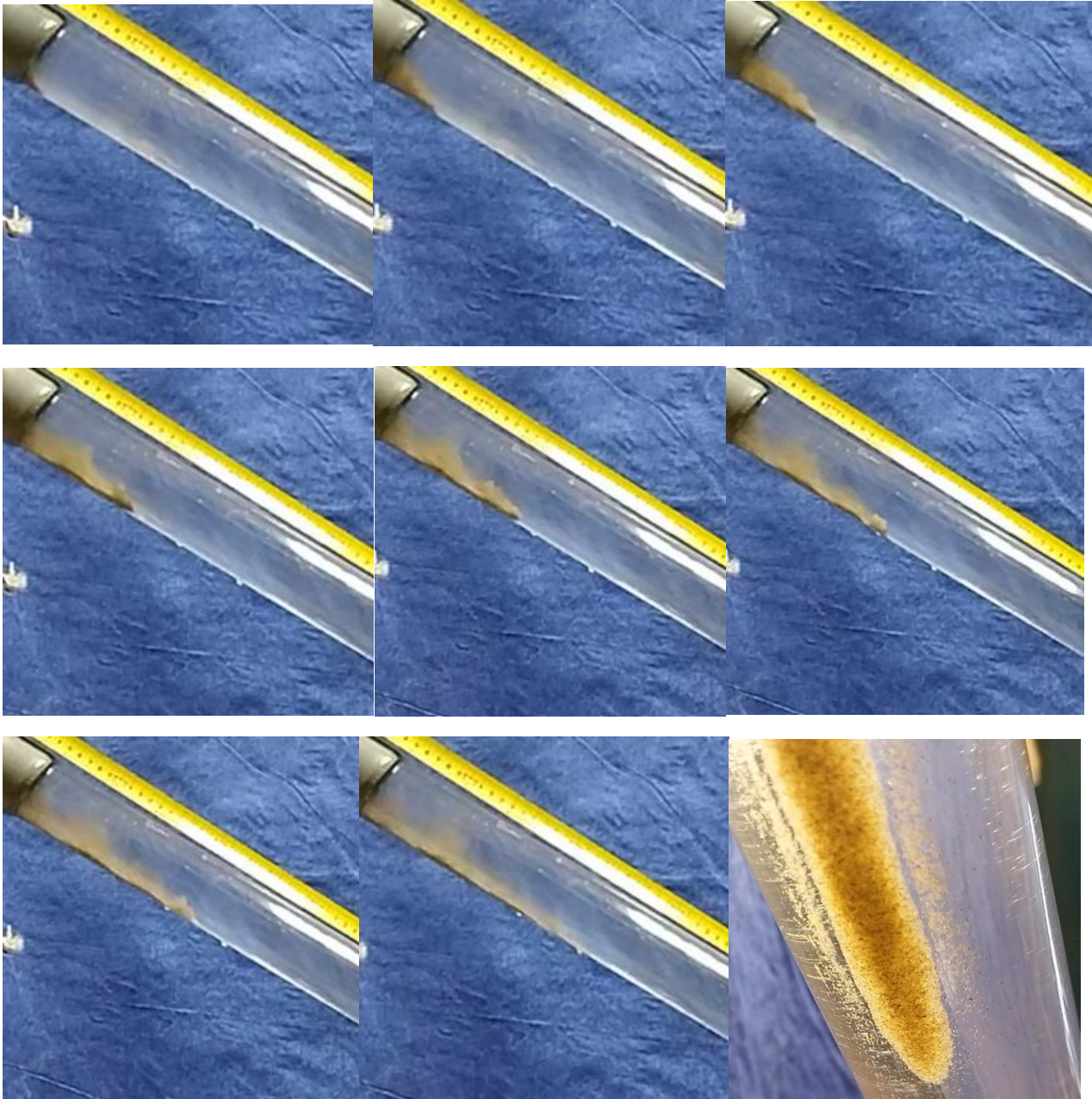


Pipe inclination 23°, hypersaline water, material 28.13 gr.

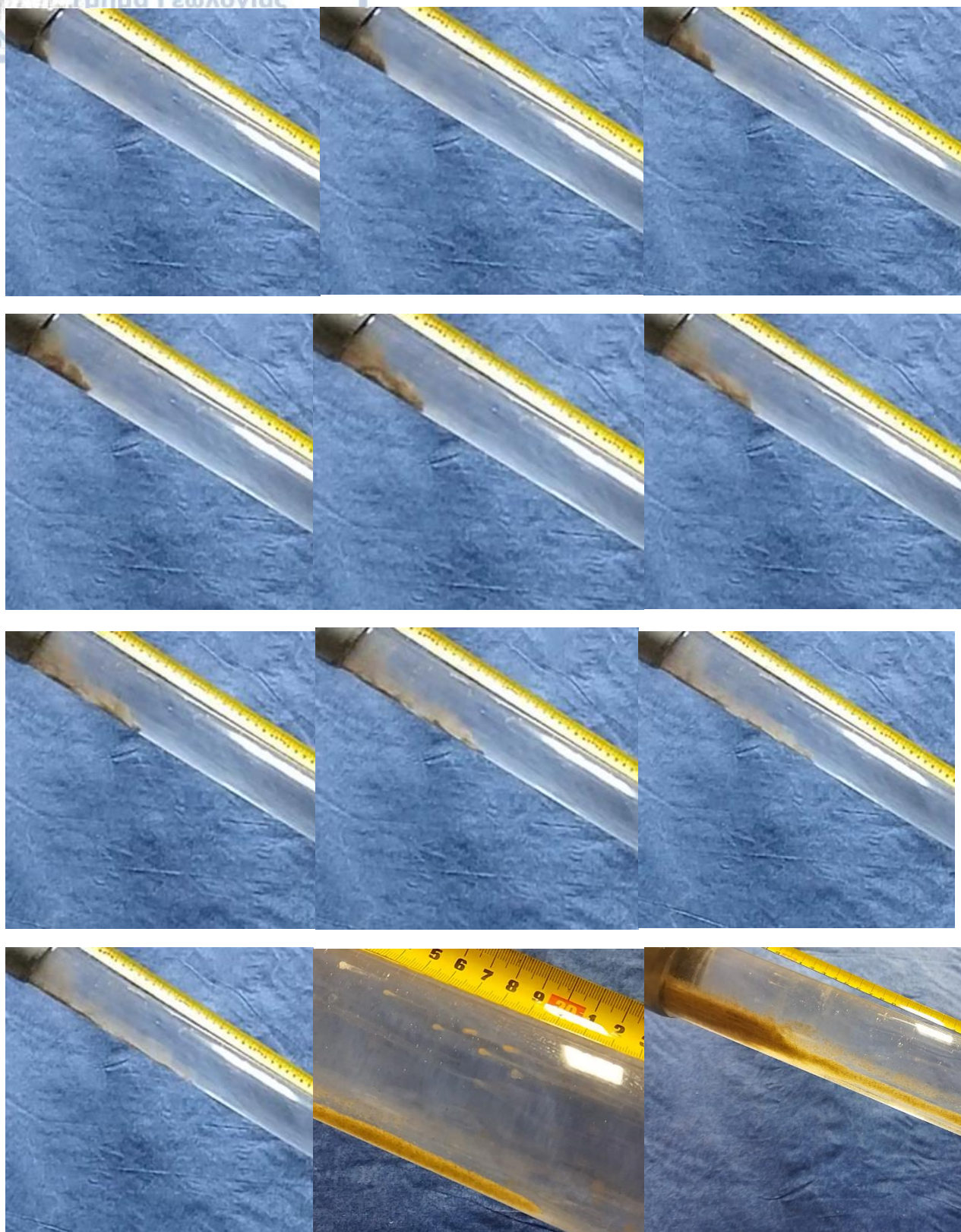


GRAIN SIZE RANGE 2-2.5φ (average 2.25φ)

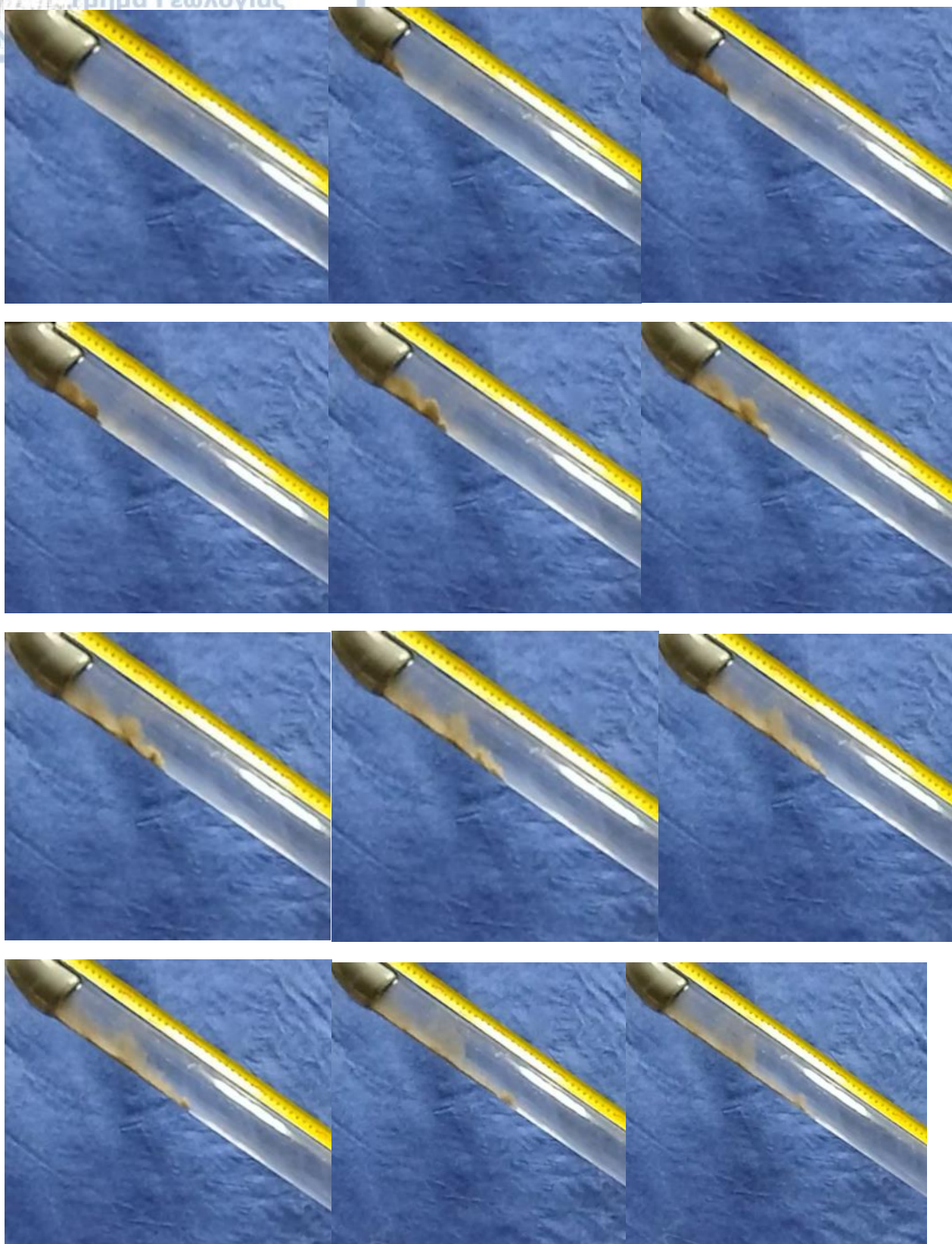
Pipe inclination 22°, tap water, material 12.82 gr.

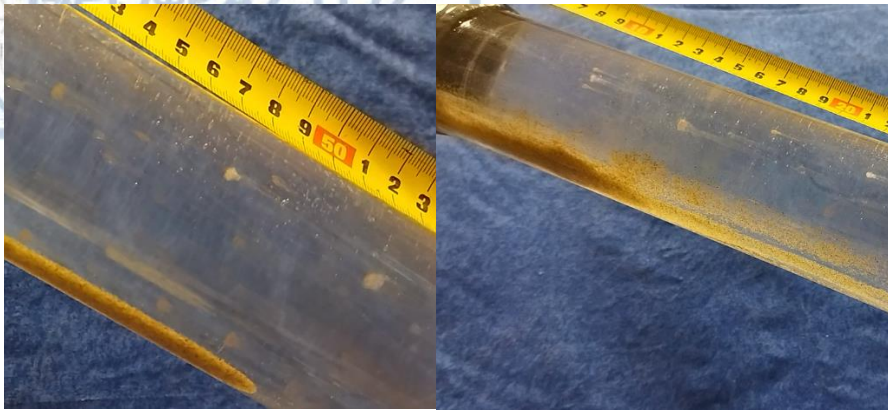


Pipe inclination 25°, tap water, material 12.82 gr.



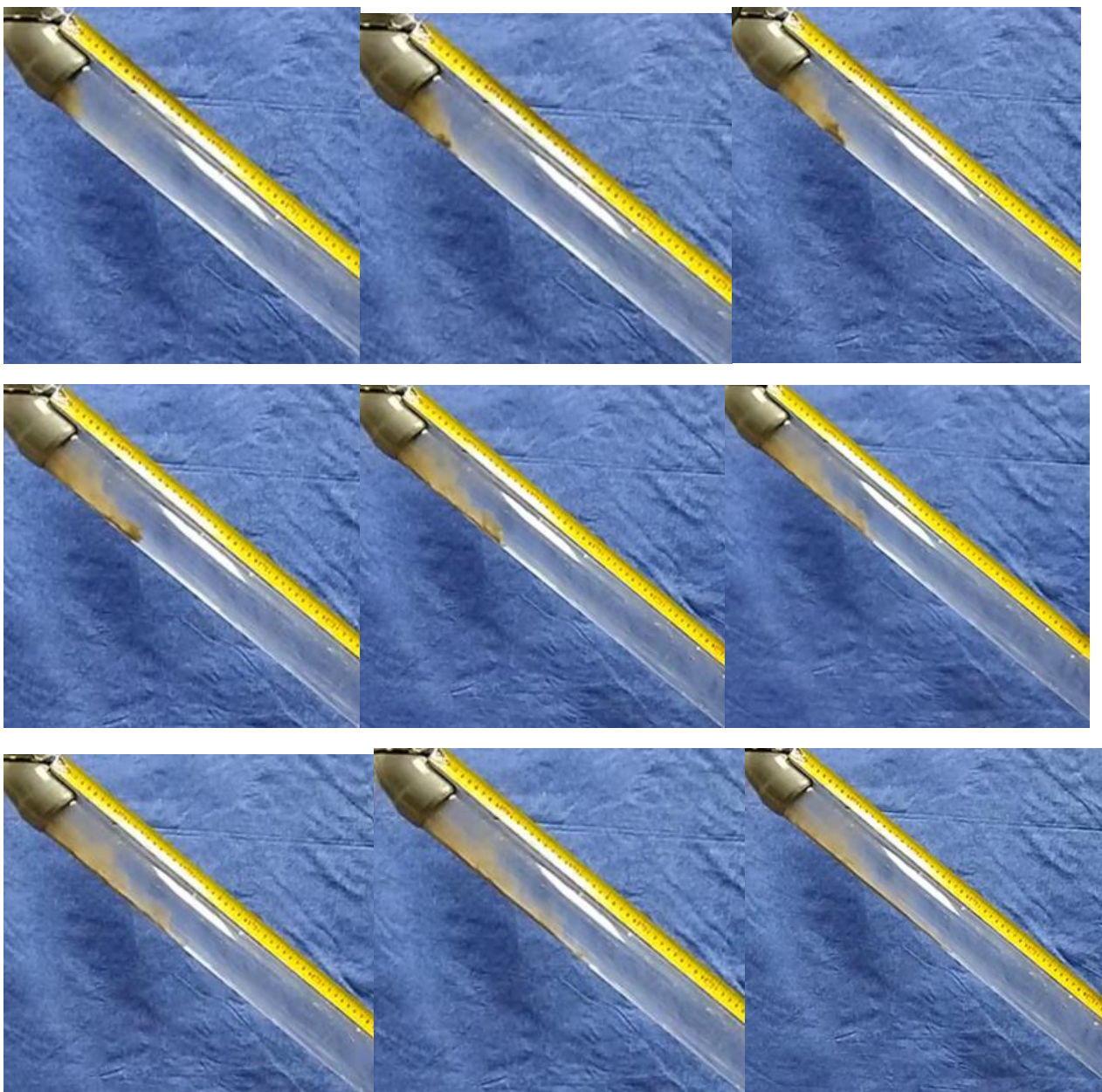
Pipe inclination 27°, tap water, material 12.82 gr.





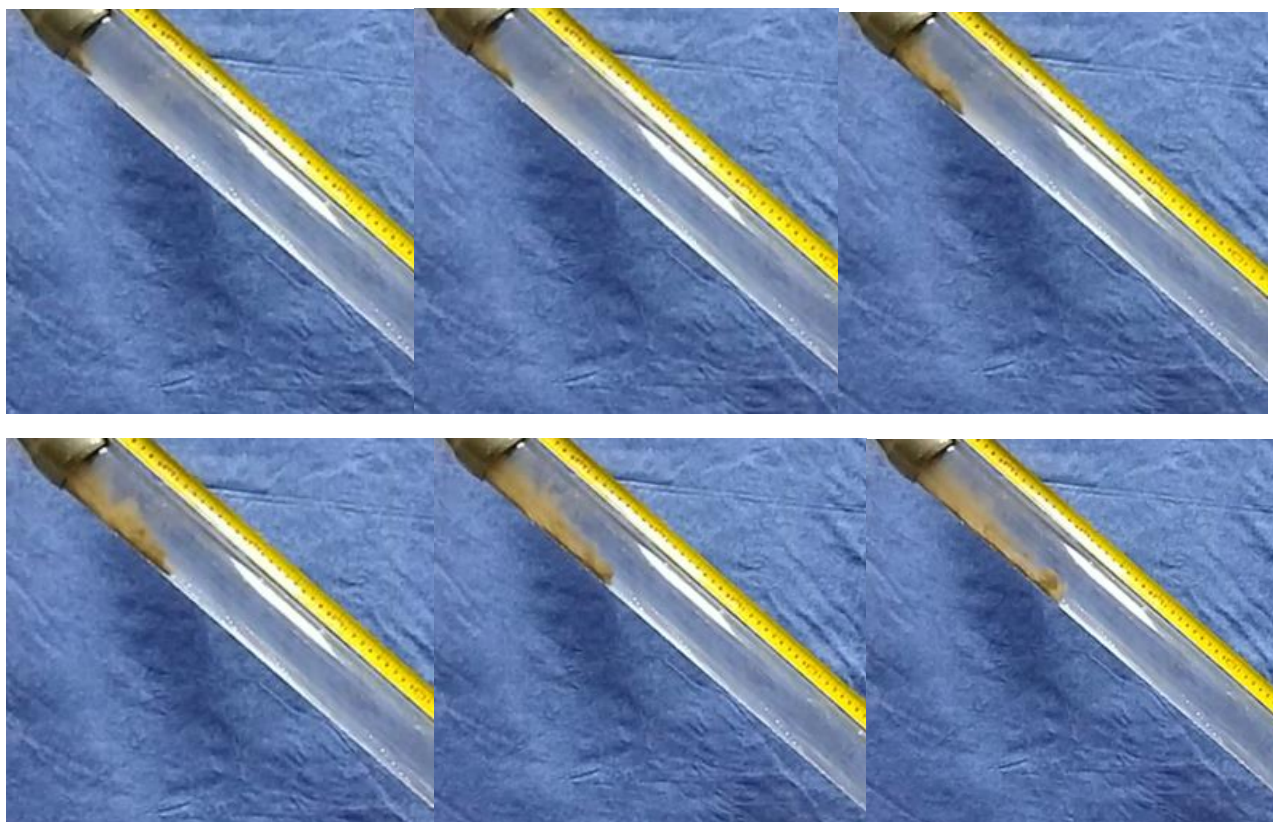
Pipe inclination 35° , tap water, material 12.82 gr.

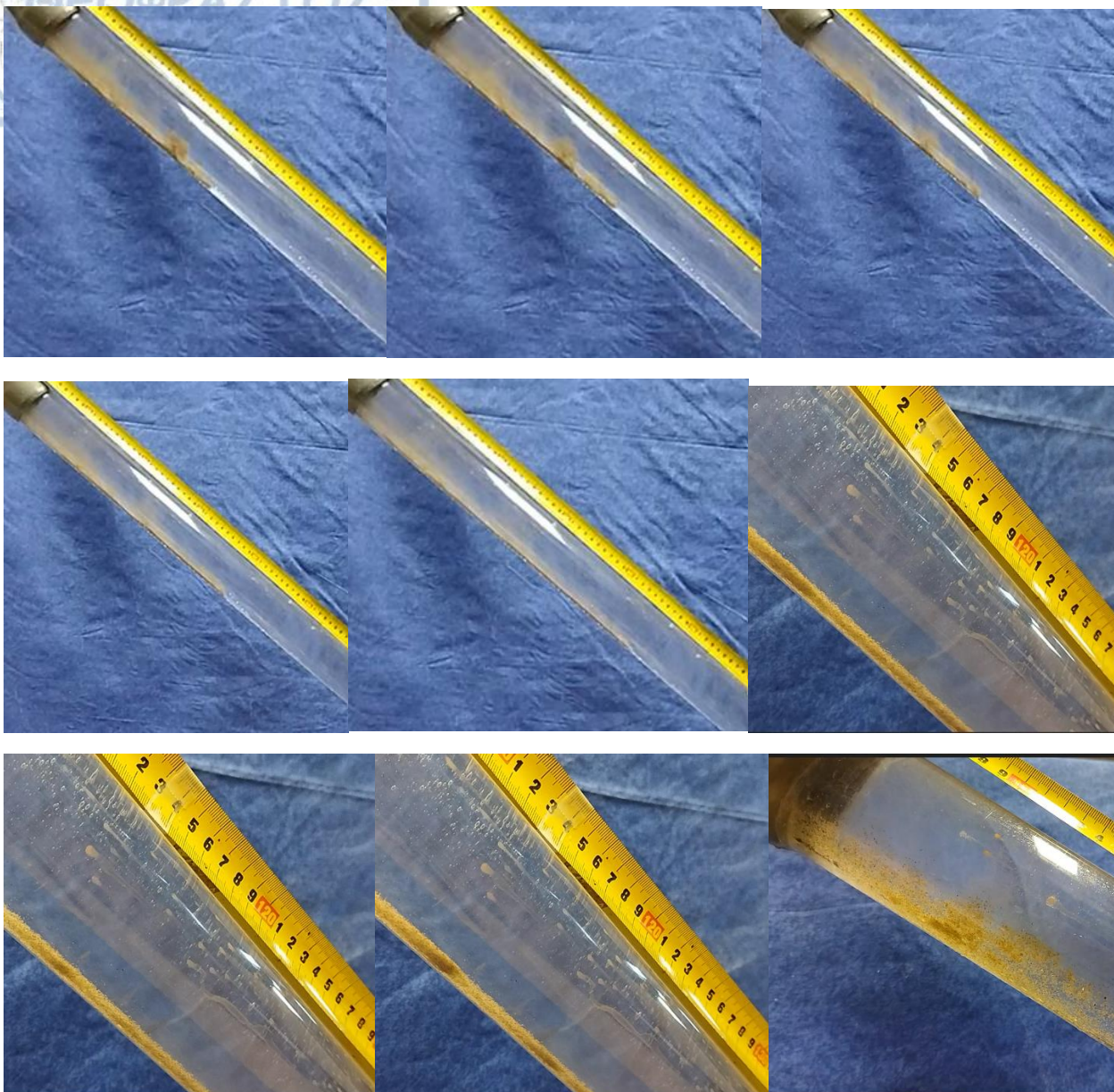
(a)

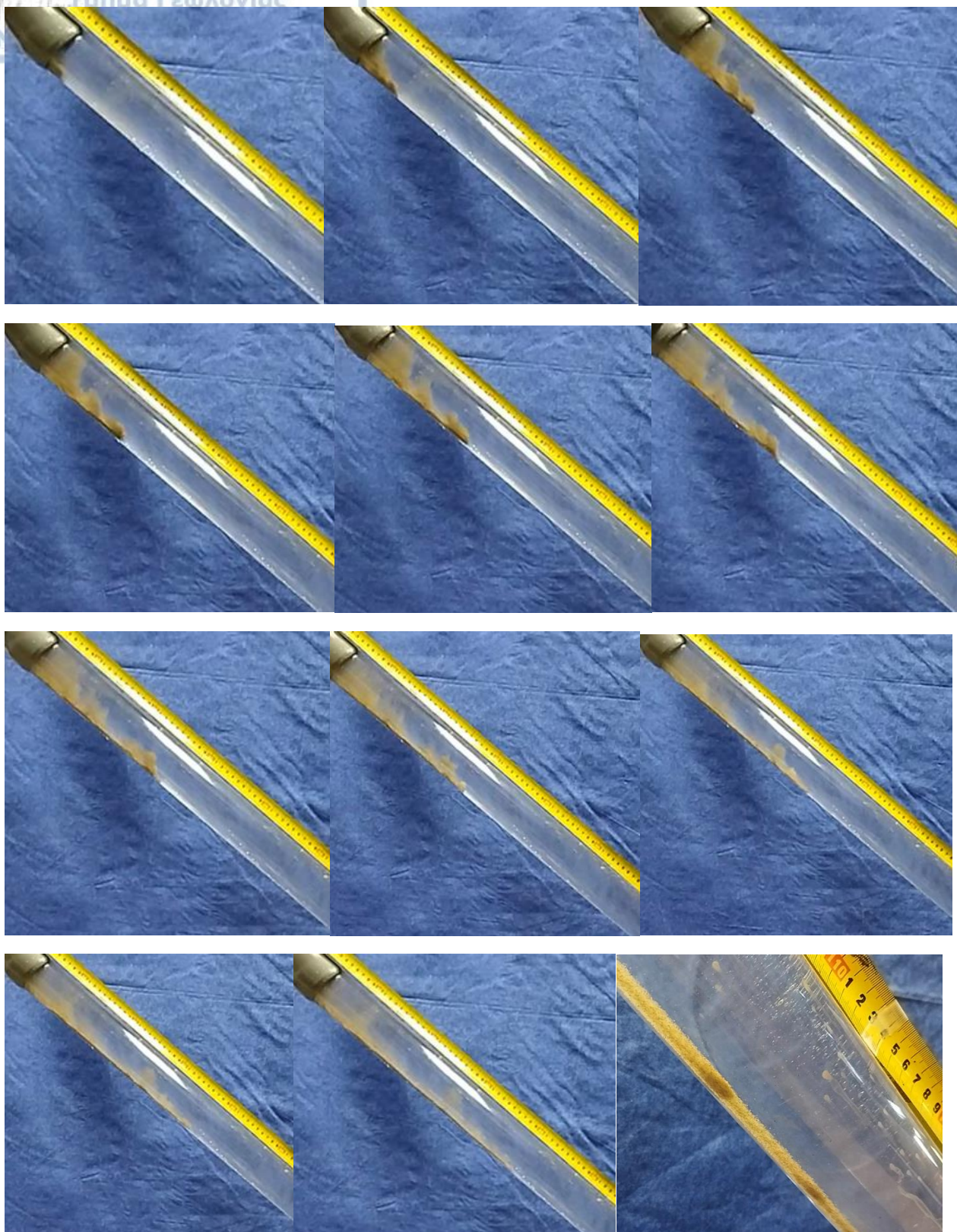




(b)



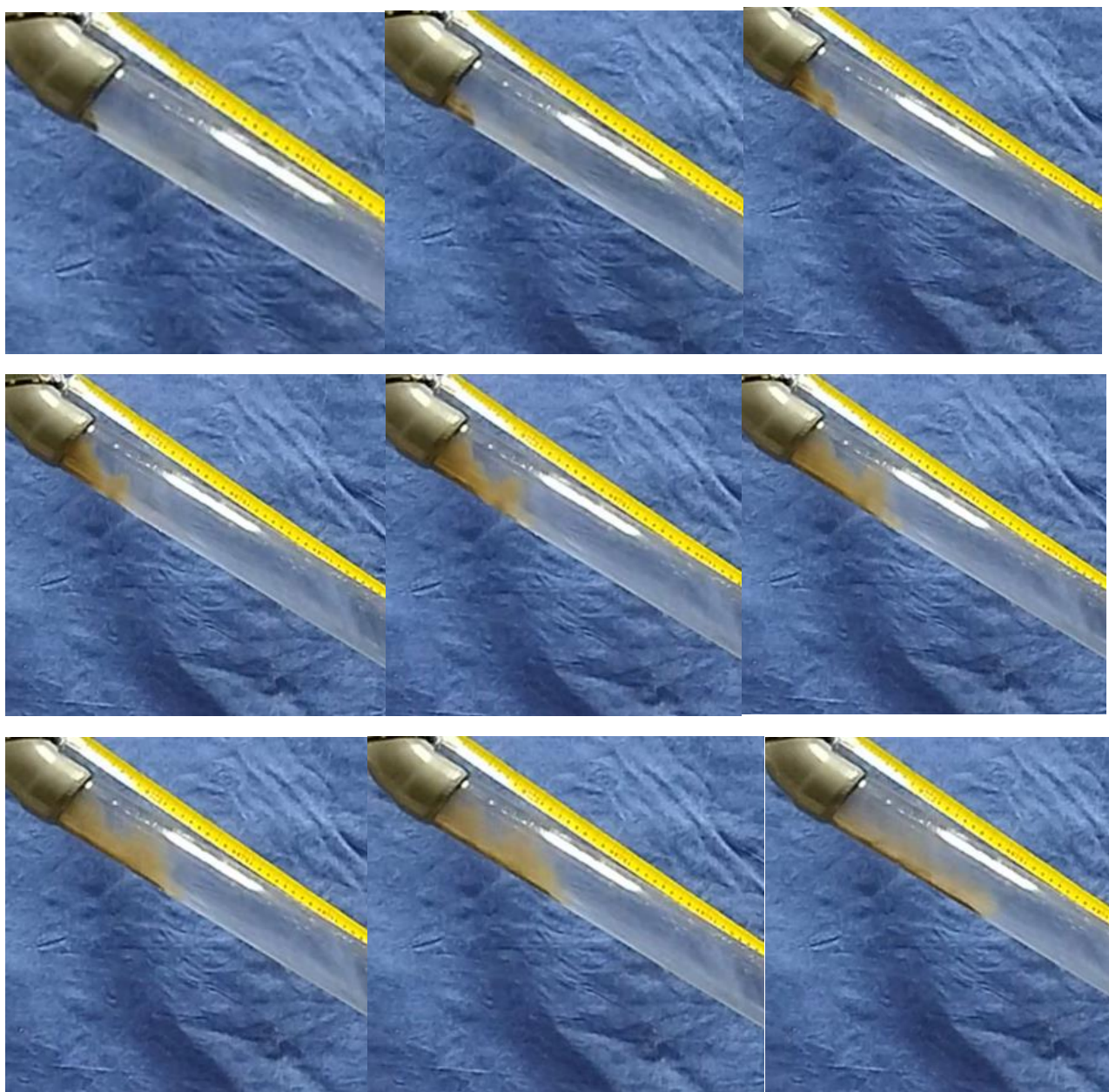


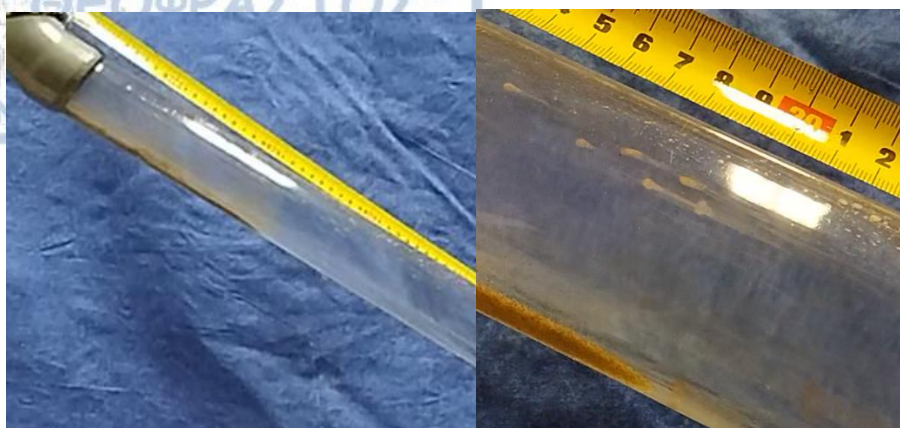




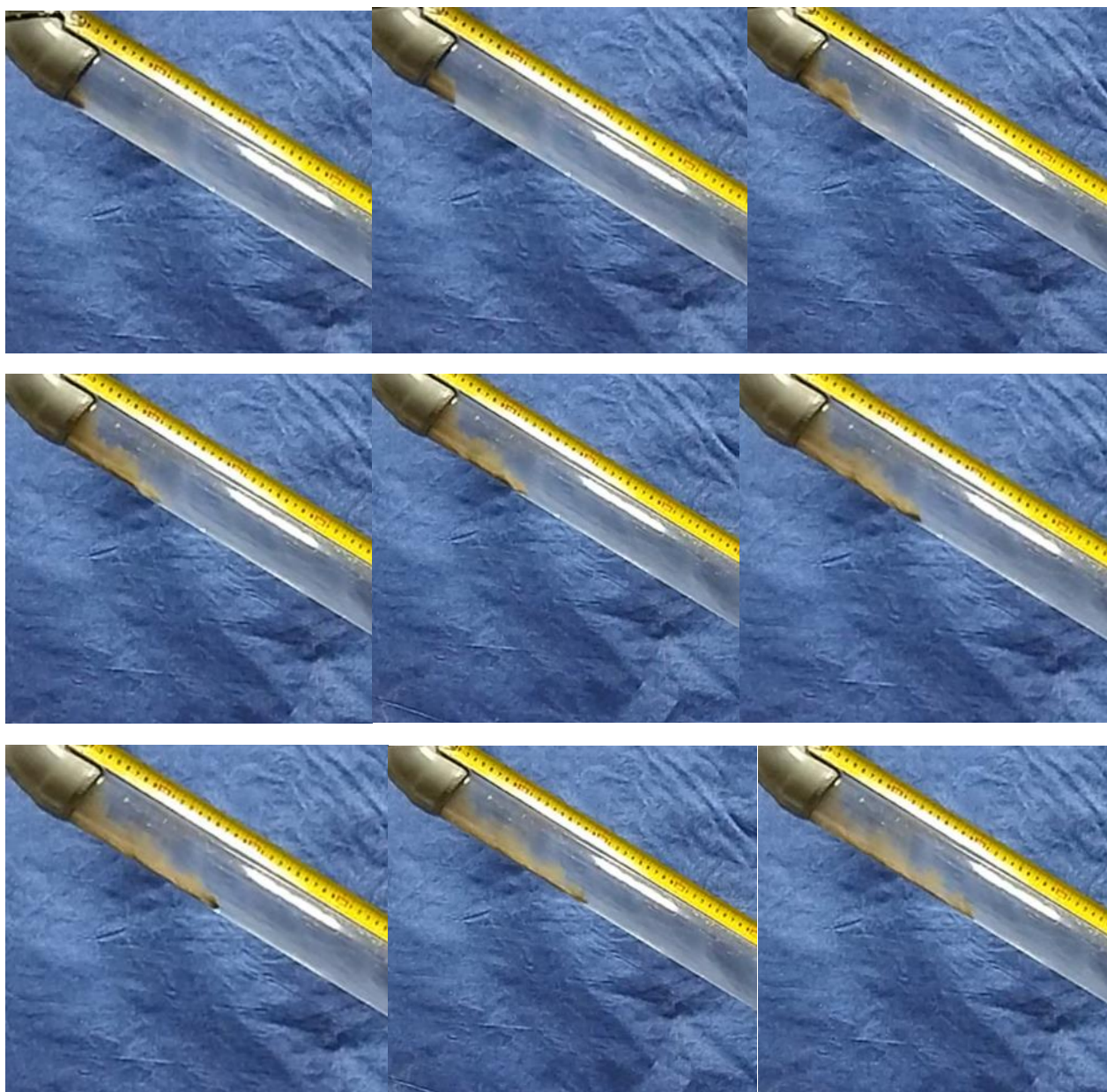
Pipe inclination 25°, hypersaline water, material 12.82gr.

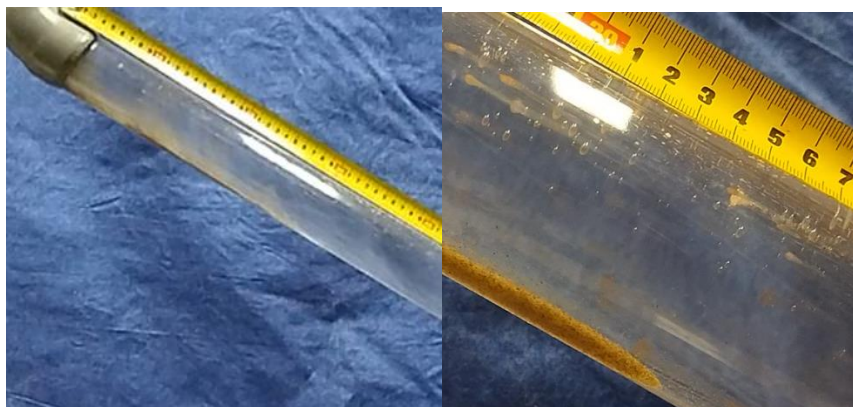
a)





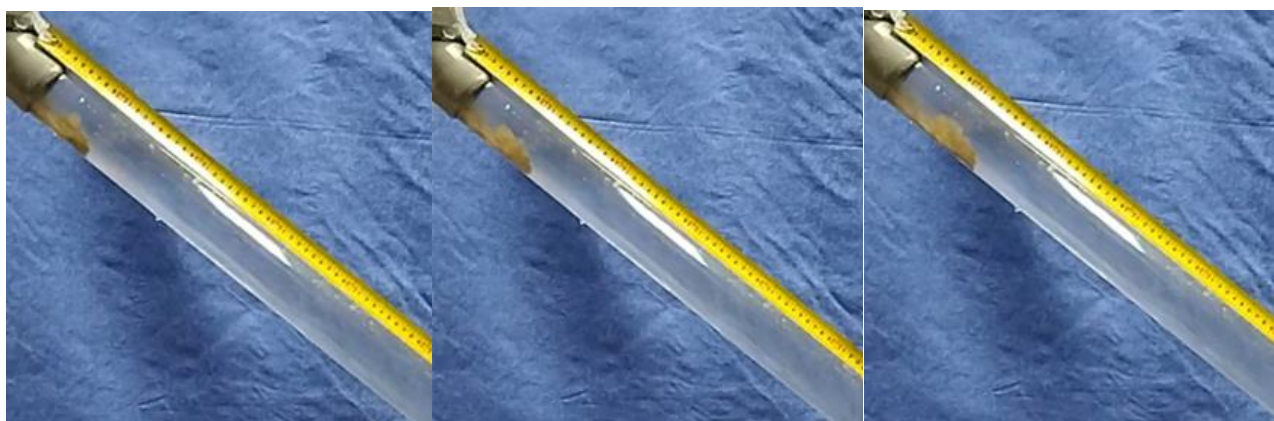
(b)

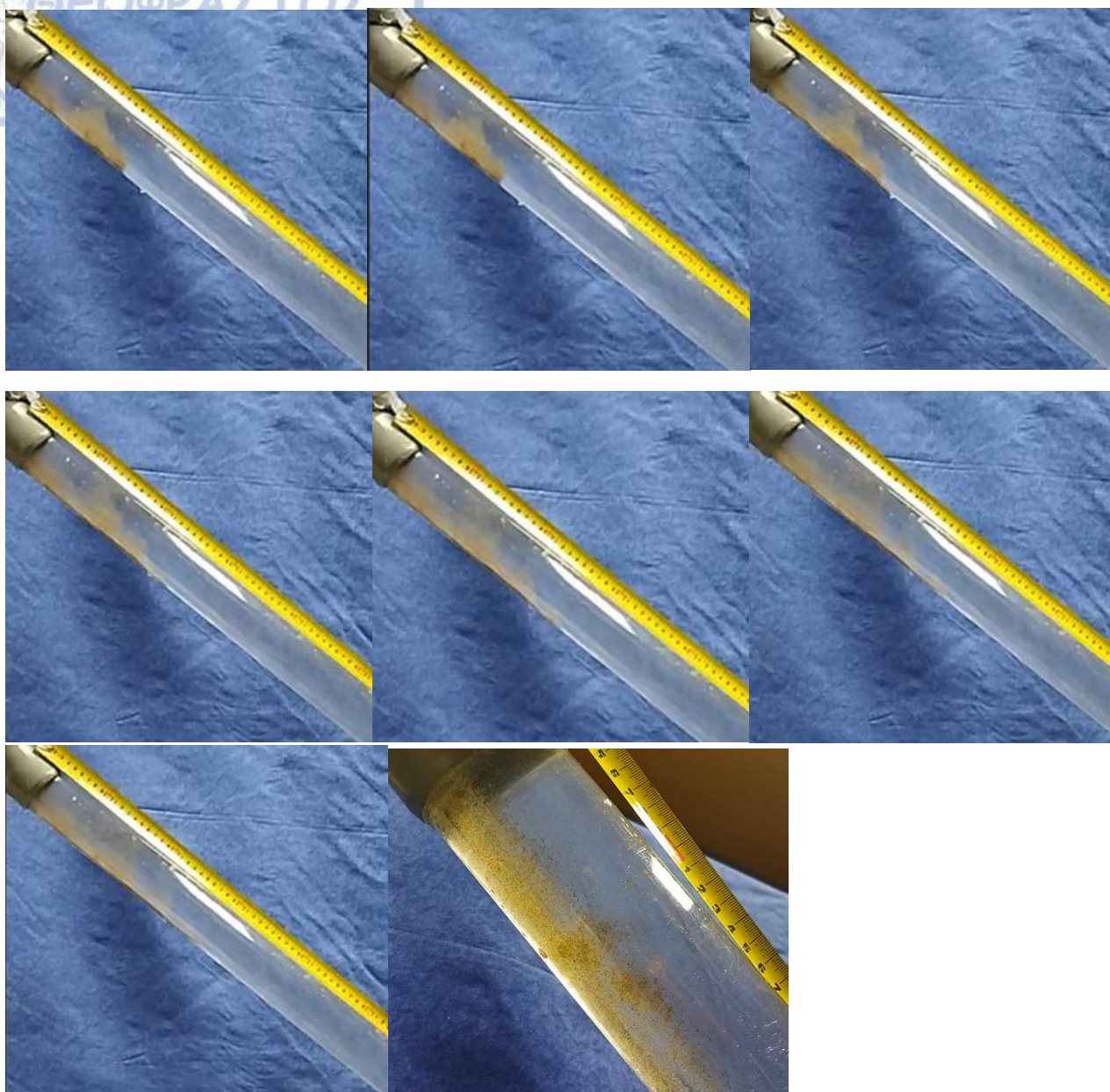




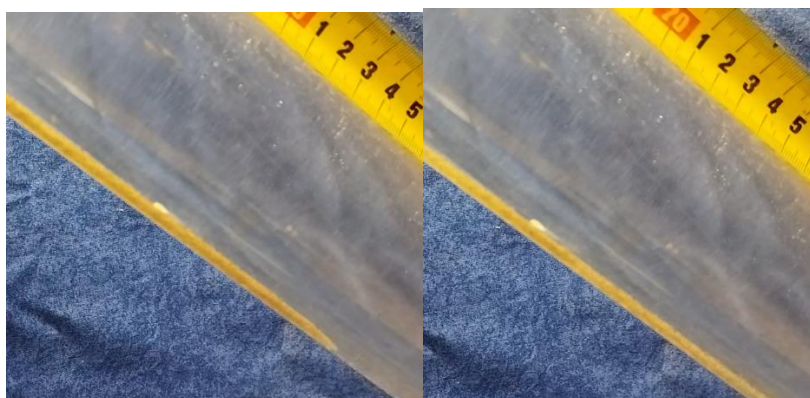
Pipe inclination 35°, hypersaline water, material 12.82 gr.

(a)





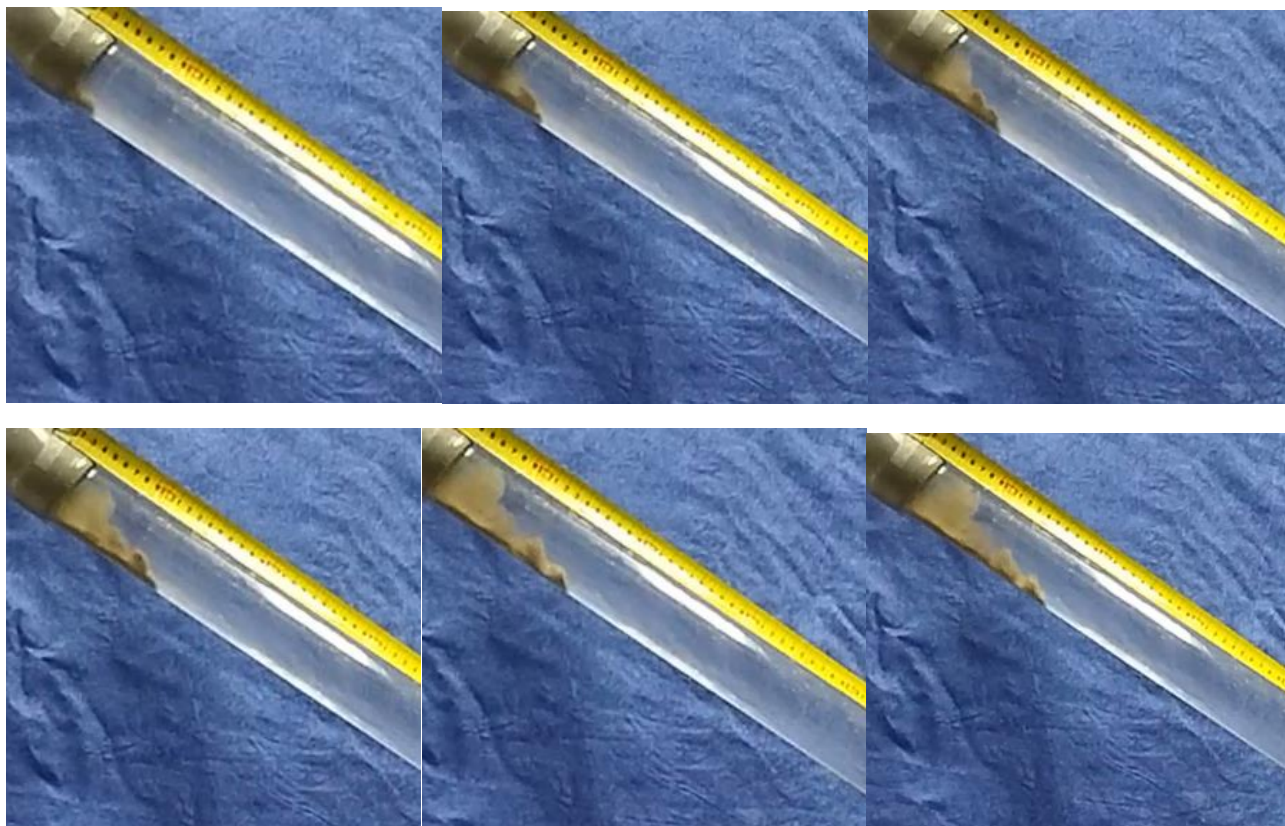
(b)

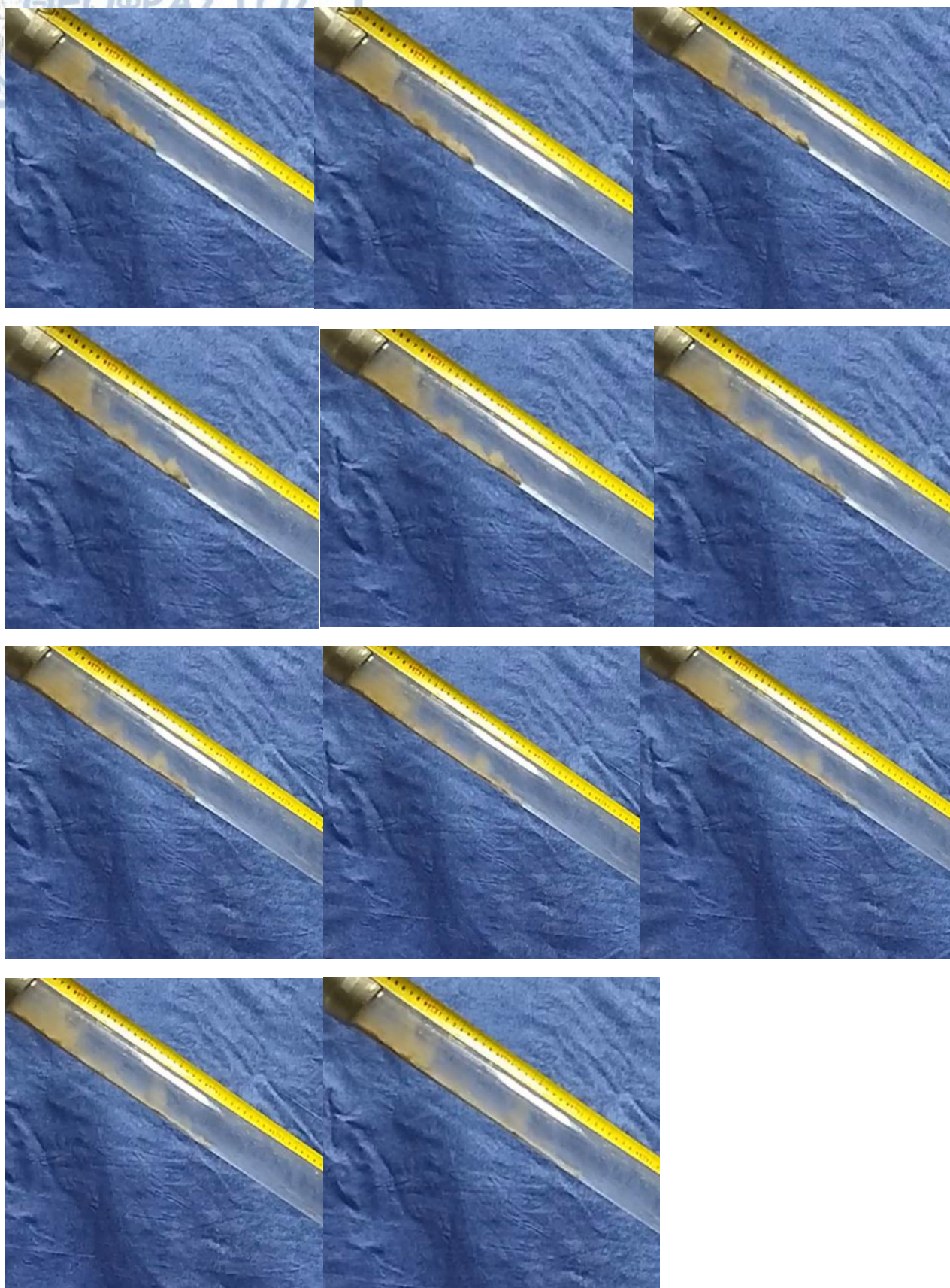




Pipe inclination 22°, tap water, material 28.78 gr.

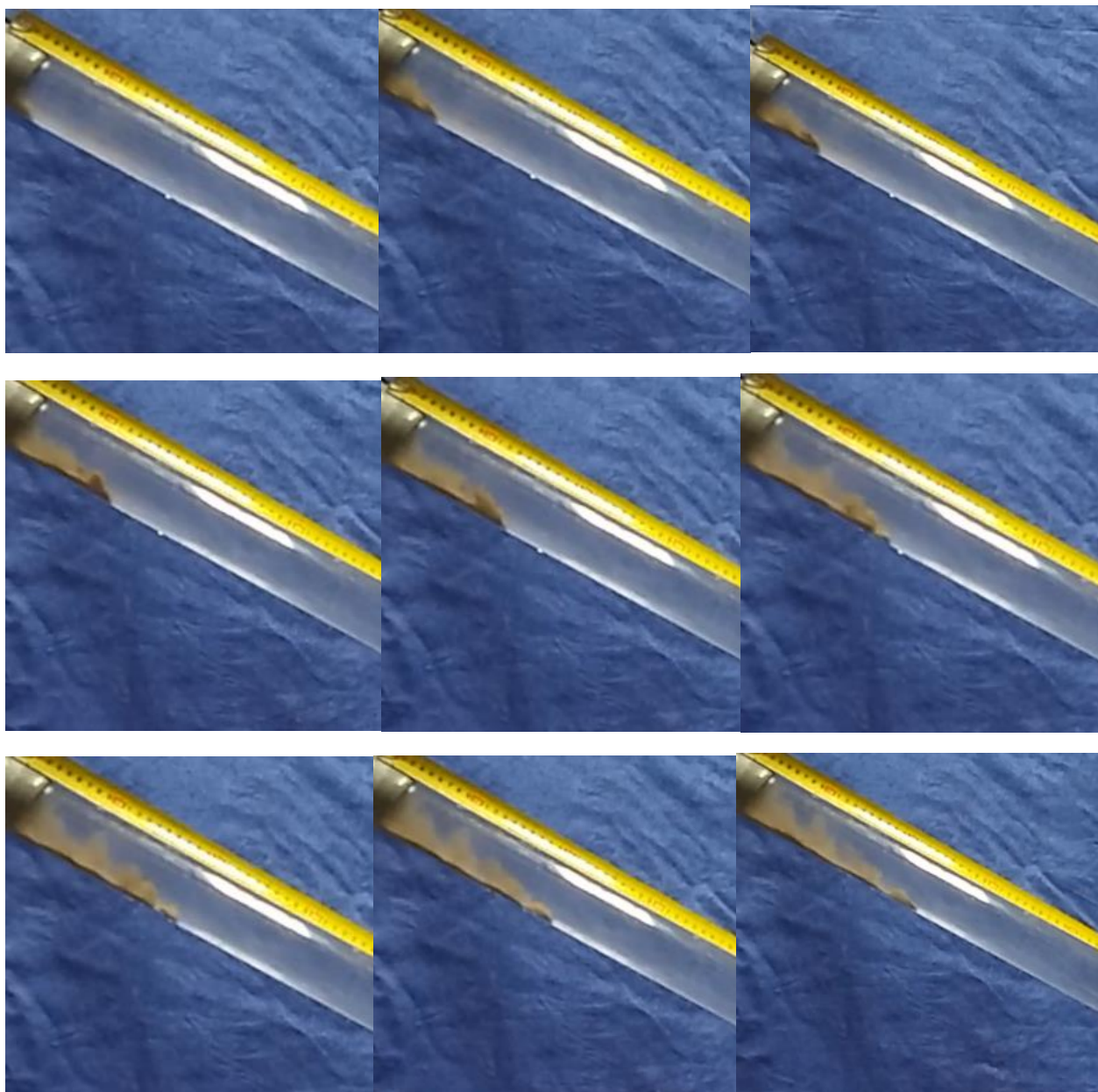
(a)

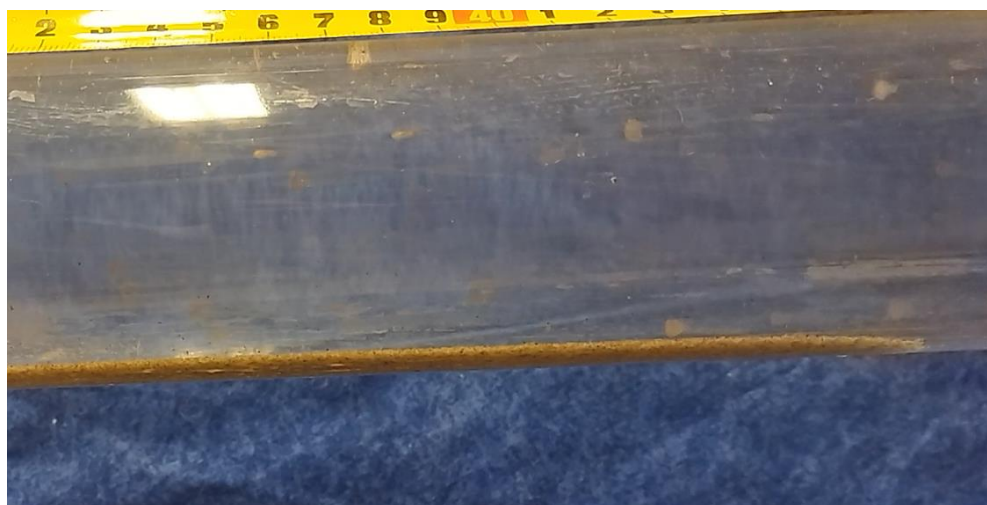
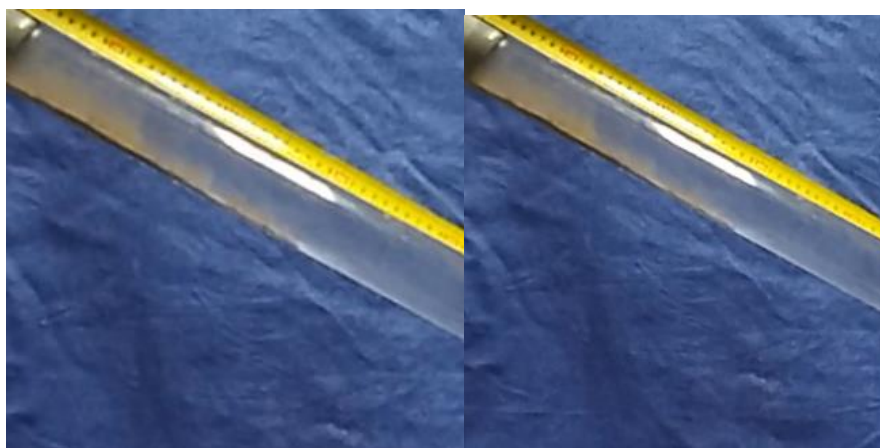






(b)

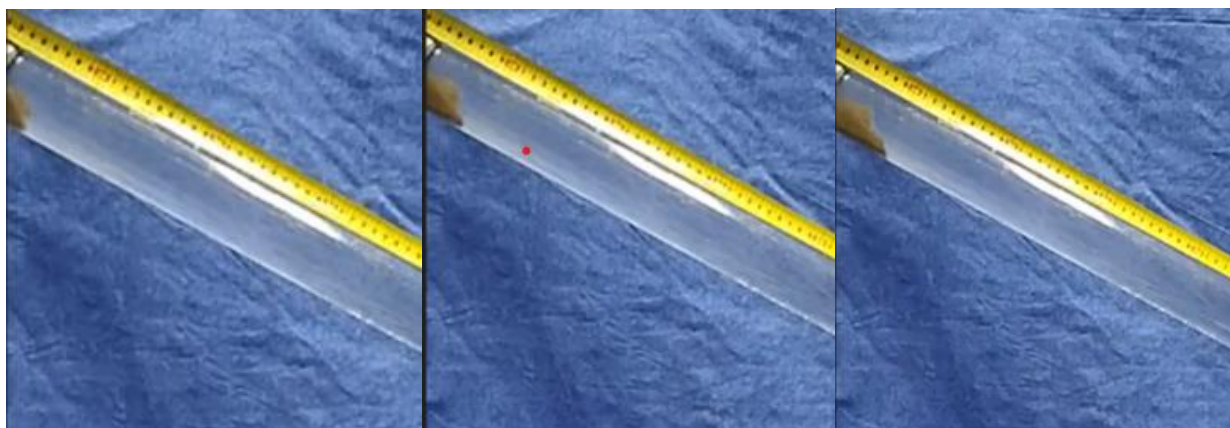


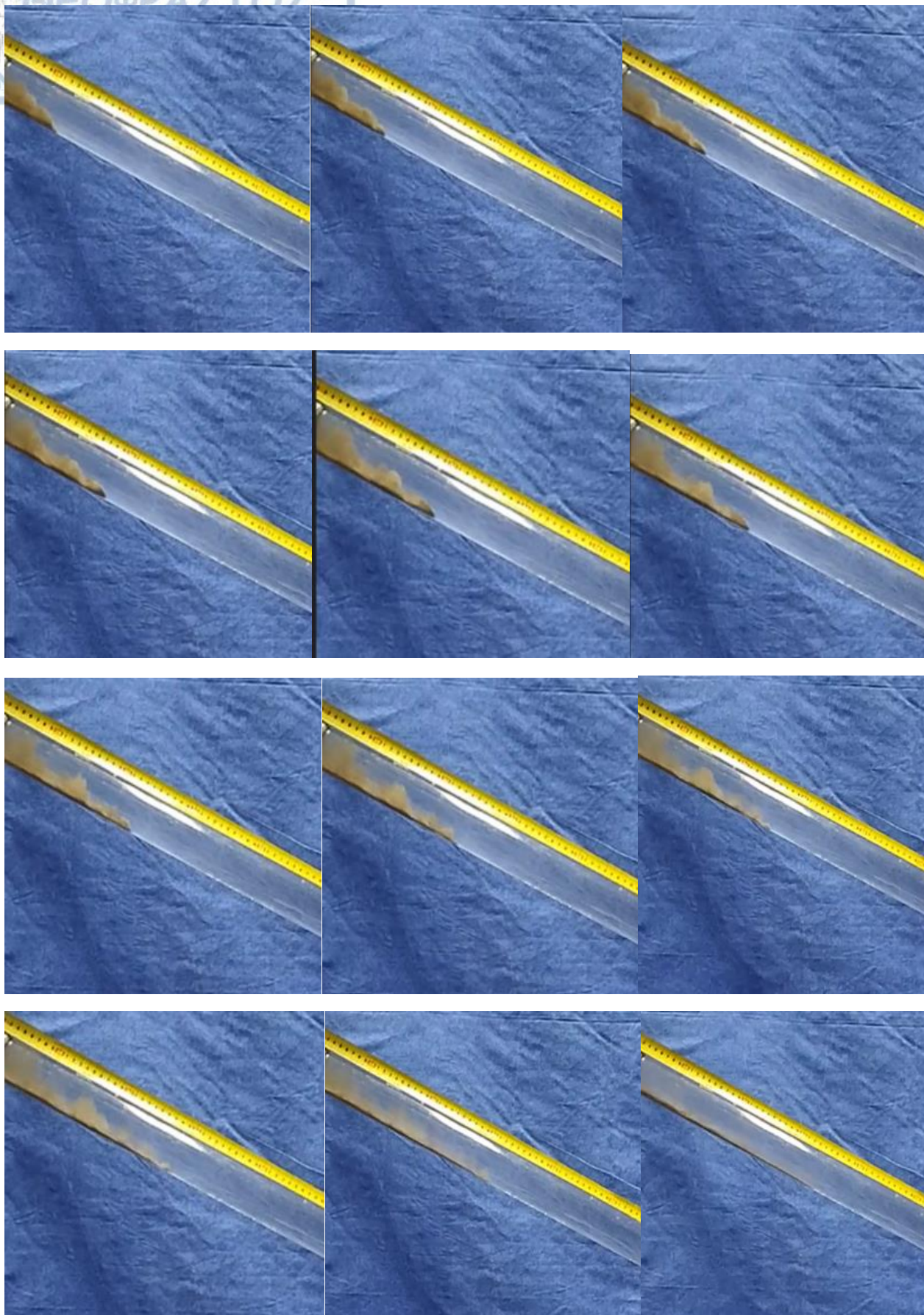


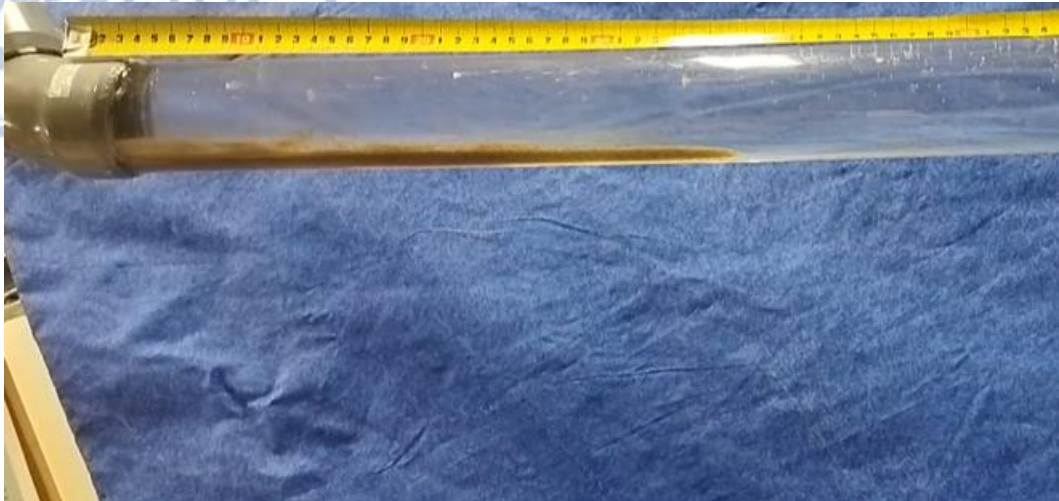


Pipe inclination 23°, hypersaline water, material 28.78 gr.

(a)





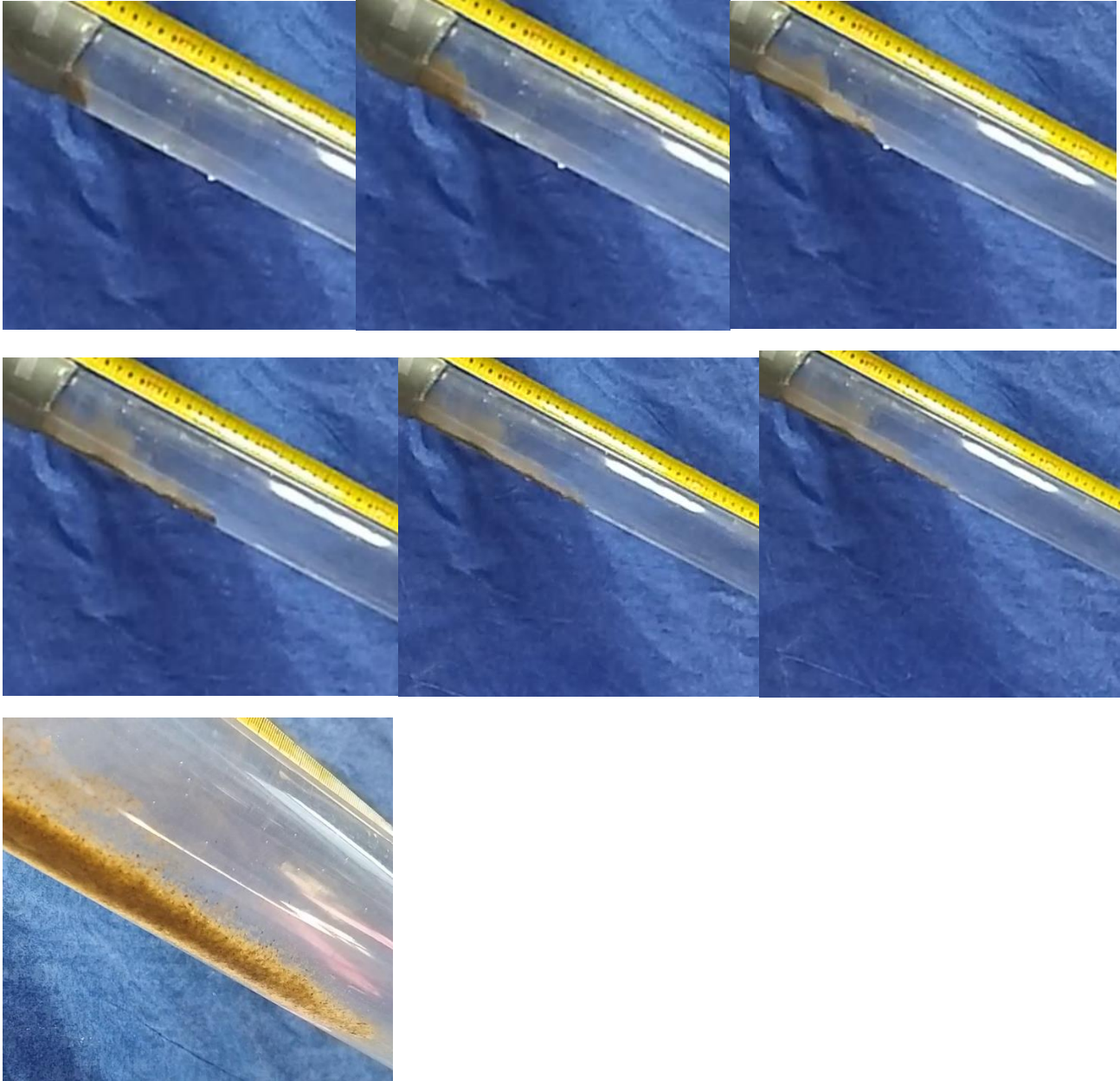


(b)

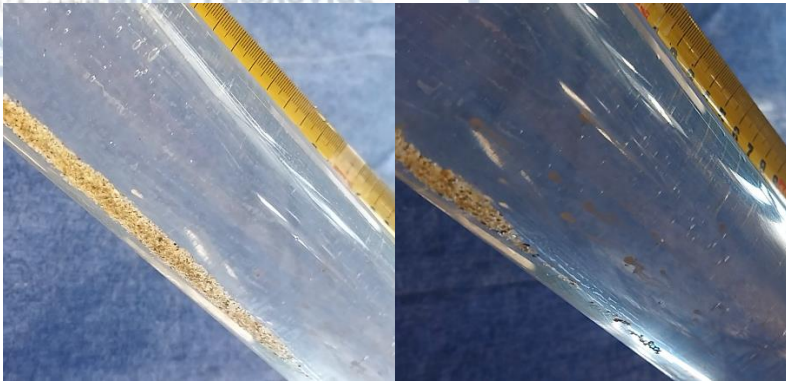


DUNE MATERIAL (-1.5- >4 φ)

Pipe inclination 20°, tap water, material 13.2 gr.

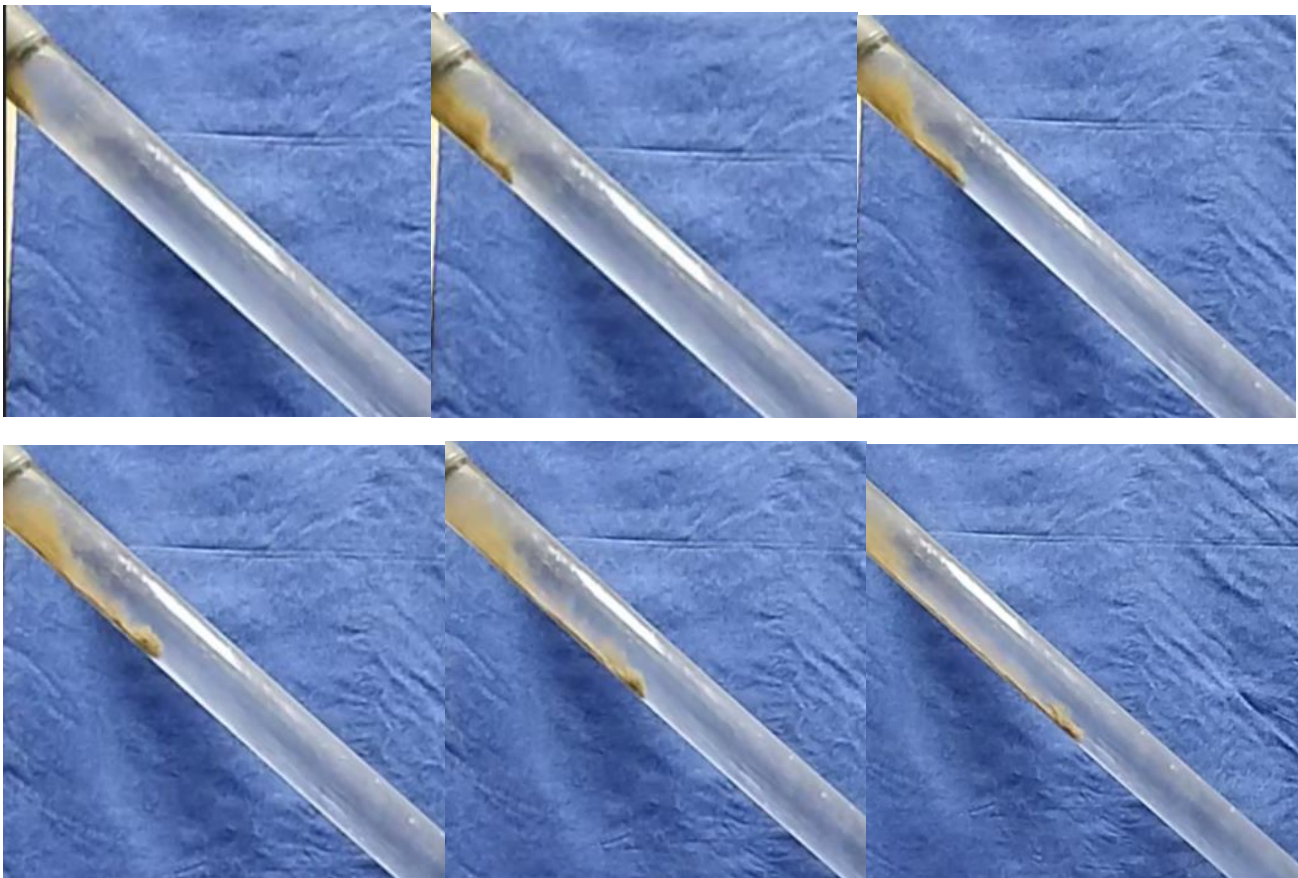


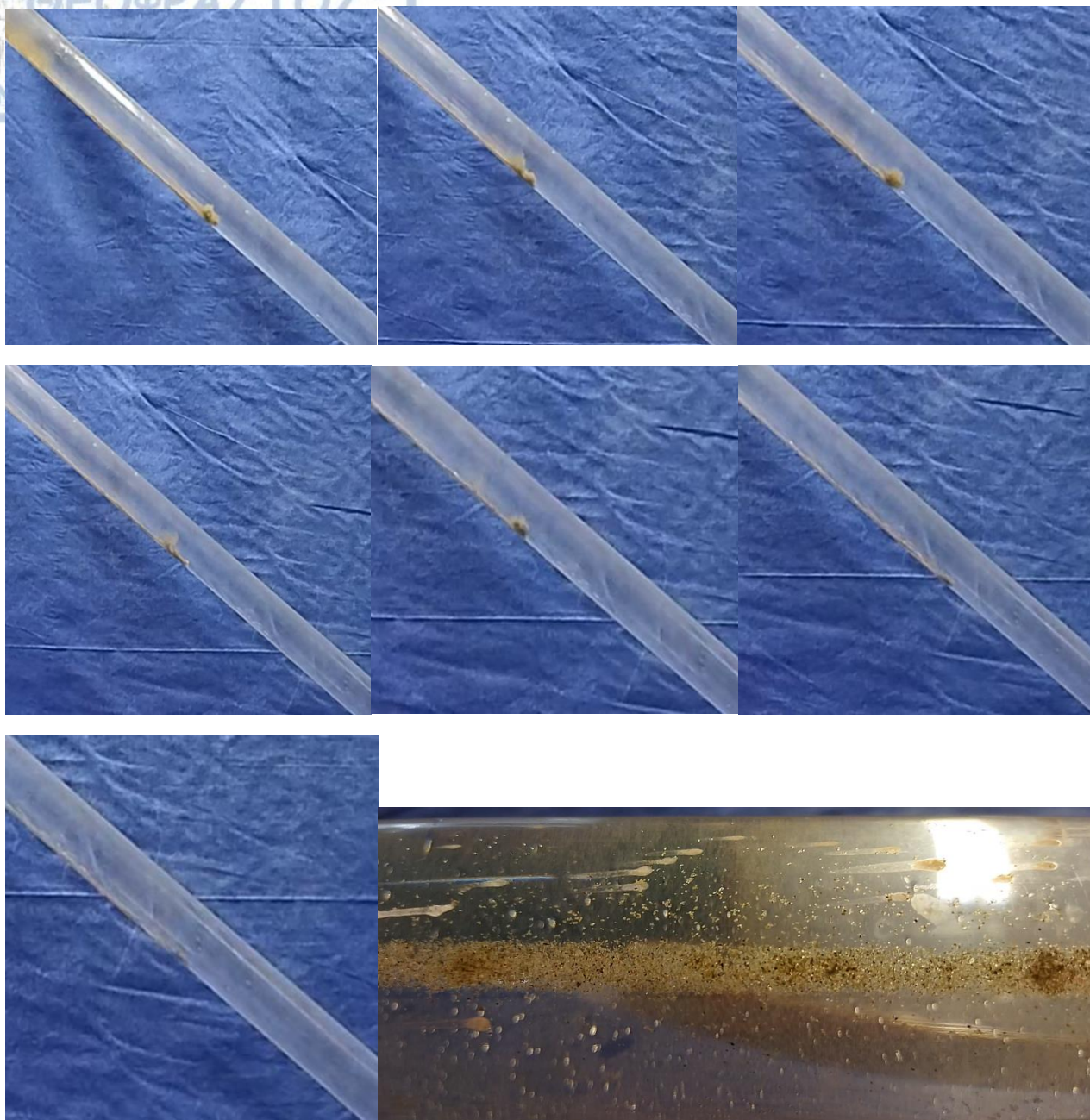
Pipe inclination 22°, tap water, material 13.2 gr.

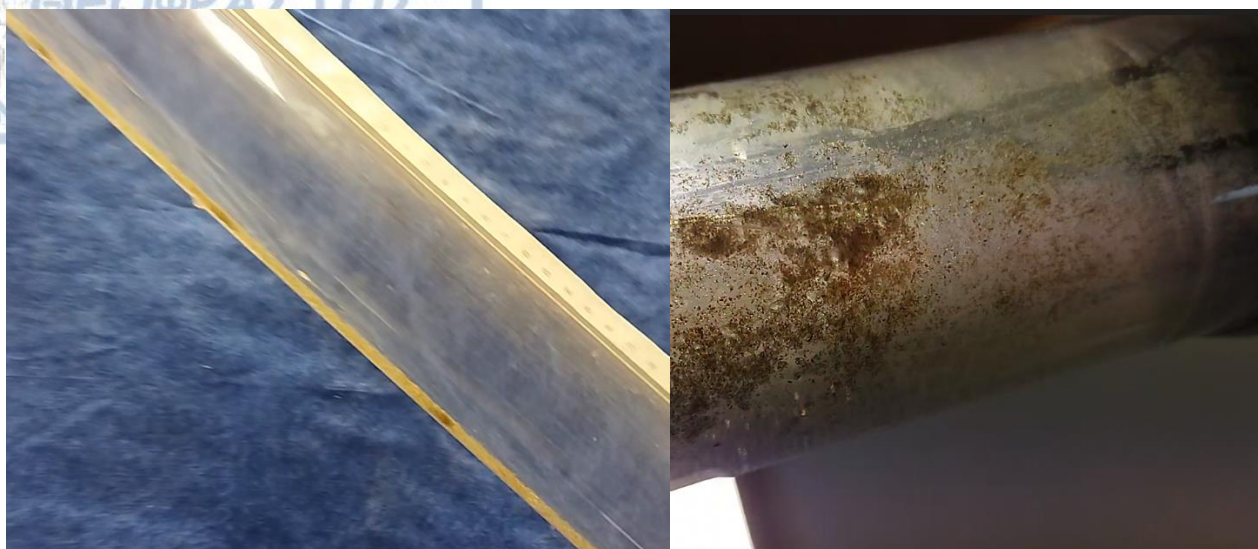


Pipe inclination 35°, tap water, material 13.2 gr.

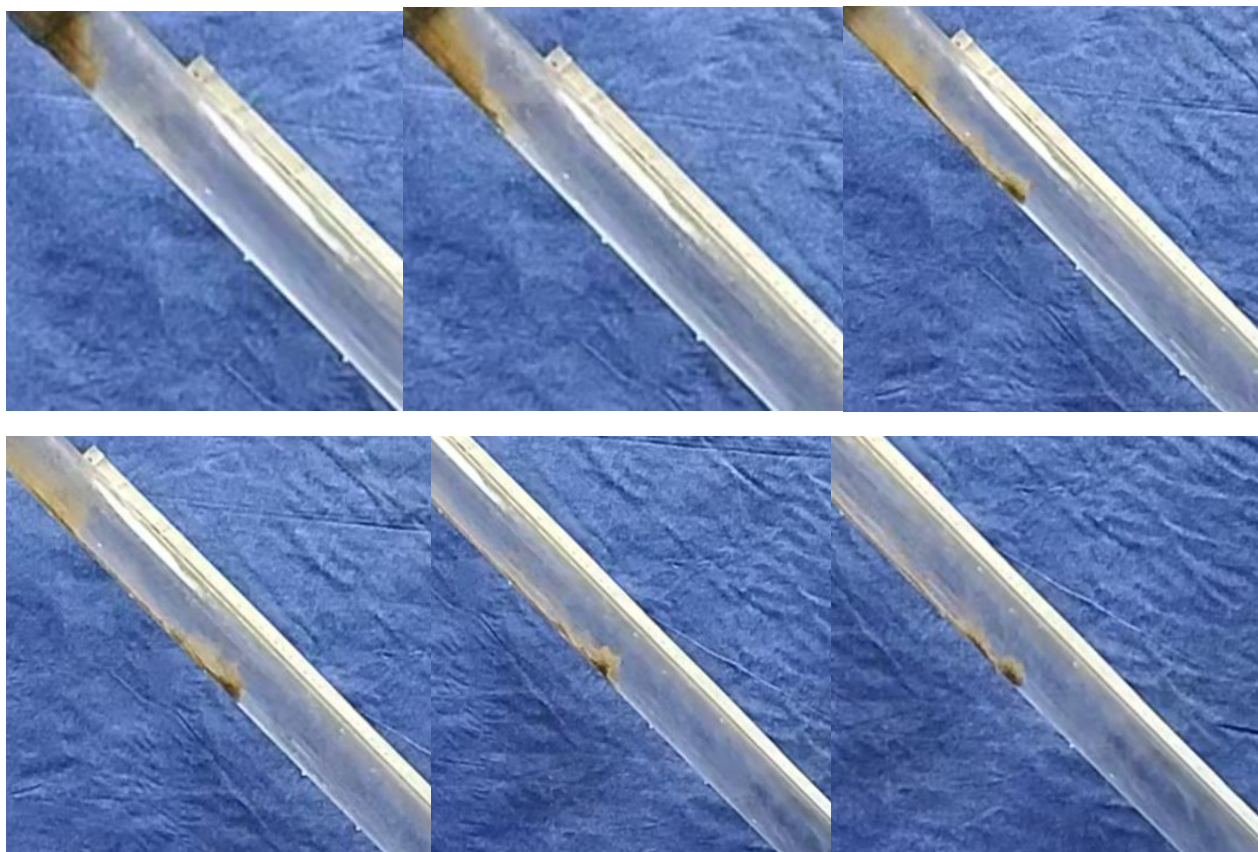
(a)

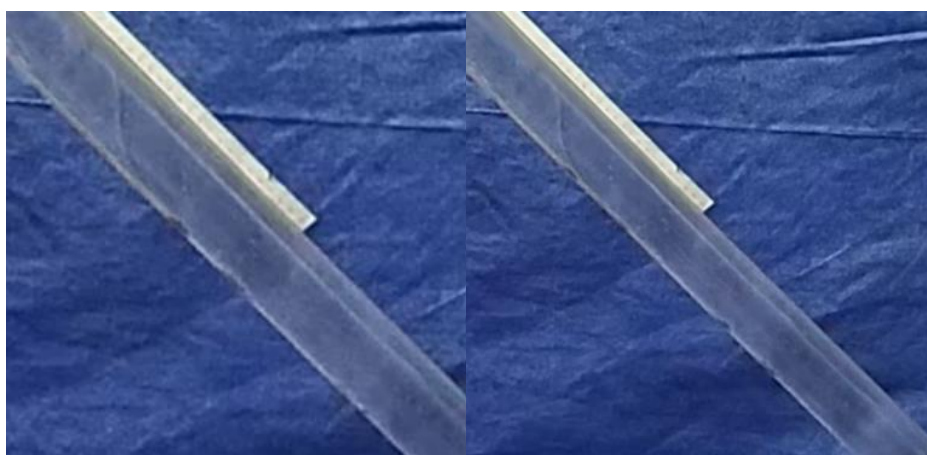
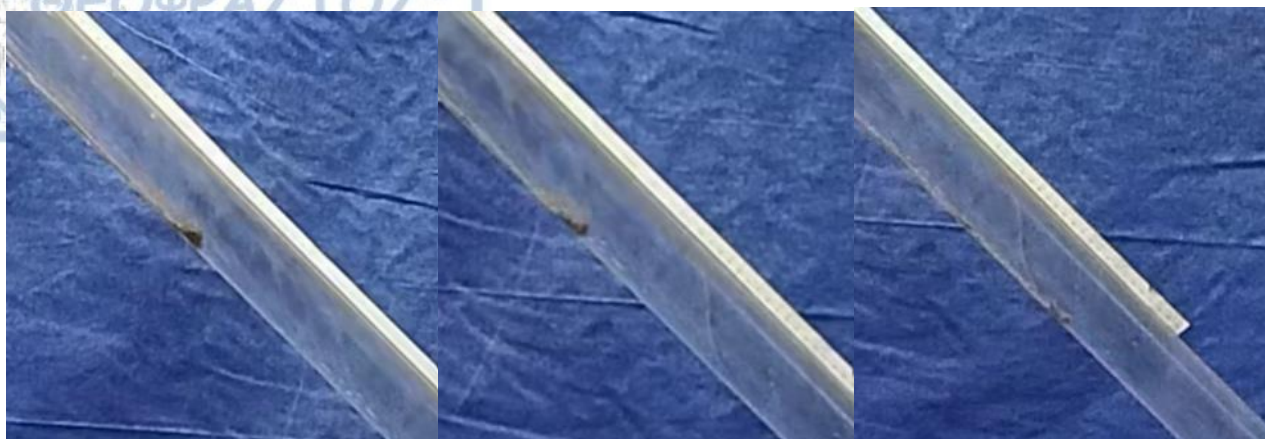






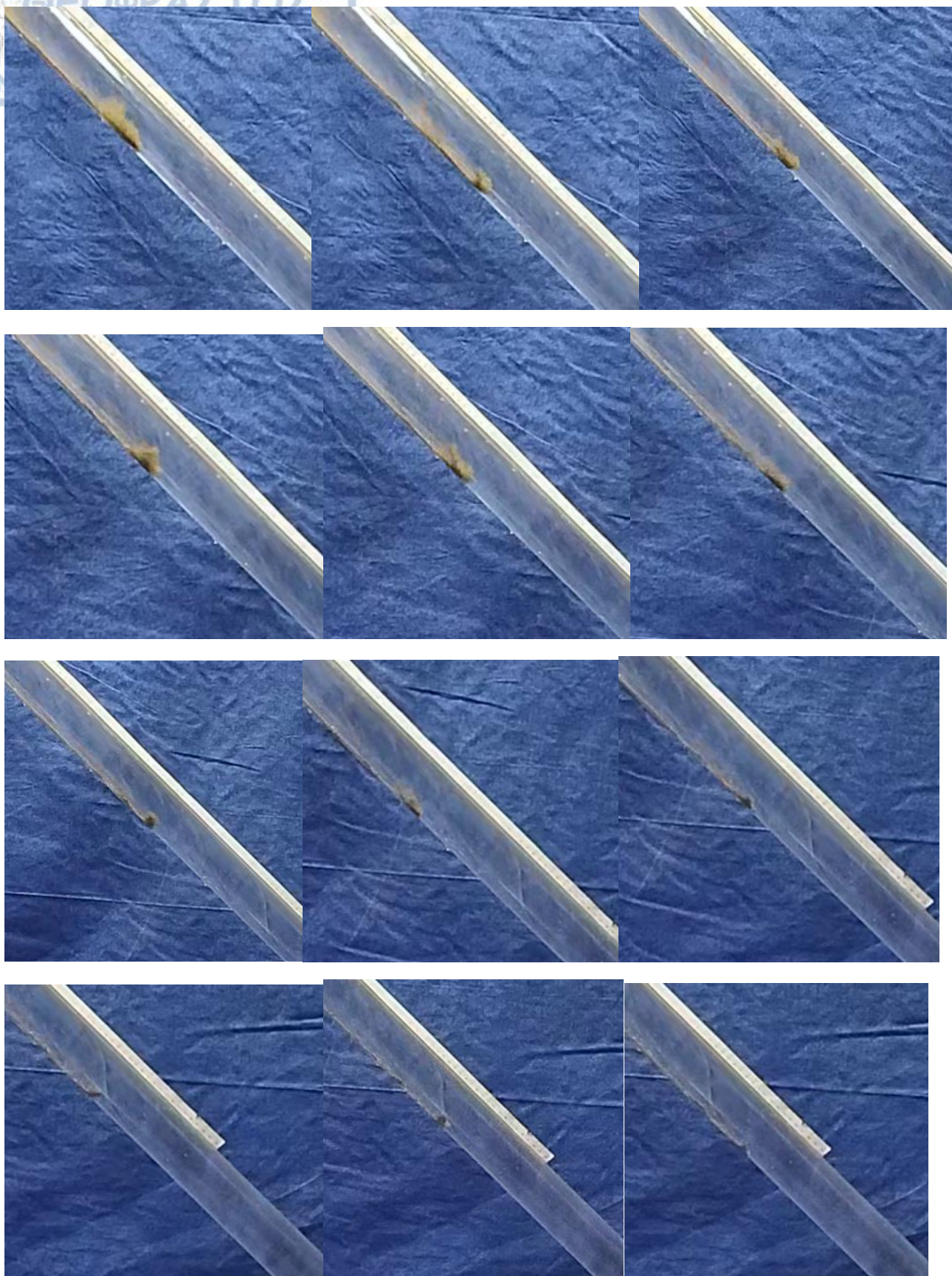
(b)

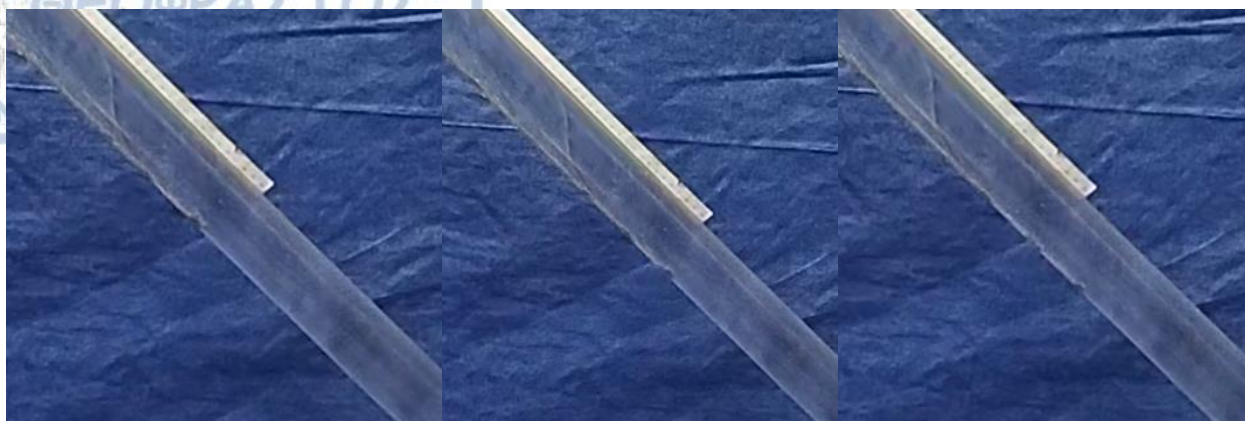




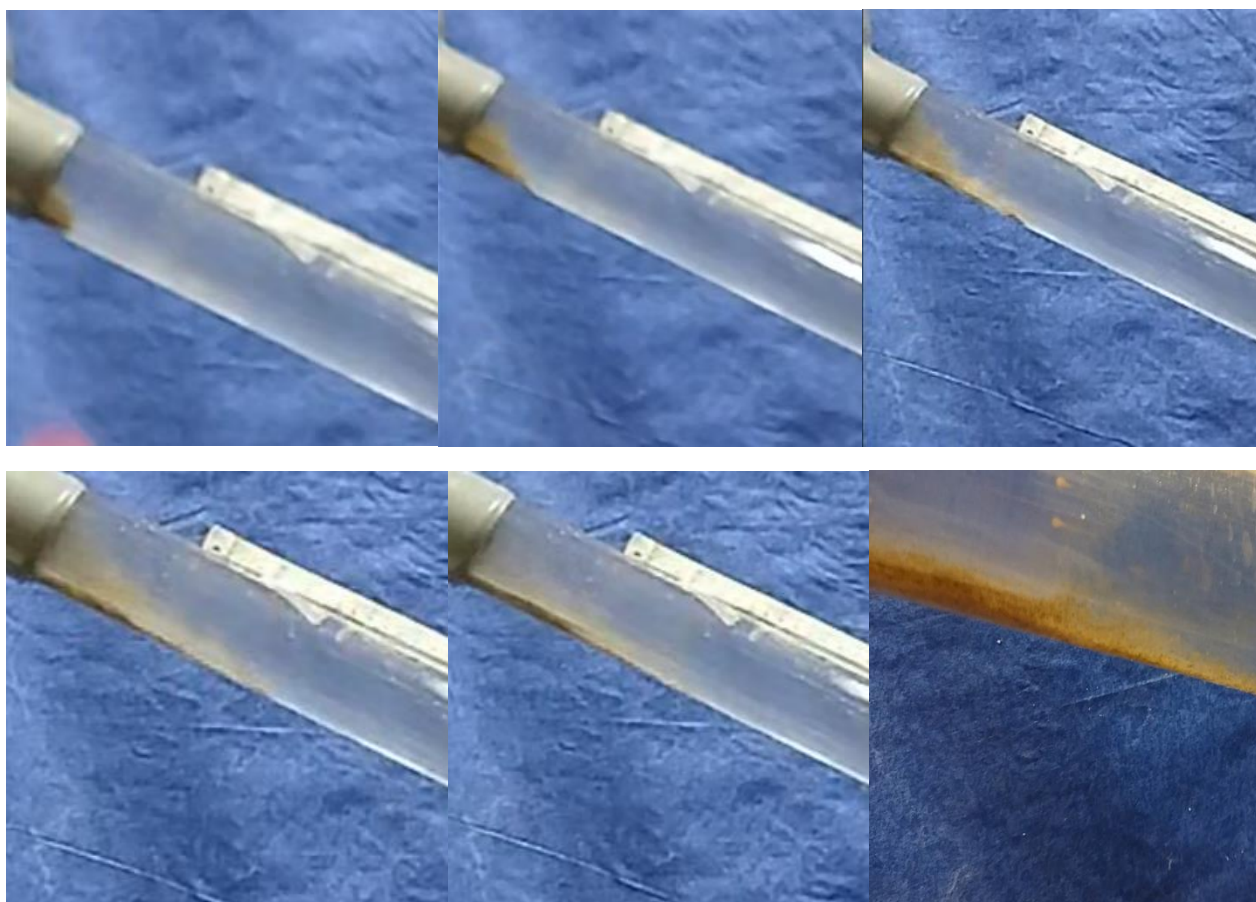
(c)



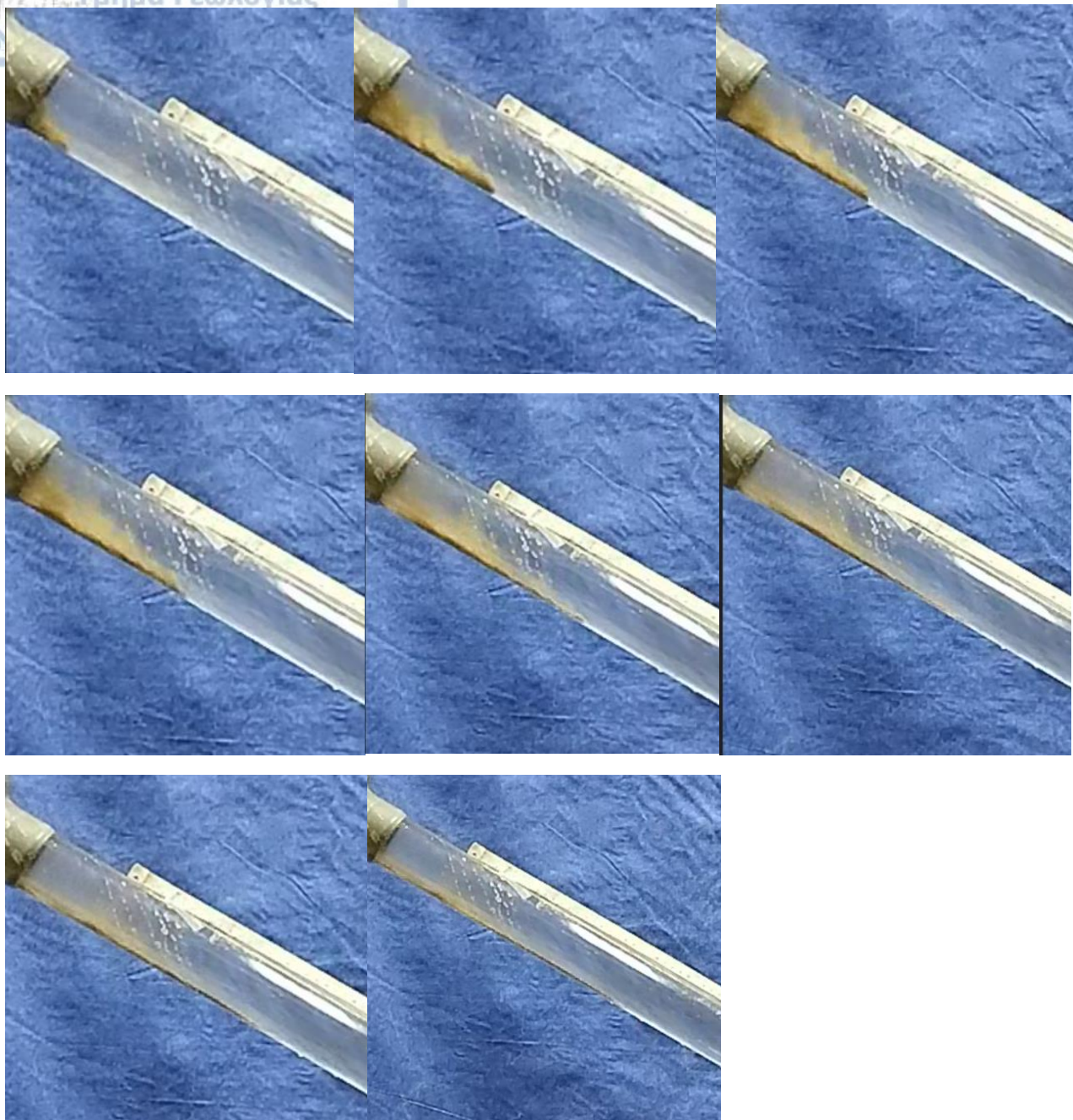




Pipe inclination 20°, hypersaline water, material 13.2 gr.

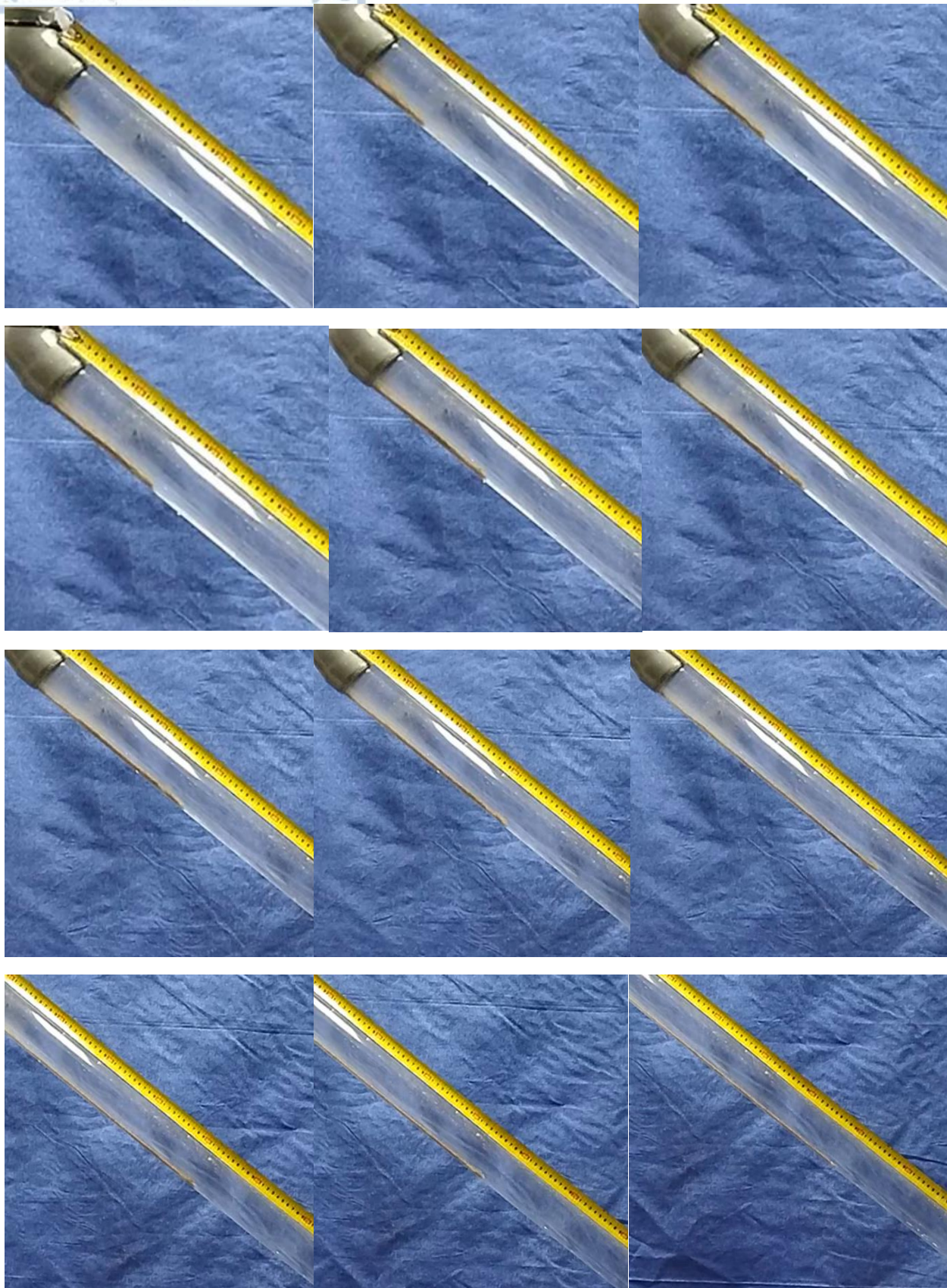


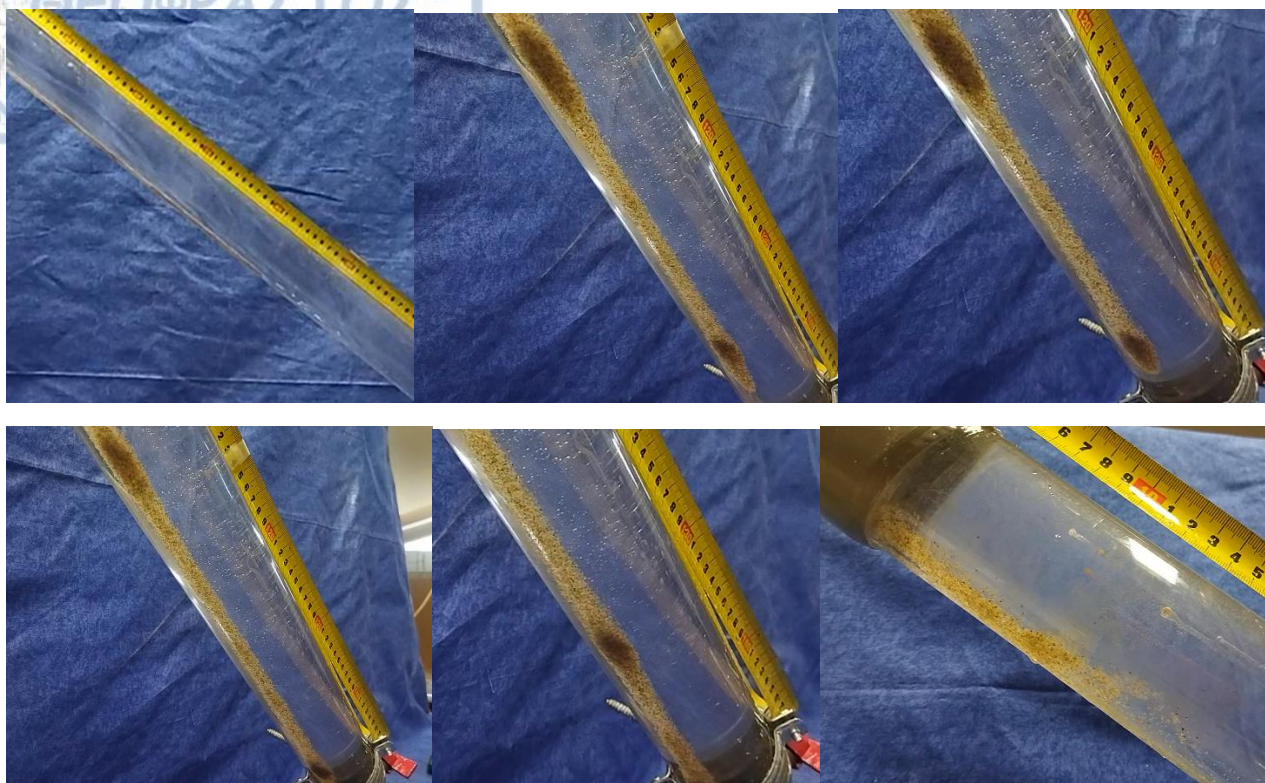
Pipe inclination 25°, hypersaline water, material 13.2 gr.



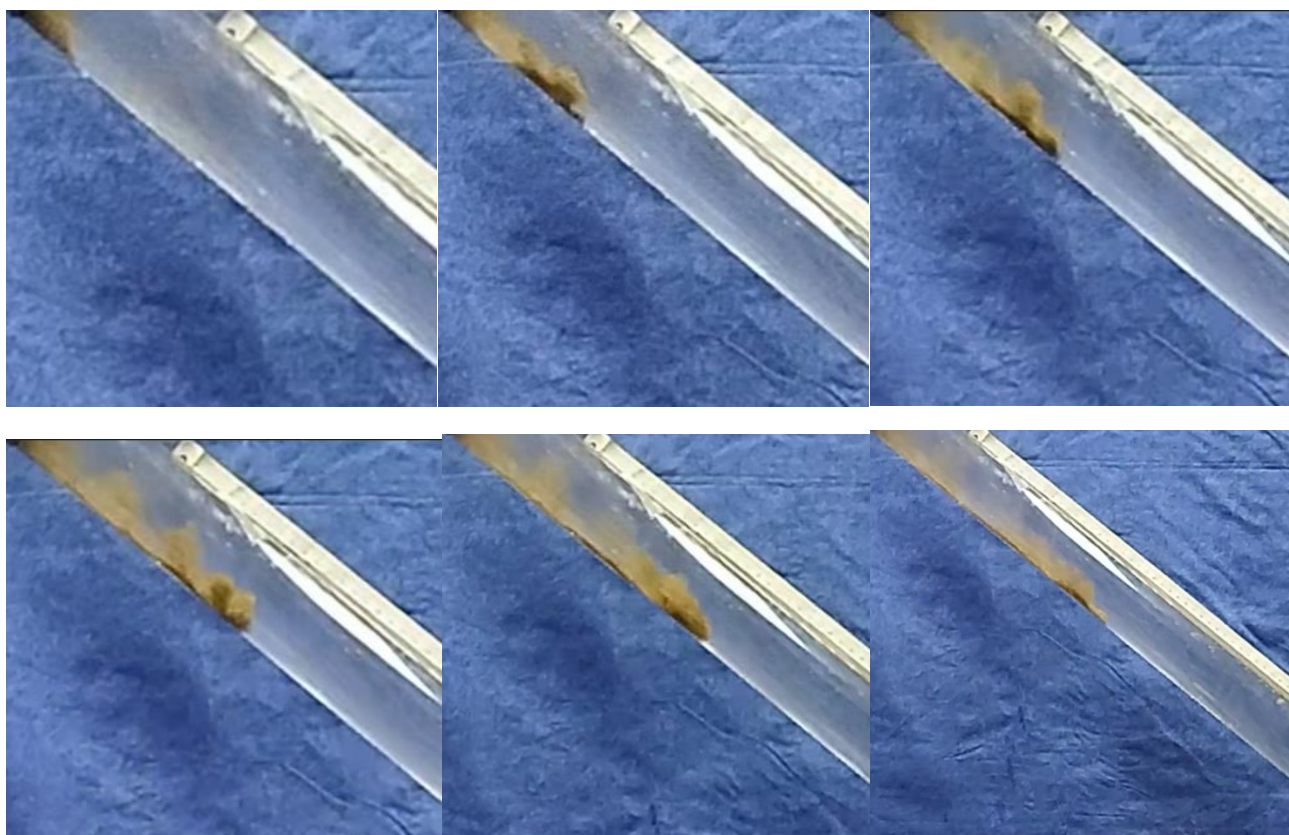
Pipe inclination 35°, hypersaline water, material 13.2 gr.

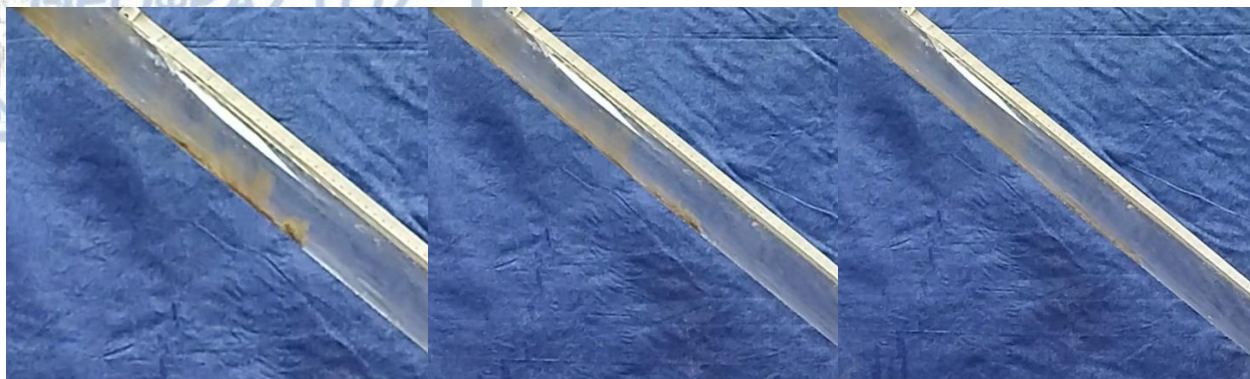
(a)





(b)



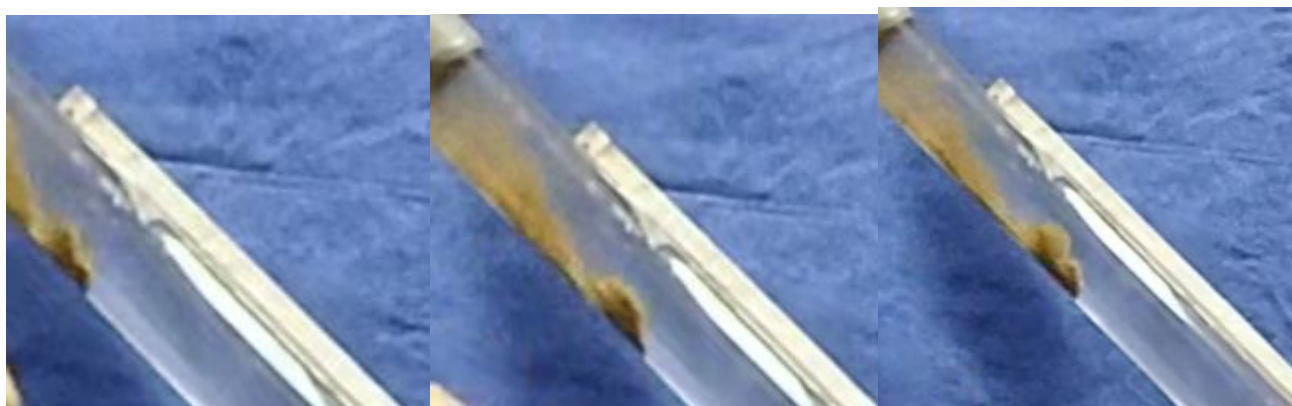


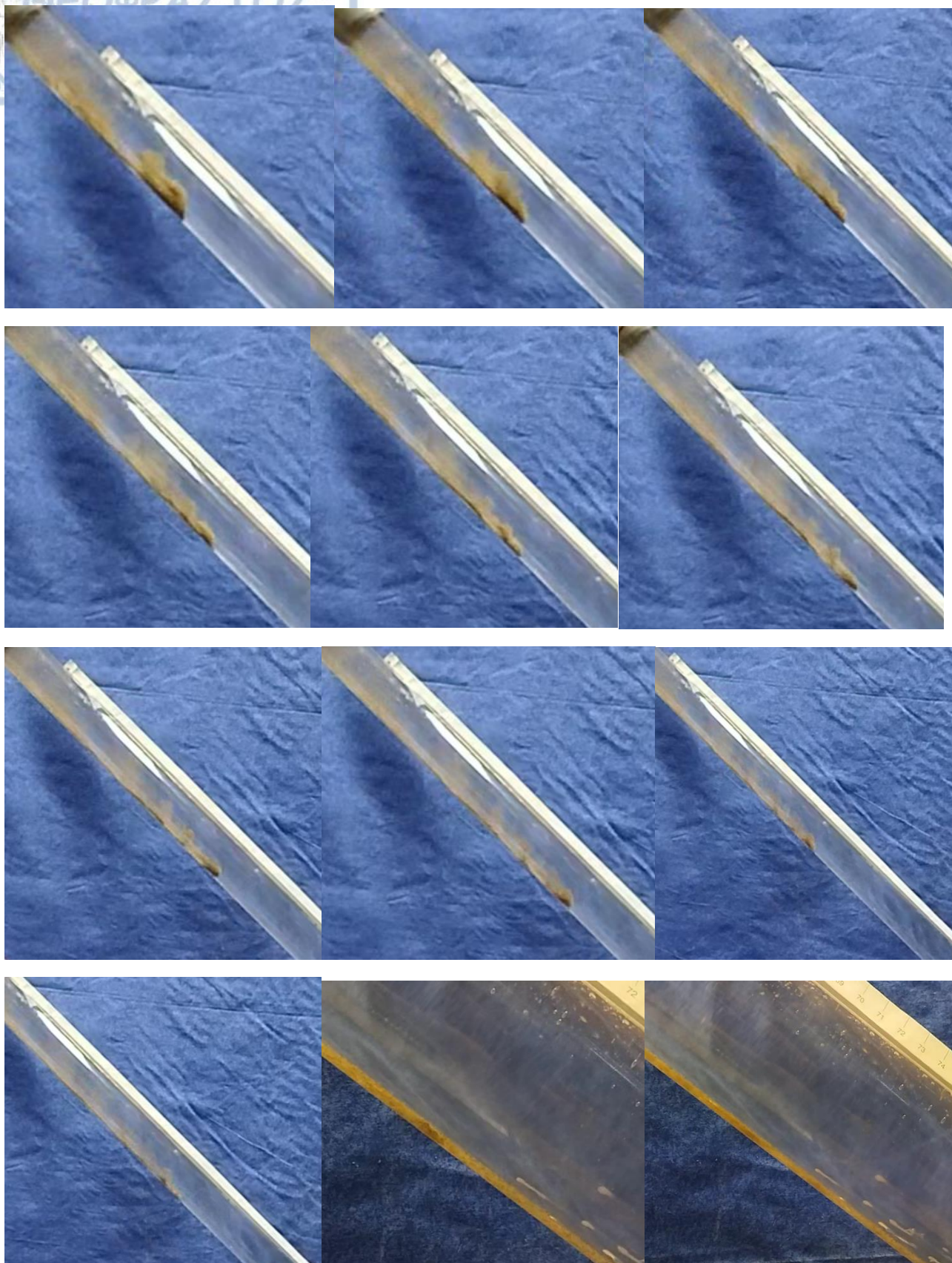
(c)





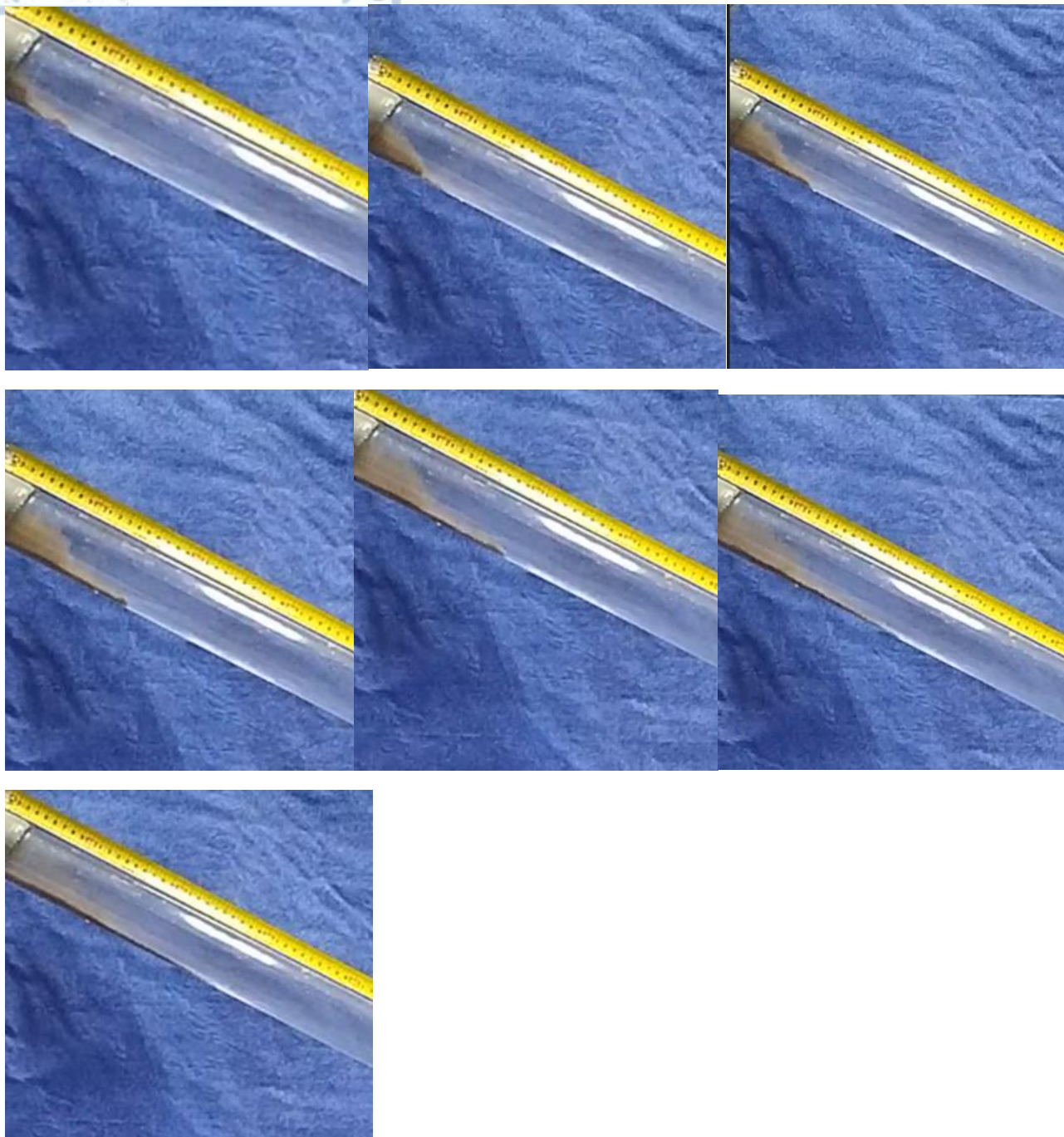
(d)





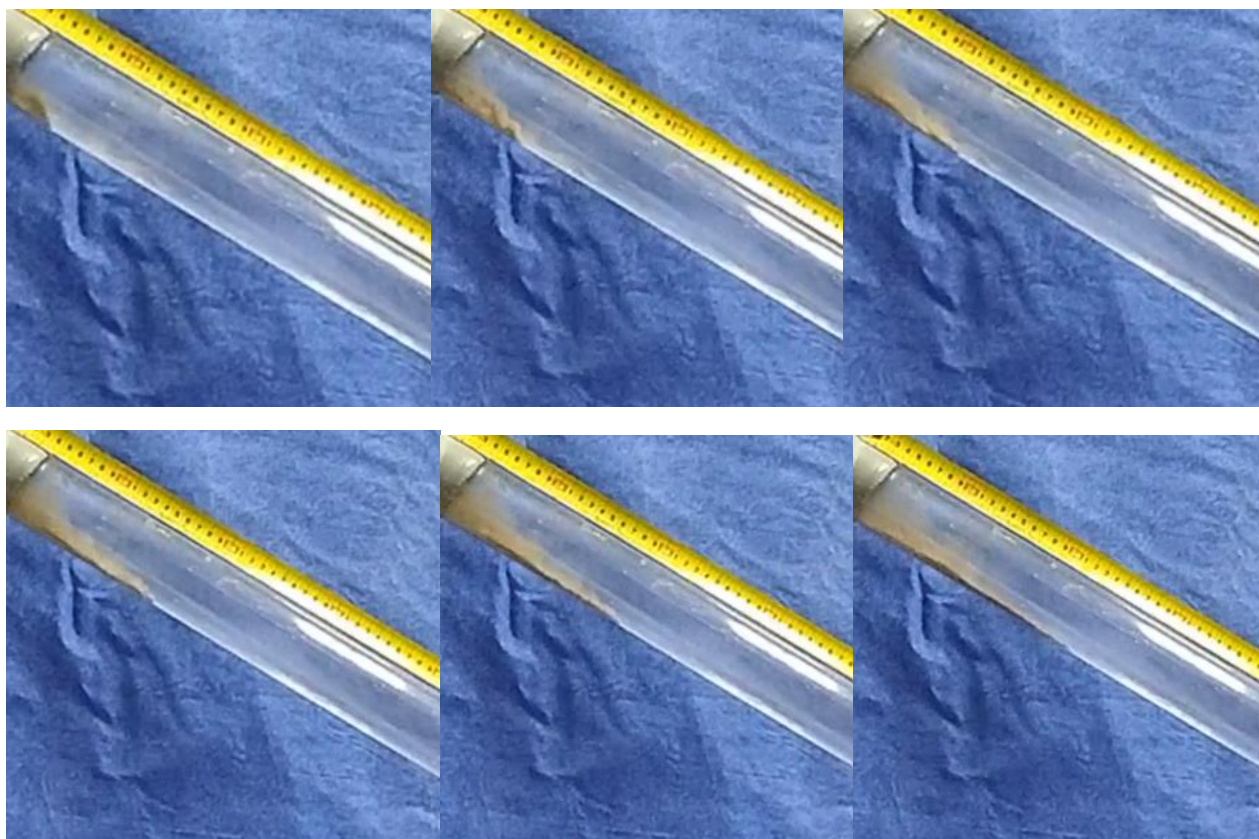
Pipe inclination 22°, tap water, material 30.07 gr.

(a)





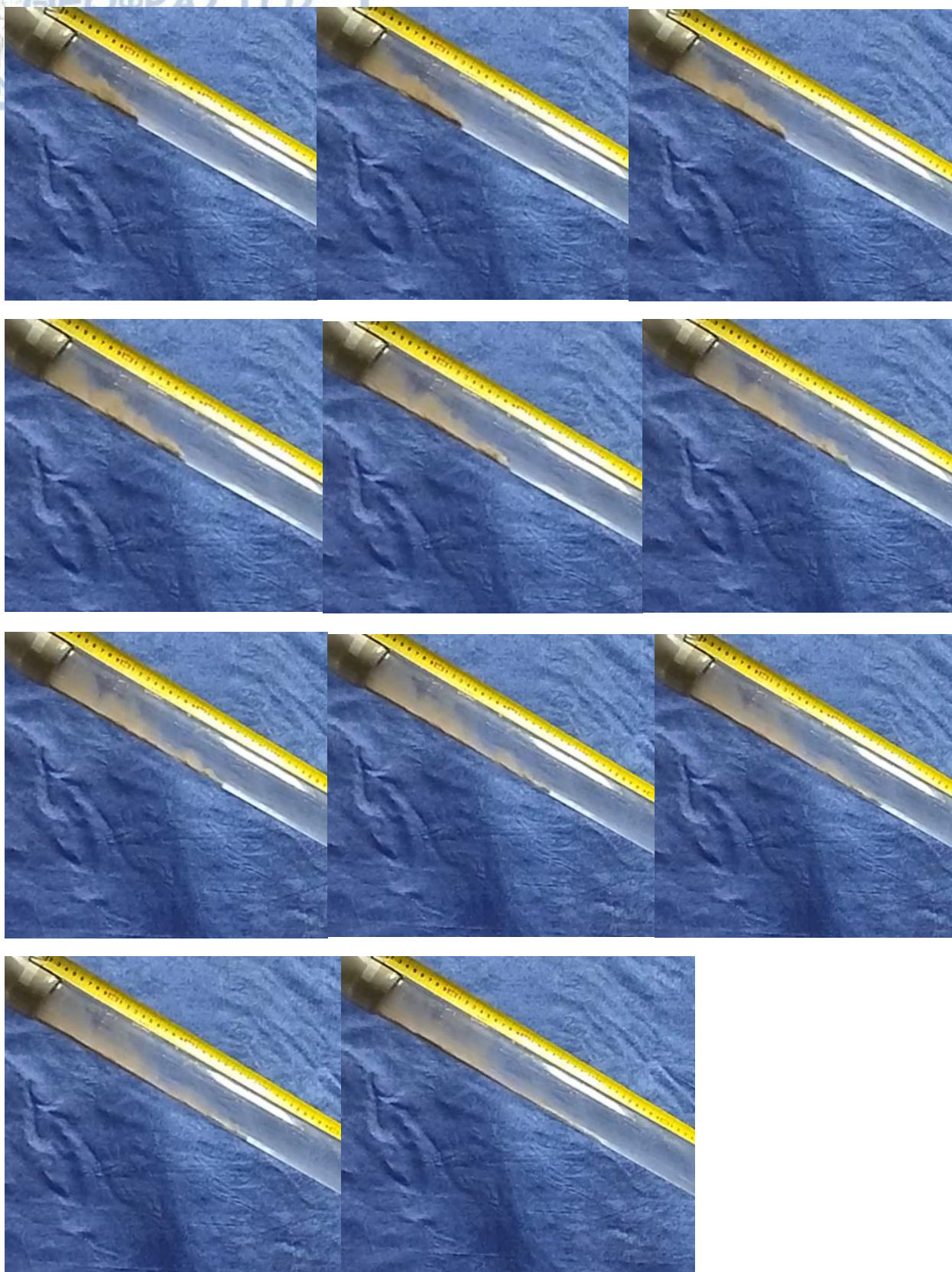
(b)





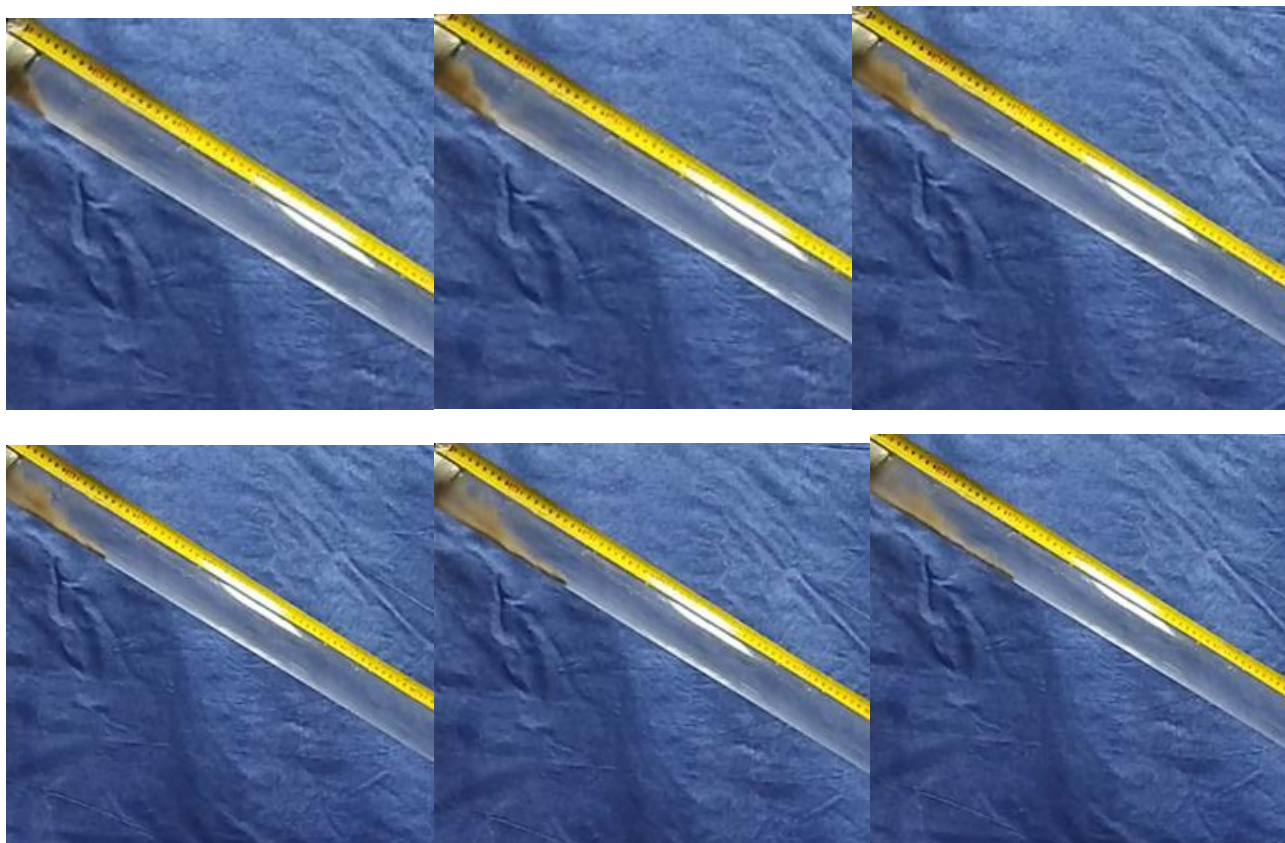
(c)







(d)



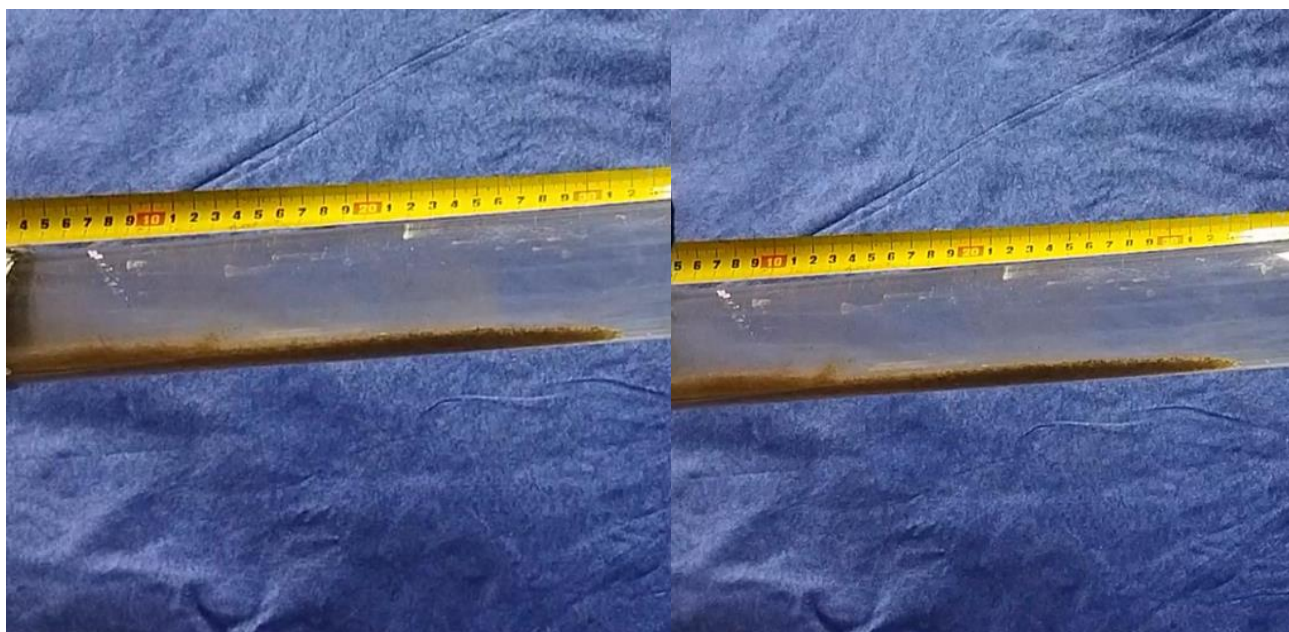


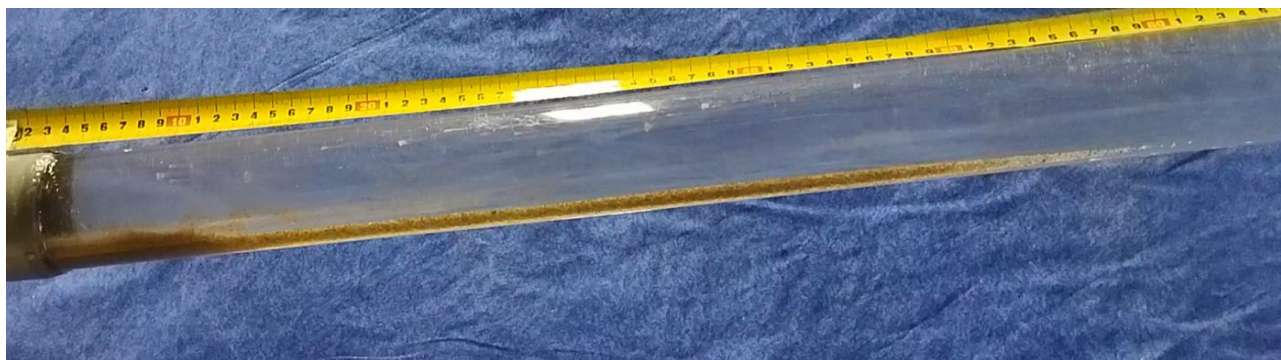
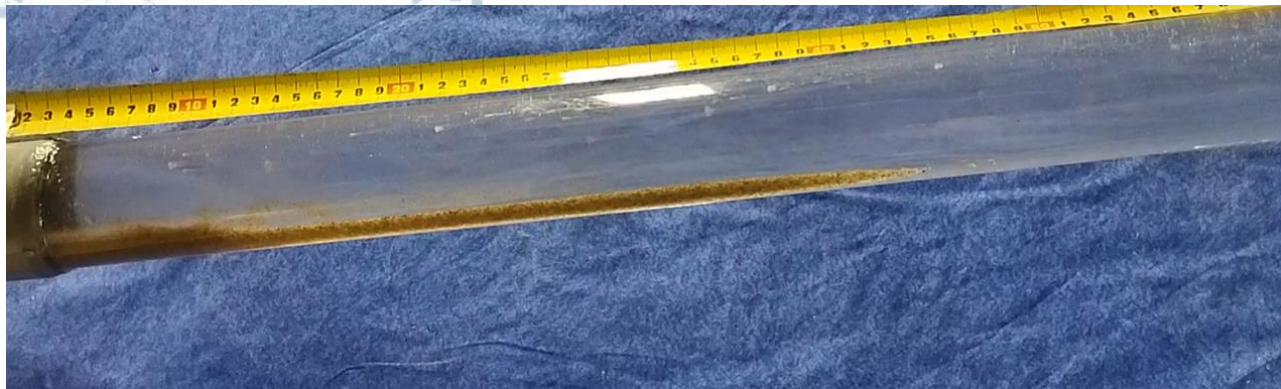
Pipe inclination 23°, hypersaline water, material 30.07 gr.

(a)









APPENTIX II

GRAIN SIZE RANGE 1-1.5 ϕ (average 1.25 ϕ)									
	FRESH WATER								
	MATERIAL 13.4 gr					MATERIAL 28.1 gr			
EXPERIMENTS (7)	1	2	3	4	5	1	2		
PIPE INCLINATION (ankles)	22	24	35	35	35	24	22		
GRAIN ROLL	NO	YES	YES	YES	YES	YES	YES		
TURBIDITE	NO	NO	YES	YES (0.4 m)	YES (0.42m)	YES (0.16 m)	YES (0.1 m)		
GRAVITY FLOW	NO	YES	YES	YES	YES	YES	YES		
GRAIN GROUPS / 10 sec	NO	NO	5	5	6	NO	NO		
GRAIN GROUPS SPEED (cm/sec)	NO	NO	10	9	8	NO	NO		
SPEED MATERIAL (cm/sec)	NO	0.5	7	4	5	0.8	0.5		
REMAINIG MATERIAL	YES	YES	YES	YES	YES	YES	YES		
TURBIDITE FRONT SPEED (cm/sec)	NO	NO	-	23	20	19	11		
HYPERSALINE WATER (SG=1160.45)									
	MATERIAL 13.4 gr					MATERIAL 28.1 gr			
	1	2	3	4	5	6	7 (+2% clay)	1	2
EXPERIMENTS (9)	22	25	27	35	35	35	35	23	23
PIPE INCLINATION (ankles)	22	25	27	35	35	35	35	23	23
GRAIN ROLL	NO	YES	YES	YES	YES	YES	YES	YES	YES
TURBIDITE	YES (0.16 m)	YES (0.18 m)	YES (0.2m)	YES (0.45 m)	YES (0.44 m)	YES (0.29 m)	YES (0.32 m)	-	-
GRAVITY FLOW	NO	YES	YES	YES	YES	YES	YES	YES	YES
GRAIN GROUPS / 30 sec	NO	NO	NO	7	6	7	8	NO	NO
GRAIN GROUPS SPEED (cm/sec)	NO	NO	NO	5	7	5	6	NO	NO
SPEED MATERIAL (cm/sec)	NO	0.3	1	-	4	3	3	0.6	0.4
REMAINIG MATERIAL	YES	YES	YES	YES	YES	YES	YES	YES	YES
TURBIDITE FRONT SPEED (cm/sec)	14	16	17	19	22	18	18	-	-

Table 5.1. Presentation of experimental results with a material grain size range of 1-1.5 ϕ (Average 1.25 ϕ).

GRAIN SIZE RANGE 2-2.5 ϕ (average 2.25 ϕ)								
	TAP WATER							
	MATERIAL 12.8 gr						MATERIAL 28.7 gr	
EXPERIMENTS (8)	1	2	3	4	5	6	1	2
PIPE INCLINATION (ankles)	22	25	27	35	35	35	22	22
GRAIN ROLL	NO	YES	YES	YES	YES	YES	YES	YES
TURBIDITE	YES (0.2 m)	YES (0.22 m)	YES (0.29 m)	YES (0.3 m)	YES (0.52m)	YES (0.45 m)	YES (0.38 m)	YES (0.26 m)
GRAVITY FLOW	NO	YES	YES	YES	YES	YES	YES	YES
GRAIN GROUPS / 30 sec	NO	NO	NO	8	10	11	NO	NO
GRAIN GROUPS SPEED (cm/sec)	NO	NO	NO	5	7	6	NO	NO
SPEED MATERIAL (cm/sec)	NO	0.5	1.5	5	6	6	0.6	0.7
REMAINIG MATERIAL	YES	YES	YES	YES	YES	YES	YES	YES
TURBIDITE FRONT SPEED (cm/sec)	17	18	20	17	22	23	23	22
	HYPERSALINE WATER (SG=1160.45)							
	MATERIAL 12.8 gr				MATERIAL 28.7 gr			
EXPERIMENTS (6)	1	2	3	4	1	2		
PIPE INCLINATION (ankles)	25	25	35	35	23	23		
GRAIN ROLL	YES	YES	YES	YES	YES	YES		
TURBIDITE	YES (0.1 m)	YES (0.24 m)	YES (0.3 m)	-	YES (0.3 m)	-		
GRAVITY FLOW	YES	YES	YES	YES	YES	YES		
GRAIN GROUPS / 30 sec	NO	NO	7	4	NO	NO		
GRAIN GROUPS SPEED (cm/sec)	NO	NO	2.5	2	NO	NO		
SPEED MATERIAL (cm/sec)	0.3	0.2	3	3	0.3	0.4		
REMAINIG MATERIAL	YES	YES	YES	YES	YES	YES		
TURBIDITE FRONT SPEED (cm/sec)	-	11	13	-	19	-		

Table 5.2. Presentation of Experimental Results with Material Particle Size Range of 2-2.5 ϕ (Mean 2.25 ϕ)

	DUNE MATERIAL (-1.5- >4 φ)									
	TAP WATER									
	MATERIAL 13.2 gr					MATERIAL 30 gr				
EXPERIMENTS (9)	1	2	3	4	5	1	2	3	4	
PIPE INCLINATION (ankles)	20	22	35	35	35	22	22	22	22	
GRAIN ROLL	NO	YES	YES	YES	YES	YES	YES	YES	YES	
TURBIDITE	YES (0.2 m)	-	YES (1.34m)	YES (1.23m)	YES (1.25m)	YES (0.2 m)	YES (0.24 m)	YES (0.35 m)	-	
GRAVITY FLOW	NO	YES	YES	YES	YES	YES	YES	YES	YES	
GRAIN GROUPS / 10 sec	NO	NO	12	13	11	YES (bigger)	NO	NO	YES (bigger)	
GRAIN GROUPS SPEED (cm/sec)	NO	NO	16	16	18	-	-	-	-	
SPEED MATERIAL (cm/sec)	NO	0.4	20	20	21	1	0.6	0.8	0.6	
REMAINIG MATERIAL	YES	YES	YES	YES	YES	YES	YES	YES	YES	
TURBIDITE FRONT SPEED (cm/sec)	19	-	27	26	28	18	18	23	-	
	HYPERSALINE WATER (SG=1160,45)									
	MATERIAL 13.2 gr					MATERIAL 30 gr				
EXPERIMENTS (9)	1	2	3	4	5	6	7	1	2	
PIPE INCLINATION (ankles)	20	23	25	35	35	35	35	22	23	
GRAIN ROLL	NO	YES	YES	YES	YES	YES	YES	YES	YES	
TURBIDITE	YES (0.13m)	-	YES (0,2m)	YES (0,69 m)	YES (-)	YES (0,64m)	YES (0,7m)	YES (0.24 m)	-	
GRAVITY FLOW	NO	YES	YES	YES	YES	YES	YES	YES	YES	
GRAIN GROUPS / 30 sec	NO	NO	NO	-	-	9	4	NO	NO	
GRAIN GROUPS SPEED (cm/sec)	NO	NO	NO	-	-	6.5	12	NO	NO	
SPEED MATERIAL (cm/sec)	NO	0.2	1.5	-	-	-	9	0.9	0.8	
REMAINIG MATERIAL	YES	YES	YES	YES	YES	YES	YES	YES	YES	
TURBIDITE FRONT SPEED (cm/sec)	15	-	20	18	22	20	21	15	-	

Table 5.3. Presentation of Experimental Results with Sediment Material of Grain Size Range -1.5 to >4 φ.

